TOPICS IN MIMO RADARS: SPARSE SENSING AND SPECTRUM SHARING

By

BO LI

A dissertation submitted to the

Graduate School—New Brunswick

Rutgers, The State University of New Jersey

in partial fulfillment of the requirements

for the degree of

Doctor of Philosophy

Graduate Program in Department of Electrical and Computer Engineering

written under the direction of

Professor Athina P. Petropulu

and approved by

_____

_____

_____

_____

New Brunswick, New Jersey

OCTOBER, 2016

ABSTRACT OF THE DISSERTATION

Topics in MIMO Radars: Sparse Sensing and Spectrum Sharing

By BO LI

Dissertation Director:

Professor Athina P. Petropulu

Recently, multiple-input multiple-output (MIMO) radars have received considerable attention due to their superior resolution. A MIMO radar system lends itself to a networked implementation, which is very desirable in both military and civilian applications. In networked radars, the transmit and receive antennas are placed on wireless connected nodes, such as vehicles, ships, airplanes, or even backpacks. The transmit antennas transmit probing waveforms, which impinge on targets and are reflected back. A fusion center collects the target echo measurements of all receive antennas and jointly processes the signals to extract the desired target parameters. This dissertation proposes to address the following two bottleneck issues associated with networked radars.

Reliable surveillance requires collection, communication and process of vast amounts of data. This is a power and bandwidth consuming task, which can be especially taxing in scenarios in which the antennas are on battery operated devices and are connected to the fusion center via a wireless link. Sparse sensing techniques are used to substantially reduce the amount of data that need to be communicated to a fusion center, while ensuring high target detection and estimation performance. In the first part, this dissertation derives the

theoretical requirements and performance guarantees for the application of compressive sensing to both MIMO radar settings, namely, the collocated MIMO radars and the distributed MIMO radars. Confirming previous simulations based observations, the theoretical results of this thesis show that exploiting the sparsity of the target vector can reduce the amount of measurements needed for successful target estimation. For compressive sensing based distributed MIMO radars, we also propose two low-complexity signal recovery approaches.

With the increasing demand of radio spectrum, the operating frequency bands of communication and radar systems often overlap, causing one system to exert interference to the other. Uncoordinated interference from communication systems may significantly harm the tactical radar functionality and vice versa. In the second part, this dissertation studies spectrum sharing between a MIMO communication system and a MIMO radar system in various scenarios. First, a cooperative spectrum sharing framework is proposed for the coexistence of MIMO radars and wireless communications. Radar transmit precoding and adaptive communication transmission are adopted, and are jointly designed to maximize signal-to-interference-plus-noise ratio (SINR) at the radar receiver subject to the communication system meeting certain rate and power constraints. Compared to the noncooperative approaches in the literature, the proposed approach has the potential to improve the spectrum utilization because it introduces more degrees of freedom. In addition, the proposed spectrum sharing framework considers several practical issues which are not addressed in literature, *e.g.*, the radar pulsed transmit pattern, targets falling in different range bins, and radar systems operating in the presence of clutter. Second, we investigate spectrum sharing between a MIMO communication system and a recently proposed sparse sensing based radar, namely the matrix completion based MIMO radar (MIMO-MC). MIMO-MC radar receivers take sub-Nyquist rate samples, and transfer them to a fusion center where the full data matrix is completed with high accuracy. MIMO-MC radars, in addition to reducing communication bandwidth and power as compared to MIMO radars, offer a significant advantage for spectrum sharing. The advantage stems from the way the sub-sampling scheme at the radar receivers modulates the interference channel from the communication system transmitters, rendering it symbol dependent and reducing its row space. This makes it easier for the communication system to design its waveforms in an adaptive fashion so that it

minimizes the interference to the radar subject to meeting rate and power constraints. Two methods are investigated to minimize the effective interference power to the radar receiver: 1) design the communication transmit covariance matrix with fixed the radar sampling scheme, and 2) jointly design the communication transmit covariance matrix and the MIMO-MC radar sampling scheme. Furthermore, we investigate joint transmit precoding for the co-existence of a MIMO-MC radar and a MIMO wireless communication system in the presence of clutter. We show that the error performance of matrix completion in MIMO-MC radars is theoretically guaranteed when precoding is employed. The radar transmit precoder, the radar sub-sampling scheme, and the communication transmit covariance matrix are jointly designed to maximize the radar SINR while meeting certain communication rate and power constraints. Efficient optimization algorithms are provided along with insight on the proposed design problem.

Acknowledgments

First of all, I would like to express my heartfelt gratitude to my advisor, Prof. Athina P. Petropulu, for her generous support and inspirational guidance throughout my Ph.D. studies. Prof. Petropulu continuously encourages me to pursue creative ideas and always stands closely to offer help. As my role model, she has taught me invaluable lessons including passions and patience for innovation, commitment to excellence, and skills for presenting ideas and writing reports/papers, which are not only helpful for doing academic research but will also be valuable assets for my career success.

Next, I would also like to thank the members of my dissertation defense committee: Prof. Waheed U. Bajwa, Prof. Vishal Patel, and Prof. Hongbin Li (Stevens Institute of Technology), for their precious time in reviewing my dissertation and valuable comments. I am also very grateful to Prof. Wade Trappe for serving as a committee member on my dissertation proposal, and for his valuable input during our collaboration. I am very grateful to members served on my oral qualifying exam: Prof. Lawrence Rabiner, Prof. Yanyong Zhang, Prof. Janne Lindqvist, Prof. Laleh Najafizadeh, and Prof. Sophocles Orfanidis.

Moreover, I also like to thank all my labmates, including Dr. Yao Yu, Dr. Jiangyuan Li, Dionysios Kalogerias, Xiaqing Yang, Chrysanthi Koumpouzi, Jing Xu, and Harshat Kumar. Additionally, I am very grateful to the graduate director, Prof. Zoran Gajic, as well as ECE staff, John Scafidi, Noraida Martinez, Ora Titus, Arletta Hoscilowicz, and Christy Lafferty, for their numerous help.

Furthermore, I am deeply grateful to my beautiful wife, Chen Zhang, a supportive companion, a true blessing from God, and an angel from heaven bringing me unending love, encouragement and happiness. Also, words couldn't express my gratitude to my parents and grandfather for encouraging me to pursue higher education. Without their support and sacrifice, I could not even attend the college. I would also like to acknowledge the support

of my sister, father-in-law, mother-in-law, and brother-in-law.

Last but not least, I thank God for the wisdom and blessings from him.

Dedication

To my beloved wife and my parents

Table of Contents

List of Tables

List of Figures

Chapter 1

Introduction

In this chapter, we provide background and literature review on multi-input multi-output (MIMO) radar, sparse sensing in MIMO radar based on compressed sensing and matrix completion, as well as spectrum sharing between radar and communication systems.

Notation: The notations in this dissertation are summarized in Table 1.1.

1.1 Radar Basics

Radar is an active sensing system using radio frequencies to determine target parameters, such as range, the direction of arrival and velocity [1, 2]. The radar transmit component transmits modulated radio waves or waveforms, which are reflected by targets in the propagation path. At the radar receive side, the target echoes are demodulated and processed to determine the target information.

To illustrate the basic principles, let us consider a monostatic pulsed radar, which transmits waveforms in short bursts or pulses [2]. The transmitted waveform is modeled as

$$\begin{aligned} x\left(t\right) &= s\left(t\right) e^{-j2\pi ft},\ t \in [0, T_{\mathrm{PRI}}] \\ &= a\left(t\right) e^{-j\varphi(t)} e^{-j2\pi ft} \end{aligned} \tag{1.1}$$

where f, $s(t)$ and T_{PRI} are the carrier frequency, the complex baseband waveform and the pulse repetition interval, respectively. The term $a(t)$ and $\varphi(t)$ represent the amplitude and phase of the waveform. The received signal can be written as

$$r\left(t\right) = \beta s\left(t - \tau_0 + \frac{2vt}{c}\right) e^{-j2\pi f(t-\tau_0) - j\nu_0 t} + n(t). \tag{1.2}$$

where β, τ_0, v, and ν_0 denote the target reflection coefficient, round trip delay from the radar to the target, the target velocity, and the Doppler shift, respectively. It holds that

Table 1.1: Notations

$\mathcal{CN}(\mu, \mathbf{\Sigma})$	the circularly symmetric complex Gaussian distribution with mean μ and covariance matrix $\mathbf{\Sigma}$
$\lvert\cdot\rvert$, $\mathrm{Tr}(\cdot)$	matrix determinant & trace
$\mathbb{N}_L^+$	the set $\{1, \ldots, L\}$
δ_{ij}	the Kronecker delta
x^+	$\max(0, x)$
$\lfloor x \rfloor$	the largest integer smaller or equal to x
$\Re(\cdot)$	the real part of a complex variable
$\mathbf{A}^T, \mathbf{A}^H$	the transpose and Hermitian transpose of $\mathbf{A}$
$\otimes$	the Kronecker product
$\circ$	the Hadamard product
$\lVert\mathbf{A}\rVert$	the spectral norm of matrix $\mathbf{A}$, *i.e.*, the largest singular value
$\lVert\mathbf{A}\rVert_*$	the nuclear norm of matrix $\mathbf{A}$, *i.e.*, the sum of singular values
$\lVert\mathbf{A}\rVert_F$	the Frobenius norm of matrix $\mathbf{A}$, *i.e.*, $\sqrt{\mathrm{Tr}(\mathbf{A}^H\mathbf{A})}$
$\mathbf{A}_{\cdot m}$	the m-th column vector of $\mathbf{A}$
$\mathbf{A}_{m\cdot}$	the m-th row vector of $\mathbf{A}$.
$[\mathbf{A}]_{i,j}$	the (i,j)-th element of matrix $\mathbf{A}$
$\mathcal{R}(\mathbf{A})$	the range (column space) of matrix $\mathbf{A}$

$\nu_0 \triangleq \frac{4\pi v f}{c}$, where c is the speed of light. $n(t)$ denotes the additive noise. The target range from the radar is $d = \frac{\tau_0 c}{2}$.

Assuming a narrowband waveform is transmitted, we can ignore the time-delay of the waveform introduced by target movements. The baseband signal can be simplified as follows

$$r(t) = \beta s(t - \tau_0) e^{j(2\pi f \tau_0 - \nu_0 t)} + n(t), \tag{1.3}$$

The received signal $r(t)$ then goes through a matched filter $s^*(t)e^{j\nu t}$, which maximizes the output SNR at time delay instant τ and Doppler shift ν. The matched filter output is given by

$$\begin{aligned} z(\tau, \nu) &= \tilde{\beta} \int_{-\infty}^{+\infty} s(t - \tau_0) s^*(t - \tau) e^{j(\nu - \nu_0)t} dt + \int_{-\infty}^{+\infty} n(t) s^*(t - \tau) e^{j\nu t} dt \\ &\triangleq \tilde{\beta} A(\tau - \tau_0, \nu - \nu_0) + \tilde{n}(\tau) \end{aligned} \tag{1.4}$$

where $\tilde{\beta}$ absorbs the constant terms, and

$$\begin{aligned} A(\tau, \nu) &\triangleq \int_{-\infty}^{\infty} s(t) s^*(t - \tau) e^{j\nu t} dt, \\ \tilde{n}(\tau) &\triangleq \int_{-\infty}^{+\infty} n(t) s^*(t - \tau) e^{j\nu t} dt. \end{aligned} \tag{1.5}$$

$|A(\tau,\nu)|$ is known as the *ambiguity function* of the radar waveform [2]. If the matched filter perfectly matched to the target echo, the filter output corresponds to the ambiguity function evaluated at $(\tau,\nu) = (0,0)$. The ambiguity function has the property that $|A(\tau,\nu)| \leq |A(0,0)|$. Therefore, the target range and velocity can be extracted by locating the peak of the matched filter output in the τ-ν plane. When there are multiple targets, multiple peaks would present in the τ-ν plane. Ideally, $|A(\tau,\nu)|$ should be a delta function, which could achieve highly accurate range and Doppler estimation and distinguish closely located multiple targets. Otherwise, a weak target can be masked by the sidelobe of a closely located strong target.

Another important target parameter is angle or DOA. Let us consider a phased array [1] with M_t transmit and M_r receive antennas as shown in Fig.1.1. Suppose that there are K targets on the same plane with the antennas, each at direction of arrival $\{\theta_k\}$ and range $\{d_k\}$ with respect to (w.r.t.) the radar phase center. During each pulse, the target echoes received at the radar RX antennas are demodulated to baseband as follows:

$$\mathbf{y}(t) = \sum_{k=1}^{K} \beta_k \mathbf{v}_r(\theta_k)\mathbf{v}_t^T(\theta_k)\mathbf{1}s(t-\tau_k) + \mathbf{n}(t),\ t \in [0, T_{PRI}], \tag{1.6}$$

where $\mathbf{n}(t) \in \mathbb{C}^{M_r}$ is the additive nose; $\mathbf{1}$ denotes the ones vector of length M_t; $\tau_k \triangleq 2d_k/c$; the time delays in the received waveform are approximated by τ_k for different radar TX-RX pairs due to the narrowband assumption; β_k is a complex amplitude contains contributions from the radar cross section, the common carrier phase delay $e^{j2\pi f_c \tau_k}$ and the Doppler shift if the k-th target is moving; the Swerling II target model is assumed, *i.e.*, the β_k's vary from pulse to pulse and have distribution $\mathcal{CN}(0,\sigma_{\beta k}^2)$; and $\mathbf{v}_r(\theta) \in \mathbb{C}^{M_r}$ is the receive steering vector defined as

$$\mathbf{v}_r(\theta) \triangleq \left[e^{j2\pi\langle \mathbf{d}_1^r, \mathbf{u}(\theta)\rangle/\lambda_c}, \ldots, e^{j2\pi\langle \mathbf{d}_{M_r}^r, \mathbf{u}(\theta)\rangle/\lambda_c}\right]^T, \tag{1.7}$$

with $\mathbf{d}_1^r \triangleq [x_m^r\ y_m^r]^T$ denoting the two-dimensional coordinates of the m-th RX antenna, $\mathbf{u}(\theta) \triangleq [\cos(\theta)\ \sin(\theta)]^T$, λ_c denoting the carrier wavelength. $\mathbf{v}_t(\theta) \in \mathbb{C}^{M_t}$ is the transmit steering vector and is respectively defined. For the case of uniform linear array (ULA), the receive steering vector is simplified as

$$\mathbf{v}_r(\theta) \triangleq \left[1, e^{j\alpha}, \ldots, e^{j(M_r-1)\alpha}\right]^T,$$

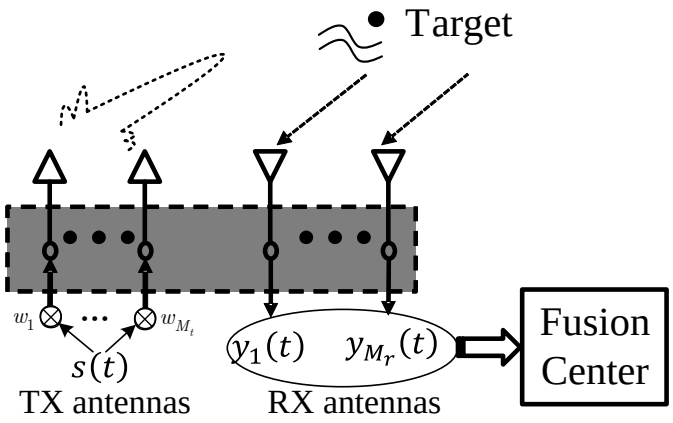

Figure 1.1: Illustration of a phased array radar with M_t transmit and M_r receive antennas. All transmit antennas transmit the same waveform $s(t)$, possibly with different weights.

where $\alpha \triangleq 2\pi d_r \sin(\theta)/\lambda_c$ is called the spatial frequency [3] and d_r is the inter distance. The spatial frequencies can be obtained by applying FFT on $\mathbf{y}(t)$, based on which the angles θ_k's can be obtained. Subspace methods, such as multiple signal classification (MUSIC), can be used to achieve more accurate DOA information [4].

1.2 MIMO Radar

Multiple-input multiple-output (MIMO) radars [5–8] have received considerable attention in recent years due to their improved performance over traditional phased array radars. Unlike the phased array radars in which all antennas transmit an identical waveform with different scalar weights [1], MIMO radars adopt independent waveforms for the transmit antennas. The target information is extracted by a bank of matched filters at the receive side. MIMO radar system can achieve high resolution with a relatively small number of transmit (TX) and receive (RX) antennas [9–12]. Depending on the locations of antennas, MIMO radars can be classified into collocated [5, 6] and widely separated [7, 8].

1.2.1 MIMO Radar with Collocated Antennas

In the collocated MIMO radars, the transmit and receive antennas are closely located and thus the target radar cross section (RCS) experienced by different transmit and receive pairs could be viewed as identical [5, 6]. Let us consider a collocated MIMO radar system

with M_t transmit and M_r receive antennas as shown in Fig.1.2. The MIMO radar employs narrowband orthogonal waveforms $s_m(t), m = 1, \ldots, M_t$, each of which contains L coded sub-pulses:

$$s_m(t) = \frac{1}{T_b} \sum_{l=1}^{L} s_{ml} \text{Rect}[t - (l-1)T_b],\ t \in [0, T_p],$$

where Rect$[t]$ equals 1 if $t \in [0, T_b]$, otherwise 0; T_b and T_p denotes the sub-pulse and pulse duration, respectively; $\mathbf{s}_m \triangleq [s_{m1}, \ldots, s_{mL}]^T$ denotes the orthogonal code vector. It holds that

$$\langle \mathbf{s}_m, \mathbf{s}_n \rangle = \int_0^{T_p} s_m(t) s_n(t) dt = \delta_{mn}.$$

Suppose that there are K targets on the same plane with the antennas, each at direction of arrival $\{\theta_k\}$ in the same range bin w.r.t. the radar phase center. During each pulse, the target echoes received at the radar RX antennas are demodulated to baseband as follows:

$$\mathbf{y}(t) = \sum_{k=1}^{K} \beta_k \mathbf{v}_r(\theta_k) \mathbf{v}_t^T(\theta_k) \mathbf{s}(t) + \mathbf{n}(t),\ t \in [0, T_{PRI}], \tag{1.8}$$

where $\mathbf{s}(t) \triangleq [s_1(t), \ldots, s_{M_t}(t)]^T$ and the other terms are defined similarly as in (1.6).

At each receive antenna, a matched filter bank composed of M_t transmit waveforms is used to separate target echoes contributed by M_t transmission. As a result, M_r receive antennas could obtain $M_t M_r$ filter output in total:

$$\mathbf{r} = \sum_{k=1}^{K} \beta_k \mathbf{v}_r(\theta_k) \otimes \mathbf{v}_t(\theta_k) + \tilde{\mathbf{n}}$$

Target estimation can be performed based on $\mathbf{Y}_R$ via standard array processing schemes [4]. In particular, for the ULA transmit array with inter-distance d_t and ULA receive array with inter-distance $d_r = M_t d_t$, we have

$$\mathbf{v}_r(\theta) \otimes \mathbf{v}_t(\theta) \equiv \left[1, e^{j\alpha}, \ldots, e^{j(M_t M_r - 1)\alpha}\right]^T,$$

where $\alpha \triangleq 2\pi d_t \sin(\theta)/\lambda_c$. Therefore, the filter output $\mathbf{r}$ can be viewed as the signal received by a virtual array of length $M_t M_r$ elements. This suggests that the collocated MIMO radar provides a much higher degree of freedom with only a small number of transmit and receive antennas. Therefore, collocated MIMO radars achieve superior spatial resolution compared with traditional radar systems [6, 12].

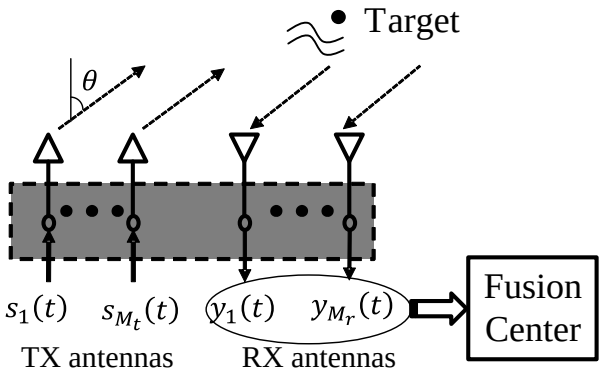

Figure 1.2: Illustration of a collocated MIMO radar system equipped with M_t transmit antennas and M_r receive antennas. Independent waveforms are used at different transmit antennas. Both transmit and receive array are ULA.

1.2.2 MIMO Radar with Widely Separated Antennas

In distributed MIMO radars, the transmit and receive antennas are widely separated from each other compared with their distance to the targets [7, 8]. For example, for an extended target of dimension 10λ and at distance 10000λ, where λ denotes the carrier wavelength, it is shown the signal propagation paths are independent if the separation between antennas of the MIMO radar is of order 1000λ. In such scenario, the transmit antennas emit independent waveforms, which propagate through independent paths from transmitters to receivers via the targets. As a result, distributed MIMO radars enjoy spatial diversity to reduce the RCS scintillation of the targets.

There are two modes to process the radar observations, namely, the non-coherent and coherent methods [7, 8]. The non-coherent method only utilizes the signal amplitude, which requires only time synchronization between transmit and receive antennas. The coherent method utilizes both amplitude and phase information, which requires both time and phase synchronization.

In summary, collocated MIMO radars exploit phase differences in target returns induced by transmit and receive antennas, to effectively increase the array aperture and achieve high resolution. Distributed MIMO radars enjoy spatial diversity, introduced by the multiple independents paths between the targets and the transmit/receive antennas, and thus achieve improved target estimation performance.

1.3 MIMO Radar Based on Sparse Sensing

Reliable surveillance requires collection, communication and process of vast amounts of data. This is a power and bandwidth consuming task, which can be especially taxing in scenarios in which the antennas are on battery operated devices and are connected to the fusion center via a wireless link. Sparse sensing techniques are used to substantially reduce the amount of data that need to be communicated to a fusion center, while ensuring high target detection and estimation performance.

1.3.1 Introduction to Compressed Sensing

Compressed sensing, or compressive sampling (CS) [13–16], is a relatively recent development for finding sparse solutions to under-determined linear systems. The theory of CS states that a sparse signal $\mathbf{s}$ can be recovered from measurements $\mathbf{z} = \mathbf{\Psi s}$ via ℓ_1-optimization as follows

$$\min \|\mathbf{s}\|_1, \quad s.t.\ \mathbf{z} = \mathbf{\Psi s} \tag{1.9}$$

where $\mathbf{s}$ is a n dimensional sparse vector with K nonzero entries and zero elsewhere; $\mathbf{\Psi}$ is the $m \times n$ dimensional measurement matrix with $m \ll n$. The recoverability of the recovery algorithm is guaranteed by the restricted isometry property (RIP) of $\mathbf{\Psi}$.

Definition 1. *Matrix $\mathbf{\Psi}$ satisfies the RIP of order K with restricted isometry constant (RIC) δ_K, shorted by RIP(K, δ_K), if δ_K is the smallest number such that for all K-sparse $\mathbf{s}$*

$$(1 - \delta_K)\|\mathbf{s}\|_2^2 \leq \|\mathbf{\Psi s}\|_2^2 \leq (1 + \delta_K)\|\mathbf{s}\|_2^2.$$

If δ_K is small enough, $\mathbf{s}$ can be recovered exactly from (1.9). For sub-Gaussian random matrix, its RIC satisfies $\delta_K \leq \delta$ with high probability provided that $m \geq c\delta^{-2} K \log n$ where c is a constant [15].

Recent works [17] show that *block* or *group sparsity*, when it exists in the signal, can be used as a prior to further reduce the number of measurements required to recover the sparse vector. Block sparsity in the sparse signal was investigated in [18–20], where the elements in the sparse signal vector appear in blocks. Let us consider a block sparse vector $\mathbf{s} \in \mathbb{C}^{MN}$ with at most K nonzero blocks out of N equal-sized blocks, *i.e.*, $M \triangleq |\mathcal{I}_n|, \forall n \in \mathbb{N}_N^+$, where

$\mathcal{I}_n$ is the index set for the n-th block. Let us denote by $\mathcal{A}_B^K$ the space in which the block sparse vectors lie.

Given the noisy measurement vector $\mathbf{z} = \mathbf{\Psi s} + \mathbf{n}$ with $\mathbf{\Psi} \in \mathbb{C}^{L \times NM}$ as the measurement matrix and $\mathbf{n} \in \mathbb{C}^L$ as the additive noise vector, the recovery of $\mathbf{s} \in \mathcal{A}_B^K$ is achieved via the following convex optimization problem

$$\min_{\mathbf{s}} \sum_{n=1}^{N} \|\mathbf{s}[\mathcal{I}_n]\|_2 \;\; s.t. \; \|\mathbf{z} - \mathbf{\Psi s}\|_2 \leq \epsilon. \tag{1.10}$$

which is referred to as mixed ℓ_2/ℓ_1-optimization program (L-OPT) [18]. The effectiveness of using L-OPT relies on the RIP of $\mathbf{\Psi}$ w.r.t. vectors in $\mathcal{A}_B^{2K}$.

Definition 2 ([21]). *For a union of certain subspaces denoted by $\mathcal{A}$, $\mathbf{\Psi}$ is said to satisfy the $\mathcal{A}$-restricted isometry property with constant $\delta \in (0,1)$, in short, $\mathcal{A}$-RIP(K,δ), if δ is the smallest value such that*

$$(1-\delta)\|\mathbf{s}\|_2^2 \leq \|\mathbf{\Psi s}\|_2^2 \leq (1+\delta)\|\mathbf{s}\|_2^2 \tag{1.11}$$

holds for all $\mathbf{s} \in \mathcal{A}$.

The above definition is for general union of subspaces. If $\mathbf{\Psi}$ satisfies the RIP over $\mathcal{A}_B^{2K}$, or equivalently, if $\mathbf{\Psi}$ satisfies the $\mathcal{A}_B$-RIP$(2K, \delta_{2K})$, then the next lemma shows that the solution of (1.10), *i.e.*, $\hat{\mathbf{s}}$, is a good approximation of $\mathbf{s}$.

Lemma 1 (Theorem 2 in [18]). *If $\mathbf{\Psi}$ satisfies the $\mathcal{A}_B$-RIP$(2K, \delta_{2K})$ with $\delta_{2K} < \sqrt{2} - 1$, then for the solution of (1.10), $\hat{\mathbf{s}}$, it holds that*

$$\|\hat{\mathbf{s}} - \mathbf{s}\|_2 \leq \frac{4\sqrt{1+\delta_{2K}}}{1-(1+\sqrt{2})\delta_{2K}}\epsilon \triangleq g(\epsilon). \tag{1.12}$$

It is shown in [18] that Gaussian measurement matrices require fewer measurements to satisfy the $\mathcal{A}_B$-RIP$(2K, \delta_{2K})$ as compared to the number of measurements needed to satisfy the RIP$(2K, \delta_{2K})$. Therefore, exploiting block sparsity in $\mathbf{s}$ reduces the required number of measurements for sparse recovery.

1.3.2 MIMO-CS: Compressed Sensing Based MIMO Radar

By exploiting the sparsity of targets in the radar scene, sparse sensing [13, 15, 16] has been studied in the context of both collocated [22–29], and distributed MIMO radars [30,

31]. MIMO-CS radar exploits the sparsity of targets in the target space and enables target estimation based on a small number of samples obtained at the receive antennas.

Suppose that we are interested in target parameters including the time delay from the transmitter to the receiver via the k-th target, i.e., τ_k , the target azimuth angle, θ_k, and Doppler frequency, f_k, for all $k \in \mathbb{N}_K^+$. To exploit the target space sparsity, the delay-angle-Doppler space is discretized on the grid $\mathcal{T} \times \Theta \times \mathcal{D}$ with $|\mathcal{T}| = N_\tau, |\Theta| = N_\theta$, and $|\mathcal{D}| = N_f$. All grid points are ordered and labeled by the index set $\mathcal{I} \triangleq \{1, \ldots, N_\tau N_\theta N_f\}$. It is assumed that the targets fall on grid points.

The transmit array emits probing pulses and each receiver obtains Nyquist rate samples from the target returns during each pulse. The fusion center collects the samples from all receivers and stacks them into vector $\mathbf{z} \in \mathbb{C}^{LPM_r}$. From the MIMO-CS radar literature, the model obeys

$$\mathbf{z} = \mathbf{\Psi}\mathbf{s} + \mathbf{n}, \tag{1.13}$$

where $\mathbf{n}$ is the interference/noise vector, $\mathbf{s} \in \mathbb{C}^{N_\tau N_\theta N_f}$ denotes the target space vector. $\mathbf{s}$ is sparse whose elements are nonzero only if the corresponding grid points are occupied by targets. $\mathbf{\Psi} \in \mathbb{C}^{(LPM_r)\times(N_\tau N_\theta N_f)}$ is the measurement matrix; its n-th column is associated with the n-th grid point. The recovery of $\mathbf{s}$ can be achieved by the ℓ_1 minimization algorithms. The estimation of the target parameters can be identified by the grid points associated with the dominant elements in recovered $\mathbf{s}$. It is well-known that the RIP [14] of the measurement matrix $\mathbf{\Psi}$ plays an important role on guaranteeing the recoverability and estimation performance of $\mathbf{s}$. In order to provide the performance of MIMO-CS radars, it is essential to characterize the RIP of $\mathbf{\Psi}$.

For collocated MIMO radars, compressed sensing has been considered and evaluated thoroughly in [22–25, 28]. The work in [26] provided the first nonuniform recovery guarantee for range-angle-Doppler estimation and the corresponding bounds on the number of transmit/receive antennas and measurements. However, the results only apply to MIMO-MC radars with virtual uniform linear array (ULA) configuration. Spatial CS for MIMO radars with random transmit/receive array was proposed in [27, 28] for angle estimation. A nonuniform recovery guarantee was provided in [27, 28] based on the isotropy property of the measurement matrix. The work in [28] also provided a uniform recovery guarantee

based on the coherence analysis of the measurement matrix. However, the analysis cannot be extended to the range-angle-Doppler estimation.

For distributed MIMO radars, the problem of target location and speed estimation was investigated in [30, 31] as a block sparse signal recovery problem. The block sparsity in the target vector arises by grouping together entries corresponding to paths between a given grid point and all transmit/receive antenna pairs. Block matching pursuit (BMP) is applied in [30] for signal support recovery. Block sparsity in distributed MIMO radars was also studied in [31], where a group Lasso approach was used to exploit the block sparsity. Simulations in [30, 31] show that exploiting block sparsity results in significant detection performance gains over methods which just consider unstructured sparsity. To the best of our knowledge, there are no theoretical works on the performance of distributed MIMO-CS radars.

1.3.3 MIMO-MC: Matrix Completion Based MIMO Radar

Reliable surveillance requires collection, communication and fusion of vast amounts of data from various antennas. This is a power and bandwidth consuming task, which can be especially taxing in scenarios in which the antennas are on battery operated devices and are connected to the fusion center via a wireless link. Recently, MIMO radars using matrix completion (MIMO-MC) [32–35] have been proposed to save power and bandwidth on the link between the receivers and the fusion center, thus facilitating the network implementation of MIMO radars.

Consider a collocated MIMO radar system with M_t TX antennas and M_r RX antennas. The targets are in the far-field of the antennas and are assumed to fall in the same range bin. Following the model of (1.8), the data matrix at the fusion center can be formulated as

$$\mathbf{Y} = \mathbf{B}\mathbf{\Sigma}\mathbf{A}^T\mathbf{S} + \mathbf{W}, \tag{1.14}$$

where the m-th row of $\mathbf{Y} \in \mathbb{C}^{M_r \times L}$ contains L samples forwarded by the m-th antenna; $\mathbf{B} = [\mathbf{v}_r(\theta_1), \ldots, \mathbf{v}_r(\theta_K)]$, $\mathbf{A} = [\mathbf{v}_t(\theta_1), \ldots, \mathbf{v}_t(\theta_K)]$, $\mathbf{\Sigma} = \mathrm{diag}(\beta_1, \ldots, \beta_K)$; $\mathbf{W}$ denotes additive noise; $\mathbf{S} = [\mathbf{s}(1), \cdots, \mathbf{s}(L)]$, with $\mathbf{s}(l) = [s_1(l), \cdots, s_{M_t}(l)]^T$ being the l-th snapshot across the transmit antennas. Let us denote the target response matrix $\mathbf{B}\mathbf{\Sigma}\mathbf{A}^T$ by $\mathbf{D} \in \mathbb{C}^{M_r \times M_t}$.

If the number of targets is smaller than M_r and L, matrix $\mathbf{DS}$ is low-rank and can

be provably recovered based on a subset of its entries [33, 35]. This observation gave rise to MIMO-MC radars [32–35], where each RX antenna sub-samples the target returns and forwards the samples to the fusion center. The sampling scheme could be a pseudo-random sequence of integers in $[1, L]$, with the fusion center knowing the random seed of each RX antenna.

In MIMO-MC radars, the partially filled data matrix at the fusion center can be mathematically expressed as follows (see [33] Scheme I)

$$\mathbf{\Omega} \circ \mathbf{Y} = \mathbf{\Omega} \circ (\mathbf{DS} + \mathbf{W}), \tag{1.15}$$

where $\mathbf{\Omega}$ is a matrix containing 0's and 1's; the 1's in the m-th row correspond to the sampled symbols of the m-th TX antenna. The sub-sampling rate, p, equals $\|\mathbf{\Omega}\|_0/(LM_r)$. When $p = 1$, the $\mathbf{\Omega}$ matrix is filled with 1's, and the MIMO-MC radar is identical to the traditional MIMO radar. At the fusion center, the completion of $\mathbf{DS}$ is formulated as the following problem [36]

$$\min_{\mathbf{M}} \|\mathbf{M}\|_* \quad \text{s.t. } \|\mathbf{\Omega} \circ \mathbf{M} - \mathbf{\Omega} \circ \mathbf{Y}\|_F \leq \delta, \tag{1.16}$$

where $\delta > 0$ is a parameter related to the noise over the sampled noise matrix entries, *i.e.*, $\mathbf{\Omega} \circ \mathbf{W}$. On denoting by $\hat{\mathbf{M}}$ the solution of (1.16), the recovery error $\|\hat{\mathbf{M}} - \mathbf{DS}\|_F$ is determined by the noise power in $\mathbf{\Omega} \circ \mathbf{W}_R$, *i.e.*, the noise enters only through the sampled entries of the data matrix. It is important to note that, assuming that the reconstruction error is small, the reconstructed $\hat{\mathbf{M}}$ has the same received target echo power as $\mathbf{DS}$ of (1.14).

MIMO-MC radars maintain the high resolution of MIMO radars, while requiring significantly fewer data to be communicated to the fusion center, thus enabling savings in sampling power, communication power and bandwidth. These savings are especially important to networked radar receivers which are battery operated and are connected to the fusion center via a wireless link. Unlike MIMO-CS, MIMO-MC does not require discretization of the target space, thus does not suffer from grid mismatch issues [37].

1.3.4 Limitations of the Existing Work on MIMO Radars with Sparse Sensing

In the literature, the effectiveness of collocated MIMO-CS radars has been studied mostly via simulations. Although there exist some theoretical results for MIMO radars with linear

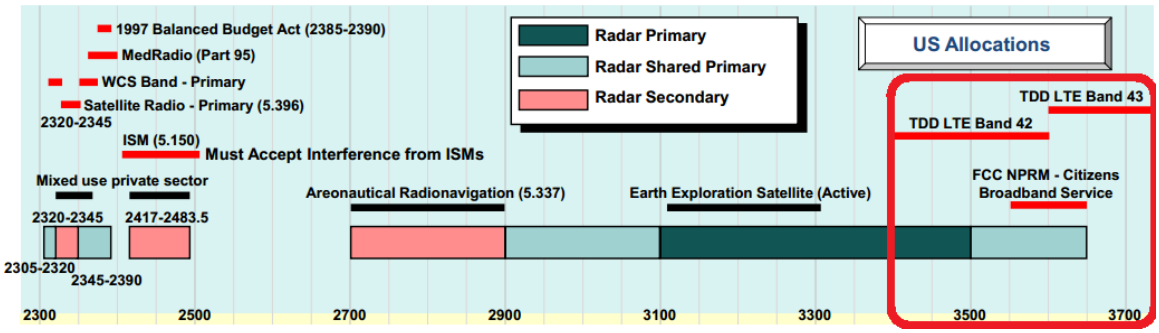

Figure 1.3: Federal Communications Commission spectrum allocation (Figure from DARPA Shared Spectrum Access for Radar and Communications (SSPARC)).

arrays [26] and for angle estimation [27, 28], those cannot be easily extended to arbitrary array configurations and range-Doppler-angle estimation.

Although simulations confirmed that exploiting block sparsity results in significant detection performance, there are no theoretical works on the performance distributed MIMO-CS radars. Existing theoretical works on collocated MIMO-CS radars [26–29] cannot be extended to the distributed MIMO radar scenario. On the other hand, sparse signal recovery techniques in radar systems introduces significant computational complexity. In [31] a group Lasso with proximal gradient algorithm (GLasso-PGA) was used, and in [38], a mixed ℓ_1/ℓ_2 norm optimization with interior point method (L-OPT-IPM) was used. GLasso-PGA and L-OPT-IPM achieve better estimation performance than BMP but involve higher computational complexity and require careful tuning of manually chosen parameters. The computation becomes prohibitive as the dimension of the sparse target vector increases.

1.4 Spectrum Sharing Between the Radar and Wireless Communication Systems

Spectrum congestion in commercial wireless communications is a growing problem as high-data-rate applications become prevalent. On the other hand, recent government studies have shown that huge chunks of spectrum held by federal agencies are underutilized in urban areas [39]. However, proposals and research on radar and communication spectrum sharing vastly emerge until recent years because of regulatory concerns. In an effort to relieve

the problem, the Federal Communications Commission (FCC) and the National Telecommunications and Information Administration (NTIA) have proposed to make available 150 megahertz of spectrum in the 3.5 GHz band, which was primarily used by federal radar systems for surveillance and air defense, to be shared by both radar and communication applications [40, 41]. From the right part of Fig. 1.3, we can see that 3.4-3.7GHz bands are shared by LTE bands and radar system. When communication and radar systems overlap in the spectrum, they exert interference to each other. This motivates us to consider the spectrum sharing between radar and communication systems. Spectrum sharing targets at enabling radar and communication systems to share the spectrum efficiently by minimizing interference effects [42–49].

The term "radar and wireless communication spectrum sharing", or "radar communication co-existence", is a rather broad concept. Generally speaking, any scenario that involves both radar and communication functionalities initialized by one or more users falls in the definition of radar and communication spectrum sharing. The key characteristic that differentiates radar and communication spectrum sharing from general cognitive radios [50] is the heterogeneousness in functionality, performance metric, and signaling for radar and communication. Radars are used for target detection and estimation, and has wide applications in civilian, military and public security purposes. The associated target detection and estimation performance is measured in terms of probability of detection, probability of false alarm, ROC, signal-to-interference-plus-noise ratio (SINR), minimum mean squared error (MMSE) and Cramer-Rao lower bound, et. al [2]. Meanwhile, wireless communication systems aim at communicating information between the transmitters and receivers. The majority of the demand for communication is from commercial and personal usage. Common performance metrics include bit error rate, channel capacity, throughout [51, 52]. The signaling used by radar and wireless communication systems are rather different. Radar waveforms can be either pulsed or continuous wave. There could also be phase or frequency modulation in radar waveforms. The choice of waveform determines fundamental radar system performance, such as SNR, range/velocity resolution and ambiguity properties [2]. Quadrature amplitude modulation (QAM) is the most extensively used signaling scheme for wireless communication systems [51, 52].

1.4.1 Related Work

For the radar and communication co-existence, the spectrum may be shared by radar and communication in time division, frequency division, space division.

Existing spectrum sharing approaches basically include three categories. The most intuitive one is avoiding interference by large physical separation distances between radar and communication systems [42, 53, 54]. The National Telecommunications and Information Administration (NTIA) reported an investigation of interference to radars operating in the band 2.7-2.9 GHz from WiMAX base stations [53]. The proposed interference mitigation options include reduction in the heights of WiMAX base stations, down-tilting of WiMAX base stations and establishing larger physical separation distances. The work in [54] studied the effect between one radar and one communication system coexisting with each other as their relative distance is varied. In [41], NTIA reported that large exclusion zones, which cover a large portion of the U.S., are required to protect cellular communication systems from high power radar signal, which essentially nulls the feasibility of the physical separation approach.

The second category is dynamic spectrum access based on spectrum sensing. Either radar or communication system is assigned as the primary or secondary user of the channel. The secondary user employs spectrum sensing techniques to identify the spectrum opportunity for nonintrusive spectrum access [55, 56][57–59]. The radar performance degradation due to in-band OFDM communication systems was studied in [60, 61], where a notch filter was used to mitigate the communication interference. Optimum joint design of OFDM radar and OFDM communication systems for spectrum sharing and carrier allocation has been considered in [62–64]. The works in [48, 49, 65] studied the synthesis of optimized radar waveforms ensuring spectral compatibility with the overlayed wireless communication systems based on a priori radio environmental map. These methods allow the radar and communication systems share the same carrier in the shared band at the cost of allowing certain amount of mutual interference. However, one can explore the spatial degree of freedom to greatly reduce the mutual interference if multiple antennas are used at both systems, as discussed in the next category.

The third category is spatial multiplexing enabled by the multiple antennas at both the radar and communication systems [43–47, 66, 67]. In [43–46, 66, 67], the radar interference to the communication system is eliminated by projecting the radar waveforms onto the null space of the interference channel from radar to communication systems. The resulted radar target detection performance was evaluated in [68, 69]. However, projection-type techniques might miss targets lying in the row space of the interference channel. In addition, the interference from the communication system to the radar was not considered. Spatial filtering at the radar receiver is proposed in [47] to reduce interference from the communication systems. This approach, however, works only if the target is not in the direction of the interference coming from the communication system. The output SINR of the optimal receive filter depends on the covariance matrix of the communication interference. Clearly, the output SINR could be further improved if the communication signaling is jointly designed.

Dual-function systems, which integrate both radar and communication functionality into one joint platform, are a special case of co-existence [70–72]. In particular, the embedding of communication signals into radar emissions for dual-functionality was reported in [73–77]. Interesting readers can refer to the review paper [78]. The radar and communication co-existence performance bounds were provided in [79, 80], where the radar estimation information rate and the communication data information rate were considered. The feasibility of merging communication and radar functionality into one common platform using OFDM signals has also been explored [81–85].

In parallel to the research on the coexistence of radar and communication systems, there are a lot of works focusing on joint radar and communication system, a new architecture which supports both the radar and communication functionality. Interesting readers can referred to the work in [65, 79, 80, 85, 86].

1.4.2 Limitations of the Existing Work on Radar-Communication Co-existence

In general, the existing literature on MIMO radar-communication systems spectrum sharing addresses interference mitigation for either solely the communication system [43–46, 66] or solely the radar [47]. While joint design of traditional radar and communication systems for spectrum sharing has been considered in [42, 62, 64], co-design of MIMO radar and

MIMO communication systems for spectrum sharing has not been addressed before. A new spectrum sharing framework can be proposed based on a higher level cooperation between the two systems. As an example, radar precoding can be introduced for new degrees of freedom of system design. The joint design of the radar precoding matrix and the communication codewords is expected to improve the overall performance. Unlike the radar waveform projection based methods [43–46], the joint design approach could potentially align the target returns and the communication interference separately in different subspaces, and thus suppress the interference without degrading the target returns.

The current work only considered the simplified scenario where multiple targets in the same range bin. In practice, multiple targets may fall in different range bins, which introduces target-dependent time variations in the radar received signal. In addition, pulsed radar operates in a particular pattern, *i.e.*, transmitting a short pulsed waveform and listening target echoes for a much longer period, which are two periods of a pulse repetition interval. At the communication receiver, radar interference only present during the radar transmit period. Furthermore,a clutter free scenario was assumed in [43–47]. However, unwanted echoes returned from ground, sea, and interfering targets, termed by clutter, can cause serious performance loss in radar systems. Realistic radar systems have to properly deal with clutter. By considering such radar operation conditions, the co-existence system model could be very different compared with that in existing works.

1.5 Contributions of the Dissertation

1.5.1 Theoretical Analysis and Efficient Algorithms for MIMO-CS Radars

For **collocated MIMO radars**, Chapter 2 considers range-angle-Doppler estimation in MIMO-CS radars with arbitrary array configuration. We analyze the restricted isometry property (RIP) of the measurement matrix. The RIP conditions involve, among other quantities, the number of transmit and receive antennas. A scheme is proposed that selects the subset of receive antennas with the smallest cardinality that meet the RIP conditions.

For **distributed MIMO radars**, we address the theoretical and computational issues for distributed MIMO radars using compressed sensing in Chapter 3. The contribution of

Chapter 3 is two-fold:

- We provide uniform recovery guarantees by analyzing the $\mathcal{A}$-RIP of the block diagonal measurement matrix. The proposed theoretical results validate the simulations based finding that the structure in the measurement matrix results in either reduction of the number of measurements needed, or improved target estimation for the same number of measurements.

- Two low-complexity approaches have been proposed to reduce the computation while maintaining the estimation performance. The first approach was an ADMM-based sparse signal recovery algorithm. The second approach decouples the location and speed estimation into two separate stages. The location estimation obtained in the first stage is used to prune the target location-speed space in the speed estimation stage.

This work has been published in

- B. Li and A. Petropulu, "RIP analysis of the measurement matrix for compressive sensing-based MIMO radars," *IEEE 8th Sensor Array and Multichannel Signal Processing Workshop (SAM)*, Spain, 2014, pp. 497-500.

- B. Li and A. P. Petropulu, "Structured sampling of structured signals," *IEEE Global Conference on Signal and Information Processing (GlobalSIP)*, Austin, TX, 2013, pp. 1009-1012.

- B. Li and A. P. Petropulu, "Efficient target estimation in distributed MIMO radar via the ADMM," *the 48th Annual Conference on Information Sciences and Systems (CISS)*, Princeton, NJ, 2014, pp. 1-5.

- B. Li and A. P. Petropulu, "Performance guarantees for distributed MIMO radar based on sparse sensing," *IEEE Radar Conference*, Cincinnati, OH, 2014, pp. 1369-1372.

- B. Li and A. P. Petropulu, "Distributed MIMO radar based on sparse sensing: Analysis and efficient implementation," in *IEEE Transactions on Aerospace and Electronic Systems*, vol. 51, no. 4, pp. 3055-3070, Oct. 2015.

1.5.2 A Joint Design Approach for Radar-Communication Co-existence under Realistic Conditions

In Chapter 4, we propose a spectrum sharing framework for the coexistence of MIMO radars and a communication system, for a scenario in which the targets fall in different range bins. The coexistence model considers the radar operation pattern, *i.e.*, transmitting a short pulsed waveform and listening target echoes for a much longer period. Radar transmit (TX) precoding and adaptive communication transmission are adopted and are jointly designed to maximize the signal-to-interference-plus-noise ratio (SINR) at the MIMO radar receiver while meeting certain rate and power constraints at the communication system. Analysis on the obtained solution indicates that a two-level constant communication rate over the radar TX period and the radar listening-only period could achieve the same radar SINR as the adaptive transmission. Based on this fact, we propose a new design with a much lower dimension which has reduced complexity without degrading the radar SINR.

In Chapter 5, we consider the co-design based spectrum sharing of a MIMO radar and a communication system for a scenario in which the radar system operates in the presence of clutter. Both the radar and the communication system use transmit precoding to maximize the radar SINR subject to the communication system meeting certain rate and power constraints. Due to the dependence of the clutter on radar precoding matrix, the optimization w.r.t. the radar precoder is a maximization of a nonconvex function over a nonconvex feasible set. Solving such problem is computationally intractable and demanding. As an efficient alternative, we propose to maximize a lower bound of the SINR. In the resulting alternating maximization problem, the alternating iteration of the communication covariance matrix reduces to one SDP problem. We show that the radar precoder always has a rank one solution. Based on this key observation, the alternating iteration of the radar precoder is solved by a sequence of second order cone programming (SOCP) problems, which are more efficient and tractable than SDP problems.

This work has been published in

- B. Li, H. Kumar and A. P. Petropulu, "A joint design approach for spectrum sharing between radar and communication systems," *IEEE International Conference on*

Acoustics, Speech and Signal Processing (ICASSP), Shanghai, 2016, pp. 3306-3310.

- B. Li and A. Petropulu, "MIMO radar and communication spectrum sharing with clutter mitigation," *IEEE Radar Conference (RadarConf)*, Philadelphia, PA, 2016, pp. 1-6.

1.5.3 Spectrum Sharing Between Matrix Completion Based MIMO Radars and MIMO Wireless Communications

By employing sparse sampling, MIMO-MC radars achieve the performance of MIMO radars but with significantly fewer data samples. Spectrum sharing will be more and more popular to enable the co-existence of radar and wireless communications sharing the scarce RF spectrum. Sparse sensing and spectrum sharing seem to be unrelated with each other in their applications to MIMO radars. The integration of these two directions has not been considered in MIMO radar literature. This dissertation bring a new perspective by answering the following key questions:

- Is it possible for MIMO radars to achieve BOTH savings in data samples and spectrum sharing with wireless communications?
- What role does sparse sensing play in the radar-communication spectrum sharing framework?
- How can transmit beamforming and clutter mitigation be integrated into the MIMO-MC radars which coexist with wireless communication systems?

Chapter 6 of this dissertation proposes ways via which a MIMO-MC radar and a MIMO communication system, in a cooperative fashion, negotiate spectrum use in order to mitigate mutual interference. The MIMO-MC radars, in addition to reducing communication bandwidth and power as compared to MIMO radars, offer a significant advantage for spectrum sharing. The advantage stems from the way the sampling scheme at the radar receivers modulates the interference channel from the communication system transmitters, rendering it symbol dependent and reducing its row space. This makes it easier for the communication

system to design its waveforms in an adaptive fashion so that it minimizes the interference to the radar subject to meeting rate and power constraints.

Chapter 7 of this dissertation proposes a design in which a MIMO radar system with matrix completion (MIMO-MC) optimally co-exists with a MIMO wireless communication system in the presence of clutter. To facilitate the co-existence, we employ transmit precoding at the radar and the communication system. First, we show that the error performance of matrix completion is theoretically guaranteed when precoding is employed. Second, the radar transmit precoder, the radar sub-sampling scheme, and the communication transmit covariance matrix are jointly designed to maximize the radar SINR while meeting certain rate and power constraints for the communication system. Efficient optimization algorithms are provided along with insight on the feasibility and properties of the proposed design.

This work has been submitted to /published in

- B. Li and A. P. Petropulu, "Spectrum sharing between matrix completion based MIMO radars and a MIMO communication system," *IEEE International Conference on Acoustics, Speech and Signal Processing (ICASSP)*, Austrilia, 2015, pp. 2444-2448.

- B. Li and A. P. Petropulu, "Radar precoding for spectrum sharing between matrix completion based MIMO radars and a MIMO communication SYSTEM," *IEEE Global Conference on Signal and Information Processing (GlobalSIP)*, Orlando, FL, 2015, pp. 737-741.

- B. Li, A. P. Petropulu and W. Trappe, "Optimum Co-Design for Spectrum Sharing between Matrix Completion Based MIMO Radars and a MIMO Communication System," in *IEEE Transactions on Signal Processing*, vol. 64, no. 17, pp. 4562-4575, Sept.1, 2016.

- B. Li and A. P. Petropulu, "Joint Transmit Designs for Co-existence of MIMO Wireless Communications and Sparse Sensing Radars in Clutter," *IEEE Transactions on Aerospace and Electronics Systems*, submitted in 2016.

1.6 Outline of the Dissertation

The dissertation is organized as follows.

In Chapter 2, we analyze the RIP of the measurement matrix in compressive sensing based collocated MIMO radars. A scheme is proposed that selects the subset of receive antennas with the smallest cardinality that meet the RIP conditions.

In Chapter 3, we confirm that exploiting block sparsity in compressive sensing based distributed MIMO radars results in significant detection performance by analyzing the $\mathcal{A}$-RIP of the block diagonal measurement matrix. Two low-complexity approaches are proposed to reduce the computation while maintaining the estimation performance.

In Chapter 4, a flexible spectrum sharing framework is proposed for the coexistence of MIMO radars and a communication system, for scenarios in which the targets fall in different range bins.

In Chapter 5, we consider the co-design based spectrum sharing of a MIMO radar and a communication system for a scenario in which the radar system operates in the presence of clutter.

Chapter 6 proposes ways via which a MIMO-MC radar and a MIMO communication system, in a cooperative fashion, negotiate spectrum use in order to mitigate mutual interference.

Chapter 7 further proposes a joint transmit design in which a MIMO radar system with matrix completion (MIMO-MC) optimally co-exists with a MIMO wireless communication system in the presence of clutter.

Finally, conclusions and possible future research directions are presented in Chapter 8 .

Chapter 2

RIP Analysis for Compressive Sensing-Based Collocated MIMO Radars

This chapter considers range-angle-Doppler estimation in collocated, compressive sensing-based MIMO (MIMO-CS) radars with arbitrary array configuration. In the literature, the effectiveness of MIMO-CS radars has been studied mostly via simulations. Although there exist some theoretical results for MIMO radars with linear arrays, those cannot be easily extended to arbitrary array configurations. This chapter analyzes the restricted isometry property (RIP) of the measurement matrix. The RIP conditions involve, among other quantities, the number of transmit and receive antennas. A scheme is proposed that selects the subset of receive antennas with the smallest cardinality that meet the RIP conditions.

2.1 Introduction

Recently, compressive sensing (CS) [14] based MIMO radars were shown to achieve the superior resolution of collocated MIMO radars with significantly fewer measurements [22, 24, 25]. If there is a small number of targets in the target space, target estimation can be formulated as a sparse signal recovery problem. The work in [26] provided the first nonuniform recovery guarantee for range-angle-Doppler estimation and the corresponding bounds on the number of transmit/receive antennas and measurements. However, the results only apply to MIMO-CS radars with virtual uniform linear array (ULA) configuration, i.e., M_r-element $\lambda/2$-spaced receive array and M_t-element $M_r\lambda/2$-spaced transmit array. Also, in [26], the angular space has to be discretized on a uniform grid with spacing $\frac{2}{M_t M_r}$. The extension of the results of [26] to general array configurations is nontrivial. Spatial CS for MIMO radars with random transmit/receive array was proposed in [27, 87] for angle estimation. A nonuniform recovery guarantee was provided in [27, 87] based on the isotropy

property of the measurement matrix. The work in [87] also provided a uniform recovery guarantee based on the coherence analysis of the measurement matrix. However, the analysis cannot be extended to the range-angle-Doppler estimation.

In this chapter, we consider the range-angle-Doppler estimation using CS-based collocated MIMO radars with arbitrary array configuration. Our goal is to provide the restricted isometry property (RIP) of the measurement matrix, which can then be readily used to derive uniform recovery guarantees. Towards this goal, we derive a unified upper bound on the entries of the Gram of the measurement matrix. To relate this with the RIP, we adopt the well-known scheme in [88] based on *Geršgorin's Disc Theorem*, which was originally applied for the RIP of Toeplitz matrices. The RIP conditions involve the number and positions of the antennas. Based on this observation, we propose a scheme that selects the subset of receive antennas with the smallest cardinality that meet the RIP conditions.

This chapter is organized as follows: Section 2.2 introduces the sparse model for collocated MIMO radar system. In Section 2.3, we present the RIP analysis of the measurement matrix. Also, we propose an optimization scheme to minimize the required number of receive antennas, which is validated in Section 2.4. Conclusions are presented in Section 2.5.

2.2 Signal Model

Consider the collocated MIMO radar system of [**Yao12**] equipped with transmit and receive arrays with M_t and M_r antennas, respectively. Let us assume that there are K moving targets and that the environment is clutter free. We are interested in target parameters including the time delay from the transmitter to the receiver via the k-th target, i.e., τ_k , the target azimuth angle, θ_k, and Doppler frequency, f_k, for all $k \in \mathbb{N}_K^+$. It holds that $\tau_k = 2d_k/v_c$ and $f_k = 2v_k f_c/v_c$, where d_k, v_k, f_c and v_c denote target range, target radial velocity, carrier frequency and speed of light, respectively. Without loss of generality, we use delay instead of range. To exploit the target space sparsity, the delay-angle-Doppler space is discretized on the grid $\mathcal{T} \times \Theta \times \mathcal{D}$ with $|\mathcal{T}| = N_\tau, |\Theta| = N_\theta$, and $|\mathcal{D}| = N_f$. All grid points are ordered and labeled by the index set $\mathcal{I} \triangleq \{1, \ldots, N_\tau N_\theta N_f\}$. It is assumed that the targets fall on grid points.

The transmit array emits P probing pulses with pulse repetition interval T_{PRI}. Each receiver obtains L T_s-spaced samples from the target returns during each pulse. The fusion center collects the samples from all receivers and stacks them into vector $\mathbf{z} \in \mathbb{C}^{LPM_r}$. From **[Yao12]**, the model obeys

$$\mathbf{z} = \mathbf{\Psi}\mathbf{s} + \mathbf{n}, \tag{2.1}$$

where $\mathbf{n}$ is the interference/noise vector, $\mathbf{s} \in \mathbb{C}^{N_\tau N_\theta N_f}$ denotes a sparse target vector whose K nonzero entries correspond to the complex reflection coefficients of the targets, and $\mathbf{\Psi} \in \mathbb{C}^{(LPM_r)\times(N_\tau N_\theta N_f)}$ is the measurement matrix; its n-th column is associated with the n-th grid point as follows

$$\mathbf{\Psi}_n = \mathbf{v}_r(\theta_n) \otimes \{\mathbf{D}(f_n) \otimes [\mathbf{X}_{\tau_n}\mathbf{v}_t(\theta_n)]\}, \forall n \in \mathcal{I}, \tag{2.2}$$

where $\otimes$ is the Kronecker product, $\mathbf{v}_r(\theta) \in \mathbb{C}^{M_r}$ is the receive steering vector defined as

$$\mathbf{v}_r(\theta) \triangleq \left[e^{j2\pi\langle \mathbf{d}_1^r, \mathbf{w}(\theta)\rangle/\lambda}, \ldots, e^{j2\pi\langle \mathbf{d}_{M_r}^r, \mathbf{w}(\theta)\rangle/\lambda}\right]^T, \tag{2.3}$$

($\mathbf{v}_t(\theta)$ is the transmit steering vector and is respectively defined) with $\mathbf{d}_m^r \triangleq [x_m^r\, y_m^r]^T$ denoting the two-dimensional coordinates of the m-th receive antenna, $\mathbf{w}(\theta) \triangleq [\cos(\theta)\ \sin(\theta)]^T$, and

$$\begin{aligned} \mathbf{D}(f) &\triangleq \left[1, e^{j2\pi f T_{PRI}}, \ldots, e^{j2\pi f T_{PRI}(P-1)}\right]^T, \\ \mathbf{X}_\tau &\triangleq [\mathbf{x}_{1,\tau}, \ldots, \mathbf{x}_{M_t,\tau}], \\ \mathbf{x}_{m,\tau} &\triangleq [x_m[\tau], \ldots, x_m[(L-1)T_s + \tau]]^T,\ m \in \mathbb{N}_{M_t}^+ \end{aligned} \tag{2.4}$$

with λ and $x_m[t]$ denote, respectively, the carrier wavelength and the sample of the m-th transmit waveform at time index t. We assume that transmit waveforms are jointly Gaussian with zero mean and variance $\sigma_0^2 = 1/L$. We assume that the targets are moving slowly, thus the Doppler effect can be approximated as constant during one pulse.

The estimation of the target parameters can be achieved by various sparse recovery algorithms, including the ℓ_1 minimization algorithms, or greedy algorithms. It is well-known that the restricted isometry property (RIP) [14] of the measurement matrix $\mathbf{\Psi}$ plays an important role on guaranteeing the recoverability and estimation performance of $\mathbf{s}$. In order to provide the performance of MIMO-CS radars, it is essential to characterize the RIP of $\mathbf{\Psi}$.

2.3 Main Results

In this section, we analyze the RIP of $\mathbf{\Psi}$. Ahead of the RIP analysis, we provide some observations on the Gram of matrix $\mathbf{\Psi}$. Let us first state one lemma which will be used later.

Lemma 2 (Lemma 5 in [88]). *Let $\mathbf{x} \in \mathbb{C}^N$ and $\mathbf{y} \in \mathbb{C}^N$ be vectors with i.i.d complex Gaussian entries with zero mean and variance σ^2. Then for every $t > 0$ it holds that*

$$Pr\left(\|\mathbf{x}\|_2^2 - \mathbb{E}\{\|\mathbf{x}\|_2^2\} \geq t\right) \leq e^{-\frac{t^2}{16N\sigma^4}}, \tag{2.5a}$$

$$Pr\left(\left|\|\mathbf{x}\|_2^2 - \mathbb{E}\{\|\mathbf{x}\|_2^2\}\right| \geq t\right) \leq 2e^{-\frac{t^2}{16N\sigma^4}}, \tag{2.5b}$$

$$Pr\left(|\langle \mathbf{x}, \mathbf{y}\rangle| \geq t\right) \leq 2e^{-\frac{t^2}{4\sigma^2(N\sigma^2 + t/2)}}. \tag{2.5c}$$

where $\langle \mathbf{x}, \mathbf{y}\rangle \triangleq \mathbf{x}^H\mathbf{y}$, and $(\cdot)^H$ denotes Hermitian transpose.

2.3.1 Observations on The Gram of The Normalized $\mathbf{\Psi}$

Note that $\mathbb{E}\{\|\mathbf{\Psi}_n\|_2^2\} = M_t M_r P$. Since in the compressive sensing literature measurement matrices with normalized columns are typically considered, we will find bounds for the diagonal and off-diagonal entries of $\mathbf{G} \triangleq \frac{\mathbf{\Psi^H\Psi}}{M_t M_r P}$, i.e., $\frac{\langle \mathbf{\Psi}_n, \mathbf{\Psi}_l\rangle}{M_t M_r P}$ for all $n, l \in \mathcal{I}$, where the inner product of two columns of $\mathbf{\Psi}$ is given by

$$\begin{aligned}\langle \mathbf{\Psi}_n, \mathbf{\Psi}_l\rangle =& \langle \mathbf{v}_r(\theta_n), \mathbf{v}_r(\theta_l)\rangle \langle \mathbf{D}(f_n), \mathbf{D}(f_l)\rangle \\ &\times \langle \mathbf{X}_{\tau_n}\mathbf{v}_t(\theta_n), \mathbf{X}_{\tau_l}\mathbf{v}_t(\theta_l)\rangle.\end{aligned} \tag{2.6}$$

When $(\tau_n, \theta_n, f_n) = (\tau_l, \theta_l, f_l)$, the inner product becomes the square of the norm, i.e., $\|\mathbf{\Psi}_n\|_2^2 = M_r P \|\mathbf{X}_{\tau_n}\mathbf{v}_t(\theta_n)\|_2^2$.

For all the entries, the following four cases are considered:

Case (i) $n = l$: In this case, we only need to consider $\|\mathbf{\Psi}_n\|_2^2$ for any $n \in \mathcal{I}$. Denote by $\mathbf{g} \in \mathbb{C}^L$ the product $\mathbf{X}_{\tau_n}\mathbf{v}_t(\theta_n)$. The i-th entry of $\mathbf{g}$ is given by $g_i = \big[x_1[(i-1)T_s + \tau_n], \ldots, x_{M_t}[(i-1)T_s + \tau_n]\big]\mathbf{v}_t(\theta_n)$, which is a weighted sum of M_t i.i.d jointly Gaussian random variables of variance $1/L$. Therefore, the entries of $\mathbf{g}$ are independent identical

distributed according to $\mathcal{CN}(0, M_t/L)$. Based on (2.5b) in Lemma 2, we get

$$\begin{aligned}&\Pr\left(\left|\|\mathbf{\Psi}_n\|_2^2 - \mathbb{E}\{\|\mathbf{\Psi}_n\|_2^2\}\right| \geq M_r P t\right)\\ &= \Pr\left(\left|\|\mathbf{g}\|_2^2 - \mathbb{E}\{\|\mathbf{g}\|_2^2\}\right| \geq t\right) \leq 2e^{-\frac{Lt^2}{16M_t^2}}.\end{aligned} \tag{2.7}$$

Substituting $\mathbb{E}\{\|\mathbf{g}\|_2^2\} = M_t$ and $t \equiv M_t t$ into (2.7), we get

$$\Pr\left(\left|\frac{\|\mathbf{\Psi}_n\|_2^2}{M_t M_r P} - 1\right| \geq t\right) \leq 2e^{-\frac{Lt^2}{16}}. \tag{2.8}$$

Case (ii) $\tau_n \neq \tau_l$: We know that $\mathbf{X}_{\tau_n}\mathbf{v}_t(\theta_n)$ has i.i.d complex Gaussian entries with zero mean and variance M_t/L; the same holds for $\mathbf{X}_{\tau_l}\mathbf{v}_t(\theta_l)$. However, the sum terms in $\langle \mathbf{X}_{\tau_n}\mathbf{v}_t(\theta_n), \mathbf{X}_{\tau_l}\mathbf{v}_t(\theta_l)\rangle$ are no longer mutually independent. Following the splitting trick of [**Li13**, 26, 88], we can split the terms into two equal-sized groups, each of which only contains mutually independent terms. Applying (2.5c) in Lemma 2 to both groups of sums and using Boole's inequality, we obtain

$$\Pr\left(|\langle \mathbf{X}_{\tau_n}\mathbf{v}_t(\theta_n), \mathbf{X}_{\tau_l}\mathbf{v}_t(\theta_l)\rangle| \geq 2t\right) \leq 4e^{-L\frac{t^2}{2M_t^2+2M_t t}}.$$

Combining with (2.6), we get

$$\begin{aligned}&\Pr\left(|\langle \mathbf{\Psi}_n, \mathbf{\Psi}_l\rangle| \geq 2M_r P t\right)\\ &\leq \Pr\left(|\langle \mathbf{\Psi}_n, \mathbf{\Psi}_l\rangle| \geq 2t\phi_{\theta_n,\theta_l}(M_r)\phi_{f_n,f_l}(P)\right)\\ &\leq 4e^{-L\frac{t^2}{2M_t^2+2M_t t}},\end{aligned} \tag{2.9}$$

where

$$\begin{aligned}\phi_{\theta_n,\theta_l}(M_r) &\triangleq |\langle \mathbf{v}_r(\theta_n), \mathbf{v}_r(\theta_l)\rangle| \in [0, M_r],\\ \phi_{f_n,f_l}(P) &\triangleq |\langle \mathbf{D}(f_n), \mathbf{D}(f_l)\rangle| \in [0, P].\end{aligned} \tag{2.10}$$

Substituting t in (2.9) by $M_t t/2$, we get

$$\Pr\left(\left|\frac{\langle \mathbf{\Psi}_n, \mathbf{\Psi}_l\rangle}{M_t M_r P}\right| \geq t\right) \leq 4e^{-L\frac{t^2}{4+4t}}. \tag{2.11}$$

Case(iii) $\tau_n = \tau_l, \theta_n \neq \theta_l$: We need to find the bound on $|\langle \mathbf{X}_{\tau_n}\mathbf{v}_t(\theta_n), \mathbf{X}_{\tau_n}\mathbf{v}_t(\theta_l)\rangle|$. According to [26, Lemma 11], we have

$$\begin{aligned}&\Pr\Bigg(\underbrace{\left|\langle \mathbf{X}_{\tau_n}\mathbf{v}_t(\theta_n), \mathbf{X}_{\tau_n}\mathbf{v}_t(\theta_l)\rangle - \langle \mathbf{v}_t(\theta_n), \mathbf{v}_t(\theta_l)\rangle\right|}_{\triangleq \chi} \geq M_t t\Bigg)\\ &\triangleq \mathcal{P}_\chi \leq 2e^{-L\frac{t^2}{C_1+C_2 t}},\end{aligned} \tag{2.12}$$

where $C_1 \approx 2.50$ and $C_2 \approx 7.69$. It is also clear that

$$\begin{aligned}\mathcal{P}_\chi &= \Pr\Big(\underbrace{M_r P|\chi| + \phi_{\theta_n,\theta_l}(M_r)\phi_{\theta_n,\theta_l}(M_t)P}_{\triangleq A} \geq \zeta\Big) \\ &\geq \Pr\Big(\underbrace{|\langle \mathbf{v}_r(\theta_n), \mathbf{v}_r(\theta_l)\rangle\langle \mathbf{D}(f_n), \mathbf{D}(f_l)\rangle\big(\chi + \langle \mathbf{v}_t(\theta_n), \mathbf{v}_t(\theta_l)\rangle\big)|}_{\triangleq B} \geq \zeta\Big) \\ &= \Pr\left(|\langle \mathbf{\Psi}_n, \mathbf{\Psi}_l\rangle| \geq \zeta\right),\end{aligned} \tag{2.13}$$

where $\zeta \triangleq M_t M_r P t + \phi_{\theta_n,\theta_l}(M_r)\phi_{\theta_n,\theta_l}(M_t)P$ and

$$\phi_{\theta_n,\theta_l}(M_t) \triangleq |\langle \mathbf{v}_t(\theta_n), \mathbf{v}_t(\theta_l)\rangle| \in [0, M_t] \tag{2.14}$$

and the second inequality holds because

$$\begin{aligned}A \geq |\langle \mathbf{v}_r(\theta_n), &\mathbf{v}_r(\theta_l)\rangle\langle \mathbf{D}(f_n), \mathbf{D}(f_l)\rangle| \\ &\times \big(|\chi| + |\langle \mathbf{v}_t(\theta_n), \mathbf{v}_t(\theta_l)\rangle|\big) \geq B.\end{aligned}$$

If $M_r M_t t \geq \phi_{\theta_n,\theta_l}(M_r)\phi_{\theta_n,\theta_l}(M_t)$, it holds that $2M_t M_r P t \geq \zeta$. Now, the bound on the inner product can be written as

$$\Pr\left(|\langle \mathbf{\Psi}_n, \mathbf{\Psi}_l\rangle| \geq 2M_t M_r P t\right) \quad \leq \mathcal{P}_\chi \tag{2.15}$$

or, equivalently, if t is substituted by $t/2$,

$$\Pr\left(\left|\frac{\langle \mathbf{\Psi}_n, \mathbf{\Psi}_l\rangle}{M_t M_r P}\right| \geq t\right) \leq 2e^{-L\frac{t^2}{4C_1 + 2C_2 t}} \tag{2.16}$$

which holds if

$$M_t M_r \geq 2/t\phi_{\theta_n,\theta_l}(M_r)\phi_{\theta_n,\theta_l}(M_t). \tag{2.17}$$

Case(iv) $\tau_n = \tau_l, \theta_n = \theta_l, f_n \neq f_l$: Consider the absolute value

$$\left|\frac{\langle \mathbf{\Psi}_n, \mathbf{\Psi}_l\rangle}{M_t M_r P}\right| = \frac{\phi_{f_n,f_l}(P)}{M_t P}\|\mathbf{X}_{\tau_n}\mathbf{v}_t(\theta_n)\|_2^2, \tag{2.18}$$

where $\phi_{f_n,f_l}(P) \triangleq |\langle \mathbf{D}(f_n), \mathbf{D}(f_l)\rangle|$. It can be viewed as the squared norm of random vector $\tilde{\mathbf{x}} \triangleq \sqrt{\frac{\phi_{f_n,f_l}(P)}{M_t P}}\mathbf{X}_{\tau_n}\mathbf{v}_t(\theta_n)$. The entries in $\tilde{\mathbf{x}}$ are i.i.d zero-mean Gaussian with variance $\sigma_1^2 = \frac{\phi_{f_n,f_l}(P)}{LP}$. Applying the unilateral bound (2.5a) in Lemma 2 gives

$$\begin{aligned}\Pr\left(\left|\frac{\langle \mathbf{\Psi}_n, \mathbf{\Psi}_l\rangle}{M_t M_r P}\right| > t\right) &\leq \exp\left(-\frac{1}{L}\left(\frac{t - L\sigma_1^2}{4\sigma_1^2}\right)^2\right) \\ &= \exp\left(-\frac{L}{16}\left(\frac{Pt}{\phi_{f_n,f_l}(P)} - 1\right)^2\right) \leq \exp\left(-\frac{Lt^2}{10}\right)\end{aligned} \tag{2.19}$$

where the last inequality holds if

$$P \geq \sqrt{2}(1/t + 1)\phi_{f_n,f_l}(P). \tag{2.20}$$

2.3.2 The RIP of The Normalized $\mathbf{\Psi}$

Equipped with the above observations, we are ready to prove the theorem regarding the RIP of the measurement matrix.

Theorem 1. *Let $\tilde{\mathbf{\Psi}}$ be the normalized measurement matrix, i.e., $\tilde{\mathbf{\Psi}} = \mathbf{\Psi}/\sqrt{M_t M_r P}$. Then, for any $\delta_K \in (0,1)$ there exist constant $C_0 \triangleq 3(4C_1 + 2C_2\delta_K)$, such that $\tilde{\mathbf{\Psi}}$ satisfies the RIP of order K with parameter δ_K with probability exceeding $(1 - 4(N_{\tau_n} N_\theta N_f)^{-1})$, whenever*

$$L \geq C_0 \delta_K^{-2} K^2 \log(N_\tau N_\theta N_f), \tag{2.21a}$$

$$M_t M_r \geq 2\delta_K^{-1} K \beta_\Theta(M_t, M_r), \tag{2.21b}$$

$$P \geq \sqrt{2}\left(\delta_K^{-1} K + 1\right) \beta_\mathcal{D}(P), \tag{2.21c}$$

where $\beta_\Theta(M_t, M_r) \triangleq \sup_{\theta_n, \theta_l \in \Theta, n \neq l} \phi_{\theta_n,\theta_l}(M_t)\phi_{\theta_n,\theta_l}(M_r)$ and $\beta_\mathcal{D}(P) \triangleq \sup_{f_n, f_l \in \mathcal{D}, n \neq l} \phi_{f_n,f_l}(P)$.

Proof. The proof of the RIP mainly follows the spirit of the proof in **[Li13]**. We only focuss on the bounds for the off-diagonal entries in the Gram of $\tilde{\mathbf{\Psi}}$. Here we choose $\delta_d \triangleq \delta_K/K$ and $\delta_o \triangleq (K-1)\delta_K/K$. The bound on the off-diagonal entries in Case (ii-iv) can be unified using (2.16) based on the fact that $(4C_1 + 2C_2 t)$ in (2.16) is always larger than $(4 + 4t)$ in (2.11) and 10 in (2.19) for any $t \geq 0$. Substituting t by $\delta_o/(K-1)$, i.e., δ_K/K, gives

$$\Pr\left(\left|\frac{\langle \mathbf{\Psi}_n, \mathbf{\Psi}_l \rangle}{M_t M_r P}\right| \geq \frac{\delta_K}{K}\right) \leq 4e^{-\frac{L\delta_K^2}{K^2(4C_1 + 2C_2\delta_K)}} \tag{2.22}$$

under conditions in (2.21b) and (2.21c), which are derived by substituting $t = \delta_K/K$ into (2.17) and (2.20), respectively. The condition in (2.21a) implies that $\frac{L\delta_K^2}{K^2(4C_1+2C_2\delta_K)} \geq 3\log(N_\tau N_\theta N_f)$. Following the steps of the standard scheme [88] proves the RIP. □

Remark 1. *Theorem 1 characterizes the RIP of normalized $\mathbf{\Psi}$ under the conditions of (2.21) for arbitrary array configuration and grid set $\mathcal{T} \times \Theta \times \mathcal{D}$. The condition in (2.21a) requires that the number of measurements scales quadratically with the number of targets and logarithmically with the number of grid points. The conditions in (2.21b) and (2.21c) involve the number of transmitters/receivers, the number of pulses, the number of the targets, the geometry of the grid and the array configuration. This dependence will be explored in the following subsection for minimizing the number of antennas involved.*

2.3.3 About $\beta_{\mathcal{D}}$ and β_{Θ}

In Theorem 1, the conditions of (2.21) are very general and can be applied on any array configuration and grid. Next, we look closer at the quantities $\beta_{\mathcal{D}}(P)$ and $\beta_{\Theta}(M_t, M_r)$, which appear in (2.21).

The quantity $\beta_{\mathcal{D}}(P)$ is determined by the pulse repetition interval, the Doppler grid $\mathcal{D}$, and the number of pulses. From the definition in (2.10), it holds that

$$\beta_{\mathcal{D}}(P) \triangleq \sup_{\substack{f_n, f_l \in \mathcal{D} \\ n \neq l}} \left| \frac{\sin(\pi P(f_n - f_l)T_{PRI})}{\sin(\pi(f_n - f_l)T_{PRI})} \right|.$$

Consider the special case where $\mathcal{D}$ is uniform with interval $\Delta_f = \frac{1}{PT_{PRI}}$ and cardinality $|\mathcal{D}| \leq P$. In this case, $\beta_{\mathcal{D}}(P) = 0$, which means that (2.21c) holds for any K (i.e., K might be larger than P). In order to increase the resolution of $\mathcal{D}$, we can increase either the number of pulses, or the pulse repetition interval.

The quantity $\beta_{\Theta}(M_t, M_r)$ is determined by the array configuration, the angular grid, Θ, and the number of transmitters /receivers. It is clear that a smaller $\beta_{\Theta}(M_t, M_r)$ is preferable since it requires a smaller $M_t M_r$. Thus, we seek to minimize $\beta_{\Theta}(M_t, M_r)$, or bound it by a small value. For arbitrary transmit/receive array and Θ, it is usually difficult to characterize $\beta_{\Theta}(M_t, M_r)$ analytically. In the MIMO-CS radar literature, some special arrays have been considered. In particular, virtual ULA MIMO radars were considered in [26], where Θ is uniform in the domain $\sin(\theta)$ with $|\Theta| = M_t M_r$ and angular grid interval $\Delta_{\sin(\theta)} = \frac{2}{M_t M_r}$. In this case, $\beta_{\Theta}(M_t, M_r)$ equals 0, which implies that K can be larger than the product $M_t M_r$. However, $M_t M_r$ equals the cardinality of Θ. Random linear array MIMO radars were considered for angle estimation in [87]; in that work, $\frac{\beta_{\Theta}(M_t, M_r)}{M_t M_r}$ is bound from above by a small value. When the locations of transmit /receive nodes can be assumed to be i.i.d random variables, it was shown in [87, Theorem 2] that $M_t M_r \propto K^2 \log^2(N_\theta)$, which is a special case of Theorem 1 for the case of random array for angle estimation.

In the following, we propose a scheme to minimize the number of receive nodes w.r.t. the nodes' positions, under the condition of (2.21b). Given the M_t-element linear transmit array with $y_m^t, \forall m \in \mathbb{N}_{M_t}^+$ and Θ, we would like to solve the following optimization problem:

$$\min_{\mathbf{y}_r} M_r \quad \text{s.t. } \beta_{\Theta}(M_t, M_r) \leq \frac{M_t M_r \delta_K}{2K} \tag{2.23}$$

where $\mathbf{y}_r = [y_1^r, \ldots, y_{M_r}^r]^T$ denotes the position vector for the receive array. Since the $\mathbf{y}_r$ appears in the exponent of the receive steering vector, the optimization problem in (2.23) is nonlinear, non-convex. To bypass the difficulty, we formulate the position optimization problem as a relaxed sensor selection problem. Specifically, given a very dense array of receive nodes at positions $\tilde{\mathbf{y}} \triangleq [\tilde{y}_1, \ldots, \tilde{y}_M]^T$, we assign a Boolean weight $w_m \in \{0, 1\}$ to each sensor and select the minimum number of sensors by solving the following problem:

$$\begin{aligned} &\min_{\mathbf{w}} \mathbf{1}^T\mathbf{w} \triangleq [1, \ldots, 1][w_1, \ldots, w_M]^T \\ &\text{s.t.} \sup_{\substack{\theta_n, \theta_l \in \Theta, \\ n \neq l}} \phi_{\theta_n, \theta_l}(M_t) f(\mathbf{w}) \leq \frac{M_t \delta_K}{2K} \mathbf{1}^T\mathbf{w} \\ &\qquad \mathbf{1}^T\mathbf{w} \geq 4,\ w_m \in \{0, 1\},\ m \in \mathbb{N}_M^+, \end{aligned} \tag{2.24}$$

where $f(\mathbf{w}) \triangleq |\langle \mathbf{w}, e^{j2\pi\tilde{\mathbf{y}}(\sin\theta_n - \sin\theta_l)/\lambda} \rangle|$, and constraint $\mathbf{1}^T\mathbf{w} \geq 4$ is imposed to prevent a naive zero vector solution. To obtain a convex relaxation, we replace the non-convex constraints $w_m \in \{0, 1\}$ by the convex constraints $w_m \in [0, 1]$. Then, the relaxed sensor selection problem turns to be

$$\begin{aligned} &\min_{\mathbf{w}} \mathbf{1}^T\mathbf{w} \\ &\text{s.t.} \sup_{\substack{\theta_n, \theta_l \in \Theta, \\ n \neq l}} \phi_{\theta_n, \theta_l}(M_t) f(\mathbf{w}) \leq \frac{M_t \delta_K}{2K} \mathbf{1}^T\mathbf{w} \\ &\qquad \mathbf{1}^T\mathbf{w} \geq 4, 0 \leq w_m \leq 1, m \in \mathbb{N}_M^+, \end{aligned} \tag{2.25}$$

which is a SOCP problem and can be solved efficiently by standard packages. A suboptimal sensor selection set can be generated from $\mathbf{w}^*$, the optimal solution of (2.25), by taking its first M_r largest entries.

Remark 2. *The proposed optimization scheme in (2.25) selects the minimum number of receive nodes for MIMO-CS radars satisfying condition (2.21b) in Theorem 1. It is similar to optimize w.r.t. the transmit array given fixed receive array. Simulation example in Section 2.4 shows that the MIMO-CS radars generated by the proposed scheme requires much fewer nodes than the ULA array and random array do.*

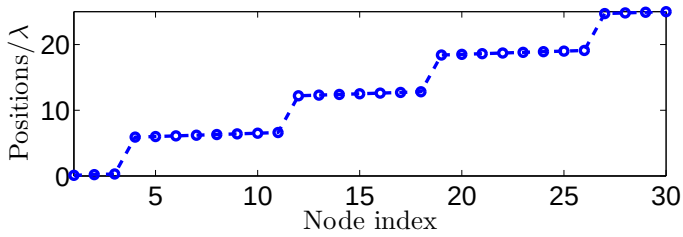

Figure 2.1: Positions of the 30 selected nodes by the proposed scheme.

2.4 A Simulation Example

In this section, we present one example to show the effectiveness of the optimization scheme proposed in Section 2.3.3. We are particularly interested in $K = 3$ targets in the angular region $\sin\theta \in [0, 0.15]$ discretized uniformly with interval $\Delta_{\sin\theta} = 0.001$. The transmit array is a ULA with $M_t = 40$ nodes and interval 25λ. The receive nodes are chosen from 0.1λ-spaced ULA with 250 nodes. The suboptimal receive array obtained from (2.25) is nonuniform with $M_r = 30$ nodes. The positions of the nodes are shown in Fig. 2.1.

For comparison, we know that the virtual array setting in [26] requires a half-wavelength linear receive array with $M_r = 50$ nodes. For random array considered in [87, Theorem 2], $M_t M_r \geq 2121$ is required. It is clear that our method produces MIMO-CS radars with the fewest nodes. We conclude that our proposed optimization scheme relaxes the requirement on $M_t M_r$ in Theorem 1.

2.5 Conclusions

We have provided the RIP analysis for MIMO-CS radars with arbitrary array configuration. The conditions involve the number of antennas, targets, transmited pulses and array geometry. Based on these conditions we have also proposed an antenna selection scheme that minimized the number of receive antennas.

Chapter 3

Distributed MIMO Radar Based on Sparse Sensing: Analysis and Efficient Implementation

In sparse sensing based distributed MIMO radars, the problem of target estimation is formulated as a sparse vector recovery problem, where the vector to be recovered is block sparse, or equivalently, the sensing matrix is block-diagonal and the sparse vector consists of equal-length blocks that have the same sparsity profile. This chapter derives the theoretical requirements and performance guarantees for the application of sparse recovery techniques to this problem. The obtained theoretical results confirm previous, simulations based observations, that exploiting the block sparsity of the target vector can further reduce the amount of measurements needed for successful target estimation. For signal recovery, two low-complexity approaches are proposed. The first one is an ADMM-based sparse signal recovery algorithm, which in addition to significantly reducing computations is also amenable to a parallel and semi-distributed implementation. The second approach decouples the location and speed estimation into two separate stages, with each stage addressing a sparse recovery problem of lower dimension while maintains high estimation accuracy.

3.1 Introduction

Multiple-input multiple-output (MIMO) radars [5–8] have received considerable attention in recent years due to their improved performance over traditional phase arrays. Depending on the placement of antennas, MIMO radars can be classified into collocated [5, 6] and widely separated [7, 8]. Collocated MIMO radars exploit phase differences in target returns induced by transmit and receive antennas, to effectively increase the array aperture and achieve high resolution. Distributed MIMO radars enjoy spatial diversity, introduced by the multiple independents paths between the targets and the transmit/receive antennas, and

thus achieve improved target estimation performance.

By exploiting the sparsity of targets in the radar scene, sparse sensing [13, 15, 16] has been studied in the context of both collocated [24, 26, 27, 29, 87], and distributed MIMO radars [30, 31]. In [30, 31], the problem of target location and speed estimation in distributed MIMO radars is investigated as a block sparse signal recovery problem. The target vector contains the attenuation coefficients for all paths between the grid points and the transmit/receive antenna pairs. If there is no target present at a certain grid point, the corresponding entries in the target vector are zero. Since the number of targets is much smaller than the number of grid points, the target vector is sparse. The block sparsity in the target vector arises by grouping together entries corresponding to paths between a given grid point and all transmit/receive antenna pairs. Block matching pursuit (BMP) is applied in [30] for signal support recovery. Simulations in [30] show that BMP outperforms the basis pursuit method, which ignores the block sparsity. The advantage of block sparsity was also studied in [31], where a group Lasso approach was used to exploit the block sparsity. Again, simulations in [31] show that exploiting block sparsity results in significant detection performance gains over methods which just consider unstructured sparsity. To the best of our knowledge, there are no theoretical works on the performance of sparse sensing based distributed MIMO radars. Although there are theoretical works on sparse sensing based collocated MIMO radars [26, 27, 29, 87], those results cannot be extended to the distributed MIMO radar scenario.

Employing sparse signal recovery techniques in radar systems, on one hand, relieves the volume of data that needs top be collected, but on the other hand, introduces significant computational complexity. In [31] a group Lasso with proximal gradient algorithm (GLasso-PGA) was used, and in [38], a mixed ℓ_1/ℓ_2 norm optimization with interior point method (L-OPT-IPM) was used. GLasso-PGA and L-OPT-IPM achieve better estimation performance than BMP but involve higher computational complexity and require careful tuning of manually chosen parameters. The computation becomes prohibitive as the dimension of the sparse target vector increases. The approach of [31] exploited the block diagonal structure of the sensing matrix to propose a decomposition of the original problem into smaller size problems, thus reducing complexity. However, the scheme of [31] did not exploit all available structural information, such as the identical sparsity profile of the sub-vectors in the target

vector.

The contribution of this chapter is two-fold: (i) it provides performance guarantees for the target location and speed estimation in sparse sensing based distributed MIMO radars, and (ii) it proposes two low-complexity approaches for target estimation. Regarding the performance guarantees, by permuting the columns of the measurement matrix we reformulate the block-sparse signal recovery problem into a problem in which the measurement matrix, $\mathbf{\Psi}$, is block diagonal (BD) and the sparse target vector, $\mathbf{s}$, contains equal-sized blocks that have the same sparsity profile. This reformulation facilitates restricted isometry property (RIP)-based performance analysis. Once the RIP of $\mathbf{\Psi}$ holds w.r.t. sparse signals with the aforementioned structure, the vector $\mathbf{s}$ can be obtained as the solution to a mixed ℓ_2/ℓ_1-optimization program (L-OPT) [18]. Our theoretical results confirm that the BD structure in $\mathbf{\Psi}$ and the sparsity structure in $\mathbf{s}$ reduce the number of measurements needed for target estimation. Further, our RIP-based analysis provides a uniform recovery guarantee, which means that once $\mathbf{\Psi}$ satisfies the RIP, target estimation can be achieved with high probability even in the worst case. In relation to the literature, the proposed RIP analysis is related to that for a Toeplitz matrix, presented in [88], except that our BD measurement matrix contains additional complex exponential factors introduced by the moving targets.

Regarding our low complexity contribution, we first propose a fast algorithm to solve the L-OPT problem based on the alternating direction method of multipliers (ADMM). This ADMM based approach is amenable to parallel implementation, which allows for reduction of running time. A semi-distributed implementation of the solution is also discussed, in which the computations are distributed among all the receive nodes, thus obviating the need of a powerful fusion center. Simulations validate the efficiency of the proposed algorithm and show that the proposed algorithm is robust over a wide range of a manually chosen parameter. Another approach to lower complexity is to reduce the dimension of the L-OPT problem. The joint location-speed space is a Cartesian product of the location space and the speed space, which produces a high dimensional sparse target vector $\mathbf{s}$. A decoupled two-stage model is proposed to lower the problem dimension. In the first stage, we derive the sparse model for the location space by absorbing the unknown target Doppler effect into the sparse target vector. The target locations are estimated via sparse recovery algorithms

with much lower dimension. In the second stage, the location estimates are used to greatly reduce the dimension of the sparse model for speed estimation. The ADMM based approach can also be integrated into both stages of the decoupled estimation framework. It is shown via simulation that the decoupled scheme reduces both the computation and the required number of measurements, while it maintains good performance. A related decoupled scheme was proposed in [25] for compressive sensing based step-frequency MIMO radar with collocated antennas. The matched filtering method was used to provide an initial estimate to reduce the space that needs to be discretized. However, while matched filtering requires large amount of measurements for high resolution and reliable estimation, our decoupled approach, provides a high resolution initial estimate with much fewer measurements.

This chapter is organized as follows. Section 3.2 provides some background and introduces notation. The sparse model for distributed MIMO radar system is presented in Section 3.3. In Section 3.4, we derive the $\mathcal{A}$-RIP of the measurement matrix, which is used to provide the performance of L-OPT in Section 3.5. In Section 3.6, an efficient algorithm based on ADMM is proposed for the target estimation. Parallel and semi-decentralized implementation schemes are discussed in Section 3.6.2. Section 3.7 presents the decoupled location and speed estimation together with discussions on the computation complexity and required number of measurements. Simulation results are given in Section 3.8, and conclusions are presented in Section 3.9.

3.2 Background on Block Sparsity

In the context of compressive sensing, the focus is to exploit the structure in the sparse signal and the measurement matrix for improving the sparse signal recovery [17]. Block sparsity in the sparse signal was investigated in [18–20], where the elements in the sparse signal vector appear in blocks.

Let us consider a block sparse vector $\mathbf{s} \in \mathbb{C}^{MN}$ with at most K nonzero blocks out of N equal-sized blocks, *i.e.*, $M \triangleq |\mathcal{I}_n|, \forall n \in \mathbb{N}_N^+$, where $\mathcal{I}_n$ is the index set for the n-th block. Let us denote by $\mathcal{A}_B^K$ the space in which the block sparse vectors lie.

Given the noisy measurement vector $\mathbf{z} = \mathbf{\Psi}\mathbf{s} + \mathbf{n}$ with $\mathbf{\Psi} \in \mathbb{C}^{L \times NM}$ as the measurement

matrix and $\mathbf{n} \in \mathbb{C}^L$ as the additive noise vector, the recovery of $\mathbf{s} \in \mathcal{A}_B^K$ is achieved via the following convex optimization problem

$$\min_{\mathbf{s}} \sum_{n=1}^{N} \|\mathbf{s}[\mathcal{I}_n]\|_2 \;\; s.t. \; \|\mathbf{z} - \mathbf{\Psi}\mathbf{s}\|_2 \leq \epsilon. \tag{3.1}$$

which is referred to as mixed ℓ_2/ℓ_1-optimization program (L-OPT) [18]. The effectiveness of using L-OPT relies on the restricted isometry property (RIP) of $\mathbf{\Psi}$ w.r.t. vectors in $\mathcal{A}_B^{2K}$.

Definition 3 ([21]). *For a union of certain subspaces denoted by $\mathcal{A}$, $\mathbf{\Psi}$ is said to satisfy the $\mathcal{A}$-restricted isometry property with constant $\delta \in (0,1)$, in short, $\mathcal{A}$-RIP(K,δ), if δ is the smallest value such that*

$$(1-\delta)\|\mathbf{s}\|_2^2 \leq \|\mathbf{\Psi}\mathbf{s}\|_2^2 \leq (1+\delta)\|\mathbf{s}\|_2^2 \tag{3.2}$$

holds for all $\mathbf{s} \in \mathcal{A}$.

The above definition is for general union of subspaces. If $\mathbf{\Psi}$ satisfies the RIP over $\mathcal{A}_B^{2K}$, or equivalently, if $\mathbf{\Psi}$ satisfies the $\mathcal{A}_B$-RIP$(2K, \delta_{2K})$, then the next lemma shows that the solution of (3.1), *i.e.*, $\hat{\mathbf{s}}$, is a good approximation of $\mathbf{s}$.

Lemma 3 (Theorem 2 in [18]). *If $\mathbf{\Psi}$ satisfies the $\mathcal{A}_B$-RIP$(2K, \delta_{2K})$ with $\delta_{2K} < \sqrt{2}-1$, then for the solution of (3.1), $\hat{\mathbf{s}}$, it holds that*

$$\|\hat{\mathbf{s}} - \mathbf{s}\|_2 \leq \frac{4\sqrt{1+\delta_{2K}}}{1-(1+\sqrt{2})\delta_{2K}}\epsilon \triangleq g(\epsilon). \tag{3.3}$$

It is shown in [18] that Gaussian measurement matrices require fewer measurements to satisfy the $\mathcal{A}_B$-RIP$(2K, \delta_{2K})$ as compared to the number of measurements needed to satisfy the RIP$(2K, \delta_{2K})$. Therefore, exploiting block sparsity in $\mathbf{s}$ reduces the required number of measurements for sparse recovery. In the following, we put the sparse sensing-based MIMO radar problems into the framework of block-sparse signal recovery, and derive the $\mathcal{A}_B$-RIP of the corresponding measurement matrix.

3.3 Distributed MIMO-CS Radar Signal Model

We consider a MIMO radar system with M_t transmit nodes (TX) and M_r receive nodes (RX), which are widely separated. Let (x_i^t, y_i^t) and (x_i^r, y_i^r) denote the locations of the i-th

transmit and receive antenna in cartesian coordinates, respectively. The i-th TX antenna transmits repeated pulses with pulse repetition interval T. Each pulse contains the modulated waveform $w_i(t)e^{j2\pi f_i t}$, where f_i is the carrier frequency, and $w_i(t)$ is the continuous-time baseband waveform. We assume that transmit waveforms are jointly Gaussian with zero mean and variance σ_0^2. Let us assume that there are K moving targets present. For simplicity, we consider a clutter-free environment [24–27, 29–31, 87]. In practice, preprocessing techniques can be employed to suppress the clutter. For example, if the covariance matrix of the clutter is known, beamforming can be used to suppress the clutter [89]. Also, if the clutter is static while the target is moving, Doppler filters [2] and the technique of change detection can be used to remove the clutter [90, 91].

The location-speed space is discretized on grid $\mathbf{\Theta} \triangleq \mathbf{\Theta}_{loc} \times \mathbf{\Theta}_{spd}$, where the location grid is $\mathbf{\Theta}_{loc} \triangleq \{(x_n, y_n), n = 1, \ldots, N_1\}$, $N_1 \triangleq N_x \times N_y$, and the speed grid is $\mathbf{\Theta}_{spd} \triangleq \{(v_x^n, v_y^n), n = 1, \ldots, N_2\}$, $N_2 \triangleq N_{vx} \times N_{vy}$. Denoting the cardinality of $\mathbf{\Theta}$ as N, it holds that $N = N_1 \times N_2$. It is assumed that the targets fall on grid points. Let us denote by Ξ the set of all different transmit and receive antenna pairs. It is clear that $|\Xi| = M_t M_r$. In the sequel, the subscript $(ij) \in \Xi$ with $i \in \mathbb{N}_{M_t}^+$ and $j \in \mathbb{N}_{M_r}^+$ denotes the pair of the i-th transmit antenna and the j-th receive antenna. Suppose that the j-th receive antenna obtains L T_s-spaced samples from each pulse transmitted by antenna i. On stacking the samples from P pulses into vector $\mathbf{z}_{ij}$ it holds that [31]

$$\mathbf{z}_{ij} = \mathbf{\Psi}_{ij}\mathbf{s}_{ij} + \mathbf{n}_{ij}, \forall (ij) \in \Xi, \tag{3.4}$$

where $\mathbf{s}_{ij} = \left[s_{ij}^1, \ldots, s_{ij}^N\right]^T$, with s_{ij}^n being non-zero only if there is a target at the n-th grid point (here n refers to a particular ordering of grid points of the 4-dimensional space into a vector of length N); $\mathbf{n}_{ij}$ denotes the additive noise; $\mathbf{\Psi}_{ij}$ is defined in term of its columns, $\mathbf{\Psi}_{ij}^n$, *i.e.*,

$$\mathbf{\Psi}_{ij}^n = \mathbf{D}(f_{ij}^n) \otimes \mathbf{w}_{i,\tau_{ij}^n}, \forall n \in \mathbb{N}_N^+, \tag{3.5}$$

where $\otimes$ denotes Kronecker product,

$$\mathbf{D}(f_{ij}^n) \triangleq \left[1, e^{j2\pi f_{ij}^n T}, \ldots, e^{j2\pi f_{ij}^n T(P-1)}\right]^T, \tag{3.6a}$$

$$\mathbf{w}_{i,\tau_{ij}^n} \triangleq \left[w_i[\tau_{ij}^n], \ldots, w_i[(L-1)T_s + \tau_{ij}^n]\right]^T \tag{3.6b}$$

with $w_i[\tau_{ij}^n]$ denoting the sample of the i-th transmit waveform at time index τ_{ij}^n. τ_{ij}^n and f_{ij}^n respectively denote the propagation time and Doppler frequency associated with the n-th grid and the (ij)-th TX/RX antenna pair. It holds that

$$f_{ij}^n = \frac{\langle (v_x^n, v_y^n), \mathbf{d}_{in}^t \rangle}{\lambda_i \|\mathbf{d}_{in}^t\|_2} + \frac{\left\langle (v_x^n, v_y^n), \mathbf{d}_{jn}^r \right\rangle}{\lambda_i \|\mathbf{d}_{jn}^r\|_2}, \tag{3.7}$$

where $\mathbf{d}_{in}^{t/r} \triangleq ((x_i^{t/r}, y_i^{t/r}) - (x_n, y_n))$ denotes the vector from the n-th grid to the i-th TX/RX antenna, and λ_i is the carrier wavelength of the i-th transmitter. In the model based on (3.5), we assume that the targets are moving relatively slowly so that the Doppler effect can be approximated as constant during one pulse, *i.e.*, $f_{ij}^n LT_s \ll 1$. In the literature, it is common to make such an assumption for pulse Doppler processing [2, 22, 24, 30]. Actually, we can show that our model works for wide range of target moving speeds by using different system parameters. Substituting the expression of f_{ij}^n in (3.7) into $f_{ij}^n LT_s \ll 1$ gives

$$\frac{\langle (v_x^n, v_y^n), \mathbf{d}_{in}^t \rangle}{\|\mathbf{d}_{in}^t\|_2} + \frac{\left\langle (v_x^n, v_y^n), \mathbf{d}_{jn}^r \right\rangle}{\|\mathbf{d}_{jn}^r\|_2} \ll \frac{c}{LT_s f_i},$$

Via the Cauchy-Schwarz inequality, we have $\|\mathbf{v}^n\|_2 \triangleq \sqrt{(v_x^n)^2 + (v_y^n)^2} \ll \frac{c}{2LT_s f_i}$ for all $n \in \mathbb{N}_N^+$. For carrier frequency $f_i = 5GHz$, waveform bandwidth $10MHz$, sampling frequency $f_s = 1/T_s = 20MHz$ and $L = 20$, the model based on (3.5) is valid for target speed much smaller than $3 \times 10^4 m/s$, which could cover speeds as high as transonic. By increasing the waveform bandwidth and the sampling frequency, the model would be valid even for supersonically moving targets. In Section 3.8, we choose waveform bandwidth $25MHz$ and sampling frequency $f_s = 50MHz$, thus the model would be valid if the target speed is much smaller than $7.5 \times 10^4 m/s$.

The fusion center collects the sample vectors from all TX/RX antenna pairs and stack them into a column vector $\mathbf{z}$ of length LPM_tM_r, *i.e.*,

$$\mathbf{z} = \left[(\mathbf{z}_{11})^T, \ldots, (\mathbf{z}_{M_tM_r})^T\right]^T = \mathbf{\Psi}\mathbf{s} + \mathbf{n}, \tag{3.8}$$

where $\mathbf{s} = \left[(\mathbf{s}_{11})^T, \ldots, (\mathbf{s}_{M_tM_r})^T\right]^T$, $\mathbf{n} = [(\mathbf{n}_{11})^T, \ldots, (\mathbf{n}_{M_tM_r})^T]^T$, and $\mathbf{\Psi} = \mathrm{diag}\big(\mathbf{\Psi}_{11}, \ldots, \mathbf{\Psi}_{M_tM_r}\big)$.

Note that each vector $\mathbf{s}_{ij}$ contains zero entries except the entries corresponding to grid points occupied by targets. Thus, the vector $\mathbf{s}$ is a concatenation of M_tM_r sub-vectors that

share the same sparsity profile, and have exactly K nonzero entries each. We can see that $\mathbf{s}$ lies in $\mathcal{A}_0^K \subset \mathbb{C}^{NM_tM_r}$, defined as

$$\begin{aligned}\mathcal{A}_0^K \triangleq \big\{\mathbf{y} \in \mathbb{C}^{NM_tM_r} \big|\, \mathbf{y} = [\mathbf{y}_1^T, \ldots, \mathbf{y}_{M_tM_r}^T]^T,\\ \mathbf{y}_j \in \mathbb{C}^N, \mathrm{supp}(\mathbf{y}_i) = \mathrm{supp}(\mathbf{y}_j),\\ |\mathrm{supp}(\mathbf{y}_j)| \leq K,\, \forall i,j \in \mathbb{N}^+_{M_tM_r}\big\},\end{aligned} \tag{3.9}$$

where $\mathbf{y}_j$'s are uniformly partitioned blocks of $\mathbf{y}$, $\mathrm{supp}(\cdot)$ denotes the index set of nonzero entries of a vector, *i.e.*, the support of a vector, and $|\cdot|$ denotes the cardinality of a set.

In the following section we provide the $\mathcal{A}$-RIP analysis of the BD measurement matrix $\mathbf{\Psi}$.

3.4 The $\mathcal{A}$-RIP of The Measurement Matrix

Let us first state two lemmas which will be used later.

Lemma 4. *Let $\mathbf{x} \in \mathbb{C}^N$ and $\mathbf{y} \in \mathbb{C}^N$ be vectors with i.i.d complex Gaussian entries with zero mean and variance σ^2. Then for every $0 < t < 4\sigma^2 N$, it holds that*

$$Pr\left(\|\mathbf{x}\|_2^2 - \mathbb{E}\{\|\mathbf{x}\|_2^2\} \geq t\right) \leq e^{-\frac{t^2}{16N\sigma^4}}, \tag{3.10a}$$

$$Pr\left(\big|\|\mathbf{x}\|_2^2 - \mathbb{E}\{\|\mathbf{x}\|_2^2\}\big| \geq t\right) \leq 2e^{-\frac{t^2}{16N\sigma^4}}. \tag{3.10b}$$

For every $t > 0$ it holds that

$$Pr\left(|\langle \mathbf{x}, \mathbf{y}\rangle| \geq t\right) \leq 2e^{-\frac{t^2}{4\sigma^2(N\sigma^2 + t/2)}}. \tag{3.11}$$

where $\langle \mathbf{x}, \mathbf{y}\rangle \triangleq \mathbf{x}^H\mathbf{y}$, and $(\cdot)^H$ denotes Hermitian transpose.

Proof. Lemma 4 is derived based on Lemma 5 and 6 in [88]. By substituting k and t in [88, Lemma 5] respectively by N and τ, we have $\Pr\left(\|\mathbf{x}\|_2^2 - \mathbb{E}\{\|\mathbf{x}\|_2^2\} \geq 2\sigma^2\sqrt{N\tau} + 2\sigma^2\tau\right) \leq e^{-\tau}$. If $\tau < N$, then it holds that $4\sigma^2\sqrt{N\tau} \geq 2\sigma^2\sqrt{N\tau} + 2\sigma^2\tau$. We have

$$\begin{aligned}&\Pr\left(\|\mathbf{x}\|_2^2 - \mathbb{E}\{\|\mathbf{x}\|_2^2\} \geq 4\sigma^2\sqrt{N\tau}\right)\\ \leq &\Pr\left(\|\mathbf{x}\|_2^2 - \mathbb{E}\{\|\mathbf{x}\|_2^2\} \geq 2\sigma^2\sqrt{N\tau} + 2\sigma^2\tau\right) \leq e^{-\tau}.\end{aligned}$$

Inequality (3.10a) is readily proved by denoting $t \triangleq 4\sigma^2\sqrt{N\tau} < 4\sigma^2 N$. Similarly, we can prove inequality (3.10b). Lastly, it is clear to see that (3.11) holds by directly substituting k in [88, Lemma 6] by N. □

Lemma 5. *Let $\{x_i\}$ and $\{y_i\}$, $i = 1, \ldots, Q$ be sequences of identically distributed, zero-mean, Gaussian variables with variance σ^2. All variables are independent except that the last I ($I \in [1, Q)$) variables of $\{x_i\}$ are the first I variables of $\{y_i\}$, i.e., $x_{i+Q-I} = y_i$ for any $i \in [1, I]$. Then*

$$Pr\left(\left|\sum_{i=1}^{Q} x_i y_i\right| \geq t\right) \leq 4\exp\left(-\frac{(Q-1)t^2}{8Q\sigma^2(Q\sigma^2 + t/2)}\right).$$

We know that $\{x_i y_i\}_{i=1}^{Q}$ are not mutually independent. Lemma 5 can be proven by a splitting trick, as in [88].

3.4.1 Observations on The Gram of The Normalized $\mathbf{\Psi}$

Note that $\mathbb{E}\{\|\mathbf{\Psi}_{ij}^n\|_2^2\} = LP\sigma_0^2$. Since in the compressive sensing literature measurement matrices with normalized columns are typically considered, we will provide observations on the normalized measurement matrix $\bar{\mathbf{\Psi}} = \mathbf{\Psi}/\sqrt{LP\sigma_0^2}$. The Gram of $\bar{\mathbf{\Psi}}$, denoted here by $\mathbf{G}$, is also block-diagonal, *i.e.*, $\mathbf{G} = \text{diag}(\mathbf{G}_{11}, \ldots, \mathbf{G}_{M_t M_r})$ where $\mathbf{G}_{ij} = \bar{\mathbf{\Psi}}_{ij}^H \bar{\mathbf{\Psi}}_{ij}$ and $\bar{\mathbf{\Psi}}_{ij} \triangleq \mathbf{\Psi}_{ij}/\sqrt{LP\sigma_0^2}$.

Consider the (n, l)-th entry in $\mathbf{G}_{ij}$. It holds that

$$\begin{aligned} \mathbf{G}_{ij}(n,l) &\equiv \frac{1}{LP\sigma_0^2}\langle \mathbf{\Psi}_{ij}^n, \mathbf{\Psi}_{ij}^l \rangle \\ &= \frac{1}{LP\sigma_0^2}\langle \mathbf{D}(f_{ij}^n), \mathbf{D}(f_{ij}^l)\rangle \langle \mathbf{w}_{i,\tau_{ij}^n}, \mathbf{w}_{i,\tau_{ij}^l}\rangle. \end{aligned} \tag{3.12}$$

The following three cases are analyzed:

Case (i) For $n = l$, *i.e.*, the diagonal entries, it holds that $\langle \mathbf{D}(f_{ij}^n), \mathbf{D}(f_{ij}^n)\rangle = P$. Now, $G_{ij}(n,n) = \frac{1}{L\sigma_0^2}\mathbf{w}_{i,\tau_{ij}^n}^T \mathbf{w}_{i,\tau_{ij}^n}$, which is the sum of squares of i.i.d Gaussian variables with $\mathbb{E}\{G_{ij}(n,n)\} = 1$. Applying (3.10b) in Lemma 4, it holds that

$$\Pr(|G_{ij}(n,n) - 1| > t) \leq 2\exp\big(-\frac{Lt^2}{16}\big). \tag{3.13}$$

Case(ii) the n-th and l-th grid points have different propagation delay, *i.e.*, $\tau_{ij}^n \neq \tau_{ij}^l$. From (3.12), it holds that $\mathbb{E}\{G_{ij}(n,l)\} = 0$ and

$$|G_{ij}(n,l)| = \frac{1}{LP\sigma_0^2}\left|\mathbf{w}_{i,\tau_{ij}^n}^T \mathbf{w}_{i,\tau_{ij}^l}\right| \phi_{f_{ij}^n, f_{ij}^l}(P), \tag{3.14}$$

where

$$\phi_{f_{ij}^n, f_{ij}^l}(P) \triangleq |\langle \mathbf{D}(f_{ij}^n), \mathbf{D}(f_{ij}^l)\rangle| \in [0, P]. \tag{3.15}$$

A probabilistic bound on $|G_{ij}(n,l)|$ can be found as

$$\Pr\big(|G_{ij}(n,l)|>t\big)\leq \Pr\bigg(\frac{1}{L\sigma_0^2}\Big|\mathbf{w}_{i,\tau_{ij}^n}^T\mathbf{w}_{i,\tau_{ij}^l}\Big|>t\bigg). \tag{3.16}$$

Now, we only need to provide the bound on the inner product of $\mathbf{w}_{i,\tau_{ij}^n}$ and $\mathbf{w}_{i,\tau_{ij}^l}$. Note that $\mathbf{w}_{i,\tau_{ij}^n}$ and $\mathbf{w}_{i,\tau_{ij}^l}$ are both sampled from the i-th waveform, and may share some common entries. The general bound (3.11) in Lemma 4 referring to two distinct i.i.d random vectors cannot be applied directly. Applying Lemma 5 for (3.16) gives

$$\Pr\big(|G_{ij}(n,l)|>t\big)\leq 4\exp\bigg(-\frac{(L-1)t^2}{8(1+t/2)}\bigg). \tag{3.17}$$

Case(iii) the n-th and l-th grid points introduce the same propagation delay ($\tau_{ij}^n=\tau_{ij}^l$) but have different Doppler frequencies ($f_{ij}^n\neq f_{ij}^l$). Consider the absolute value

$$|G_{ij}(n,l)|=\frac{1}{LP\sigma_0^2}\mathbf{w}_{i,\tau_{ij}^n}^T\mathbf{w}_{i,\tau_{ij}^n}\phi_{f_{ij}^n,f_{ij}^l}(P), \tag{3.18}$$

which can be viewed as the squared norm of random vector $\sqrt{\frac{1}{LP\sigma_0^2}\phi_{f_{ij}^n,f_{ij}^l}(P)}\mathbf{w}_{i,\tau_{ij}^n}$ with i.i.d zero-mean Gaussian entries with variance $\sigma_1^2=\frac{1}{LP}\phi_{f_{ij}^n,f_{ij}^l}(P)$. Applying the unilateral bound (3.10a) in Lemma 4 , we have

$$\begin{aligned}\Pr\left(|G_{ij}(n,l)|>t\right)&\leq\exp\left(-\frac{1}{L}\left(\frac{t-L\sigma_1^2}{4\sigma_1^2}\right)^2\right)\\&=\exp\left(-\frac{L}{16}\left(\frac{Pt}{\phi_{f_{ij}^n,f_{ij}^l}(P)}-1\right)^2\right)\leq\exp\left(-\frac{Lt^2}{16}\right),\end{aligned} \tag{3.19}$$

where the last inequality holds if

$$P\geq(1/t+1)\phi_{f_{ij}^n,f_{ij}^l}(P). \tag{3.20}$$

3.4.2 $\mathcal{A}$-RIP of The Normalized Measurement Matrix

Equipped with the above observations, we will first establish the RIP of $\bar{\mathbf{\Psi}}$ w.r.t. sparse vectors in $\mathcal{A}_1^K\subset\mathbb{C}^{NM_tM_r}$, which is defined as

$$\begin{aligned}\mathcal{A}_1^K\triangleq\big\{\mathbf{y}\in\mathbb{C}^{NM_tM_r}\big|\,\mathbf{y}=[\mathbf{y}_1^T,\ldots,\mathbf{y}_{M_tM_r}^T]^T,\mathbf{y}_j\in\mathbb{C}^N,\\|\mathrm{supp}(\mathbf{y}_i)|=|\mathrm{supp}(\mathbf{y}_j)|\leq K,\,\forall i,j\in\mathbb{N}_{M_tM_r}^+\big\}\end{aligned}$$

where $\mathbf{y}_j$'s are uniformly partitioned blocks of $\mathbf{y}$. It holds that $\mathcal{A}_0^K\subset\mathcal{A}_1^K$.

Theorem 2. *For any $\delta_K \in (0,1)$, $\bar{\mathbf{\Psi}}$ satisfies $\mathcal{A}_1$-RIP(K, δ_K) with probability exceeding $(1 - 4(N\sqrt{M_t M_r})^{-1})$ whenever*

$$L \geq 48\delta_K^{-1} K^2 \log(N\sqrt{M_t M_r}) + 1, \tag{3.21a}$$

$$P \geq (\delta_K^{-1} K + 1)\beta(P), \tag{3.21b}$$

where

$$\beta(P) \triangleq \sup_{(ij)\in\Xi} \phi_{ij}(P) \triangleq \sup_{\substack{f_{ij}^n \neq f_{ij}^l, \\ (ij)\in\Xi}} \phi_{f_{ij}^n, f_{ij}^l}(P). \tag{3.22}$$

Proof. See Appendix 3.A □

Note that the technique used to prove Theorem 1 can only exploit the structure characterized by $\mathcal{A}_1^K$, and not the additional structure characterized by $\mathcal{A}_0^K$. Vectors in $\mathcal{A}_0^K$ consist of sub-vectors that have the same support. However, only the support cardinality of the sub-vectors matters in the proof of $\mathcal{A}$-RIP presented in Appendix 3.A. The positions of the nonzero entries would introduce no difference to the bound for the off-diagonal entries in (3.44). In the next section, the $\mathcal{A}_1$-RIP of $\bar{\mathbf{\Psi}}$ in Theorem 2 will be relaxed to the $\mathcal{A}_0$-RIP, which is further used to guarantee the effectiveness of applying L-OPT.

Remark 3. *In the proof of Theorem 2, the sparsity structures in $\bar{\mathbf{\Psi}}$ and $\mathbf{s}$ is exploited to reduce the required number of measurements. To emphasize the advantage of the block-sparse structure in our scenario, we compare to a scenario in which the block-structure is ignored, and the recovery is based on a full Toeplitz matrix of size $LM_tM_r \times NM_tM_r$ and a sparse vector with KM_tM_r nonzero entries at arbitrary locations. From [88], a full Toeplitz matrix satisfies the RIP if L is of the order of $\mathcal{O}(K^2 M_t M_r \log(N\sqrt{M_t M_r}))$, which is M_tM_r times larger than the bound in (3.21a). Comparing that to (3.21a) suggests that exploiting the block sparsity reduces the number of samples needed. This validates previous simulation-based observations [31] and results in Section 3.8.2 of this chapter, suggesting that exploiting the structure in both $\mathbf{\Psi}$ and $\mathbf{s}$ allows for reduction of the number of samples, L, needed for target estimation.*

Remark 4. *From (3.21b), we know that the number of required pulses is determined by $\beta(P)$, which is the maximum of $\phi_{f_{ij}^n, f_{ij}^l}(P)$ over the Doppler grid set for all TX/RX pairs.*

From the definitions in (3.6a) and (3.15), it holds that

$$\beta(P) \triangleq \sup_{\substack{f_{ij}^n \neq f_{ij}^l, \\ (ij)\in\Xi}} \left| \frac{\sin\left(\pi P(f_{ij}^n - f_{ij}^l)T\right)}{\sin\left(\pi(f_{ij}^n - f_{ij}^l)T\right)} \right|.$$

The quantity $\beta(P)$ is determined by the pulse repetition interval T, the number of pulses, P, and the Doppler grid set. From the definition in (3.7), the Doppler grid set further depends on the speed grid set $\mathbf{\Theta}_2$, the antennas position and even the target location grid set $\mathbf{\Theta}_1$. Therefore, it is rather difficult to analytically characterize $\beta(P)$. Generally speaking, in order to increase the speed resolution, we can increase either the number of pulses, or the pulse repetition interval. For a given MIMO radar configuration and target space discretization, we can use numerical methods to find the minimum P that satisfies (3.21b). In Section 3.8.1, we present an example to show how P is chosen.

3.5 Performance of Distributed MIMO Radars Using Sparse Sensing

To apply the L-OPT for the sparse model in (3.8), we permute the columns of $\mathbf{\Psi}$ and correspondingly permute the entries of $\mathbf{s}$ to generate block sparsity in the target vector. Then, $\mathbf{s}$ is recovered by solving the problem

$$\min \sum_{n=1}^{N} \|\mathbf{s}[\mathcal{I}_n]\|_2 \;\; s.t. \; \|\mathbf{z} - \mathcal{P}_M(\mathbf{\Psi})\mathcal{P}_v(\mathbf{s})\|_2 \leq \epsilon_0. \tag{3.23}$$

where $\mathcal{P}_M$ is the column permutation matrix applied on $\mathbf{\Psi}$ and $\mathcal{P}_v : \mathcal{A}_0^K \rightarrow \mathcal{A}_B^K$ is the corresponding permutation operator applied on $\mathbf{s}$; $\mathcal{I}_n$, $\forall n \in \mathbb{N}_N^+$, is the set with cardinality $M_t M_r$ containing the indices of the n-th entries from all sub-vectors $\mathbf{s}_{ij}$; ϵ_0 is a manually chosen parameter related to the norm of vector $\mathbf{n}$. In the above, $\mathcal{P}_v(\mathbf{s}) = [\mathbf{s}[\mathcal{I}_1], \ldots, \mathbf{s}[\mathcal{I}_N]]^T$ is block sparse.

The reconstructed target location-speed scene $\hat{\mathbf{s}}$ contains location and speed and target complex Radar Cross Section (RCS) information on all K targets. Let us use as performance metric the error $\|\hat{\mathbf{s}} - \mathbf{s}\|_2$. As shown in Lemma 3, the effectiveness of (3.23) is guaranteed if $\mathcal{P}_M(\mathbf{\Psi})$ satisfies the $\mathcal{A}_B$-RIP$(2K, \delta_{2K})$. Combining with the $\mathcal{A}$-RIP analysis of Section 3.4, the following proposition provides an error bound when applying L-OPT for the recovery of $\mathbf{s}$, along with the requirements on the number of measurements and pulses.

Proposition 1. *Consider the signal model in (3.8). For any $\delta_{2K} < \sqrt{2}-1$, if L and P satisfy that*

$$L \geq 192\delta_{2K}^{-1}K^2\log(N\sqrt{M_tM_r})+1, \tag{3.24a}$$

$$P \geq (2\delta_{2K}^{-1}K+1)\beta(P), \tag{3.24b}$$

then for any $\mathbf{s}\in\mathcal{A}_0^K$, the error in the solution of the L-OPT problem of (3.23) is bounded as

$$\|\hat{\mathbf{s}}-\mathbf{s}\|_2 \leq g\left(\frac{\epsilon_0}{\sqrt{LP\sigma_0^2}}\right) \tag{3.25}$$

with probability exceeding $(1-4(N\sqrt{M_tM_r})^{-1})$.

Proof. According to Theorem 2, $\bar{\mathbf{\Psi}}$ satisfies the $\mathcal{A}_1$-RIP$(2K,\delta_{2K})$ with probability exceeding $(1-4(N\sqrt{M_tM_r})^{-1})$ under conditions:

$$L \geq 48\delta_{2K}^{-1}(2K)^2\log(N\sqrt{M_tM_r})+1,$$
$$P \geq (\delta_{2K}^{-1}(2K)+1)\beta(P),$$

which are obtained by substituting K and δ_K in (3.21) respectively by $2K$ and δ_{2K}. As we can see, the above two conditions are equivalent to those in (3.24). Since $\mathcal{A}_0^{2K}\subset\mathcal{A}_1^{2K}$, we know that $\bar{\mathbf{\Psi}}$ also satisfies the $\mathcal{A}_0$-RIP$(2K,\delta_{2K}^0)$ with $\delta_{2K}^0\leq\delta_{2K}$. In [92, Proposition 1], we have shown that the $\mathcal{A}_B$-RIP of $\mathcal{P}_M(\bar{\mathbf{\Psi}})$ is equivalent to the $\mathcal{A}_0$-RIP of $\bar{\mathbf{\Psi}}$. Applying Lemma 3 to (3.23) for the normalized measurement matrix $\bar{\mathbf{\Psi}}$ proves the claims of the proposition. □

Remark 5. *The significance of Proposition 1 is that it guarantees theoretically that sparse modeling and block sparse recovery algorithms can be effectively applied to distributed MIMO radars. If there is no additive noise, i.e., $\epsilon_0=0$, based on (3.25), $\mathbf{s}$ can be recovered exactly. When noise is present, the performance is stable in the sense that the estimation error is bounded for any $\mathbf{s}\in\mathcal{A}_0^K$. In the proof of Proposition 1, the $\mathcal{A}_B$-RIP of $\mathcal{P}_M(\bar{\mathbf{\Psi}})$ is established via its equivalence to the $\mathcal{A}_0$-RIP of $\bar{\mathbf{\Psi}}$. The direct block-RIP analysis for $\mathcal{P}_M(\bar{\mathbf{\Psi}})$ is difficult, because $\mathcal{P}_M(\bar{\mathbf{\Psi}})$ has a complicated structure. Also, the $\mathcal{A}_0$-RIP of $\bar{\mathbf{\Psi}}$ is established indirectly via the $\mathcal{A}_1$-RIP analysis of $\bar{\mathbf{\Psi}}$. Since $\mathcal{A}_0^{2K}$ is only a small subset of $\mathcal{A}_1^{2K}$, the $\mathcal{A}_0$-RIP of $\bar{\mathbf{\Psi}}$ may be satisfied with much weaker conditions on L and P which are required by the $\mathcal{A}_1$-RIP*

of $\bar{\mathbf{\Psi}}$. That is to say that the L-OPT in (3.23) may perform well with smaller L and P than those in (3.24).

Remark 6. *In the compressive sensing literature, there are two kinds of sparse recovery guarantees: the uniform and non-uniform [93]. A uniform guarantee means that once $\mathbf{\Psi}$ satisfies the $\mathcal{A}_0$-RIP, target estimation can be achieved with high probability for any $\mathbf{s} \in \mathcal{A}_0^K$. A uniform recovery guarantee attracts a lot of research interest in the compressive sensing literature [15, 18, 21, 88, 93] and applications in collocated MIMO radars [29, 87]. Proposition 1 provides bounds on L and P for the uniform recovery guarantee including the worst case. On the other hand, the simulation gives the average performance for given L and P. This explains why much smaller L and P perform well in the simulation in Section 3.8. As one can see both in Theorem 1 and Preposition 1, the bound on L scales quadratically with the sparsity level K. The quadratically scaled bound is the proved tightest bound for many structured measurement matrices [29, 87, 88, 93]. To the best of our knowledge, Theorem 1 is the first result on the $\mathcal{A}$-RIP of the measurement matrix $\mathbf{\Psi}$ with block diagonal structure in sparse sensing based distributed MIMO radars, modeled via (8). Although there might be the possibility to break the quadratic bottleneck on L, that would call for complete different techniques and it is out of the scope of this chapter.*

Remark 7. *The L-OPT problem is convex and can be solved directly using the interior point method with complexity of $\mathcal{O}((NM_rM_t)^3)$. This means that the computational cost may be prohibitive if the dimension- NM_tM_r is large. In the following two sections, we tackle the computation issue in two ways, namely, we propose an ADMM-based algorithm with lower complexity (see Section 3.6), and we propose decoupling the location and speed estimation, which effectively lowers the dimensionality of the problem (see Section 3.7).*

3.6 Fast Signal Recovery based on ADMM

In this section, we present an ADMM-based approach for solving the L-OPT problem for the general case of moving targets. Preliminary results of our work, for the case of stationary targets can be found in [94].

Note that $\mathbf{z}, \mathbf{\Psi}, \mathbf{s}$ and $\mathbf{n}$ are all complex. The majority of ADMM literature deals with

real variables. However, we can easily reformulate our problem with real variables as follows.

$$\underbrace{(\mathbf{z}\otimes\mathcal{F}_v)}_{\triangleq\tilde{\mathbf{z}}}=\underbrace{(\mathbf{\Psi}\otimes\mathcal{F}_M)}_{\triangleq\tilde{\mathbf{\Psi}}}\underbrace{(\mathbf{s}\otimes\mathcal{F}_v)}_{\triangleq\tilde{\mathbf{s}}}+\underbrace{(\mathbf{n}\otimes\mathcal{F}_v)}_{\triangleq\tilde{\mathbf{n}}}, \tag{3.26}$$

where the operators $\mathcal{F}_v$ and $\mathcal{F}_M$ are defined in terms of the real and imaginary parts of $z\in\mathbb{C}$, *i.e.*, respectively, $\Re\{z\}$ and $\Im\{z\}$, as follows.

$$\mathcal{F}_v(z)\triangleq[\Re\{z\},\Im\{z\}]^T,\ \mathcal{F}_M(z)\triangleq\begin{bmatrix}\Re\{z\} & -\Im\{z\}\\ \Im\{z\} & \Re\{z\}]\end{bmatrix}.$$

For any vector $\mathbf{v}$, $\mathbf{v}\otimes\mathcal{F}_v$ applies the operator $\mathcal{F}_v$ on all the entries of $\mathbf{v}$. Similarly, for any matrix $\mathbf{M}$, $\mathbf{M}\otimes\mathcal{F}_M$ applies the operator $\mathcal{F}_M$ on all the entries of $\mathbf{M}$. It is clear that $\tilde{\mathbf{\Psi}}$ is still block diagonal with $\tilde{\mathbf{\Psi}}_{ij}\triangleq(\mathbf{\Psi}_{ij}\otimes\mathcal{F}_M)\in\mathbb{R}^{(2LP)\times(2N)}$ as is its (ij)-th diagonal block; and $\tilde{\mathbf{s}}$ is composed by M_tM_r sub-vectors $\tilde{\mathbf{s}}_{ij}\triangleq(\mathbf{s}_{ij}\otimes\mathcal{F}_v)\in\mathbb{R}^{2N}$ that share the same sparsity profile and have exactly $2K$ nonzero real entries.

The L-OPT problem corresponding to (3.26) is given by

$$\min\sum_{n=1}^{N}\|\tilde{\mathbf{s}}[\mathcal{I}_n]\|_2\ \ s.t.\ \|\tilde{\mathbf{z}}-\tilde{\mathbf{\Psi}}\tilde{\mathbf{s}}\|_2\leq\epsilon_0, \tag{3.27}$$

where the set $\mathcal{I}_n,\forall n\in\mathbb{N}_N^+$, with cardinality $2M_tM_r$, contains the indices of the $(2n-1)$-th and $(2n)$-th entries from all equal-length sub-vectors $\tilde{\mathbf{s}}_{ij},\forall(ij)\in\Xi$. The equivalent unconstrained problem, known as group Lasso, is as follows:

$$\min\ \frac{1}{2}\|\tilde{\mathbf{z}}-\tilde{\mathbf{\Psi}}\tilde{\mathbf{s}}\|_2^2+\lambda\sum_{n=1}^{N}\|\tilde{\mathbf{s}}[\mathcal{I}_n]\|_2 \tag{3.28}$$

where λ is the regularization parameter. The second term enforce the solution to be group sparse. If prior information on the sparse target vector exists, it can be incorporated by introducing constraints, *i.e.*,

$$\begin{aligned}&\min\ \frac{1}{2}\|\tilde{\mathbf{z}}-\tilde{\mathbf{\Psi}}\tilde{\mathbf{s}}\|_2^2+\lambda\sum_{n=1}^{N}\|\tilde{\mathbf{s}}[\mathcal{I}_n]\|_2\\ &s.t.\ \tilde{\mathbf{s}}\in\Omega^{2NM_tM_r},\end{aligned} \tag{3.29}$$

where $\Omega^{2NM_tM_r}$ can be any general convex set, determined by the prior. In this chapter, we consider complex attenuation factors with magnitude less than ω_0, which means $|s_{ij}^n|\in[0,\omega_0]\triangleq\Omega$. Such prior can be obtained, for example, based on the distance between the

region of interest and the TX/RX pairs. Thus, the constraint $\tilde{\mathbf{s}} \in \Omega^{2NM_tM_r}$ is satisfied if $\|\left[\tilde{\mathbf{s}}[2i-1], \tilde{\mathbf{s}}[2i]\right]\|_2 \in \Omega,\ \forall i \in \mathbb{N}^+_{NM_tM_r}$, where $\tilde{\mathbf{s}}[i]$ denotes the i-th entry of $\tilde{\mathbf{s}}$.

In the following, we use the alternating direction method of multipliers (ADMM) [95] to solve the problem.

3.6.1 A Fast Algorithm Based on the ADMM

We introduce auxiliary variables $\mathbf{y}$ and $\mathbf{x}$ and rewrite (3.29) as

$$\begin{aligned} \min\ & \frac{1}{2}\|\tilde{\mathbf{z}} - \tilde{\mathbf{\Psi}}\tilde{\mathbf{s}}\|_2^2 + \sum_{n=1}^{N} \lambda \|\mathbf{y}_n\|_2 \\ s.t.\ & \mathbf{y}_n = \mathbf{D}_n \tilde{\mathbf{s}},\ \forall n \in \mathbb{N}^+_N, \\ & \mathbf{x} = \tilde{\mathbf{s}}, \mathbf{x} \in \Omega^{2NM_tM_r}, \end{aligned} \tag{3.30}$$

where $\mathbf{D}_n$ is the matrix of dimension $(2M_tM_r) \times (2NM_tM_r)$ that selects the entries in $\tilde{\mathbf{s}}$ indexed by $\mathcal{I}_n$; the vector $\mathbf{y}$ is defined as $[\mathbf{y}_1^T, \ldots, \mathbf{y}_N^T]^T$. We have $\mathbf{y} = \mathbf{D}\tilde{\mathbf{s}}$ where $\mathbf{D} = [\mathbf{D}_1^T, \ldots, \mathbf{D}_N^T]$ permutates $\tilde{\mathbf{s}}$ into $\mathbf{y}$. The auxiliary variable $\mathbf{y}$ is to isolate $\tilde{\mathbf{s}}$ from the group sparsity-inducing term $\sum\|\cdot\|_2$; the magnitude constraint is now imposed on $\mathbf{x}$ instead of $\tilde{\mathbf{s}}$.

Let us now apply the ADMM after grouping the variables into two blocks, *i.e.*, $(\mathbf{y}, \mathbf{x})$ and $\tilde{\mathbf{s}}$. The augmented Lagrangian of the above optimization problem can be written as follows

$$\begin{aligned} \mathcal{L}(\tilde{\mathbf{s}}, \mathbf{y}, \mathbf{x}; \mu, \nu) = & \frac{1}{2}\|\tilde{\mathbf{z}} - \tilde{\mathbf{\Psi}}\tilde{\mathbf{s}}\|_2^2 + \nu^T(\mathbf{x} - \tilde{\mathbf{s}}) + \frac{\rho_2}{2}\|\mathbf{x} - \tilde{\mathbf{s}}\|_2^2 \\ & + \sum_{n=1}^{N} \left(\lambda\|\mathbf{y}_n\|_2 + \mu_n^T(\mathbf{y}_n - \mathbf{D}_n\tilde{\mathbf{s}}) + \frac{\rho_1}{2}\|\mathbf{y}_n - \mathbf{D}_n\tilde{\mathbf{s}}\|_2^2\right), \end{aligned} \tag{3.31}$$

where $\rho_1, \rho_2 > 0$ and $\mu \triangleq [\mu_1^T, \ldots, \mu_N^T]^T \in \mathbb{R}^{2NM_tM_r}$ and $\nu \in \mathbb{R}^{2NM_tM_r}$ are the Lagrangian multipliers.

Based on the framework of ADMM, we can solve (3.30) by alternatively iterating over $\mathbf{y}, \mathbf{x}$ and $\tilde{\mathbf{s}}$. The $\mathbf{y}$-subproblem is well studied in the literature [57] and its solution is given explicitly by the shrinkage operator

$$\mathbf{y}_n^{k+1} = \max\left\{\|\bar{\mathbf{s}}_n^k\|_2 - \frac{\lambda}{\rho_1}, 0\right\} \frac{\bar{\mathbf{s}}_n^k}{\|\bar{\mathbf{s}}_n^k\|_2},\ \forall n \in \mathbb{N}^+_N, \tag{3.32}$$

where $\bar{\mathbf{s}}_n^k \triangleq \mathbf{D}_n\tilde{\mathbf{s}}^k - \mu_n^k/\rho_1$. In total, the computation cost of (3.32) scales as $\mathcal{O}(NM_tM_r)$.

For the $\mathbf{x}$-subproblem, we have

$$\mathbf{x}^{k+1} = \mathcal{P}_\Omega\left(\tilde{\mathbf{s}}^{k+1} - \frac{\nu^k}{\rho_2}\right), \tag{3.33}$$

where $\mathcal{P}_\Omega(\mathbf{x})$ projects $\big(\mathbf{x}[2i-1], \mathbf{x}[2i]\big)$ onto the region $\{(x,y)|x^2+y^2 \leq \omega_0\}$, $\forall i \in \mathbb{N}^+_{NM_tM_r}$. The overall computation of (3.33) involves $\mathcal{O}(NM_tM_r)$ operations.

The $\tilde{\mathbf{s}}$-subproblem is a least squares problem. The minimizer is attained if

$$0 = \frac{\partial}{\partial \tilde{\mathbf{s}}} \mathcal{L}(\tilde{\mathbf{s}}, \mathbf{y}^{k+1}, \mathbf{x}^{k+1}; \mu^k, \nu^k) = \mathbf{A}\tilde{\mathbf{s}} - \mathbf{b}^k, \tag{3.34}$$

where $\mathbf{A} = \tilde{\mathbf{\Psi}}^T\tilde{\mathbf{\Psi}} + (\rho_1+\rho_2)\mathbf{I}_{2NM_tM_r}$ and $\mathbf{b}^k = \tilde{\mathbf{\Psi}}^T\tilde{\mathbf{z}} + \mathbf{D}^T\mu^k + \rho_1\mathbf{D}^T\mathbf{y}^{k+1} + \nu^k + \rho_2\mathbf{x}^{k+1}$, and $\mathbf{I}_N$ denotes the identity matrix of dimension $N \times N$. The solution can be obtained by solving the following system of linear equations

$$\mathbf{A}\tilde{\mathbf{s}}^{k+1} = \mathbf{b}^k. \tag{3.35}$$

Given the signal model, $\mathbf{A}$ is fixed for all iterations. The computational effort for $\mathbf{b}^k$ in each iteration only involves permutation and addition of vectors; this is because $\tilde{\mathbf{\Psi}}^T\tilde{\mathbf{z}}$ is also fixed. In addition, $\mathbf{A}$ is block diagonal because $\tilde{\mathbf{\Psi}}^T\tilde{\mathbf{\Psi}}$ is block diagonal. The system of (3.35) can be written into a set of subsystems of linear equations as follows

$$\mathbf{A}_m\tilde{\mathbf{s}}_m^{k+1} = \mathbf{b}_m^k,\ \forall m \in \mathbb{N}^+_{M_tM_r}, \tag{3.36}$$

where $\mathbf{A}_m$ denotes the m-th diagonal block of matrix $\mathbf{A}$; $\mathbf{v}_m$ denotes the m-th uniformly partitioned block of vector $\mathbf{v}$. From the definition of $\mathbf{A}$, we know that

$$\mathbf{A}_m = \tilde{\mathbf{\Psi}}_{ij}^T\tilde{\mathbf{\Psi}}_{ij} + (\rho_1+\rho_2)\mathbf{I}_{2N},\ \forall m \in \mathbb{N}^+_{M_tM_r}, \tag{3.37}$$

where $j = \lfloor \frac{m-1}{M_t} \rfloor + 1$ and $i = m - (j-1)M_t$. $\lfloor a \rfloor$ denotes the largest integer that is smaller than a. From the definition of $\mathbf{A}_m$, it is easy to show that $\mathbf{A}_m$ is symmetric and positive definite for any $\rho_1, \rho_2 > 0$. Therefore, each system in (3.36) can be solved efficiently using iterative methods, such as the Preconditioned Conjugate Gradient (PCG) method, with cost about $\mathcal{O}(N^2)$ operations. The total number of operations to solve (3.35) is of the order of $\mathcal{O}(N^2M_tM_r)$.

Finally, the update for multipliers μ and ν can be carried out as

$$\nu^{k+1} = \nu^k + \rho_2(\mathbf{x}^{k+1} - \tilde{\mathbf{s}}^{k+1}), \tag{3.38a}$$

$$\mu^{k+1} = \mu^k + \rho_1(\mathbf{y}^{k+1} - \mathbf{D}\tilde{\mathbf{s}}^{k+1}), \tag{3.38b}$$

with linear complexity $\mathcal{O}(NM_tM_r)$.

The convergence of the above iterations is guaranteed by results in the ADMM literature [95]. The iterations stop when the decrease of the objective value in (3.29) drops below certain threshold or the number of iterations exceeds certain value.

Remark 8. *The bounds on L and P of Proposition 1 apply to (3.27) and (3.28) exactly in the same way as to (3.23). The problems in (3.27) and (3.23) are identical because the transformation only involves the separation of real and imaginary parts. Also, (3.28) is equivalent to (3.27) because (3.28) and (3.27) are the dual problems of each other. It can be shown using convex analysis techniques [96] that for any $\lambda > 0$ the solution of (3.28) is a minimizer of (3.27) for certain ϵ_0. The same bounds on L and P of Proposition 1 also guarantee to solve (3.29), which result in a smaller recovery error than (3.23). The bounded constraint in (3.29) reduces the feasible set in (3.23) by incorporating prior information on $\mathbf{s}$. This means that the solution of (3.29) is at least as accurate as that of (3.23) with the same conditions on L and P of Proposition 1. As shown in the simulations, the additional constraint indeed improves the accuracy of the solution over other methods that also use the same L and P.*

Remark 9. *The advantages of the proposed algorithm can be summarized as follows. First, the computational cost is low. As we know, solving (3.30) using an interior point method would involve $\mathcal{O}((NM_tM_r)^3)$ operations [97]. For the proposed algorithm, the computational cost in each iteration is dominated by solving the system of linear equations (3.35), which is $\mathcal{O}(N^2M_tM_r)$. The reduction of computations is more significant as the number of antennas increases. Second, the estimation accuracy of $\mathbf{s}$ is improved by introducing the amplitude constraints on the sparse target vector. Also, the performance is robust over wide range of regularization parameter λ. This is validated via simulations in Section 3.8. Lastly, due to the block diagonal structure in $\mathbf{\Psi}$, the update of $\tilde{\mathbf{s}}^{k+1}$ in (3.35) can be achieved by updating independent sub-vectors in $\tilde{\mathbf{s}}^{k+1}$. The good separability in the update of all variables affords a parallel and decentralized implementation, as discussed in the next section.*

3.6.2 Parallel and Semi-distributed Implementation

Parallel Implementation

In the $(k+1)$th iteration, it is clear that all pairs $(\mathbf{x}^k[2i-1], \mathbf{x}^k[2i])$ in $\mathbf{x}^k$ are updated independent of the others, thus, the computations can be done in parallel. A similar parallel scheme applies to μ^k and ν^k, and the update of $\mathbf{y}_n^k$. The subsystems in (3.36) can also be solved in parallel. Assuming that there are multiple computing units available at the fusion center, the target estimation running time can be significantly reduced. The parallel implementation here is different from the decoupled Lasso of [31], because here, the identical sparsity profile in the sub-vectors of the target vector is utilized via the auxiliary variable $\mathbf{y}$.

Fusion Center Aided Semi-Distributed Implementation

The ADMM based approach described in Section 3.6.1 requires a fusion center to perform all the computations. However, a semi-distributed implementation is also possible. For each iteration, $\mathbf{x}$ (respectively for $\mathbf{s}$ and ν) can be divided into blocks, each of which can be updated locally at the receive antenna. However, the update of $\mathbf{y}$ and μ cannot be done locally. A fusion center performs the update of $\mathbf{y}$ and μ.

The fusion center aided semi-distributed scheme is summarized in Algorithm 1. In the implementation of Algorithm 1, $\tilde{\mathbf{s}}_m^{k+1} \in \mathbb{R}^{2N}$ (respectively for $\nu_m^{k+1}, \mathbf{x}_m^{k+1}$), $\forall m \in \mathbb{N}^+_{M_t M_r}$, denotes the m-th block of uniformly partitioned $\tilde{\mathbf{s}}^{k+1}$. $\mathbf{y}_m^{k+1} \in \mathbb{R}^N$ denotes the m-th block of uniformly partitioned $\mathbf{D}^T\mathbf{y}^{k+1}$. The receive node j updates $\mathbf{x}_m^{k+1}, \nu_m^{k+1}$ and $\mathbf{s}_m^{k+1}$ for all $m \in \mathcal{T}_j \triangleq \{(j-1)M_t + i | i \in \mathbb{N}^+_{M_t}\}$. The fusion center updates $\mathbf{y}$ and μ. Thus, the computation cost is $\mathcal{O}(N^2 M_t)$ at each node and $\mathcal{O}(NM_tM_r)$ at the fusion center. One can see that the computations are distributed among all receive nodes. The computation and memory required by the fusion center is only linear in the dimension of sparse vector $\mathbf{y}$, which is significantly lower than that of the fusion center of Section 3.6.1. Thus, even one of the receivers can be assigned to serve as the fusion center, and perform the update of $\mathbf{y}$ and μ. In each iteration, each node communicates $\tilde{\mathbf{s}}_m^{k+1}$ and $\mathbf{y}_m^{k+1}$ to the fusion center. However, the communication load decreases in a few iterations, because the nonzero entries in $\tilde{\mathbf{s}}_m^{k+1}$

and $\mathbf{y}_m^{k+1}$ would be on the order of $\mathcal{O}(K)$.

A fully distributed scheme would also be possible, but would require consensus. However, consensus-based implementations converge slowly, which would be a problem in target estimation and tracking applications.

Algorithm 1 Semi-Distributed Implementation

One peer receive node is chosen as the fusion center.
Input $\tilde{\mathbf{\Psi}}, \tilde{\mathbf{z}}, \lambda, \rho_1, \rho_2$
Initialization $\tilde{\mathbf{s}}^{(0)} = \mathbf{x}^{(0)} = \mathbf{y}^{(0)} = 0$, $\mu^{(0)} = \nu^{(0)} = 0$
Iteration
Fusion Center:
  compute $\mathbf{y}_n^{k+1}$, $\forall n \in \mathbb{N}_N^+$ by (3.32);
Node $j \in \mathbb{N}_{M_r}^+$: for all $m \in \mathcal{T}_j$
  download $\mathbf{y}_m^{k+1}$ from the fusion center;
  compute $\mathbf{x}_m^{k+1} = \mathcal{P}_\Omega(\tilde{\mathbf{s}}_m^{k+1} - \nu_m^k/\rho_2)$;
  compute $\tilde{\mathbf{s}}_m^{k+1}$ by solving (3.36);
  compute $\nu_m^{k+1} = \nu_m^k + \rho_2(\mathbf{x}_m^{k+1} - \tilde{\mathbf{s}}_m^{k+1})$;
  upload $\tilde{\mathbf{s}}_m^{k+1}$ to the fusion center;
Fusion Center:
  compute μ^{k+1} by (3.38b);

3.7 Decoupled location and speed estimation

Instead of jointly estimating the target location-speed in the discretized location-speed space $\mathbf{\Theta} = \mathbf{\Theta}_{loc} \times \mathbf{\Theta}_{spd}$ (dimension $N = N_1 \times N_2$) we can decouple the estimation into target location estimation and the speed estimation. As it will be shown, such decoupling lowers complexity and required fewer measurements.

3.7.1 The Decoupled Signal Model

First, we describe the sparse model in the discretized target location space, $\mathbf{\Theta}_{loc}$, of dimension N_1, where $N_1 \ll N$. For target location estimation, it suffices to collect the measurements from one pulse only. During the p-th pulse (for some fixed p), the sample vector $\mathbf{z}_{ij}^p \in \mathbb{C}^L$, corresponding to the (ij)-th TX/RX antenna pair node pair, equals

$$\mathbf{z}_{ij}^p = \mathbf{\Psi}_{ij}^p \mathbf{s}_{ij}^p + \mathbf{n}_{ij}^p, \ \forall (ij) \in \Xi, \tag{3.39}$$

where $\mathbf{n}_{ij}^p \in \mathbb{C}^L$ denotes the additive noise. The matrix $\mathbf{\Psi}_{ij}^p \in \mathbb{R}^{L\times N_1}$ has $\mathbf{w}_{i,\tau_{ij}^n}$ as its n-th column. The vector $\mathbf{s}_{ij}^p \in \mathbb{C}^{N_1}$ is K-sparse and its n-th entry equals $\mathbf{s}_{ij}^p(n) = \beta_{ij}^k e^{2\pi f_{ij}^k T(p-1)}$, if there is a target at the n-th grid point (here β_{ij}^k is the corresponding target reflectivity); otherwise it equals 0. For slowly moving targets, the Doppler effect can be approximated as constant during one pulse, thus, the Doppler effect here is absorbed into $\mathbf{s}_{ij}^p$. At the fusion center, the sample vector corresponding to the p-th pulse, formed based on all TX/RX pairs, $\mathbf{z}^p \in \mathbb{C}^{LM_tM_r}$, equals

$$\mathbf{z}^p = \left[(\mathbf{z}_{11}^p)^T, \ldots, (\mathbf{z}_{M_tM_r}^p)^T\right]^T = \mathbf{\Psi}^p\mathbf{s}^p + \mathbf{n}^p, \tag{3.40}$$

where $\mathbf{s}^p = \left[(\mathbf{s}_{11}^p)^T, \ldots, (\mathbf{s}_{M_tM_r}^p)^T\right]^T$, $\mathbf{n}^p = [(\mathbf{n}_{11}^p)^T, \ldots, (\mathbf{n}_{M_tM_r}^p)^T]^T$, and $\mathbf{\Psi}^p = \text{diag}(\mathbf{\Psi}_{11}^p, \ldots, \mathbf{\Psi}_{M_tM_r}^p)$.

The location vector $\mathbf{s}^p$ can be recovered by applying the L-OPT method of Section 3.2. The recovery performance is given in the following proposition.

Proposition 2. *Consider the location estimation model in (3.40). For any $\delta_{2K} < \sqrt{2}-1$, if L is such that*

$$L \geq 192\delta_{2K}^{-1}K^2\log(N_1\sqrt{M_tM_r}) + 1, \tag{3.41}$$

then the error of the L-OPT solution, $\hat{\mathbf{s}}^p$, is bounded as $\|\hat{\mathbf{s}}^p - \mathbf{s}^p\|_2 \leq g\left(\epsilon_p/\sqrt{L\sigma_0^2}\right)$ with probability exceeding $(1-4(N_1\sqrt{M_tM_r})^{-1})$.

The proof of Proposition 2 follows the same spirit as that of Proposition 1. The key is to show that $\mathbf{\Psi}^p$ satisfies the $\mathcal{A}_1$-RIP$(2K, \delta_{2K})$ given the conditions on L, which can be proven along the lines of Section 3.4.

Once we obtain the target locations from $\hat{\mathbf{s}}^p$, we can use them to reduce the dimension of the speed estimation problem. Let $\mathbf{\Theta}_{loc,\mathcal{I}}$ be the pruned target location space. If the number of targets, K, is known, then $\mathbf{\Theta}_{loc,\mathcal{I}}$ consists of the grid points corresponding to the K largest entries of the recovered $\mathbf{s}_{ij}^p$. If K is unknown, we keep a slightly larger portion of the location grid points in $\mathbf{\Theta}_{loc,\mathcal{I}}$. The sparse model in (3.8) can be applied for $\mathbf{\Theta}_{loc,\mathcal{I}} \times \mathbf{\Theta}_{spd}$ instead of the entire space $\mathbf{\Theta}$. On denoting $\tilde{K} \triangleq |\mathbf{\Theta}_{loc,\mathcal{I}}|$, it holds that $\tilde{K} \sim \mathcal{O}(K) \ll N_1$. The number of measurements can also be reduced due to the lower dimension of the location-speed space $\mathbf{\Theta}_{loc,\mathcal{I}} \times \mathbf{\Theta}_{spd}$. During each pulse, the (ij)-th TX/RX pair will only use $\tilde{L} \ll L$ measurements.

Let us denote by $\mathcal{I}_r$ the index set that selects $\tilde{L}P$ measurements during all P pulses, and by $\mathcal{I}_c$ the index set that selects $\mathbf{\Theta}_{loc,\mathcal{I}} \times \mathbf{\Theta}_{spd}$ out of $\mathbf{\Theta}$. The sparse model for speed estimation becomes

$$\mathbf{z}_{\mathcal{I}_r} = \mathbf{\Psi}_{\mathcal{I}} \mathbf{s}_{\mathcal{I}_c} + \mathbf{n}_{\mathcal{I}_r}, \tag{3.42}$$

where $\mathbf{z}_{\mathcal{I}_r} \in \mathbb{C}^{\tilde{L}PM_tM_r}$ consists of entries of $\{\mathbf{z}_{ij}\}_{(ij)\in\Xi}$ indexed by $\mathcal{I}_r$, and similarly for $\mathbf{s}_{\mathcal{I}_c} \in \mathbb{C}^{\tilde{K}N_2M_tM_r}$ and $\mathbf{n}_{\mathcal{I}_r} \in \mathbb{C}^{\tilde{L}PM_tM_r}$; $\mathbf{\Psi}_{\mathcal{I}} \in \mathbb{C}^{\tilde{L}PM_tM_r \times \tilde{K}N_2M_tM_r}$ is the corresponding block diagonal matrix. The diagonal blocks of $\mathbf{\Psi}_{\mathcal{I}}$ consist of rows and columns of $\{\mathbf{\Psi}_{ij}\}_{(ij)\in\Xi}$ respectively indexed by $\mathcal{I}_r$ and $\mathcal{I}_c$. Note that $\mathbf{s}_{\mathcal{I}_c}$ can be uniformly partitioned into M_tM_r K-sparse sub-vectors, which share the same sparse profile. The final location-speed estimation can be achieved based on $\mathbf{s}_{\mathcal{I}_c}$, by solving an L-OPT problem (see (3.42)).

3.7.2 Complexity and Discussion

The decoupled location and speed estimation scheme needs to solve two sparse recovery problems. If the interior point method is adopted to solve the L-OPT problems, the total computation cost would be $\mathcal{O}((N_1M_tM_r)^3 + (\tilde{K}N_2M_tM_r)^3)$. Recall that solving (3.8) using the interior point method requires cost of $\mathcal{O}((N_1N_2M_tM_r)^3)$. The computation saving comes from the lower dimensions of the decoupled scheme than that of the original problem in (3.8). Moreover, in (3.40), the measurement matrix $\mathbf{\Psi}^p$ is block diagonal, and the sparse vector $\mathbf{s}^p$ has group sparsity. Thus, the ADMM-based algorithm in Section 3.6 can be used to recover $\mathbf{s}^p$. It is easy to show that the Gram matrix of $\mathbf{\Psi}^p$ is block diagonal, symmetric and positive semidefinite. The computation of the ADMM-based algorithm will be $\mathcal{O}(N_1^2M_tM_r)$. Similarly for (3.42), the ADMM-based algorithm can also be used to recover $\mathbf{s}_{\mathcal{I}_c}$ with cost $\mathcal{O}(\tilde{K}^2N_2^2M_tM_r)$. The decoupled location and speed estimation using the ADMM further reduces the computational complexity. The parallel technique (or semi-distributed implementation) can also be applied here to distribute the computations among multiple processors (or receiver nodes).

The decoupled scheme requires LM_tM_r measurements from the p-th pulse for location estimation and $(P-1)\tilde{L}M_tM_r$ from the rest $(P-1)$ pulses for the final speed estimation. Thus, the receivers can operate at sampling frequency $1/T_s$ during the first pulse, and reduce the sampling frequency to $\frac{\tilde{L}}{LT_s}$ thereafter. Compared to the joint estimation scheme, less

measurements are needed.

Given fixed amount of measurements, the estimation performance is better for smaller location-speed space $\mathbf{\Theta}_{loc,\mathcal{I}} \times \mathbf{\Theta}_{spd}$ once it contains the location grid points possessed by targets. Since the dimension of $\mathbf{\Theta}_{loc,\mathcal{I}} \times \mathbf{\Theta}_{spd}$ is controlled by $\tilde{K}$, it is expected that the estimation error achieves the minimum when $\tilde{K} = K$ if the locations of K targets are estimated correctly in the first stage. We will show in the simulation that this happens even for reasonable low SNRs. It is also shown that the estimation error of the decouple scheme with partial measurements may even be lower than that of the joint scheme using all the measurements.

3.8 Numerical Results

We consider a MIMO radar system with M_t TX and M_r RX antennas, distributed uniformly on a circle of radius of $6,000m$ and $3,000m$, respectively. Each TX radar transmits pulses with pulse repetition interval 0.125 ms and $5GHz$ carrier frequency. The variance of Gaussian waveform is $\sigma_0^2 = 1$. Each RX radar works with sampling frequency of 50MHz on the received baseband signal, which are corrupted by zero-mean Gaussian noise with variance σ_n^2. The signal-to-noise ratio (SNR) is defined as $10\log_{10}(\sigma_0^2/\sigma_n^2)$.

The probing space is discretized on a $N_x \times N_y$ grid, starting from point $[8000m, 8000m]$ with grid spacing equal to $10m$. The velocity space in default is fixed as a uniform 4×1 grid on $v_x \in [100, 130]m/s$, $v_y = 100m/s$ *i.e.*, $N_{vx} = 4, N_{vy} = 1$, unless otherwise is stated. We randomly generate K targets on the grid. The magnitude of the complex reflection coefficients for each target in each trial is randomly generated from uniform distribution in the range of $[0.1, 0.8]$.

All the simulations are carried out on a PC with Intel Core i7 CPU and 8GB memory. The number of independent trials is 100 unless otherwise stated.

3.8.1 On The Number of Pulses P

We first illustrate the choice of the number of pulses P via the inequality $\beta(P)/P \leq \delta_{2K}/(2K + \delta_{2K})|_{\delta_{2K}=\sqrt{2}-1} \triangleq \gamma_0$ when only a single target is considered, *i.e.*, $K = 1$. We

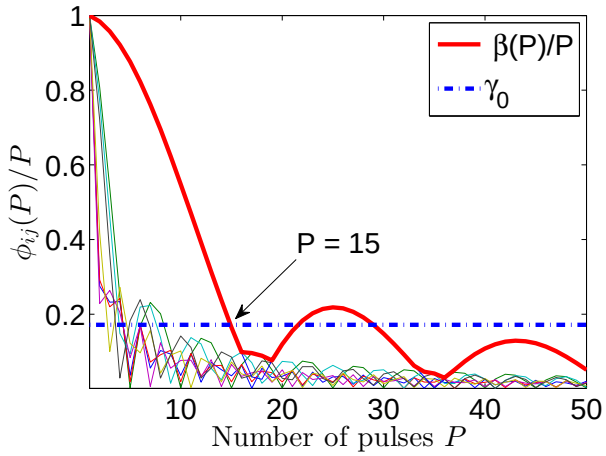

Figure 3.1: Results on the choice of the number of pulses, P.

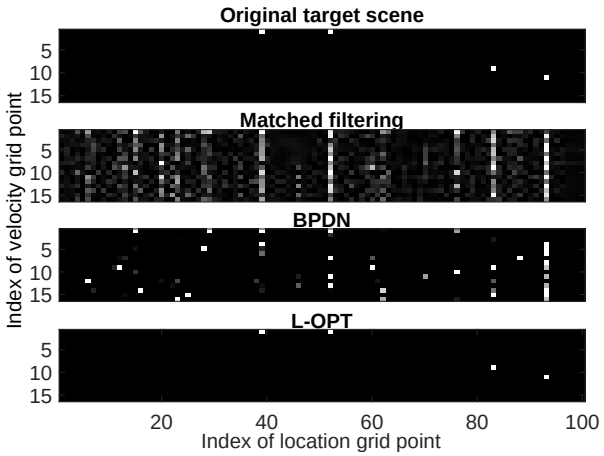

Figure 3.2: An illustration of target scene estimation. The MIMO radar system has $M_t = 2$ receive and $M_r = 4$ transmit antennas. We sample $L = 50$ samples per pulse from $P = 6$ pulses. There are $K = 4$ targets. The target space of interest is with parameters $N_x = 25, N_y = 4, N_{vx} = 4$ and $N_{vy} = 4$.

consider $M_t = 2, M_r = 4$. For the case of $N_x = 25, N_y = 4$, Fig. 3.1 shows values of $\phi_{ij}(P)/P$ for all TX/RX pairs under different values of P. We choose the smallest P such that the maximum of $\phi_{ij}(P)/P$, $\forall(ij) \in \Xi$, is smaller than γ_0, *i.e.*, $\beta(P)/P \leq \gamma_0$. Based on Proposition 1, this value guarantees the performance under the worst cases. In the following simulation, we will show that even a smaller P works well.

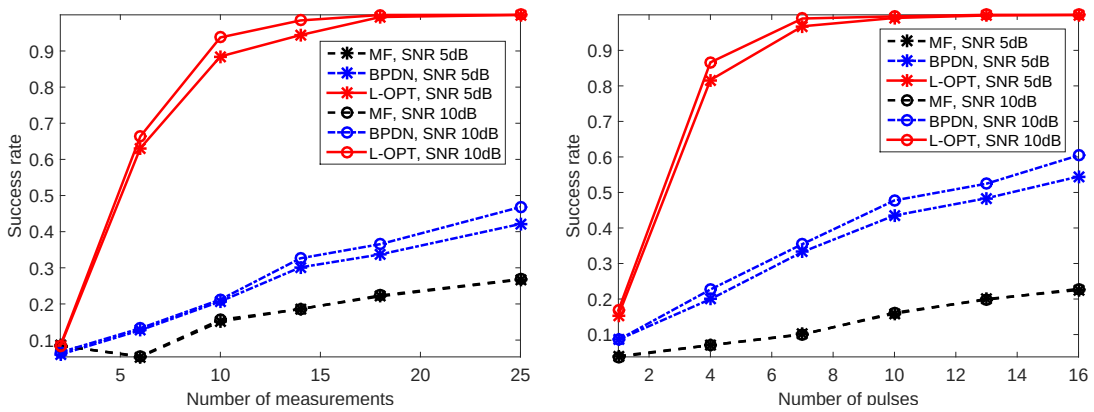

Figure 3.3: Performance for the Matched Filtering (MF), the BPDN and the L-OPT methods. (a) Results under different number of measurements and SNRs, $K = 20, P = 3$; (b) Results under different number of pulses and SNRs, $K = 20, L = 6$.

3.8.2 The Advantage of Exploiting Group Sparsity

It can be seen from Theorem 2 that exploiting the sparsity in the target vector reduces the required measurements, or equivalently, it improves the performance with the same amount of measurements. In this simulation, we evaluate the advantage of exploiting the sparsity structure in the target vector. We consider $M_t = 2, M_r = 4, N_x = 25$ and $N_y = 4$. For the proposed L-OPT based method in (3.23), we use the interior point method with $\epsilon_0 = 2\sqrt{LM_tM_r}\sigma_n$ [38]. For comparison, we implement BPDN which just minimizes the ℓ_1-norm of $\mathbf{s}$ and ignores the sparsity structure in $\mathbf{s}$. The constraint in BPDN is exactly the same as that for L-OPT method. The parameter ϵ_0 for BPDN is chosen the same as that for L-OPT. Also, the traditional matched filtering (MF) approach [2] is also implemented for comparison. The MF method uses the same L and P as the sparsity-based methods. The received signal is correlated with the transmitted signal distorted by different Doppler shifts and time delays.

An illustration of target scene estimation is presented in Fig. 3.2. The MIMO radar system has $M_t = 2$ receive and $M_r = 4$ transmit antennas. We sample $L = 50$ samples per pulse from $P = 6$ pulses. There are $K = 4$ targets. The target space of interest is with parameters $N_x = 25, N_y = 4, N_{vx} = 4$ and $N_{vy} = 4$. The traditional MF method has complexity of $\mathcal{O}(LPNM_tM_r)$, which is much lower compared to that of the BPDN and the L-OPT methods. However, the target scene estimate by the MF method is corrupted by

lots of false peaks. The BPDN method achieves a relative cleaner target scene estimate, but the strong false peaks may still degrade the target estimation results. The L-OPT method utilizes the group sparsity in $\mathbf{s}$, which helps to remove the false peaks in the estimate. It can be seen from Fig. 3.2 that the L-OPT method indeed achieves the best target scene estimation.

In Fig. 3.3(a), we plot the successful recovery rates by the MF, the BPDN and the L-OPT methods under different number of measurements, L, and SNRs with $K = 20, P = 3$. The recovery rate of the L-OPT method drops dramatically if L is smaller than 10. This observation validates the claim in Proposition 1 that L should be larger than certain value to maintain a high probability of target location and speed estimation. Based on (3.24a) in Proposition 1, the bound on L is 5×10^5, which is much larger than the values of L here. As discussed in Remark 5, the L-OPT method performs well with much smaller L and P than those in (3.24). In Fig. 3.3(b), we plot the successful recovery rates under different number of pulses, P, with $K = 20, L = 6$. Similar observations can be made for the number of pulses. From both Fig. 3.3(a) and (b), the successful recovery rates of the L-OPT method are higher than those of the BPDN method under all the settings. As implied by Theorem 2, L-OPT outperforms BPDN because it exploits the sparsity structure in $\mathbf{s}$. In addition, the sparsity based methods, both the BPDN and the L-OPT methods, outperform the traditional MF method in terms of the success rate of target estimation.

3.8.3 Efficient Algorithm Based on The ADMM

In this section, we evaluate the efficient algorithm based on the ADMM proposed in Section 3.6.1. We consider the same simulation setting in Section 3.8.2 except that the SNR is set to be 5 dB. The dimension of the target vector in (3.26) is 6400×1 with $16 \times K$ nonzero entries. The BOMP [30] method, the GLasso-PGA method [31] and the L-OPT method using the interior point method (L-OPT-IPM) are implemented for comparison. For GLasso-PGA, we choose $\lambda = 0.02$ for the best performance. For L-OPT-IPM, we set $\epsilon_0 = 2\sqrt{LPM_tM_r}\sigma_n$ with knowledge of $\sigma_n^2 = \sigma_0^2 10^{10/SNR}$. For the proposed ADMM based method, preconditioned conjugate gradient is used to solve the system of (3.35). The estimation error $\|\hat{\mathbf{s}} - \mathbf{s}\|_2$ and the CPU running time are used as the performance metrics. All results are averaged over

100 independent trials.

We first fix $K = 10, P = 3$ and evaluate the root of total squared error $\|\hat{\mathbf{s}} - \mathbf{s}\|_2$ under different number of measurements L. The results are plotted in Fig. 3.4. The proposed algorithm, labeled as ADMM-based in the legend, achieves lower estimation errors with less CPU run time as compared to GLasso-PGA and L-OPT-IPM under all L's. The CPU run time of the proposed algorithm remains less than $10s$, while the run time of L-OPT-IPM grows superlinearly with L. We should note that the L-OPT-IPM solves the problem of (3.23), while the ADMM method solves the problem of (3.29). Compared to the problem of (3.23), there is an additional bounded constraint in (3.29), which changes the optimization problem. The additional constraint in (3.29) imposes a smaller feasible set, which may introduce the denoising effect because the noise-corrupted candidates outside the feasible set are excluded. In contrast, the solution of (3.23) obtained by the L-OPT-IPM method may fall out of the feasible set in (3.29). As shown in Fig. 3.4, the additional constraint in (29) improves the accuracy of the solution with the same L and P over the L-OPT-IPM method.

Next, we consider the performance of the proposed scheme for different number of targets and fixed number of measurements $L = 20$ and pulses $P = 3$. The results are plotted in Fig. 3.5. For all values of K, the proposed ADMM-based algorithm achieves lower estimation errors than the GLasso-PGA method using around one quarter CPU running time.

Fig. 3.6 shows the performance of the proposed scheme for different number of pulses and fixed number of measurements $L = 10$ and targets $K = 10$. The ADMM-based method achieves the smallest estimation errors, and takes much less CPU runtime than the GLasso-PGA method does.

It is noted that the MF method takes much less CPU runtime compared to the sparsity based methods because its complexity is $\mathcal{O}(LPNM_tM_r)$. However, the sparsity based methods achieve lower estimation errors and higher success rates at the cost of complexity increase.

In the above simulation, L-OPT-IPM requires knowledge of the noise variance σ_n^2. The regularization parameter λ in GLasso-PGA and the proposed algorithm also need to be

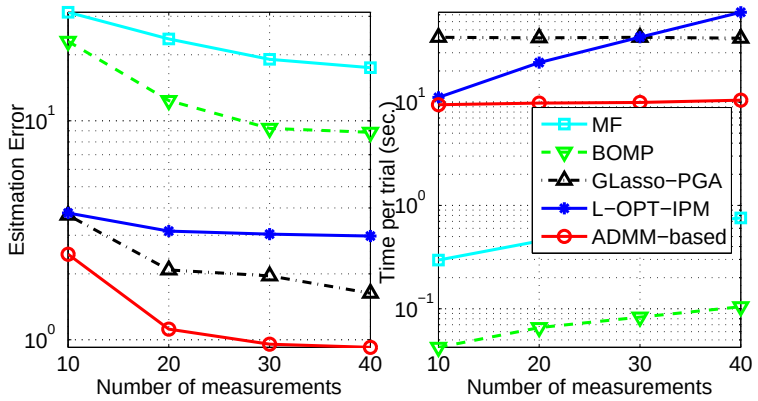

Figure 3.4: Performance under different number of measurements with $K = 10$ and $P = 3$; for GLasso-PGA $\lambda = 0.02$; and for the proposed ADMM-based method $\lambda = 4$, $\rho_1 = \rho_2 = 1$.

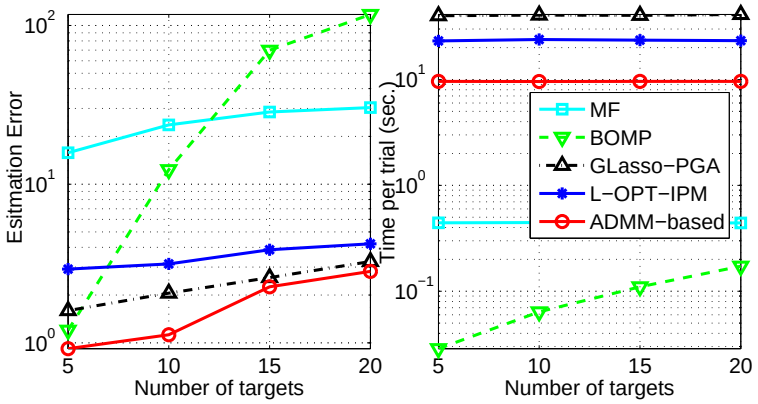

Figure 3.5: Performance under different number of targets with $L = 20$ and $P = 3$; for GLasso-PGA $\lambda = 0.02$; and for the proposed ADMM-based method $\lambda = 4$, $\rho_1 = \rho_2 = 1$.

manually tuned. In fact, the choice of such parameters are critical for the estimation performance. In Fig. 3.7, we plot the estimation errors for a wide range of λ. We observe that the estimation error of the proposed ADMM-based algorithm remains very small for a wide range of λ's, while for GLasso-PGA, the range of good λ's is very narrow. The robustness to λ makes the proposed algorithm good candidate for real world applications.

3.8.4 The Performance of the Decoupled Scheme

In this section, we evaluate the performance of the decouple scheme proposed in Section 3.7 under different values of $\tilde{L}$ and $\tilde{K}$. Recall that $\tilde{K}$ is the number of location grid points kept after the location estimation stage, and $\tilde{L}$ is the number of measurements used to achieve final location and speed estimation in the second stage. We aim to illustrate the extent to

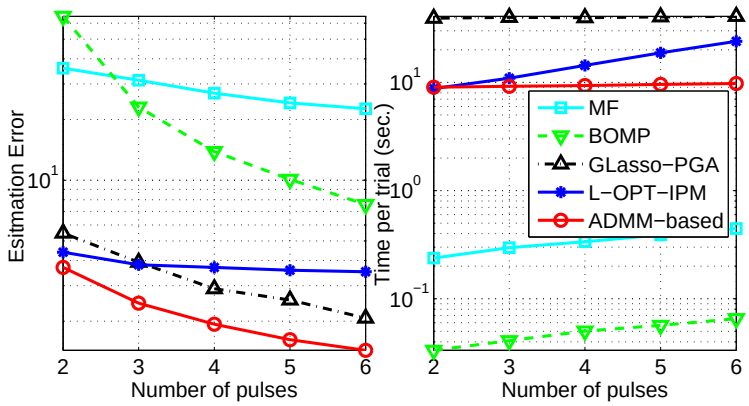

Figure 3.6: Performance under different number of pulses with $K = 10$ and $L = 10$; for GLasso-PGA $\lambda = 0.02$; and for the proposed ADMM-based method $\lambda = 4$, $\rho_1 = \rho_2 = 1$.

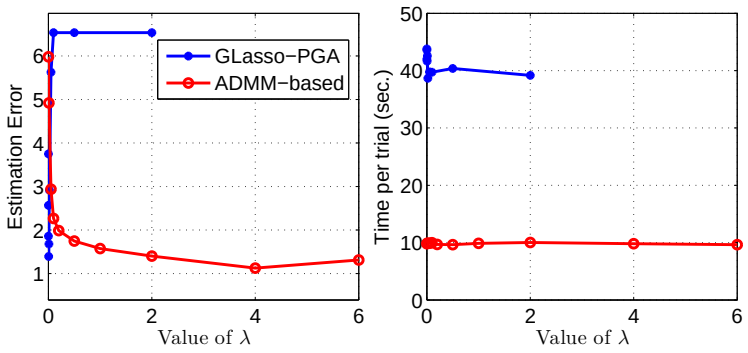

Figure 3.7: Performance under different values of λ with $K = 10, L = 20$ and $P = 3$.

which $\tilde{K}$ and $\tilde{L}$ can be reduced. For comparison, the joint location and speed estimation is implemented using the ADMM-based algorithm in Section 3.6, which is referred to as the joint scheme. We consider $M_t = 2, M_r = 4, N_x = 25$ and $N_y = 4$. The number of targets, measurements and pulses are fixed as $K = 10, L = 50$, and $P = 3$. The performance metrics used in this subsection are the successful recovery rate, root of the total squared error, and the CPU running time.

Fig. 3.8 shows the performance under different values of $\tilde{L}$. The performance of the joint scheme remains constant and serves as the reference because it is not affected by $\tilde{L}$. As for the decoupled scheme, the successful recovery rate goes up if more number of measurements are used. Also, the estimation accuracy of $\mathbf{s}$ increases when more measurements are used. The success rate and the estimation error of the decoupled scheme become very close to that of the joint scheme when only $\tilde{L} = 20$ out of $L = 50$ measurements (40%) are used. The location and speed estimation is correct with high probability even when we only keep 20% the measurements. The running time of the decoupled scheme is less than one tenth of that of the joint scheme. Note that the decoupled scheme estimation error becomes even smaller than that of the joint scheme when $\tilde{L}$ is large enough. It is because that the dimension of the location-speed space in the second stage of the decoupled scheme is much smaller than that used in the joint scheme, *i.e.*, $\tilde{K}N_2 \ll N_1N_2$.

The performance results under different values of $\tilde{K}$ are plotted in Fig. 3.9. The success rate results in Fig. 3.9(a) show that the success rate of the decouple scheme is 100% even if $\tilde{K} = K$. This means that the location estimation is accurate and stable in noise (5dB and 0dB are shown in the figure). The estimation error results in Fig. 3.9(b) indicate that the error is large if $\tilde{K}$ is smaller that K. If $\tilde{K}$ is set properly larger than K, the estimation error of the decoupled scheme is lower than that of the joint scheme. Also, note that once the correct location grid points are kept, the smaller the $\tilde{K}$ is, the smaller the dimension of the pruned space in the decoupled scheme is, and thus the smaller the estimation error is.

Based on the simulations in the subsection, we conclude that the decoupled scheme can reduce both the computation and the required number of measurements, while maintaining high estimation accuracy in practice.

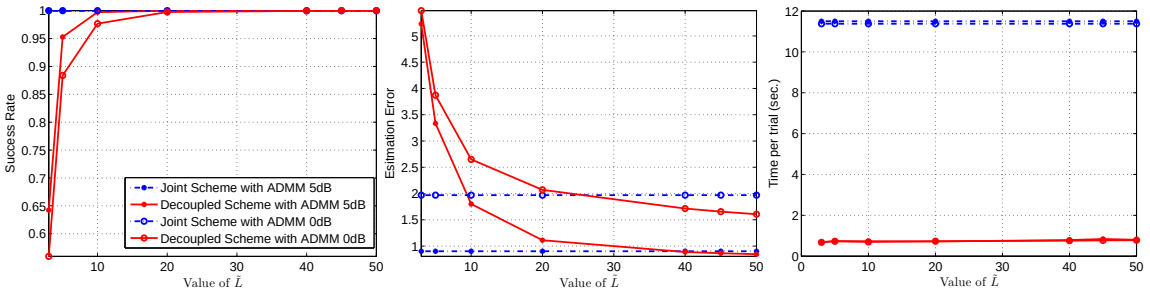

(a) (b) (c)

Figure 3.8: Performance of the decoupled scheme under different values of $\tilde{L}$ with $\tilde{K} = 2K$. (a) the successful recovery rate, (b) the estimation error, and (c) the CPU running time per trial in seconds.

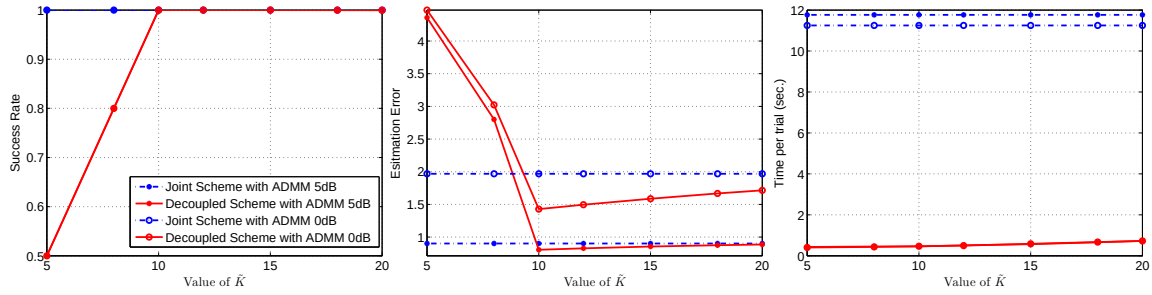

(a) (b) (c)

Figure 3.9: Performance of the decouple scheme under different values of $\tilde{K}$ with $\tilde{L} = 0.8L$. (a) the successful recovery rate, (b) the estimation error, and (c) the CPU running time per trial in seconds.

3.8.5 Off-grid targets and grid refinement

In all the previous simulations, all targets are assumed to be on the grid. In this section, we consider the case in which the targets may be between the grid points. For a certain target space, a dense grid would generate a problem with large dimension, the solution of which would demand high computational cost. On the other hand, a coarse grid would introduce large estimation errors. One could use the grid refinement scheme [97] to reduce the complexity while maintaining estimation performance. Let us consider the location and velocity estimation of $K = 4$ moving targets. The true target parameters are given in the second row of Table 3.1. The target space of interest is $x \in [8000, 8200], y \in [8000, 8100], v_x \in [100, 180]$ and $v_y \in [100, 140]$. In a dense uniform grid $\mathbf{\Theta}_d$ with $N_x = 41, N_y = 21, N_{vx} = 9$ and $N_{vy} = 5$, the location and velocity grid spacings would be $5m$ and $10m/s$, respectively, for which all targets fall on the grid. However, the corresponding total number of grid points

Table 3.1: The estimated target locations and velocities by a three-level grid refinement scheme. The results are given in the form of $[x, y, v_x, v_y]$ with metrics m and m/s respectively for location and velocity.

	Target 1	Target 2	Target 3	Target 4
True	[8025,8015,120,100]	[8085,8035,140,120]	[8125,8055,160,120]	[8185,8075,180,140]
1st est.	[8020,8020,120,100]	[8080,8040,140,120]	[8120,8060,160,120]	[8180,8080,180,140]
2nd est.	[8020,8020,120,100]	[8080,8040,140,120]	[8120,8060,160,120]	[8180,8080,180,140]
3rd est.	[8025,8015,120,100]	[8085,8035,140,120]	[8125,8055,160,120]	[8185,8075,180,140]

and the dimension of the sparse target vector $\mathbf{s}$ are $N = 38745$ and $NM_tM_r = 309960$, respectively. It is too time demanding to estimate targets using $\mathbf{\Theta}_d$. We instead use a three-level grid refinement scheme. An initial coarse grid $\mathbf{\Theta}_c$ with $N_x = 11, N_y = 6, N_{vx} = 5$ and $N_{vy} = 3$ is used to discretize the target space, which reduces the total number of grid points to 990. The location and velocity grid spacings are $20m$ and $20m/s$, respectively. Note that for this grid, all four targets fall between grid points. The first round estimate $\hat{\mathbf{s}}_1$ is obtained from the reconstructed target vector using the L-OPT method and $\mathbf{\Theta}_c$. A refined grid $\mathbf{\Theta}_r$ is generated in the neighborhood of the dominant peaks in $\hat{\mathbf{s}}_1$ with location grid spacing $10m$ and velocity grid spacing $10m/s$. The total number of grid points in the refined grid is 2153, which is still very small compared to that of $\mathbf{\Theta}_d$. Note that all four targets still fall off the refined grid. The second round estimate $\hat{\mathbf{s}}_2$ is obtained and the grid refinement procedure is repeated for a second time. Finally, we obtain the third round estimate $\hat{\mathbf{s}}_3$ using a further refined grid $\mathbf{\Theta}_{r'}$ with 2924 grid points, $5m$ location grid spacing and $10m/s$ velocity grid spacing. The true and estimated target scenes in the location space are shown in Fig. 3.10, where the vectors $\hat{\mathbf{s}}_1$, $\hat{\mathbf{s}}_2$ and $\hat{\mathbf{s}}_3$ are mapped onto grid $\mathbf{\Theta}_d$ by interpolating with zeroes. The estimated target locations and velocities are given in Table 3.1. We observe that the grid refinement scheme can effectively reduce the computational complexity and achieve accurate target estimation. Also, in the first two rounds, the off-grid targets are captured by the closest grid points. This indicates that the proposed methods are robust to off-grid targets.

3.9 Conclusions

We have considered moving target estimation using distributed, sparsity based MIMO radars. We have provided the uniform recovery guarantee by analyzing the $\mathcal{A}$-RIP of the

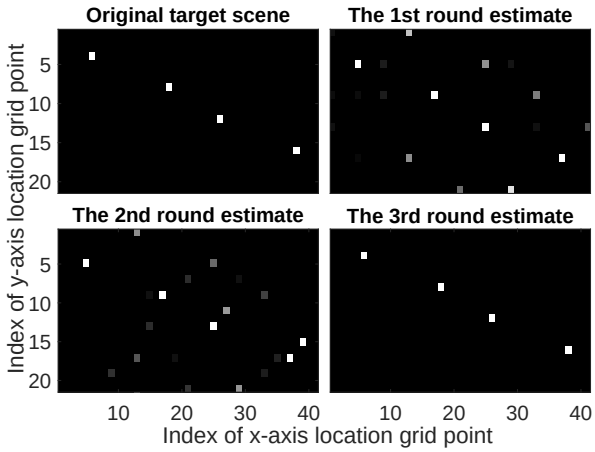

Figure 3.10: The estimated target scene in location space by a three-level grid refinement scheme.

block diagonal measurement matrix. The proposed theoretical results validate that the structures in both $\mathbf{\Psi}$ and $\mathbf{s}$ result in reduction of the number of measurements needed, or result in improved target estimation for the same L.

Two low-complexity approaches have been proposed to reduce the computation while maintaining the estimation performance. The first approach was an ADMM-based sparse signal recovery algorithm. Simulation results have indicated that this approach significantly lowers the computational complexity for target estimation with improved accuracy as compared to the approaches using proximal gradient algorithm and interior point method. The second approach decouples the location and speed estimation into two separate stages. The location estimation obtained in the first stage is used to prune the target location-speed space in the speed estimation stage. Simulations have indicated that the decoupled scheme can reduce both the computation and the required number of measurements, while maintaining high estimation accuracy.

3.A Proof of Theorem 2

Proof. Here we only focuss on the bounds for the off-diagonal entries in the Gram of $\bar{\mathbf{\Psi}}$, $\mathbf{G} = \bar{\mathbf{\Psi}}^H \bar{\mathbf{\Psi}}$. For the diagonal entries, *i.e.*, $n = l$ as in case (i), the union bound can be easily obtained based on (3.13).

The off-diagonal entries may be from either case (ii) or case (iii). In order to arrive at a

uniform union bound, we need to unify the bounds in (3.17) and (3.19) for these two cases. Inequality (3.17) for case (ii) can be relaxed as

$$\Pr\left(|G_{ij}(n,l)| > t\right) \leq 4\exp\left(-\frac{L-1}{16}t^2\right). \tag{3.43}$$

Under condition (3.20), the probabilistic bound in (3.19) for case (iii) can be relaxed to the same as that in (3.43) for case (ii).

Following the classical procedure of RIP analysis in [88], we need to evaluate the radii of the Gergošin's discs for the sub-matrix of $\mathbf{G}$ constructed based on the support of $\mathbf{s}$. Recall that $\bar{\mathbf{\Psi}}$ is block diagonal and there are only K nonzero entries in each sub-vector $\mathbf{s}_{ij}$ in $\mathbf{s}$. Therefore, there are only $(K-1)$ instead of $(K-1)M_tM_r$ off-diagonal entries contributing to the radii of the Gergošin's discs. This reduction comes from the BD structure of $\tilde{\mathbf{\Psi}}$ and the sparsity profile of $\mathbf{s}$ characterized by $\mathcal{A}_1^K$. Here we choose $\delta_d \triangleq \frac{\delta_K}{K}$ and $\delta_o \triangleq \frac{(K-1)\delta_K}{K}$. Substituting t with $\delta_o/(K-1)$ in (3.43) gives the unified bound for any of the off-diagonal entries, *i.e.*,

$$\Pr\left(|G_{ij}(n,l)| > \frac{\delta_K}{K}\right) \leq 4\exp\left(-\frac{(L-1)\delta_K^2}{16K^2}\right). \tag{3.44}$$

under the condition of (3.21b), which is derived by substituting $t = \delta_K/K$ into (3.20). Following the steps of [88] the proof follows. □

Chapter 4

A Joint Design Approach for Spectrum Sharing between Radar and Communication Systems

A joint design approach is proposed for the coexistence of MIMO radars and a communication system, for a scenario in which the targets fall in different range bins. Radar transmit precoding and adaptive communication transmission are adopted, and are jointly designed to maximize signal-to-interference-plus-noise ratio (SINR) at the radar receiver subject to the communication system meeting certain rate and power constraints. We start with the design of a system in which knowledge of the target information is used. Such design can be used to benchmark the performance of schemes that do not use target information. Then, we propose a design which does not require target information. In both cases, the optimization problems are nonconvex w.r.t. the design variables and have high computational complexity. Alternating optimization and sequential convex programming techniques are used to find a local maximum. Based on the analysis of the obtained solution, we propose a reduced dimensionality design, which has reduced complexity without degrading the radar SINR. Simulation results validate the effectiveness of the proposed spectrum sharing framework.

4.1 Introduction

The operating frequency bands of communication and radar systems often overlap, causing one system to exert interference to the other. For example, the high UHF radar systems overlap with GSM communication systems, and the S-band radar systems partially overlap with Long Term Evolution (LTE), and WiMax systems [42, 43, 53, 98]. Spectrum sharing is a new line of work whose goal is to enable radar and communication systems to share the spectrum efficiently by minimizing interference effects [42–49].

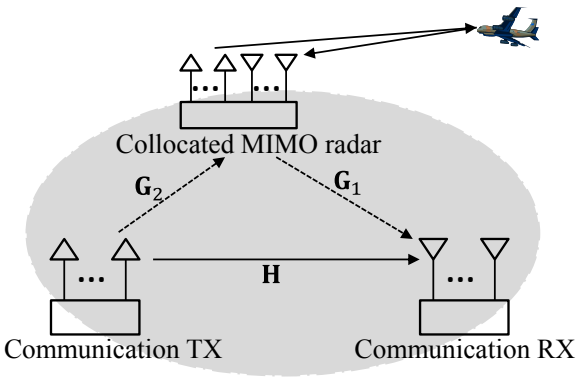

Figure 4.1: A MIMO communication system sharing spectrum with a colocated MIMO radar system.

Spectrum sharing between MIMO radar and communication systems has been considered in [43–46], where the radar interference to the communication system is eliminated by projecting the radar waveforms onto the null space of the interference channel from radar to communication systems. However, projection-type techniques might miss targets lying in the row space of the interference channel. Spatial filtering at the radar receiver is proposed in [47] to reject interference from the communication systems. This approach, however, works only if the target is not in the direction of the interference coming from the communication system.

Most of the existing radar-communication spectrum sharing literature addresses interference mitigation either for the communication systems [43–46], or for the radar [47]. To the best of our knowledge, co-design of radar and communication systems for spectrum sharing was proposed in [99–101] for the first time. Compared to the radar design approaches of [43–47], the joint design has the potential to improve the spectrum utilization due to increased number of design degrees of freedom. However, the results of [99–101] were developed for a scenario in which all targets fall in the same range bin, and the propagation delay is properly compensated.

In this chapter, we propose a spectrum sharing framework for the coexistence of MIMO radars and a communication system, for a scenario in which the targets fall in different range bins. The coexistence model considers the radar operation pattern, *i.e.*, transmitting a short pulsed waveform and listening target echoes for a much longer period. Radar transmit (TX) precoding and adaptive communication transmission are adopted and are jointly

designed. Unlike the radar waveform projection based methods, the joint design approach could potentially align the target returns and the communication interference separately in different subspaces, and thus suppress the interference without degrading the target returns. We formulate the design problem as maximization of SINR at the radar receiver subject to the communication system meeting certain rate and power constraints. We start with the design of a system in which knowledge of the target information (e.g., delays, reflectivities) is used. Such design can be used to benchmark the performance of schemes that do not use target information. Then, we propose a design which does not require target information. In both cases, the optimization problems are nonconvex w.r.t. the design variables and have high computational complexity. Alternating optimization and sequential convex programming techniques are used to find a local maximum. Analysis on the obtained solution indicates that a two-level constant communication rate over the radar TX period and the radar listening-only period could achieve the same radar SINR as the adaptive transmission. Based on this fact, we propose a new design with a much lower dimension which has reduced complexity without degrading the radar SINR. Simulation results validate the effectiveness of the proposed spectrum sharing methods over methods based on noncooperative spectrum access.

This chapter is organized as follows. Section 4.2 introduces the coexistence model of a MIMO radar system and a communication system. The proposed spectrum sharing method is given in Section 4.3. Numerical results and conclusions are provided respectively in Sections 4.4 and 4.5.

4.2 System Models

Consider a MIMO communication system which coexists with a MIMO radar system as shown in Fig. 4.1, sharing the same carrier frequency. The MIMO radar system uses $M_{t,R}$ TX and $M_{r,R}$ RX collocated antennas for target detection/estimation. The communication transmitter and receiver are equipped with $M_{t,C}$ and $M_{r,C}$ antennas, respectively. The communication channel is denoted as $\mathbf{H} \in \mathbb{C}^{M_{r,C} \times M_{t,C}}$. The interference channel from the radar TX antennas to the communication receiver is denoted as $\mathbf{G}_1 \in \mathbb{C}^{M_{r,C} \times M_{t,R}}$ [43, 44, 46]; the interference channel from the communication transmitter to the radar RX antennas

is denoted as $\mathbf{G}_2 \in \mathbb{C}^{M_{r,R} \times M_{t,C}}$. It is assumed that the channels $\mathbf{H}$, $\mathbf{G}_1$ and $\mathbf{G}_2$ are block fading [102] and perfectly known at the communication transmitter. In practice, the channel state information can be obtained through the transmission of pilot signals [43, 103]. The detailed signal models for the MIMO radar and communication systems are described in the sequel. We do not assume perfect carrier phase synchronization between the two systems. A graphical illustration of the received signal at the radar and communication receivers is provided in Fig. 4.2.

The MIMO radar employs narrowband orthogonal waveforms, each of which contains L coded sub-pulses, each of duration T_b. Let $\mathbf{s}_m \triangleq [s_{m1}, \ldots, s_{mL}]^T$ denote the orthogonal code vector for the m-th TX antenna. It holds that $\langle \mathbf{s}_m, \mathbf{s}_n \rangle = \delta_{mn}$. The waveforms are first precoded by matrix $\mathbf{P} \in \mathbb{C}^{M_{t,R} \times M_{t,R}}$, and then transmitted over carrier f_c periodically, with pulse repetition interval T_{PRI}. Suppose that there are K targets on the same plane with the antennas, each at directions of arrival $\{\theta_k\}$ and range $\{d_k\}$ w.r.t. the radar phase center. During each pulse, the target echoes and communication interference received at the radar RX antennas are demodulated to baseband and sampled every T_b seconds. The discrete time signal model for sampling time index $l \in \mathbb{N}_{\tilde{L}}^+$ is expressed as

$$\mathbf{y}_R(l) = \sum_{k=1}^{K} \beta_k \mathbf{v}_r(\theta_k) \mathbf{v}_t^T(\theta_k) \mathbf{P} \mathbf{s}(l - l_k) + \mathbf{G}_2 \mathbf{x}(l) e^{j\alpha_2(l)} + \mathbf{w}_R(l), \tag{4.1}$$

where $\tilde{L} = \lfloor T_{PRI}/T_b \rfloor$ denotes the total number of samples in one PRI; $\mathbf{y}_R(l)$ and $\mathbf{x}(l)$ respectively denote the radar received signal and communication waveform symbol at time lT_b; $\mathbf{s}(l) = [s_{1l}, \ldots, s_{M_{t,R}l}]^T$; $\mathbf{w}_R(l)$ is noise distributed as $\mathcal{CN}(\mathbf{0}, \sigma_R^2 \mathbf{I})$; $l_k = \lfloor \tau_k / T_b \rfloor$ with $\tau_k \triangleq 2d_k/v_c$; β_k denotes the complex radar cross section for the k-th target; the Swerling II target model is assumed, *i.e.*, the β_k's vary from pulse to pulse and have distribution $\mathcal{CN}(0, \sigma_{\beta k}^2)$; and $\mathbf{v}_r(\theta) \in \mathbb{C}^{M_{r,R}}$ is the receive steering vector defined as

$$\mathbf{v}_r(\theta) \triangleq \left[e^{j2\pi \langle \mathbf{d}_1^r, \mathbf{u}(\theta) \rangle / \lambda_c}, \ldots, e^{j2\pi \langle \mathbf{d}_{M_{r,R}}^r, \mathbf{u}(\theta) \rangle / \lambda_c} \right]^T,$$

with $\mathbf{d}_1^r \triangleq [x_m^r \, y_m^r]^T$ denoting the two-dimensional coordinates of the m-th RX antenna, $\mathbf{u}(\theta) \triangleq [\cos(\theta) \, \sin(\theta)]^T$, and λ_c denoting the carrier wavelength. $\mathbf{v}_t(\theta) \in \mathbb{C}^{M_{t,R}}$ is the transmit steering vector and is respectively defined. The second term on the right hand side of (4.1) denotes the interference due to the communication transmission $\mathbf{x}(l) \in \mathbb{C}^{M_{t,C}}$. $e^{j\alpha_2(l)}$ is introduced to denote the random phase offset resulting from the random phase jitter of the oscillators at the communication transmitter and the MIMO radar receiver

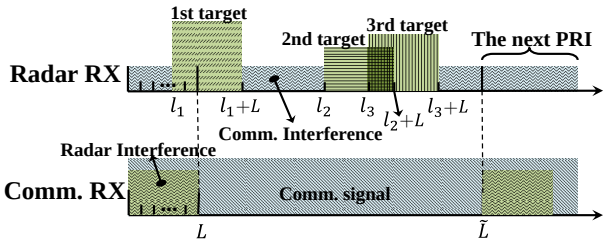

Figure 4.2: An illustration of the received signal at radar and communication receivers. At the radar receiver, echoes returned from three targets are present during periods $\mathcal{L}_k, k = 1, 2, 3$ with $\mathcal{L}_k \triangleq \{l_k, ..., l_k + L - 1\}$, while the interference from the communication system is present during the whole PRI. Echoes from the second and third targets overlap with each other. At the communication receiver, the radar interference is only present during the first L symbols.

Phase-Locked Loops [100]. In the literature [104–106], phase jitter is modeled as zero-mean Gaussian process. Note that $\mathbf{s}(l)$ is nonzero only for $l \in \mathbb{N}_L^+$. The echo from the k-th target appears starting from l_k and lasts for L samples.

The MIMO communication system uses the same carrier frequency f_c. The baseband signal at the communication receiver is sampled according to the symbol rate T_s, which could be different than the radar waveform symbol duration T_b. In this chapter, we only consider the matched case, *i.e.*, $T_s = T_b$; the extension of the proposed methods to the mismatched case is straightforward [100]. The discrete time communication signal has the following form

$$\mathbf{y}_C(l) = \mathbf{H}\mathbf{x}(l) + \mathbf{G}_1\mathbf{P}\mathbf{s}(l)e^{j\alpha_1(l)} + \mathbf{w}_C(l),\ l \in \mathbb{N}_{\tilde{L}}^+, \tag{4.2}$$

where $\mathbf{x}(l) \in \mathbb{C}^{M_{t,C}}$ denotes the transmit vector at the communication transmitter at time index l; $e^{j\alpha_1(l)}$ denotes the random phase offset between the radar TX carrier and the communication RX reference carrier [100]; the additive noise $\mathbf{w}_C(l)$ has distribution $\mathcal{CN}(\mathbf{0}, \sigma_C^2\mathbf{I})$. Note that the radar waveform $\mathbf{s}(l)$ equals zero when $l > L$, which means that the communication system is interference free during this period. The above model assumes that the radar transmission is the only interference, while the target returns do not reach the communication system.

4.3 Proposed Spectrum Sharing Framework

The figure of merit for the communication system is the achievable channel capacity. For the communication receiver, there are two distinct periods: one containing $l \in \mathbb{N}_{\tilde{L}}^+ \setminus \mathbb{N}_L^+$, during which only additive noise is present, and another one containing $l \in \mathbb{N}_L^+$, during which both

interference and noise are present. Let the interference covariance during the latter period be $\mathbf{R}_{\mathrm{Ci}l} = \mathbf{G}_1\mathbf{P}\mathbb{E}\{\mathbf{s}(l)\mathbf{s}^H(l)\}\mathbf{P}^H\mathbf{G}_1^H$. In this chapter, as in [101] we choose $\mathbf{S}$ as a random orthonormal matrix. Note that the entries of $\mathbf{S}$ are not independent anymore. However, based on [107, Theorem 3], if $M_{t,R} = \mathcal{O}(L/\ln L)$, the entries of $\mathbf{S}$ can be approximated by i.i.d. Gaussian random variables with distribution $\mathcal{N}(0, 1/L)$. The communication system is aware that $\mathbf{S}$ is orthonormal but has no access to the specific realization of $\mathbf{S}$. Based on the above, the radar interference covariance matrix equals $\mathbf{R}_{\mathrm{Ci}l} \equiv \mathbf{R}_{\mathrm{Ci}} \triangleq \mathbf{G}_1\mathbf{\Phi}\mathbf{G}_1^H$ for any $l \in \mathbb{N}_L^+$, where $\mathbf{\Phi} \triangleq \mathbf{P}\mathbf{P}^H/L$ is positive semidefinite.

The overall communication system capacity can be maximized using adaptive rate transmission [52, 108]. For $l \in \mathbb{N}_L^+$, the *instaneous* capacity is unknown because the interference plus noise is not necessarily Gaussian due to the random phase offset $\alpha_1(l)$. In this chapter, we are interested in a lower bound of the capacity. However, Gaussian noise with covariance matrix equal to the actual noise covariance is the worst-case noise for additive noise channels [109]. The lower bound of the capacity is given by $\underline{C}(\mathbf{R}_{xl}, \mathbf{\Phi}) \triangleq \log_2\left|\mathbf{I} + \mathbf{R}_{\mathrm{Cin}l}^{-1}\mathbf{H}\mathbf{R}_{xl}\mathbf{H}^H\right|$, which is achieved when the codeword $\mathbf{x}(l)$, $l \in \mathbb{N}_L^+$ is distributed as $\mathcal{CN}(0, \mathbf{R}_{xl})$. Similar to the definition of ergodic capacity [108], the overall communication capacity should be the average over $\tilde{L}$ symbols, *i.e.*,

$$\mathrm{C}_{\mathrm{avg}}(\{\mathbf{R}_{xl}\}, \mathbf{\Phi}) \triangleq 1/\tilde{L}\sum\nolimits_{l=1}^{\tilde{L}} \log_2\left|\mathbf{I} + \mathbf{R}_{\mathrm{Cin}l}^{-1}\mathbf{H}\mathbf{R}_{xl}\mathbf{H}^H\right|, \tag{4.3}$$

where $\{\mathbf{R}_{xl}\}$ denotes the set of all $\mathbf{R}_{xl}$'s, and $\mathbf{R}_{\mathrm{Cin}l}$ equals $\mathbf{R}_{\mathrm{Ci}} + \sigma_C^2\mathbf{I}$ if $l \in \mathbb{N}_L^+$, otherwise $\sigma_C^2\mathbf{I}$.

For the radar system, the SINR has been commonly used as figure of merit in the waveform design literature with the prior knowledge of targets and the surrounding environment [110–113]. The covariance of the interference exerted at the radar RX antennas during the l-th symbol equals $\mathbb{E}\{\mathbf{G}_2\mathbf{x}(l)e^{j\alpha_2(l)}e^{-j\alpha_2(l)}\mathbf{x}^H(l)\mathbf{G}_2^H\} = \mathbf{G}_2\mathbf{R}_{xl}\mathbf{G}_2^H$. The echoes returned from the k-th target are present during $\mathcal{L}_k \triangleq \{l_k, \cdots, l_k + L - 1\}$, and have covariance $\mathbf{D}_k\mathbf{\Phi}\mathbf{D}_k^H$ for any $l \in \mathcal{L}_k$, where $\mathbf{D}_k \triangleq \sigma_{\beta k}\mathbf{v}_r(\theta_k)\mathbf{v}_t^T(\theta_k)$. The local SINR associated with the k-th target is averaged over $\mathcal{L}_k$ [112]

$$\mathrm{SINR}_k = 1/L\sum\nolimits_{l\in\mathcal{L}_k} \mathrm{Tr}\big(\mathbf{R}_{\mathrm{Rin}l}^{-1}\mathbf{D}_k\mathbf{\Phi}\mathbf{D}_k^H\big), \tag{4.4}$$

where $\mathbf{R}_{\text{Rin}l} \triangleq \mathbf{G}_2\mathbf{R}_{xl}\mathbf{G}_2^H + \sigma_R^2\mathbf{I}$. The overall SINR is defined as

$$\text{SINR} \triangleq \frac{1}{K}\sum_{k=1}^{K}\text{SINR}_k(\{\mathbf{R}_{xl}\}_{\mathcal{L}_k}, \mathbf{\Phi}).$$

In the following, we first present the formulation based on target prior information, *i.e.*, knowledge based spectrum sharing, and then the formulation for the worst case design strategy, which does not rely on target information, *i.e.*, robust spectrum sharing.

1) Knowledge-based spectrum sharing. In some cases, targets information can be maintained from the detection and tracking history [111, 114]. Since in most cases such information does not exist, the design for this case will be used to benchmark other methods that are more practical. Assuming that $\{\sigma_{\beta k}^2\}$, $\{l_k\}$, and $\{\theta_k\}$ are known, the design problem is to maximize the radar SINR, subject to satisfying the communication rate and TX power constraints:

$$(\mathbf{P}_1) \quad \max_{\{\mathbf{R}_{xl}\}\succeq 0, \mathbf{\Phi}\succeq 0} \text{SINR, s.t. } \text{C}_{\text{avg}}(\{\mathbf{R}_{xl}\}, \mathbf{\Phi}) \geq C, \tag{4.5a}$$

$$\sum\nolimits_{l=1}^{\tilde{L}} \text{Tr}\left(\mathbf{R}_{xl}\right) \leq P_C, L\text{Tr}\left(\mathbf{\Phi}\right) \leq P_R, \tag{4.5b}$$

The constraint of (4.5a) restricts the communication rate to be at least C, in order to avoid service outage. The constraints of (4.5b) restrict the total communication and radar TX power to be no larger than P_C and P_R, respectively.

2) Robust spectrum sharing with unknown $\{\sigma_{\beta k}^2\}$ and $\{l_k\}$. Here we consider the scenario where the radar searches in particular directions of interest given by set $\{\theta_k\}$ for targets with unknown RCS variances and delays [3, 113]. The worst possible target RCS variances are given by $\{\sigma_{\beta k}^2\} \equiv \sigma_\beta^2$, where σ_β^2 is the smallest target RCS variance that could be detected by the radar. Since $\mathcal{L}_k$ is unknown, the local SINR_k associated with the k-th target is relaxed to the whole PRI

$$\text{SINR}_k' = 1/\tilde{L}\sum\nolimits_{l\in\mathbb{N}_{\tilde{L}}^+} \text{Tr}\left(\mathbf{R}_{\text{Rin}l}^{-1}\mathbf{D}_k\mathbf{\Phi}\mathbf{D}_k^H\right), \tag{4.6}$$

where $\mathbf{D}_k \triangleq \sigma_\beta \mathbf{v}_r(\theta_k)\mathbf{v}_t^T(\theta_k)$. The overall SINR is given by $\text{SINR}' \triangleq 1/K\sum_{k=1}^{K}\text{SINR}_k'$. Now, the spectrum sharing problem can be formulated as

$$(\mathbf{P}_2) \quad \max_{\{\mathbf{R}_{xl}\}\succeq 0, \mathbf{\Phi}\succeq 0} \text{SINR}', \text{ s.t. same constraints as in } (\mathbf{P}_1).$$

Both $(\mathbf{P}_1)$ and $(\mathbf{P}_2)$ are nonconvex w.r.t. variable pair $(\{\mathbf{R}_{xl}\}, \mathbf{\Phi})$. In the following, we will focus on the algorithm that solves $(\mathbf{P}_2)$, which could also be adapted to solve $(\mathbf{P}_1)$.

4.3.1 Iterative algorithm for solving $(\mathbf{P}_2)$

A solution can be obtained via alternating optimization. Let $(\{\mathbf{R}_{xl}^n\}, \mathbf{\Phi}^n)$ be the variable at the n-th iteration. *First*, we solve $\{\mathbf{R}_{xl}^n\}$ while fixing $\mathbf{\Phi}$ to be $\mathbf{\Phi}^{n-1}$:

$$\begin{aligned}(\mathbf{P_R}) \ &\max_{\{\mathbf{R}_{xl}\}\succeq 0} 1/K \sum_{k=1}^{K} \mathrm{SINR}_k'(\{\mathbf{R}_{xl}\}, \mathbf{\Phi}^{n-1}) \\ &\text{s.t. } \mathrm{C_{avg}}(\{\mathbf{R}_{xl}\}, \mathbf{\Phi}^{n-1}) \geq C, \sum_{l=1}^{\tilde{L}} \mathrm{Tr}\left(\mathbf{R}_{xl}\right) \leq P_C.\end{aligned} \tag{4.7}$$

Let us rewrite the objective as $\sum_{l=1}^{\tilde{L}} f(\mathbf{R}_{xl})$, with

$$f(\mathbf{R}_{xl}) \triangleq \mathrm{Tr}\left(\left(\mathbf{G}_2\mathbf{R}_{xl}\mathbf{G}_2^H + \sigma_R^2\mathbf{I}\right)^{-1}\mathcal{D}^{n-1}\right), \tag{4.8}$$

where $\mathcal{D}^{n-1} = \sum_{k=1}^{K} \mathbf{D}_k\mathbf{\Phi}^{n-1}\mathbf{D}_k^H$, and constant scale factors are omitted. It can be shown that $f(\mathbf{R}_{xl})$ is convex w.r.t $\mathbf{R}_{xl}$. Problem $(\mathbf{P_R})$ is nonconvex w.r.t. $\mathbf{R}_{xl}$, because it maximizes a convex function. The sequential convex programming technique is used to find a local optimal solution [**Boyd**]. $f(\mathbf{R}_{xl})$ can be approximated by the first order Taylor series expansion at $\bar{\mathbf{R}}_{xl}$ as

$$\begin{aligned}f(\mathbf{R}_{xl}) \approx &\tilde{f}(\mathbf{R}_{xl}) \triangleq f(\bar{\mathbf{R}}_{xl}) \\ &+ \mathrm{Tr}\left[\left(\frac{\partial f(\mathbf{R}_{xl})}{\partial \Re(\mathbf{R}_{xl})}\right)^T_{\mathbf{R}_{xl}=\bar{\mathbf{R}}_{xl}} (\mathbf{R}_{xl} - \bar{\mathbf{R}}_{xl})\right],\end{aligned}$$

where $\frac{\partial f(\mathbf{R}_{xl})}{\partial \Re(\mathbf{R}_{xl})} = -[\mathbf{G}_2^H\mathbf{R}_{\mathrm{Rin}l}^{-1}\mathcal{D}^{n-1}\mathbf{R}_{\mathrm{Rin}l}^{-1}\mathbf{G}_2]^T$.

We can see that $\tilde{f}(\mathbf{R}_{xl})$ is now an affine function of $\mathbf{R}_{xl}$. Problem $(\mathbf{P_R})$ can be approximated by the following convex problem:

$$\begin{aligned}(\tilde{\mathbf{P}}_{\mathbf{R}}) \ &\max_{\{\mathbf{R}_{xl}\}\succeq 0} \sum_{l=1}^{\tilde{L}} \tilde{f}(\mathbf{R}_{xl}) \\ &\text{s.t. } \mathrm{C_{avg}}(\{\mathbf{R}_{xl}\}, \mathbf{\Phi}^{n-1}) \geq C, \sum_{l=1}^{\tilde{L}} \mathrm{Tr}\left(\mathbf{R}_{xl}\right) \leq P_C.\end{aligned} \tag{4.9}$$

which can be solved with available convex programming packages. The original problem $(\mathbf{P_R})$ could be solved via several iterations of solving $(\tilde{\mathbf{P}}_{\mathbf{R}})$. At each iteration, $\{\bar{\mathbf{R}}_{xl}\}$ is updated with the optimal solution of the previous iteration. The iteration stops when the increase of SINR is small. In addition, we observe that both the objective and constraints are separable functions of $\{\mathbf{R}_{xl}\}$. Dual decomposition technique could be used to solve (4.9) with lower computation complexity.

Second, the obtained $\{\mathbf{R}_{xl}^n\}$ are used to solve the following problem for $\mathbf{\Phi}^n$:

$$(\mathbf{P}_\Phi) \max_{\mathbf{\Phi}\succeq 0} \mathrm{Tr}\left(\mathbf{Q}^n\mathbf{\Phi}\right) \text{ s.t. } \mathrm{C_{avg}}(\{\mathbf{R}_{xl}^n\}, \mathbf{\Phi}) \geq C, L\mathrm{Tr}\left(\mathbf{\Phi}\right) \leq P_R,$$

where $\mathbf{Q}^n \triangleq \sum_{k=1}^{K} \mathbf{D}_k^H\left[\sum_{l=1}^{\tilde{L}}\left(\mathbf{G}_2\mathbf{R}_{xl}^n\mathbf{G}_2^H + \sigma_R^2\mathbf{I}\right)^{-1}\right]\mathbf{D}_k$.

Let $C_l(\mathbf{R}_{xl}^n, \mathbf{\Phi}) \triangleq \log_2 \left|\mathbf{I} + \mathbf{R}_{\text{Cin}l}^{-1}\mathbf{H}\mathbf{R}_{xl}^n\mathbf{H}^H\right|$; this is function of $\mathbf{\Phi}$ only if $l \in \mathbb{N}_L^+$. The first constraint in $(\mathbf{P}_\Phi)$ can be rewritten as $\sum_{l=1}^{L} C_l(\mathbf{R}_{xl}^n, \mathbf{\Phi}) \geq \tilde{L}C - \sum_{l=L+1}^{\tilde{L}} C_l(\mathbf{R}_{xl}^n) \triangleq \tilde{C}^n$. We could express $C_l(\mathbf{R}_{xl}^n, \mathbf{\Phi})$, $\forall l \in \mathbb{N}_L^+$, as follows

$$\begin{aligned} C_l(\mathbf{R}_{xl}^n, \mathbf{\Phi}) &= \log_2 \left|\mathbf{R}_{\text{Cin}l} + \mathbf{H}\mathbf{R}_{xl}^n\mathbf{H}^H\right| - \log_2 \left|\mathbf{R}_{\text{Cin}l}\right| \\ &= \log_2 \left|\mathbf{G}_1\mathbf{\Phi}\mathbf{G}_1^H + \tilde{\mathbf{R}}_{xl}^n\right| - \log_2 \left|\mathbf{G}_1\mathbf{\Phi}\mathbf{G}_1^H + \sigma_C^2\mathbf{I}\right|, \end{aligned} \tag{4.10}$$

where $\tilde{\mathbf{R}}_{xl}^n \triangleq \sigma_C^2\mathbf{I} + \mathbf{H}\mathbf{R}_{xl}^n\mathbf{H}^H$. We can see that $C_l(\mathbf{R}_{xl}^n, \mathbf{\Phi})$ is in the form of a concave function plus a convex function. It can be shown that $C_l(\mathbf{R}_{xl}^n, \mathbf{\Phi})$ is actually a convex function of $\mathbf{\Phi}$. Thus, $(\mathbf{P}_\Phi)$ is nonconvex because the above constraint imposes a nonconvex feasible set on $\mathbf{\Phi}$. A similar problem is considered in [101, Eq. (5)]. As in [101], we introduce a slack variable $\mathbf{\Psi}$ to overcome the non-convexity and apply alternating optimization again as an inner iteration. Let $(\mathbf{\Phi}^{ni}, \mathbf{\Psi}^{ni})$ be the variables at the i-th inner iteration corresponding to the n-th outer alternating iteration. $\mathbf{\Phi}^{ni}$ is initialized as $\mathbf{\Phi}^{n-1}$ for $i = 0$. Given $\mathbf{\Phi}^{n(i-1)}$, $\mathbf{\Psi}^{ni}$ is obtained as follows

$$\mathbf{\Psi}^{ni} = \left(\mathbf{G}_1\mathbf{\Phi}^{n(i-1)}\mathbf{G}_1^H + \sigma_C^2\mathbf{I}\right)^{-1}. \tag{4.11}$$

Based on $\mathbf{\Psi}^{ni}$, $\mathbf{\Phi}^{ni}$ is obtained by solving the following problem

$$\begin{aligned} (\mathbf{P}'_\Phi) \quad & \max_{\mathbf{\Phi}\succeq 0} \text{Tr}\left(\mathbf{Q}^n\mathbf{\Phi}\right), \quad \text{s.t.} \;\; L\text{Tr}\left(\mathbf{\Phi}\right) \leq P_R, \\ & \sum_{l\in\mathbb{N}_L^+} \log_2 \left|\mathbf{I} + \mathbf{G}_1^H(\tilde{\mathbf{R}}_{xl}^n)^{-1}\mathbf{G}_1\mathbf{\Phi}\right| - L\text{Tr}\left(\mathbf{G}_1^H\mathbf{\Psi}^{ni}\mathbf{G}_1\mathbf{\Phi}\right) \geq C', \end{aligned}$$

where $C' \triangleq \tilde{C}^n + L\left\{\sigma_C^2\text{Tr}(\mathbf{\Psi}^{ni}) - \log_2\left|\mathbf{\Psi}^{ni}\right| - M_{r,C}\right\} - \sum_{l\in\mathbb{N}_L^+} \log_2 \left|\tilde{\mathbf{R}}_{xl}^n\right|$. $(\mathbf{P}'_\Phi)$ is convex w.r.t. $\mathbf{\Phi}$ and thus can be solved using available software packages **[Boyd]**.

The complete proposed spectrum sharing algorithm alternately solves $(\mathbf{P}_R)$ and $(\mathbf{P}_\Phi)$ as stated above. It is easy to show that the value of SINR is nondecreasing during the alternating iterations. Also, the SINR has a upper bound. Therefore, the algorithm converges. The iteration stops if the improvement of SINR is smaller than a certain threshold.

4.3.2 Discussion

The adaptive transmission technique adopted by the communication system greatly increases the complexity of the spectrum sharing problem $(\mathbf{P}_2)$. The following property can be used to reduce the complexity of solving $(\mathbf{P}_2)$ without any performance degradation.

Proposition 3. *Suppose that* $\{\mathbf{R}_{xl}\}$ *is initialized by* $\{\mathbf{R}_{xl}\} \equiv \mathbf{R}_x^0$. *Then, the optimal value of* $(\mathbf{P}_R)$ *in every iteration of the proposed algorithm could be achieved by* $\{\mathbf{R}_{xl}^n\}$ *such that for any* $l, l' \in \mathbb{N}_L^+$ *(or* $l, l' \in \mathbb{N}_{\tilde{L}}^+ \setminus \mathbb{N}_L^+$*), it holds that* $\mathbf{R}_{xl}^n = \mathbf{R}_{xl'}^n$.

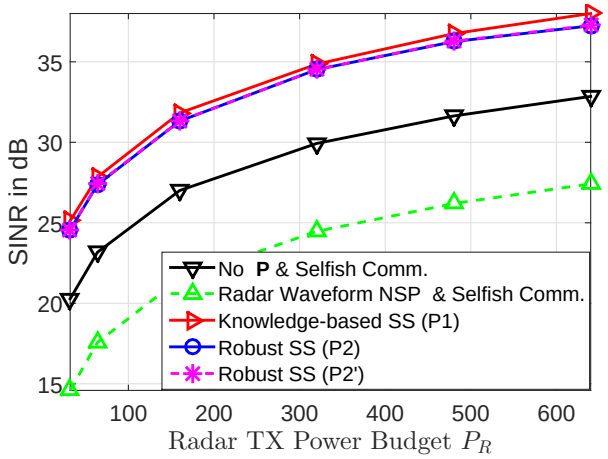

Figure 4.3: SINR performance vs different values of radar TX power.

The proof can be found in Section 4.A. The above proposition indicates that it suffices to use only two matrix variables, $\mathbf{R}_{x1}$ and $\mathbf{R}_{x2}$, as the communication transmission covariance matrices respectively for two periods, the one during which radar transmits and the one during which radar only receives. The spectrum sharing problem can be reformulated as following

$$(\mathbf{P}_2') \quad \max_{\{\mathbf{R}_{xl}\}\succeq 0, \mathbf{\Phi}\succeq 0} \ \frac{1}{K}\sum_{l=1}^{2} \mathrm{Tr}\left(\eta_l \mathbf{R}_{\mathrm{Rin}l}^{-1} \sum\nolimits_{k=1}^{K} \mathbf{D}_k \mathbf{\Phi} \mathbf{D}_k^H\right)$$

$$\text{s.t.} \ \sum_{l=1}^{2} \eta_l C_l(\mathbf{R}_{xl}, \mathbf{\Phi}) \geq C, \sum_{l=1}^{2} \eta_l \tilde{L}\mathrm{Tr}\left(\mathbf{R}_{xl}\right) \leq P_C, L\mathrm{Tr}\left(\mathbf{\Phi}\right) \leq P_R,$$

where $\eta_1 \triangleq L/\tilde{L}$ is called the duty cycle and $\eta_2 = 1 - \eta_1$. Again, alternating optimization and sequential convex programming techniques used in Section 4.3.1 could be applied to solve $(\mathbf{P}_2')$, which could achieve the same radar SINR objective as $(\mathbf{P}_2)$. We can observe that the robust communication transmission scheme for unknown target ranges is constant rate transmission over two periods. This is reasonable in the sense that the achieved radar SINR would be constant across different target ranges, and thus abrupt SINR degradation for certain target ranges would be avoided.

4.4 Numerical Results

We next conduct some simulation results to quantify the comparative performance of the designs based on solving $(\mathbf{P}_1)$, $(\mathbf{P}_2)$, $(\mathbf{P}_2')$, and also include results based the projection method of [46].

We set the number of samples per PRI to $\tilde{L} = 32$, the number of radar waveform symbols to $L = 8$, the noise variance to $\sigma_C^2 = \sigma_R^2 = 0.01$, and the number of antennas

to $M_{t,R} = M_{r,R} = M_{t,C} = M_{r,C} = 4$. The MIMO radar system consists of collocated TX and RX antennas forming half-wavelength uniform linear arrays. The radar waveforms are chosen from the rows of a random orthonormal matrix [99]. There are three stationary targets at angles $-60°$, $0°$ and $60°$ w.r.t. to the arrays, and the corresponding target propagation delays are $6, 18$ and 22. This corresponds to the scenario depicted in Fig. 4.2. For the communication capacity and power constraints, we take $C = 24$ bits/symbol and $P_C = \tilde{L}M_{t,C}$ (the power is normalized by the power of the radar waveform). The interference channels $\mathbf{G}_1$ and $\mathbf{G}_2$ are generated with entries which are independent and distributed as $\mathcal{CN}(0, 0.01)$. The channel $\mathbf{H}$ has independent entries, distributed as $\mathcal{CN}(0, 1)$. The communication covariance matrix and the radar precoding matrix are jointly optimized according to $(\mathbf{P}_1)$, $(\mathbf{P}_2)$ and $(\mathbf{P}_2')$ in Section 4.3. For comparison, we implement methods based on uniform precoding, *i.e.*, $\mathbf{P} = \sqrt{LP_R/M_{t,R}}\mathbf{I}$, and null space projection (NSP) precoding, *i.e.*, $\mathbf{P} = \sqrt{LP_R/M_{t,R}}\mathbf{V}\mathbf{V}^H$, where $\mathbf{V}$ contains the basis of the null space of $\mathbf{G}_1$ [46]. In both of the aforementioned methods, selfish communication is considered, *i.e.*, the communication system minimizes the transmit power to achieve capacity C without any concern about the interferences it exerts to the radar system.

Fig. 4.3 shows the SINR results for different values of the radar transmit power budget (P_R). The radar power budget per antenna ranges from 1 to 20 times of the communication power budget per antenna. The highest SINR, as expected, corresponds to the case in which pretty much everything is known about the targets, *i.e.*, via the joint design of $\mathbf{P}$ and $\{\mathbf{R}_{xl}\}$ resulting from $(\mathbf{P}_1)$. Interestingly, the design of $(\mathbf{P}_2)$, which uses no knowledge about the targets incurs an SINR loss of 1 dB only. Also interestingly, the low complexity spectrum sharing method of $(\mathbf{P}_2')$, which does not use any knowledge about the targets, achieves the same SINR performance as $(\mathbf{P}_2)$. For this particular example, as compared to $(\mathbf{P}_2)$, in $(\mathbf{P}_2')$ the number of matrix variables is reduced from 33 to 3.

As expected, the selfish communication schemes with no precoding involves no cooperation between the radar and communication systems, and thus achieves the worst performance. The projection-type method of [46] performs even worse, because targets may fall in the row space of $\mathbf{G}_1$.

4.5 Conclusion

We have considered a general spectrum sharing framework between a MIMO radar and a MIMO communication system. Depending on the availability of target range information, a knowledge-based and a robust spectrum sharing approach were proposed to maximize the radar SINR while satisfying the communication requirements. The resulting nonconvex problems were solved by using alternating optimization and sequential convex programming. Simulation results have validated the effectiveness of the proposed spectrum sharing methods. We would like to point out that radar and communication coexistence is a new line of work with limitations and challenges. It calls for not only more research efforts on system modeling and design, but also cooperation across public and private sectors on regulation and policy revision.

4.A Proof of Proposition 3

Proof. The proposition can be proved using induction. We focus on the proof for $l, l' \in \mathbb{N}_L^+$ in the following. The proof for $l, l' \in \mathbb{N}_{\tilde{L}}^+ \setminus \mathbb{N}_L^+$ is similar.

From the proposition, we know that $\{\mathbf{R}_{xl}\}$ is initialized such that $\mathbf{R}_{xl}^0 = \mathbf{R}_{xl'}^0 = \mathbf{R}_x^0$, $\forall l, l' \in \mathbb{N}_L^+$. We need to show that the optimal value of $(\mathbf{P}_R)$ in the n-th iteration is also achieved by $\{\mathbf{R}_{xl}^n\}$ such that $\mathbf{R}_{xl}^n = \mathbf{R}_{xl'}^n$, $\forall l, l' \in \mathbb{N}_L^+$. Because $\{\mathbf{R}_{xl}^n\}$ is obtained via several inner iterations of solving $(\tilde{\mathbf{P}}_{\mathbf{R}})$, it suffices to show that the above property could be passed on between the iterations of solving $(\tilde{\mathbf{P}}_{\mathbf{R}})$.

Suppose that, in the $(i-1)$-th inner iteration, the optimal value of $(\tilde{\mathbf{P}}_R)$ is achieved by $\{\mathbf{R}_{xl}^{n(i-1)}\}$ such that $\mathbf{R}_{xl}^{n(i-1)} = \mathbf{R}_{xl'}^{n(i-1)}$, $\forall l, l' \in \mathbb{N}_L^+$. During the i-th iteration, $\{\mathbf{R}_{xl}^{ni*}\}$ is obtained by solving $(\tilde{\mathbf{P}}_R)$ with $\{\bar{\mathbf{R}}_{xl}\} = \{\mathbf{R}_{xl}^{n(i-1)}\}$. We will show that $\mathbf{R}_{xl}^{ni} \equiv 1/L \sum_{l=1}^L \mathbf{R}_{xl}^{ni*} \triangleq \mathbf{R}_x^{ni}$, $\forall l \in \mathbb{N}_L^+$ is also feasible and achieves the same radar SINR as $\{\mathbf{R}_{xl}^{ni*}\}_{l \in \mathbb{N}_L^+}$ does. Based on the concavity of $C_l(\mathbf{R}_{xl}, \cdot)$, we have

$$\sum_{l=1}^{L} C_l(\mathbf{R}_{xl}^{ni*}, \cdot) \leq L C_l\left(\mathbf{R}_x^{ni}, \cdot\right).$$

For the communication transmission power, it trivially holds that $\sum_{l=1}^L \mathrm{Tr}(\mathbf{R}_{xl}^{ni*}) = L\mathrm{Tr}(\mathbf{R}_x^{ni})$. Therefore, $\{\mathbf{R}_x^{ni}\}$ is also feasible. The objective $\tilde{f}(\mathbf{R}_{xl})$ of $(\tilde{\mathbf{P}}_R)$ in the i-th iteration is affine

w.r.t. $\mathbf{R}_{xl}$ with coefficient depending on $\bar{\mathbf{R}}_{xl} = \mathbf{R}_{xl}^{n(i-1)}$. Given that $\mathbf{R}_{xl}^{n(i-1)} = \mathbf{R}_{xl'}^{n(i-1)}$, $\forall l, l' \in \mathbb{N}_L^+$, the affine functions $\tilde{f}(\cdot)$ for are identical for any $l \in \mathbb{N}_L^+$. Therefore, $\{\mathbf{R}_x^{ni}\}$ achieves the same objective value as $\{\mathbf{R}_{xl}^{ni*}\}_{l \in \mathbb{N}_L^+}$ does.

Proposition 3 is proved. □

Chapter 5

MIMO Radar and Communication Spectrum Sharing with Clutter Mitigation

We address the co-existence of MIMO radars and a MIMO communication system. Unlike previous works, we consider a scenario in which the radar system operates in the presence of clutter. Both the radar and the communication system use transmit precoding. Initially, spectrum sharing is formulated as a problem that maximizes the radar SINR subject to the communication system meeting certain rate and power constraints. Due to the dependence of the clutter on the radar precoding matrix, the optimization w.r.t. the radar precoder is a maximization of a nonconvex function over a nonconvex feasible set. Since solving such problem is computationally intractable, we propose to maximize a lower bound of the SINR. In the resulting alternating maximization problem, the alternating iteration of the communication TX covariance matrix reduces to one SDP problem, while the iteration of the radar precoder is solved by a sequence of SOCP problems, which are more efficient and tractable than SDP. Simulation results validate the effectiveness of the proposed spectrum sharing method for scenarios with clutter.

5.1 Introduction

Spectrum sharing targets at enabling radar and communication systems to share the spectrum efficiently by minimizing interference effects [42–49, 63]. The existing radar and communication spectrum sharing literature addresses interference mitigation either for the communication systems [43–46], or for the radar [47]. To the best of our knowledge, co-design of radar and communication systems for spectrum sharing was proposed in [99–101, 115] for the first time. Compared to radar design approaches of [43–47], the joint design has the potential to improve the spectrum utilization due to increased number of design degrees of

freedom. However, a clutter free scenario was assumed in [43–47].

In this chapter, we consider the co-design based spectrum sharing of a MIMO radar and a communication system for a scenario in which the radar system operates in the presence of clutter. Both the radar and the communication system use transmit precoding. Initially, spectrum sharing is formulated as a problem that maximizes the radar SINR subject to the communication system meeting certain rate and power constraints. Usually, the joint design problem can be solved using alternating optimization. Due to the dependence of the clutter on radar precoding matrix, the optimization w.r.t. the radar precoder is a maximization of a nonconvex function over a nonconvex feasible set. Solving such problem is computationally intractable and demanding. In addition, the objective is also nonlinear and nonconvex w.r.t. the communication covariance matrix. The joint design problem requires to solve a sequence of semidefinte programming (SDP) problems in every alternating iteration of either design variable; as such it has high computational complexity. As an efficient alternative, we propose to maximize a lower bound of the SINR. In the resulting alternating maximization problem, the alternating iteration of the communication covariance matrix reduces to one SDP problem. We show that the radar precoder always has a rank one solution. Based on this key observation, the alternating iteration of the radar precoder is solved by a sequence of second order cone programming (SOCP) problems, which are more efficient and tractable than SDP problems. Simulation results validate the effectiveness of the proposed spectrum sharing method for scenarios with clutter.

The chapter is organized as follows. Section 5.2 introduces the coexistence model of a MIMO radar system and a communication system. The proposed spectrum sharing method is given in Section 5.3. Numerical results and conclusions are provided respectively in Sections 5.4 and 5.5.

5.2 System Models

Consider a MIMO communication system which coexists with a MIMO radar system as shown in Fig. 4.1, sharing the same carrier frequency. The MIMO radar system uses $M_{t,R}$ TX and $M_{r,R}$ RX collocated antennas for target detection/estimation. The communication

transmitter and receiver are equipped with $M_{t,C}$ and $M_{r,C}$ antennas, respectively. The communication channel is denoted as $\mathbf{H} \in \mathbb{C}^{M_{r,C} \times M_{t,C}}$. The interference channel from the radar TX antennas to the communication receiver is denoted as $\mathbf{G}_1 \in \mathbb{C}^{M_{r,C} \times M_{t,R}}$ [43, 44, 46]; the interference channel from the communication transmitter to the radar RX antennas is denoted as $\mathbf{G}_2 \in \mathbb{C}^{M_{r,R} \times M_{t,C}}$. It is assumed that the channels $\mathbf{H}$, $\mathbf{G}_1$ and $\mathbf{G}_2$ are block fading [102] and perfectly known at the communication transmitter. In practice, the channel state information can be obtained through the transmission of pilot signals [43, 103]. The detailed signal models for the MIMO radar and communication systems are described in the sequel. We do not assume perfect carrier phase synchronization between the two systems.

The MIMO radar employs narrowband orthogonal waveforms, each of which contains L coded sub-pulses, each of duration T_b. Let $\mathbf{s}_m \triangleq [s_{m1}, \ldots, s_{mL}]^T$ denote the orthogonal code vector for the m-th TX antenna. It holds that $\langle \mathbf{s}_m, \mathbf{s}_n \rangle = \delta_{mn}$. In this chapter, we choose $\mathbf{S}$ as a random orthonormal matrix [101], which is obtained through performing the Gram-Schmidt orthogonalization on a matrix whose entries are i.i.d. Gaussian random variables. Note that the entries of $\mathbf{S}$ are not independent anymore. However, based on [107, Theorem 3], if $M_{t,R} = \mathcal{O}(L/\ln L)$, the entries of $\mathbf{S}$ can be approximated by i.i.d. Gaussian random variables with distribution $\mathcal{N}(0, 1/L)$. The waveforms are first precoded by matrix $\mathbf{P} \in \mathbb{C}^{M_{t,R} \times M_{t,R}}$, and then transmitted over carrier f_c periodically, with pulse repetition interval T_{PRI}. Suppose that there are one target and K point clutters in the same range bin w.r.t. the radar phase center. During each pulse, the target echoes and communication interference received at the radar RX antennas are demodulated to baseband and sampled every T_b seconds. The discrete time signal model for sampling time index $l \in \mathbb{N}_{\tilde{L}}^{+}$ is expressed as

$$\begin{aligned} \mathbf{y}_R(l) &= \beta_0 \mathbf{v}_r(\theta_0)\mathbf{v}_t^T(\theta_0)\mathbf{P}\mathbf{s}(l - l_0) + \mathbf{G}_2\mathbf{x}(l)e^{j\alpha_2(l)} \\ &\quad + \sum_{k=1}^{K} \beta_k \mathbf{v}_r(\theta_k)\mathbf{v}_t^T(\theta_k)\mathbf{P}\mathbf{s}(l - l_0) + \mathbf{w}_R(l), \end{aligned} \tag{5.1}$$

where $\tilde{L} = \lfloor T_{PRI}/T_b \rfloor$ denotes the total number of samples in one PRI; $\mathbf{y}_R(l)$ and $\mathbf{x}(l)$ respectively denote the radar received signal and communication waveform symbol at time lT_b; $\mathbf{s}(l) = [s_{1l}, \ldots, s_{M_{t,R}l}]^T$; $\mathbf{w}_R(l)$ is noise distributed as $\mathcal{CN}(\mathbf{0}, \sigma_R^2\mathbf{I})$; $l_0 = \lfloor \tau_0/T_b \rfloor$ with $\tau_0 \triangleq 2d_0/v_c$, d_0 being the range of the target and v_c being the speed of light; β_0 and β_k,

$\forall k \in \mathbb{N}_K^+$, denote the complex radar cross sections for the target and the k-th point clutter, respectively; the Swerling II target model is assumed, *i.e.*, the β_0 varies from pulse to pulse and has distribution $\mathcal{CN}(0, \sigma_{\beta 0}^2)$; and $\mathbf{v}_r(\theta) \in \mathbb{C}^{M_{r,R}}$ is the receive steering vector defined as

$$\mathbf{v}_r(\theta) \triangleq \left[e^{j2\pi\langle \mathbf{d}_1^r, \mathbf{u}(\theta)\rangle/\lambda_c}, \ldots, e^{j2\pi\langle \mathbf{d}_{M_{r,R}}^r, \mathbf{u}(\theta)\rangle/\lambda_c}\right]^T,$$

with $\mathbf{d}_m^r \triangleq [x_m^r \, y_m^r]^T$ denoting the two-dimensional coordinates of the m-th RX antenna, $\mathbf{u}(\theta) \triangleq [\cos(\theta) \, \sin(\theta)]^T$, and λ_c denoting the carrier wavelength. $\mathbf{v}_t(\theta) \in \mathbb{C}^{M_{t,R}}$ is the transmit steering vector and is respectively defined. The second term on the right hand side of (5.1) denotes the interference due to the communication transmission $\mathbf{x}(l) \in \mathbb{C}^{M_{t,C}}$. $e^{j\alpha_2(l)}$ is introduced to denote the random phase offset resulted from the random phase jitters of the oscillators at the communication transmitter and the MIMO radar receiver Phase-Locked Loops [100]. In the literature [104–106], phase jitters are modeled as zero-mean Gaussian processes.

The MIMO communication system uses the same carrier frequency f_c. The baseband signal at the communication receiver is sampled according to the symbol rate T_s, which could be different that the radar waveform symbol duration T_b. In this chapter, we only consider the matched case, *i.e.*, $T_s = T_b$; the extension of the proposed methods to the mismatched case is straightforward [100]. The discrete time communication signal has the following form

$$\mathbf{y}_C(l) = \mathbf{H}\mathbf{x}(l) + \mathbf{G}_1\mathbf{P}\mathbf{s}(l)e^{j\alpha_1(l)} + \mathbf{w}_C(l), \; l \in \mathbb{N}_{\tilde{L}}^+, \tag{5.2}$$

where $\mathbf{x}(l) \in \mathbb{C}^{M_{t,C}}$ denotes the transmit vector at the communication transmitter at time index l; $e^{j\alpha_1(l)}$ denotes the random phase offset between the radar TX carrier and the communication RX reference carrier [100]; the additive noise $\mathbf{w}_C(l)$ has distribution $\mathcal{CN}(\mathbf{0}, \sigma_C^2\mathbf{I})$. Note that the radar waveform $\mathbf{s}(l)$ equals zero when $l > L$, which means that the communication system is interference free during this period. The above model assumes that the radar transmission is the only interference, while the target and clutter returns do not reach the communication system.

5.3 Spectrum Sharing with Clutter Mitigation

We first derive the communication rate and radar SINR in terms of communication and radar waveforms.

For the communication system, the covariance of interference plus noise is given by

$$\mathbf{R}_{\text{Cin}l} = \begin{cases} \mathbf{G}_1 \mathbf{\Phi} \mathbf{G}_1^H + \sigma_C^2 \mathbf{I} & l \in \mathbb{N}_L^+ \\ \sigma_C^2 \mathbf{I} & l \in \mathbb{N}_{\tilde{L}}^+ \setminus \mathbb{N}_L^+ \end{cases} \tag{5.3}$$

where $\mathbf{\Phi} \triangleq \mathbf{P}\mathbf{P}^H/L$ is positive semidefinite. For $l \in \mathbb{N}_L^+$, the *instaneous* information rate is unknown because the interference plus noise is not necessarily Gaussian due to the random phase offset $\alpha_1(l)$. Instead, we are interested in a lower bound of the rate, which is given by [109]

$$\underline{C}(\mathbf{R}_x, \mathbf{\Phi}) \triangleq \log_2 \left| \mathbf{I} + \mathbf{R}_{\text{Cin}l}^{-1} \mathbf{H} \mathbf{R}_x \mathbf{H}^H \right|,$$

which is achieved when the codeword $\mathbf{x}(l)$, $l \in \mathbb{N}_L^+$ is distributed as $\mathcal{CN}(0, \mathbf{R}_x)$. The average communication rate over $\tilde{L}$ symbols is as follows

$$\text{C}_{\text{avg}}(\mathbf{R}_x, \mathbf{\Phi}) \triangleq \eta \underline{C}(\mathbf{R}_x, \mathbf{\Phi}) + (1-\eta)\underline{C}(\mathbf{R}_x, \mathbf{0}), \tag{5.4}$$

where $\eta \triangleq L/\tilde{L}$ is called the radar duty cycle.

For the radar system, the covariance of the communication interference exerted at the radar RX antennas equals $\mathbb{E}\{\mathbf{G}_2 \mathbf{x}(l) e^{j\alpha_2(l)} e^{-j\alpha_2(l)} \mathbf{x}^H(l) \mathbf{G}_2^H\} = \mathbf{G}_2 \mathbf{R}_x \mathbf{G}_2^H$. Suppose that each of the clutter amplitude β_k is an independent complex Gaussian variable with zero mean and variance $\sigma_{\beta k}^2$. The above clutter model is widely considered in the literature [113, 116, 117]. The clutter covariance matrix is given as $\mathbf{R}_c = \sum_{k=1}^K \mathbf{C}_k \mathbf{\Phi} \mathbf{C}_k^H$ with $\mathbf{C}_k = \sigma_{\beta k} \mathbf{v}_r(\theta_k) \mathbf{v}_t^T(\theta_k)$. Incorporating the additive noise and interference from both clutter and the communication system, the radar SINR is given as

$$\text{SINR}(\mathbf{R}_x, \mathbf{\Phi}) = \text{Tr}\left(\left(\mathbf{R}_{\text{Rin}} + \mathbf{R}_c \right)^{-1} \mathbf{D}_0 \mathbf{\Phi} \mathbf{D}_0^H \right), \tag{5.5}$$

where $\mathbf{R}_{\text{Rin}} \triangleq \mathbf{G}_2 \mathbf{R}_x \mathbf{G}_2^H + \sigma_R^2 \mathbf{I}$ and $\mathbf{D}_0 = \sigma_{\beta 0} \mathbf{v}_r(\theta_0) \mathbf{v}_t^T(\theta_0)$.

Here we consider the scenario where the radar searches in particular directions of interest given by set $\{\theta_k\}$ for targets with unknown RCS variances and delays [3, 113]. The worst possible target RCS variance is given by $\{\sigma_0^2\}$, which is the smallest target RCS variance

that could be detected by the radar. We assume that $\{\sigma_{\beta k}^2\}$ and $\{\theta_k\}$ are known. In practice, these clutter parameters could be estimated when target is absent [116].

The spectrum sharing problem when clutter is present can be formulated as follows

$$(\mathbf{P}_1) \max_{\mathbf{R}_x \succeq 0, \mathbf{\Phi} \succeq 0} \text{SINR, s.t. } \mathrm{C}_{\text{avg}}(\mathbf{R}_x, \mathbf{\Phi}) \geq C, \tag{5.6a}$$

$$\tilde{L}\mathrm{Tr}\left(\mathbf{R}_x\right) \leq P_C, L\mathrm{Tr}\left(\mathbf{\Phi}\right) \leq P_R. \tag{5.6b}$$

Note that the objective in $(\mathbf{P}_1)$ is not affine w.r.t. $\mathbf{\Phi}$ because the clutter covariance in SINR depends on $\mathbf{\Phi}$. One natural solution is the sequential convex programming using the first order Taylor expansion of the SINR. Solving the sequence of approximated problems increases the computational complexity. It is even worse when the sequential convex programming is embedded in every alternating iterations w.r.t. $\mathbf{R}_x$ and $\mathbf{\Psi}$.

In this chapter, we propose a more efficient alternative where we maximize a lower bound of the SINR. To tackle the nonconvexity in the objective function, we propose to maximize a lower bound of the objective function

$$\text{SINR} \geq \frac{\sigma_{\beta 0}^2 M_{r,R}^2 \mathrm{Tr}(\mathbf{\Phi}\mathbf{D}_t)}{\mathrm{Tr}(\mathbf{\Phi}\mathbf{C}) + \mathrm{Tr}(\mathbf{R}_x\mathbf{B}) + \sigma_R^2 M_{r,R}}, \tag{5.7}$$

where $\mathbf{D}_t \triangleq \mathbf{v}_t^*(\theta_0)\mathbf{v}_t^T(\theta_0)$, $\mathbf{C} \triangleq \sum_{k=1}^K \mathbf{C}_k^H \mathbf{v}_r(\theta_0)\mathbf{v}_r^H(\theta_0)\mathbf{C}_k$ and $\mathbf{B} \triangleq \mathbf{G}_2^H \mathbf{v}_r(\theta_0)\mathbf{v}_r^H(\theta_0)\mathbf{G}_2$. The lower bound is derived based on Cauchy-Schwarz inequality and is tight if the clutter plus interference is spectrally white, *i.e.*, $(\mathbf{R}_{\text{Rin}} + \mathbf{R}_c) \propto \mathbf{I}$. The approximate problem is now given as

$$\begin{aligned}(\mathbf{P}_1') \max_{\mathbf{R}_x \succeq 0, \mathbf{\Phi} \succeq 0} & \frac{\sigma_{\beta 0}^2 M_{r,R}^2 \mathrm{Tr}(\mathbf{\Phi}\mathbf{D}_t)}{\mathrm{Tr}(\mathbf{\Phi}\mathbf{C}) + \mathrm{Tr}(\mathbf{R}_x\mathbf{B}) + \sigma_R^2 M_{r,R}}, \\ & \text{s.t. same constraints as}(\mathbf{P}_1).\end{aligned} \tag{5.8}$$

Alternate optimization is applied to solve $(\mathbf{P}_1')$. The alternating iterations w.r.t. $\mathbf{R}_x$ and $\mathbf{\Phi}$ are discussed in the following two subsections.

5.3.1 The Alternating Iteration w.r.t. $\mathbf{R}_x$

With fixed $\mathbf{\Phi}$, the optimization w.r.t. $\mathbf{R}_x$ can be formulated as the following equivalent convex problem

$$\min_{\mathbf{R}_x \succeq 0} \mathrm{Tr}(\mathbf{R}_x\mathbf{B}) \text{ s.t. } \mathrm{C}_{\text{avg}}(\mathbf{R}_x, \mathbf{\Phi}) \geq C, \tilde{L}\mathrm{Tr}\left(\mathbf{R}_x\right) \leq P_C. \tag{5.9}$$

Problem (5.9) can be solved using available SDP solvers [118].

$$\mathbf{A} \triangleq -\left(\frac{\partial C_{\text{avg}}(\mathbf{R}_x, \mathbf{\Phi})}{\partial \Re(\mathbf{\Phi})}\right)^T_{\mathbf{\Phi}=\bar{\mathbf{\Phi}}} = \mathbf{G}_1^H[(\mathbf{G}_1\mathbf{\Phi}\mathbf{G}_1^H + \sigma_C^2\mathbf{I})^{-1} - (\mathbf{G}_1\mathbf{\Phi}\mathbf{G}_1^H + \sigma_C^2\mathbf{I} + \mathbf{H}\mathbf{R}_x\mathbf{H}^H)^{-1}]\mathbf{G}_1\big|_{\mathbf{\Phi}=\bar{\mathbf{\Phi}}}. \tag{5.10}$$

5.3.2 The Alternating Iteration w.r.t. $\mathbf{\Phi}$

For the optimization of $\mathbf{\Phi}$ with fixed $\mathbf{R}_x$, the constraint in (5.6a) is nonconvex w.r.t. $\mathbf{\Phi}$. The first order Taylor expansion of $\mathrm{C}_{\text{avg}}(\mathbf{R}_x, \mathbf{\Phi})$ at $\bar{\mathbf{\Phi}}$ is given as

$$\mathrm{C}_{\text{avg}}(\mathbf{R}_x, \mathbf{\Phi}) \approx \mathrm{C}_{\text{avg}}(\mathbf{R}_x, \bar{\mathbf{\Phi}}) - \mathrm{Tr}\left[\mathbf{A}(\mathbf{\Phi} - \bar{\mathbf{\Phi}})\right],$$

where $\mathbf{A}$ is given in (5.10) on the top of next page.

The sequential convex programming technique is applied to solve $\mathbf{\Phi}$ by repeatedly solve the following approximate optimization problem

$$\max_{\mathbf{\Phi}\succeq 0} \frac{\mathrm{Tr}(\mathbf{\Phi}\mathbf{D}_t)}{\mathrm{Tr}(\mathbf{\Phi}\mathbf{C}) + \rho}, \text{ s.t. } \mathrm{Tr}\left(\mathbf{\Phi}\mathbf{A}\right) \leq \tilde{C}/L, \mathrm{Tr}\left(\mathbf{\Phi}\right) \leq P_R/L. \tag{5.11}$$

where $\tilde{C} = L[\underline{C}(\mathbf{R}_x, \bar{\mathbf{\Phi}}) + \mathrm{Tr}(\bar{\mathbf{\Phi}}\mathbf{A})] + (\tilde{L} - L)\underline{C}(\mathbf{R}_x, \mathbf{0}) - \tilde{L}C$, $\rho = \mathrm{Tr}(\mathbf{R}_x\mathbf{B}) + \sigma_R^2 M_{r,R}$ are real positive constants w.r.t. $\mathbf{\Phi}$, and $\bar{\mathbf{\Phi}}$ is updated as the solution of the previous repeated problem. Problem (5.11) could be formulated as a semidefinite programming problem (SDP) via Charnes-Cooper Transformation [116, 119]. However, in each alternating iteration w.r.t. $\mathbf{\Phi}$, it is required to solve several iterations of SDP due to the sequential convex programming, which could be computational demanding if $\mathbf{\Phi}$ has large dimensions. In the following, we will show that (5.11) always has rank one solution, and thus it could be further solved using more efficient second order conic programming (SOCP). To do so, we introduce the following SDP problem

$$\min_{\mathbf{\Phi}\succeq 0} \mathrm{Tr}\left(\mathbf{\Phi}\right) \text{ s.t. } \mathrm{Tr}\left(\mathbf{\Phi}\mathbf{A}\right) \leq \tilde{C}/L, \frac{\mathrm{Tr}(\mathbf{\Phi}\mathbf{D}_t)}{\mathrm{Tr}(\mathbf{\Phi}\mathbf{C}) + \rho} \geq \gamma, \tag{5.12}$$

where γ is a real positive constant. The following proposition relates the optimal solutions of problems (5.11) and (5.12).

Proposition 4. *If γ in (5.12) is chosen to be the maximum achievable SINR of (5.11), denoted as $SINR_{max}$, the optimal $\mathbf{\Phi}$ of (5.12) is also optimal for (5.11).*

Proof. Denote $\mathbf{\Phi}_1^*$ and $\mathbf{\Phi}_2^*$ the optimal solutions of (5.11) and (5.12), respectively. It is clear that $\mathbf{\Phi}_1^*$ is feasible point of (5.12). This means that $\mathrm{Tr}(\mathbf{\Phi}_2^*) \leq \mathrm{Tr}(\mathbf{\Phi}_1^*) \leq P_R/L$. Therefore,

$\mathbf{\Phi}_2^*$ is a feasible point of (5.11). It holds that

$$\mathrm{SINR}_{\max} \equiv \frac{\mathrm{Tr}(\mathbf{\Phi}_1^*\mathbf{D}_t)}{\mathrm{Tr}(\mathbf{\Phi}_1^*\mathbf{C})+\rho} \geq \frac{\mathrm{Tr}(\mathbf{\Phi}_2^*\mathbf{D}_t)}{\mathrm{Tr}(\mathbf{\Phi}_2^*\mathbf{C})+\rho} \geq \mathrm{SINR}_{\max}.$$

It is only possible when all the equalities hold. In other words, $\mathbf{\Phi}_2^*$ is optimal for (5.11). The claim is proved. □

Based on the above proposition, the optimal solution of (5.11) can be obtained by solving (5.12) using a bisection search for γ. Given an interval $[l, u]$ which contains $\mathrm{SINR}_{\max}$, we start from solving (5.12) with $\gamma = \frac{l+u}{2}$. If the optimal solution of (5.12) is feasible for (5.11), this means that $\mathrm{SINR}_{\max}$ is larger than $\frac{l+u}{2}$, and the interval is updated by its upper half; otherwise, the interval is updated by its lower half. The above procedure is repeated until the interval is sufficient small. The remaining issue is to find an algorithm that solves (5.12) more efficiently than SDP does.

In order to characterize the optimal solution of (5.12), we need the following key lemma:

Lemma 6. *Matrix* $\mathbf{A}$ *defined in (5.10) is positive semidefinite.*

Proof. For simplicity of notation, we denote that $\mathbf{X} \triangleq \mathbf{G}_1\mathbf{\Phi}\mathbf{G}_1^H + \sigma_C^2\mathbf{I} \succ 0$ and $\mathbf{Y} \triangleq \mathbf{H}\mathbf{R}_x\mathbf{H}^H \succeq 0$. It is easy to see that $\mathbf{A}$ is Hermitian because both $\mathbf{X}^{-1}$ and $(\mathbf{X}+\mathbf{Y})^{-1}$ are Hermitian. It is sufficient to show that $\mathbf{M} \triangleq \mathbf{X}^{-1} - (\mathbf{X}+\mathbf{Y})^{-1}$ is positive semidefinite. We have that

$$\mathbf{X}^{-1} - (\mathbf{X}+\mathbf{Y})^{-1} = \mathbf{X}^{-1}\mathbf{Y}(\mathbf{X}+\mathbf{Y})^{-1},$$

which could be shown by right multiplying $(\mathbf{X}+\mathbf{Y})$ on both sides of the equality. Since $\mathbf{X}$, $\mathbf{Y}$ and $\mathbf{M}$ are Hermitian, we have

$$\mathbf{M} = \mathbf{X}^{-1}\mathbf{Y}(\mathbf{X}+\mathbf{Y})^{-1} = (\mathbf{X}+\mathbf{Y})^{-1}\mathbf{Y}\mathbf{X}^{-1}.$$

Since $(\mathbf{X}+\mathbf{Y})^{-1}$ is invertible, there exists a unique positive definite matrix $\mathbf{V}$, such that $(\mathbf{X}+\mathbf{Y})^{-1} = \mathbf{V}^2$. Simple algebra manipulation shows that

$$\begin{aligned}\mathbf{V}^{-1}\mathbf{M}\mathbf{V}^{-1} &= (\mathbf{V}^{-1}\mathbf{X}^{-1}\mathbf{V}^{-1})(\mathbf{V}\mathbf{Y}\mathbf{V}) \\ &= (\mathbf{V}\mathbf{Y}\mathbf{V})(\mathbf{V}^{-1}\mathbf{X}^{-1}\mathbf{V}^{-1}),\end{aligned}$$

i.e., $\mathbf{V}^{-1}\mathbf{M}\mathbf{V}^{-1}$ is a product of two commutable positive semidefinite matrices $\mathbf{V}^{-1}\mathbf{X}^{-1}\mathbf{V}^{-1}$ and $\mathbf{V}\mathbf{Y}\mathbf{V}$. Therefore, $\mathbf{V}^{-1}\mathbf{M}\mathbf{V}^{-1}$ and thus $\mathbf{M}$ is positive semidefinite. □

Based on Lemma 6, we prove the following result by following the approach in [119]:

Proposition 5. *Suppose that (5.12) is feasible. Then, the optimal solution of (5.12) must be rank one and unique. Moreover, (5.11) always has rank one solution.*

Proof. Problem (5.12) is an SDP, whose Karush-Kuhn-Tucker (KKT) conditions are given as

$$\mathbf{\Psi} + \lambda_2 \mathbf{D}_t = \mathbf{I} + \lambda_1 \mathbf{A} + \lambda_2 \gamma \mathbf{C} \tag{5.13a}$$

$$\mathbf{\Psi}\mathbf{\Phi} = \mathbf{0} \tag{5.13b}$$

$$\mathbf{\Psi} \succeq 0, \mathbf{\Phi} \succeq 0, \lambda_1 \geq 0, \lambda_2 \geq 0 \tag{5.13c}$$

$$\mathrm{Tr}(\mathbf{\Phi}\mathbf{D}_t) \geq \gamma \mathrm{Tr}(\mathbf{\Phi}\mathbf{C}) + \gamma\rho \tag{5.13d}$$

where $\mathbf{\Psi} \succeq 0, \lambda_1 \geq 0, \lambda_2 \geq 0$ are dual variables. From (5.13a), we have

$$\mathrm{rank}(\mathbf{\Psi}) + \mathrm{rank}(\lambda_2 \mathbf{D}_t) \geq \mathrm{rank}(\mathbf{I} + \lambda_1 \mathbf{A} + \lambda_2 \gamma \mathbf{C}).$$

Recall that $\mathrm{rank}(\mathbf{D}_t) = 1$. Since $\mathbf{A}$ and $\mathbf{C}$ are PSD, the matrix on right hand side of (5.13a) has full rank. Therefore, $\mathrm{rank}(\mathbf{\Psi})$ is not smaller than $M_{t,R} - 1$. From (5.13b) and (5.13d) we conclude that the optimal $\mathbf{\Phi}$ must be a rank one matrix.

The uniqueness of optimal solution could be proved via contradiction. The second claim on the solution of (5.11) follows from Proposition 4. □

Proposition 5 implies that when there is only one target, the transmit beamforming is the optimal radar precoding strategy for the spectrum sharing between the MIMO radar and the communication systems along with clutter mitigation for radar, as formulated in $(\mathbf{P}_1')$. Based on Proposition 5, we denote that $\mathbf{\Phi} = \mathbf{u}\mathbf{u}^H$, where $\mathbf{u}$ is a vector of dimension $M_{t,R}$. Problem (5.12) can be reformulated as

$$\begin{aligned} \min_{\mathbf{u}} \|\mathbf{u}\|^2 \text{ s.t. } & \|\mathbf{A}^{1/2}\mathbf{u}\|^2 \leq \tilde{C}/L, \\ & \gamma \mathbf{u}^H \mathbf{C} \mathbf{u} + \gamma\rho \leq \left(\mathbf{u}^H \mathbf{v}_t^*(\theta_0)\right)^2. \end{aligned} \tag{5.14}$$

Note that if $\mathbf{u}$ is a solution of (5.14), so is $e^{jw}\mathbf{u}$ for any real w. Without loss of generality, we restrict $\mathbf{u}^H \mathbf{v}_t^*(\theta_0)$ is real and nonnegative. Problem (5.14) is equivalent to the following

SOCP

$$\begin{aligned}\min_{\mathbf{u},t}\ t \text{ s.t. } \ \|\mathbf{u}\|_2 \le t,\ \left\|\mathbf{A}^{1/2}\mathbf{u}\right\|_2 \le \sqrt{\tilde{C}/L},\\ \left\|\begin{bmatrix}\gamma\mathbf{C} & \\ & \gamma\rho\end{bmatrix}^{1/2}\begin{bmatrix}\mathbf{u}\\ 1\end{bmatrix}\right\|_2 \le \mathbf{u}^H\mathbf{v}_t^*(\theta_0).\end{aligned} \tag{5.15}$$

The proposed efficient spectrum sharing algorithm in presence of clutter using a lower bound of the radar SINR is outlined in Algorithm 2.

Algorithm 2 The proposed algorithm for spectrum sharing with clutter mitigation ($\mathbf{P}_1'$).

1: **Input:** $\mathbf{D}_0, \mathbf{C}_n, \mathbf{H}, \mathbf{G}_1, \mathbf{G}_2, P_{C/R}, C, \sigma^2_{C/R}, \delta_1$
2: **Initialization:** $\mathbf{\Phi} = \frac{P_R}{LM_{t,R}}\mathbf{I}$, $\mathbf{R}_x = \frac{P_C}{\tilde{L}M_{t,C}}\mathbf{I}$;
3: **repeat**
4: Update $\mathbf{R}_x$ by solving (5.9) with fixed $\mathbf{\Phi}$;
5: Update $\mathbf{\Phi}$ by solving a sequence of approximated problem (5.11), which is in turn achieved by bisection search and repeatedly solving (5.15) using SOCP solvers;
6: **until** $|\text{SINR}^n - \text{SINR}^{n-1}| < \delta_1$
7: **Output:** $\mathbf{R}_x, \mathbf{P} = \mathbf{u}$

5.4 Simulation Results

In this section, we provide two simulation examples to quantify the performance of the proposed spectrum sharing method with clutter mitigation. We set the number of samples per PRI to $\tilde{L} = 32$, the number of radar waveform symbols to $L = 8$, the noise variance to $\sigma_C^2 = \sigma_R^2 = 0.01$, and the number of antennas to $M_{t,R} = M_{r,R} = 16, M_{t,C} = 8, M_{r,C} = 4$. The MIMO radar system consists of collocated TX and RX antennas forming half-wavelength uniform linear arrays. The radar waveforms are chosen from the rows of a random orthonormal matrix [99]. There are one stationary targets with RCS variance $\sigma_{\beta 0}^2 = 5 \times 10^{-5}$ and eight point clutters. All clutter RCS variances are set to be identical and are denoted by σ_β^2, which is decided by the prescribed clutter to noise ratio (CNR) $10\log\sigma_\beta^2/\sigma_R^2$. The target angle θ_0 w.r.t. the array is randomly generated; clutter scatters are with angles in $[\theta_0 - 20^\circ, \theta_0 - 10^\circ]$ and $[\theta_0 + 10^\circ, \theta_0 + 20^\circ]$. For the communication capacity and power constraints, we take $C = 24$ bits/symbol and $P_C = \tilde{L}M_{t,C}$ (the power is normalized by the power of the radar waveform). The interference channels $\mathbf{G}_1$ and $\mathbf{G}_2$ are generated with

entries which are independent and distributed as $\mathcal{CN}(0, 0.1)$. The channel $\mathbf{H}$ has independent entries, distributed as $\mathcal{CN}(0, 1)$. The proposed spectrum sharing method with clutter mitigation jointly designs the communication covariance matrix and the radar precoder according to the algorithm presented in Section 5.3. For comparison, we also implement the method based on the Charnes-Cooper transformation of (5.11) and SDP. The aforementioned spectrum sharing algorithms are respectively labeled by "precoding with clutter mitigation (SOCP)" and "precoding with clutter mitigation (SDP)" in the figures. We also implement the spectrum sharing method without the consideration of clutter mitigation, labeled by "precoding without clutter mitigation", and method based on uniform precoding, *i.e.*, $\mathbf{P} = \sqrt{LP_R/M_{t,R}}\mathbf{I}$.

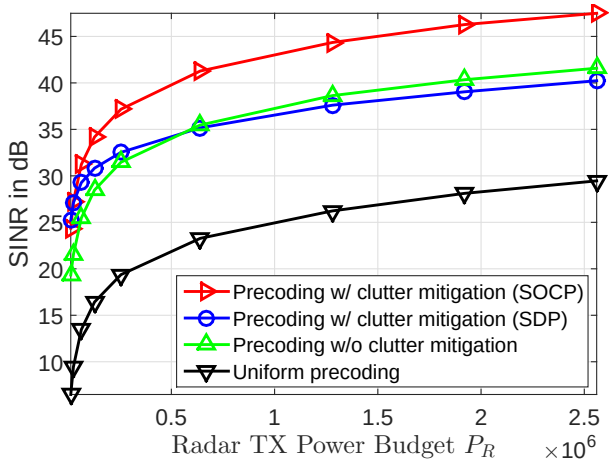

Figure 5.1: SINR performance under different values of radar TX power.

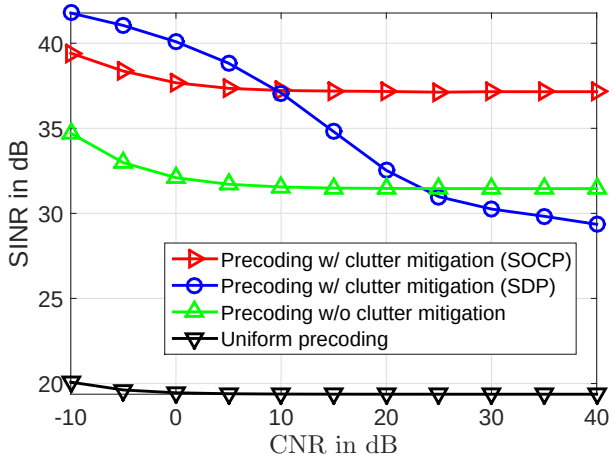

Figure 5.2: SINR performance under different clutter to noise ratios (CNR).

Fig. 5.1 shows the SINR results for different values of the radar transmit power budget P_R. The CNR is fixed as 20 dB. The radar power budget per antenna ranges from 100

to $20,000$ times of the communication power budget per antenna. Fig. 5.2 shows the SINR results under different clutter to noise ratios. The radar power budget is fixed as $P_R = 2.56 \times 10^5$. We can observe that the proposed method achieves the highest SINR while the uniform precoding based method achieves the lowest SINR. The method "precoding without clutter mitigation" improves the SINR over uniform precoding because it focuses more power on the target. Our proposed method achieves higher SINR than the method without clutter mitigation because our method can effectively reduce the power transmitted on the clutter. Note that the performance of the SDP based method degrades greatly as the CNR increases, even worse than the spectrum sharing method without considering clutter mitigation. This indicates that the SDP based method is very sensitive to CNR. A rigorous treatment on this phenomenon will be considered in the future work.

Comparing with the spectrum sharing method using SDP based precoding design, our proposed SOCP based precoding design is more tractable and computationally efficient. From Fig. 5.1 and Fig. 5.2, we can see that the proposed method outperforms the SDP based method when CNR is larger than 10 dB. The CPU time required by the SDP method increase dramatically with $M_{t,R}$, while the proposed SOCP based method increase mildly with $M_{t,R}$.

5.5 Conclusion

We have proposed an efficient spectrum sharing method for a MIMO radar and a communication system operating in a scenario with clutter. The radar and communication system signals were optimally designed by minimizing a lower bound for the SINR at the radar receive antennas. We have shown that the radar precoder always has a rank one solution. Based on this key observation, the alternating iteration of the radar precoder has been solved by a sequence of SOCP problems, which are more efficient and tractable than applying SDP directly. Simulation results have shown that the proposed spectrum sharing method can effectively increase the radar SINR for various scenarios with clutter.

Chapter 6

Optimum Co-Design for Spectrum Sharing Between Matrix Completion Based MIMO Radars and a MIMO Communication System

Spectrum sharing enables radar and communication systems to share the spectrum efficiently by minimizing mutual interference. Recently proposed multiple input multiple output radars based on sparse sensing and matrix completion (MIMO-MC), in addition to reducing communication bandwidth and power as compared to MIMO radars, offer a significant advantage for spectrum sharing. The advantage stems from the way the sampling scheme at the radar receivers modulates the interference channel from the communication system transmitters, rendering it symbol dependent and reducing its row space. This makes it easier for the communication system to design its waveforms in an adaptive fashion so that it minimizes the interference to the radar subject to meeting rate and power constraints. Two methods are proposed. First, based on the knowledge of the radar sampling scheme, the communication system transmit covariance matrix is designed to minimize the effective interference power (EIP) to the radar receiver, while maintaining certain average capacity and transmit power for the communication system. Second, a joint design of the communication transmit covariance matrix and the MIMO-MC radar sampling scheme is proposed, which achieves even further EIP reduction.

6.1 Introduction

Spectrum sharing is an emerging technology that can be applied to enable radar and communication systems to share the spectrum efficiently by minimizing mutual interference [42–49, 62, 64, 66].

In this chapter we study spectrum sharing between a special class of collocated MIMO

radars and a MIMO communication system. The rationale behind considering a MIMO-type radar system is the high resolution which such systems can achieve with a relatively small number of transmit (TX) and receive (RX) antennas [9–12]. A MIMO radar system lends itself to a networked implementation, which is very desirable in both military and civilian applications. A networked radar is a configuration of TX and RX antennas. The TX antennas transmit probing waveforms, and target information is extracted by jointly processing the measurements of all RX antennas. This processing can be done at a fusion center, *i.e.*, a network node endowed with more computational power than the rest of the nodes. Reliable surveillance requires collection, communication and fusion of vast amounts of data from various antennas. This is a power and bandwidth consuming task, which can be especially taxing in scenarios in which the antennas are on battery operated devices and are connected to the fusion center via a wireless link. Recently, MIMO radars using compressive sensing (MIMO-CS) [22–24, 28], and MIMO radars via matrix completion (MIMO-MC) [32–35] have been proposed to save power and bandwidth on the link between the receivers and the fusion center, thus facilitating the network implementation of MIMO radars. MIMO-MC radars transmit orthogonal waveforms from their multiple TX antennas. Each RX antenna samples the target returns in a pseudo-random sub-Nyquist fashion and forwards the samples to the fusion center, along with the seed of the random sampling sequence. By collecting the samples of all RX antennas, and based on knowledge of each antenna's sampling scheme, the fusion center constructs a matrix, refereed to as the data matrix (see [33] Scheme I), in which only the entries corresponding to sampled times contain non-zero values. Subsequently, the missing entries, corresponding to non-sampled times, are provably recovered via MC techniques. In MIMO-MC radars the interference is confined to the sampled entries of the data matrix, while after matrix completion the target echo power is preserved. Unlike MIMO-CS, MIMO-MC does not require discretization of the target space, thus does not suffer from grid mismatch issues [37].

Spectrum sharing between a MIMO radar and a communication system has been considered in [43–46, 66], where the radar interference is eliminated by projecting the radar waveforms onto the null space of the interference channel between the MIMO radar transmitters and the communication system. In [47], a radar receive filter was proposed to mitigate the

interference from the communication systems. However, null space projection-type or spatial filtering-type techniques might miss targets aligned with the the interference channel. In general, the existing literature on MIMO radar-communication systems spectrum sharing addresses interference mitigation for either solely the communication system [43–46, 66] or solely the radar [47]. While joint design of traditional radar and communication systems for spectrum sharing has been considered in [42, 62, 64], co-design of MIMO radar and MIMO communication systems for spectrum sharing has not been addressed before, with the exception of our preliminary results in [99, 101]. In practice, however, the two systems are often aware of the existence of each other, and they could share information, which could be exploited for co-design. Recent developments in cognitive radios [120] and cognitive radars [121] could provide the tools for information sharing and channel feedback, thus facilitating the cooperation between radar and communication systems.

Motivated by the cooperative methods in cognitive radio networks [102, 122, 123], we propose ways via which a MIMO-MC radar and a MIMO communication system, in a cooperative fashion, negotiate spectrum use in order to mitigate mutual interference. In addition to reducing communication bandwidth and power, MIMO-MC radars offer a significant advantage for spectrum sharing. The advantage stems from the way the sampling scheme at the radar receivers modulates the interference channel from the communication system transmitters, rendering it symbol dependent and reducing its row space. This makes it easier for the communication system to design its waveforms in an adaptive fashion so that it minimizes the interference to the radar subject to meeting rate and power constraints. Two methods are proposed. The first method is a cooperative design; for a fixed radar sampling scheme, which is known to the communication system, the communication system optimally selects its precoding matrix to minimize the interference to the radar. The second method is a joint design, whereby the radar sampling scheme as well as the communication system precoding matrix are optimally selected to minimize the interference to the radar. For the first method, an efficient algorithm for solving the corresponding optimization problem is proposed based on the Lagrangian dual decomposition (see Algorithm 3). For the second method, alternating optimization is employed to solve the corresponding optimization problem. The candidate sampling scheme needs to be such that the resulting data matrix can

be completed. Recent work [124] showed that for matrix completion, the sampling locations should correspond to a binary matrix with large spectral gap. Since the spectral gap of a matrix is not affected by column and row permutations, we propose to search for the optimum sampling matrix among matrices which are row and column permutations of an initial sampling matrix with large spectral gap.

This chapter is organized as follows. Section 6.3 introduces the signal model when the MIMO-MC radar and communication systems coexist. The problem of a MIMO communication system sharing the spectrum with a MIMO-MC radar system is studied in Section 6.4. Numerical results, discussions and conclusions are provided in Section 6.5-6.7.

6.2 Background on MIMO-MC Radars

Consider a collocated MIMO radar system with $M_{t,R}$ TX antennas and $M_{r,R}$ RX antennas. The targets are in the far-field of the antennas and are assumed to fall in the same range bin. The radar operates in two phases; in the first phase the TX antennas transmit waveforms and the RX antennas receive target returns, while in the second phase, the RX antennas forward their measurements to a fusion center. In each pulse, the m-th, $m \in \mathbb{N}^{+}_{M_{t,R}}$, antenna transmits a coded waveform containing L symbols $\{s_m(1), \cdots, s_m(L)\}$ of duration T_R each. Each RX antenna samples the target returns every T_R seconds, *i.e.*, samples each symbol exactly once. Following the model of [32–34], the data matrix at the fusion center can be formulated as

$$\mathbf{Y}_R = \gamma\rho\mathbf{D}\mathbf{S} + \mathbf{W}_R, \tag{6.1}$$

where the m-th row of $\mathbf{Y}_R \in \mathbb{C}^{M_{r,R}\times L}$ contains the L samples forwarded by the m-th antenna; γ and ρ respectively denote the path loss corresponding to the range bin of interest, and the radar transmit power; $\mathbf{D} \in \mathbb{C}^{M_{r,R}\times M_{t,R}}$ denotes the target response matrix, which depends on the target reflectivity, angle of arrival and target speed (details can be found in [33]); $\mathbf{S} = [\mathbf{s}(1), \cdots, \mathbf{s}(L)]$, with $\mathbf{s}(l) = [s_1(l), \cdots, s_{M_{t,R}}(l)]^T$ being the l-th snapshot across the transmit antennas. The transmit waveforms are assumed to be orthogonal, *i.e.*, it holds that $\mathbf{S}\mathbf{S}^H = \mathbf{I}$ [33]; $\mathbf{W}_R$ denotes additive noise. After matched filtering at the fusion center,

target estimation can be performed based on $\mathbf{Y}_R$ via standard array processing schemes [4].

If the number of targets is smaller than $M_{r,R}$ and L, matrix $\mathbf{DS}$ is low-rank and can be provably recovered based on a subset of its entries [33, 35]. This observation gave rise to MIMO-MC radars [32–35], where each RX antenna sub-samples the target returns and forwards the samples to the fusion center. The sampling scheme could be a pseudo-random sequence of integers in $[1, L]$, with the fusion center knowing the random seed of each RX antenna. In MIMO-MC radars, the partially filled data matrix at the fusion center can be mathematically expressed as follows (see [33] Scheme I)

$$\mathbf{\Omega} \circ \mathbf{Y}_R = \mathbf{\Omega} \circ (\gamma\rho\mathbf{DS} + \mathbf{W}_R), \tag{6.2}$$

where $\circ$ denotes Hadamard product and $\mathbf{\Omega}$ is a matrix containing 0's and 1's; the 1's in the m-th row correspond to the sampled symbols of the m-th TR antenna. The sub-sampling rate, p, equals $\|\mathbf{\Omega}\|_0/(LM_{r,R})$. When $p = 1$, the $\mathbf{\Omega}$ matrix is filled with 1's, and the MIMO-MC radar is identical to the traditional MIMO radar. At the fusion center, the completion of $\gamma\rho\mathbf{DS}$ is formulated as the following problem [36]

$$\min_{\mathbf{M}} \|\mathbf{M}\|_* \quad \text{s.t. } \|\mathbf{\Omega} \circ \mathbf{M} - \mathbf{\Omega} \circ \mathbf{Y}_R\|_F \leq \delta, \tag{6.3}$$

where $\delta > 0$ is a parameter related to the noise over the sampled noise matrix entries, *i.e.*, $\mathbf{\Omega} \circ \mathbf{W}_R$. On denoting by $\hat{\mathbf{M}}$ the solution of (6.3), the recovery error $\|\hat{\mathbf{M}} - \gamma\rho\mathbf{DS}\|_F$ is determined by the noise power in $\mathbf{\Omega} \circ \mathbf{W}_R$, *i.e.*, the noise enters only through the sampled entries of the data matrix. It is important to note that, assuming that the reconstruction error is small, the reconstructed $\hat{\mathbf{M}}$ has the same received target echo power as $\gamma\rho\mathbf{DS}$ of (6.1).

Early studies on matrix completion theory suggested that the low-rank matrix reconstruction requires that the entries are sampled uniformly at random. However, recent works [124] showed that non-uniform sampling would still work, as long as the sampling matrix has large spectral gap (*i.e.*, large gap between the largest and second largest singular values).

6.3 System Model

Consider a MIMO communication system which coexists with a MIMO-MC radar system as shown in Fig. 4.1, sharing the same carrier frequency. The MIMO-MC radar operates

in two phases, *i.e.*, in Phase 1 the RX antennas obtain measurements of the target returns, and in Phase 2, the RX antennas forward the obtained samples to a fusion center. The communication system interferes with the radar system during both phases. In the following, we will address spectrum sharing during the first phase only. The interference during the second phase can be viewed as the interference between two communication systems; addressing this problem has been covered in the literature [102, 122].

Suppose that the two systems have the same symbol rate and are synchronized in terms of sampling times (see Section 6.5 for the mismatched case). We do not assume perfect carrier phase synchronization between the two systems. The data matrix at the radar fusion center, and the received matrix at the communication RX antennas during L symbol durations can be respectively expressed as

Radar fusion center:

$$\mathbf{\Omega} \circ \mathbf{Y}_R = \underbrace{\mathbf{\Omega} \circ (\gamma \rho \mathbf{D} \mathbf{S})}_{\text{signal}} + \underbrace{\mathbf{\Omega} \circ (\mathbf{G}_2 \mathbf{X} \mathbf{\Lambda}_2)}_{\text{interference}} + \underbrace{\mathbf{\Omega} \circ \mathbf{W}_R}_{\text{noise}}, \tag{6.4a}$$

Communication receiver:

$$\mathbf{Y}_C = \underbrace{\mathbf{H}\mathbf{X}}_{\text{signal}} + \underbrace{\rho \mathbf{G}_1 \mathbf{S} \mathbf{\Lambda}_1}_{\text{interference}} + \underbrace{\mathbf{W}_C}_{\text{noise}}, \tag{6.4b}$$

where

- $\mathbf{Y}_R$, $\rho, \mathbf{D}$, $\mathbf{S}$, $\mathbf{W}_R$, and $\mathbf{\Omega}$ are defined in Section 6.2.
- $\mathbf{X} \triangleq [\mathbf{x}(1), \ldots, \mathbf{x}(L)]$; $\mathbf{x}(l) \in \mathbb{C}^{M_{t,C} \times 1}$ denotes the transmit vector by the communication TX antennas during the l-th symbol duration. The rows of $\mathbf{X}$ are codewords from the code-book of the communication system.
- $\mathbf{W}_C$ and $\mathbf{W}_R$ denote the additive noise; their elements are assumed to be independent identically distributed as $\mathcal{CN}(0, \sigma_C^2)$ and $\mathcal{CN}(0, \sigma_R^2)$, respectively.
- $\mathbf{H} \in \mathbb{C}^{M_{r,C} \times M_{t,C}}$ denotes the communication channel, where $M_{r,C}$ and $M_{t,C}$ denote respectively the number of RX and TX antennas of the communication system; $\mathbf{G}_1 \in \mathbb{C}^{M_{r,C} \times M_{t,R}}$ denotes the interference channel from the radar TX antennas to the communication system RX antennas; $\mathbf{G}_2 \in \mathbb{C}^{M_{r,R} \times M_{t,C}}$ denotes the interference channel from the communication TX antennas to the radar RX antennas. All channels

are assumed to be flat fading and remain the same over L symbol intervals [43, 44, 46, 102].

- $\mathbf{\Lambda}_1$ and $\mathbf{\Lambda}_2$ are diagonal matrices. The l-th diagonal entry of $\mathbf{\Lambda}_1$, *i.e.*, $e^{j\alpha_{1l}}$, denotes the random phase offset between the MIMO-MC radar carrier and the communication receiver reference carrier at the l-th sampling time. The l-th diagonal entry of $\mathbf{\Lambda}_2$, *i.e.*, $e^{j\alpha_{2l}}$, denotes the random phase offset between the communication transmitter carrier and the MIMO-MC radar reference carrier at the l-th sampling time. The phase offsets arise due to random phase jitter of the radar oscillator and the oscillator at the communication receiver Phase-Locked Loops. In the literature [104–106], the phase jitter of oscillator $\alpha(t)$ is modeled as a zero-mean Gaussian process. In this chapter, we model $\{\alpha_{1l}\}_{l=1}^{L}$ as a sequence of zero-mean Gaussian random variables with variance σ_α^2. Modern CMOS oscillators exhibit very low phase noise, e.g., -94 dB below the carrier power per Hz (*i.e.*, -94dBc/Hz) at an offset of $2\pi \times 1$ MHz, which yields phase jitter variance $\sigma_\alpha^2 \approx 2.5 \times 10^{-3}$ [125].

The following assumptions are made:

- *About the synchronization of sampling times*- In the above model, we assume that the radar receivers and the communication system sample in a time synchronous manner. Although this assumption is later relaxed in Section 6.5, we next provide an example of radar and communication parameter settings suggesting that the aforementioned assumption is applicable in real world systems. The typical range resolution for an S-band search and acquisition radar is between $100m$ and $600m$ [126, 127]. Thus, for range resolution of $cT_b/2 = 300m$, where $c = 3 \times 10^8 m/s$ denotes the speed of light, the radar sub-pulse duration is $T_b = 2\mu s$. In order to have identical symbol rate for two systems, the communication symbol duration should be $2\mu s$, which corresponds to signal bandwidth of 0.5 MHz. This symbol interval value falls in the typical range of symbol interval values in LTE systems [128].

- *About channel fading*- We assume that $\mathbf{H}$, $\mathbf{G}_1$ and $\mathbf{G}_2$ are flat fading, which is valid when the channel coherence bandwidth is larger than the signal bandwidth [51, 52,

129], *i.e.*, when the transmitted signals are narrowband. Consider the symbol interval value $2\mu s$ and signal bandwidth 0.5 MHz given above. In a LTE macro-cell, the coherence bandwidth is in the order of 1 MHz [128, 130]. The typical values of LTE channel coherence bandwidth are much larger than the signal bandwidth of 0.5 MHz, thus making the flat fading channel assumption valid. Since the radar and communication systems use the same carrier and signal bandwidth, the flat fading assumption is valid for all $\mathbf{H}$, $\mathbf{G}_1$ and $\mathbf{G}_2$. In the radar-communication system coexistence literature [43–46, 66], the flat fading assumption is quite typical. If the narrowband assumption is not valid then perhaps one could consider an OFDM scenario, where the flat fading model would apply on each carrier [62, 64].

- *About channel information feedback*- The channels $\mathbf{H}$ and $\mathbf{G}_2$ are also assumed to be perfectly known at the communication TX antennas. In practice, such channel information can be obtained at the radar RX antennas through the transmission of pilot signals [43, 103]. Viewing the radar system as the primary user of a cognitive radio system and the MIMO communication system as the secondary user, techniques similar to those of [102, 122, 123],[131] can be used to estimate and feed back the channel information between the primary and secondary systems.

Let $\mathbf{S}_{\text{obs}} \triangleq \rho\mathbf{G}_1\mathbf{S}$ be the radar interference as viewed by the communication system. This can be obtained during times that the communication system does not transmit. Since the radar transmission power ρ is very high, $\rho\mathbf{G}_1\mathbf{S}$ can be estimated with high accuracy. Based on $\mathbf{S}_{\text{obs}}$, the communication receivers can eliminate some of the interference via direct subtraction. However, due to the high power of the radar [53] and the unknown phase offset, there will always be residual interference, *i.e.*,

$$\rho\mathbf{G}_1\mathbf{S}(\mathbf{\Lambda}_1 - \mathbf{I}) \approx \rho\mathbf{G}_1\mathbf{S}\mathbf{\Lambda}_\alpha \equiv \mathbf{S}_{\text{obs}}\mathbf{\Lambda}_\alpha, \tag{6.5}$$

where $\mathbf{\Lambda}_\alpha = \text{diag}(j\alpha_{11}, \cdots, j\alpha_{1L})$, and the approximation is based on the fact that $\{\alpha_{1l}\}_{l=1}^{L}$ are small. In the above, we assume that the radar waveforms have not changed between the time the interference is estimated and used in (6.5). The signal at the communication receiver after interference cancellation equals

$$\tilde{\mathbf{Y}}_C = \mathbf{H}\mathbf{X} + \mathbf{S}_{\text{obs}}\mathbf{\Lambda}_\alpha + \mathbf{W}_C. \tag{6.6}$$

This residual interference is not circularly symmetric, and thus the communication channel capacity is achieved by non-circularly symmetric Gaussian codewords, whose covariance and complementary covariance matrix would need to be designed simultaneously [132]. Here, we consider circularly symmetric complex Gaussian codewords $\mathbf{x}(l) \sim \mathcal{CN}(0, \mathbf{R}_{xl})$, which achieve a lower bound of the channel capacity [109, 132]. This reduces the complexity of the design since we only need to design the transmit covariance matrix $\mathbf{R}_{xl}$.

Unless special measures are taken, the interference from the radar transmissions, *i.e.*, $\mathbf{S}_{\text{obs}}\mathbf{\Lambda}_\alpha$, will reduce the communication system capacity, and the interference from the communication system transmission, *i.e.*, $\mathbf{\Omega} \circ (\mathbf{G}_2\mathbf{X}\mathbf{\Lambda}_2)$ will degrade the completion of the data matrix and as a result the target detection/estimation. The application of traditional spatial filtering on $\mathbf{\Omega} \circ \mathbf{Y}_\mathbf{R}$ for eliminating the communication system interference is not straightforward and to the best of our knowledge has not been previously addressed. For the case with complete samples, the optimal detector to maximize the SINR is matched filtering following a whitening filter. However, in the case of partially sampled $\mathbf{Y}_\mathbf{R}$, *i.e.*, $\mathbf{\Omega} \circ \mathbf{Y}_\mathbf{R}$, $\mathbf{S}$ cannot be fully matched due to the sub-sampling operator. Also, the interference plus noise at the whitening filter output would not be white anymore. Further, note that the recovery of $\gamma\rho\mathbf{DS}$ via matrix completion in (6.3) is based on $(\mathbf{\Omega} \circ \mathbf{Y}_R)$. Even if we somehow find the spatial filter $\mathbf{W}$ that maximizes the SINR, the filter output $\mathbf{W}(\mathbf{\Omega} \circ \mathbf{Y}_R)$ cannot be used by the matrix completion formulation in (6.3), which follows the formulation in the MIMO-MC radar [32–35] and general matrix completion literature [36]. The extension of the matrix completion working with the additional filtering matrix is out the scope of this chapter. Of course, one could apply filtering on the recovered data matrix $\mathbf{DS}$ as post processing. However, such post-filtering would first need the matrix completion to be successful.

The approach that we propose here for addressing the radar and comm systems interference is a design for the communication TX signals, or a co-design of the communication TX signals and the radar sub-sampling scheme, so that we minimize the interference at the radar RX antennas for successful matrix completion, while satisfying certain communication system rate requirements.

6.4 Spectrum Sharing Between MIMO-MC Radar and a MIMO Communication System

First, let us provide expressions for the communication TX power and channel capacity, and the interference power at the MIMO-MC radar receiver. The total transmit power of the communication TX antennas equals

$$\mathbb{E}\{\mathrm{Tr}(\mathbf{X}\mathbf{X}^H)\} = \mathbb{E}\left\{\mathrm{Tr}\left(\sum_{l=1}^{L}\mathbf{x}(l)\mathbf{x}^H(l)\right)\right\} = \sum_{l=1}^{L}\mathrm{Tr}(\mathbf{R}_{xl}),$$

where $\mathbf{R}_{xl} \triangleq \mathbb{E}\{\mathbf{x}(l)\mathbf{x}^H(l)\}$.

Due to the sampling performed at the MIMO-MC radar receiver, the *effective interference power* (EIP) at the radar RX nodes can be expressed as:

$$\begin{aligned}
\mathrm{EIP} \triangleq& \mathbb{E}\left\{\mathrm{Tr}\left(\boldsymbol{\Omega}\circ(\mathbf{G}_2\mathbf{X}\boldsymbol{\Lambda}_2)\left(\boldsymbol{\Omega}\circ(\mathbf{G}_2\mathbf{X}\boldsymbol{\Lambda}_2)\right)^H\right)\right\}\\
=&\mathbb{E}\left\{\mathrm{Tr}\left([\mathbf{G}_{21}\mathbf{x}(1)\ldots\mathbf{G}_{2L}\mathbf{x}(L)]\boldsymbol{\Lambda}_2\boldsymbol{\Lambda}_2^H[\mathbf{G}_{21}\mathbf{x}(1)\ldots\mathbf{G}_{2L}\mathbf{x}(L)]^H\right)\right\}\\
=&\mathbb{E}\left\{\mathrm{Tr}\left(\sum_{l=1}^{L}\mathbf{G}_{2l}\mathbf{x}(l)\mathbf{x}^H(l)\mathbf{G}_{2l}^H]\right)\right\}\\
=&\sum_{l=1}^{L}\mathrm{Tr}\left(\mathbf{G}_{2l}\mathbf{R}_{xl}\mathbf{G}_{2l}^H\right) = \sum_{l=1}^{L}\mathrm{Tr}\left(\boldsymbol{\Delta}_l\mathbf{G}_2\mathbf{R}_{xl}\mathbf{G}_2^H\right),
\end{aligned} \tag{6.7}$$

where $\mathbf{G}_{2l} \triangleq \boldsymbol{\Delta}_l\mathbf{G}_2$, with $\boldsymbol{\Delta}_l = \mathrm{diag}(\boldsymbol{\Omega}_{\cdot l})$. We note that the EIP at sampling time l contains the interference corresponding only to 1's in $\boldsymbol{\Omega}_{\cdot l}$. Thus, the effective interference channel during the l-th symbol duration is $\mathbf{G}_{2l}$. In the following, the EIP is used as the figure of merit for MIMO-MC radars as it affects the performance of matrix completion and further target estimation (see simulation results in Section 6.6.1). Before matrix completion and any target estimation, the EIP should be minimized. From another perspective, the EIP is a reasonable surrogate of the radar SINR, which is widely used as figure of merit in the literature [111, 113], as in this chapter we do not assume any prior information on target parameters.

In the coexistence model of (6.4a) and (6.6), both the effective interference channel $\mathbf{G}_{2l}$, and the interference covariance matrix at the communication receiver, *i.e.*, $\mathbf{R}_{\mathrm{int}l} \triangleq \sigma_\alpha^2\mathbf{S}_{\mathrm{obs}}(l)\mathbf{S}_{\mathrm{obs}}^H(l)$, vary between sampling times. Thus, the optimum scheme for the communication transmitter would be adaptive/dynamic transmission. A symbol dependent covariance matrix, *i.e.*, $\mathbf{R}_{xl}$, would need to be designed for each symbol duration in order

to match the variation of $\mathbf{G}_{2l}$ and $\mathbf{R}_{\text{int}l}$.

The channel $\mathbf{G}_{2l}$ can be equivalently viewed as a fast fading channel with perfect channel state information at both the transmitter and receiver [52, 108]. Similar to the definition of ergodic capacity [108], the achieved capacity is the average over L symbols, *i.e.*,

$$\mathrm{C}_{\text{avg}}(\{\mathbf{R}_{xl}\}) \triangleq \frac{1}{L}\sum\nolimits_{l=1}^{L} \log_2 \left|\mathbf{I} + \mathbf{R}_{wl}^{-1}\mathbf{H}\mathbf{R}_{xl}\mathbf{H}^H\right|, \tag{6.8}$$

where $\{\mathbf{R}_{xl}\}$ denotes the set of all $\mathbf{R}_{xl}$'s and $\mathbf{R}_{wl} \triangleq \mathbf{R}_{\text{int}l} + \sigma_C^2\mathbf{I}$ for all $l \in \mathbb{N}_L^+$.

The adaptive transmission could be implemented using the V-BLAST transmitter architecture [52, Chapter 7], where the precoding matrix for symbol index l is set to $\mathbf{R}_{xl}^{1/2}$. This idea is also used in the transceiver architecture for achieving the capacity of a fast fading MIMO channel with full channel state information [52, Chapter 8.2.3], and is also discussed in [129, Chapter 9]. The adaptive transmission in response to highly mobile, fast fading channels requires the transmitter to vary the rate, power and even the coding strategy. The main bottleneck of the system is not due to the complexity of designing and implementing the variable transmission parameters, but rather due to the feedback delay of the fast fading channel. In our case, the latter issue is not relevant because the channel variations are introduced by the MC technique and radar waveforms, which are available at the communication transmitter.

In this section, spectrum sharing between the communication system and the MIMO-MC radar is achieved by minimizing the interference power at the MIMO-MC radar RX node, while satisfying the communication rate and TX power constraints of the communication system. The design variables are the communication TX covariance matrices and/or the radar sub-sampling scheme. In the following we will consider two approaches, namely, a cooperative and a joint design approach.

6.4.1 Cooperative Spectrum Sharing

In the *cooperative approach*, the MIMO-MC radar shares its sampling scheme $\mathbf{\Omega}$ with the communication system. The spectrum sharing problem can be formulated as

$$(\mathbf{P}_1) \quad \min_{\{\mathbf{R}_{xl}\}\succeq 0} \text{EIP}(\{\mathbf{R}_{xl}\}) \text{ s.t. } \sum\nolimits_{l=1}^{L} \text{Tr}\left(\mathbf{R}_{xl}\right) \leq P_t \tag{6.9a}$$

$$\text{C}_{\text{avg}}(\{\mathbf{R}_{xl}\}) \geq C, \tag{6.9b}$$

where the constraint of (6.9a) restricts the total transmit power at the communication TX antennas to be no larger than P_t. The constraint of (6.9b) restricts the communication average capacity during L symbol durations to be at least C, in order to provide reliable communication and avoid service outage. $\{\mathbf{R}_{xl}\} \succeq 0$ imposes the positive semi-definiteness on the solution.

Problem $(\mathbf{P}_1)$ is convex and involves multiple matrix variables, the joint optimization w.r.t. which requires high computational complexity. Fortunately, we observe that both the objective and constraints are separable functions of $\{\mathbf{R}_{xl}\}$. An efficient algorithm for solving the above problem can be implemented based on the Lagrangian dual decomposition [118] as follows.

An Efficient Algorithm Based on Dual Decomposition

The Lagrangian of $(\mathbf{P}_1)$ can be written as

$$\mathcal{L}(\{\mathbf{R}_{xl}\}, \lambda_1, \lambda_2) = \text{EIP}(\{\mathbf{R}_{xl}\}) + \lambda_2 \left(C - \text{C}_{\text{avg}}(\{\mathbf{R}_{xl}\})\right) + \lambda_1 \left(\sum\nolimits_{l=1}^{L} \text{Tr}\left(\mathbf{R}_{xl}\right) - P_t\right),$$

where $\lambda_1 \geq 0$ is the dual variable associated with the transmit power constraint, and $\lambda_2 \geq 0$ is the dual variable associated with the average capacity constraint. The dual problem of $(\mathbf{P}_1)$ is

$$(\mathbf{P}_1\text{-}\mathbf{D}) \ \max_{\lambda_1,\lambda_2\geq 0} g(\lambda_1, \lambda_2),$$

where $g(\lambda_1, \lambda_2)$ is the dual function defined as

$$g(\lambda_1, \lambda_2) = \inf_{\{\mathbf{R}_{xl}\}\succeq 0} \mathcal{L}(\{\mathbf{R}_{xl}\}, \lambda_1, \lambda_2).$$

The domain of the dual function, *i.e.*, $\text{dom}\, g$, is $\lambda_1, \lambda_2 \geq 0$ such that $g(\lambda_1, \lambda_2) > -\infty$. It is also called dual feasible if $(\lambda_1, \lambda_2) \in \text{dom}\, g$. It is interesting to note that $g(\lambda_1, \lambda_2)$ can be

obtained by solving L independent subproblems, each of which can be written as follows

$$(\mathbf{P}_1\text{-sub}) \min_{\mathbf{R}_{xl}\succeq 0} \mathrm{Tr}\left(\left(\mathbf{G}_2^H\boldsymbol{\Delta}_l\mathbf{G}_2+\lambda_1\mathbf{I}\right)\mathbf{R}_{xl}\right)-\lambda_2\log_2\left|\mathbf{I}+\mathbf{R}_{wl}^{-1}\mathbf{H}\mathbf{R}_{xl}\mathbf{H}^H\right|. \tag{6.10}$$

Before giving the solution of ($\mathbf{P}_1$-sub), let us first state some observations.

Observation 1) The average capacity constraint should be active at the optimal point. This means that the achieved capacity is always C and $\lambda_2 > 0$. To show this, let us assume that the optimal point $\{\mathbf{R}_{xl}^*\}$ achieves $\mathrm{C}_{\mathrm{avg}}(\{\mathbf{R}_{xl}^*\}) > C$. Then we can always shrink $\{\mathbf{R}_{xl}^*\}$ until the average capacity reduces to C, which would also reduce the objective. Thus, we end up with a contradiction. By complementary slackness, the corresponding dual variable is positive, *i.e.*, $\lambda_2 > 0$.

Observation 2) $\left(\mathbf{G}_2^H\boldsymbol{\Delta}_l\mathbf{G}_2+\lambda_1\mathbf{I}\right)$ is positive definite for all $l\in\mathbb{N}_L^+$. This can be shown by contradiction. Suppose that there exists l such that $\mathbf{G}_2^H\boldsymbol{\Delta}_l\mathbf{G}_2+\lambda_1\mathbf{I}$ is singular. Then it must hold that $\mathbf{G}_2^H\boldsymbol{\Delta}_l\mathbf{G}_2$ is singular and $\lambda_1 = 0$. Therefore, we can always find a nonzero vector $\mathbf{v}$ lying in the null space of $\mathbf{G}_2^H\boldsymbol{\Delta}_l\mathbf{G}_2$. At the same time, it holds that $\mathbf{R}_{wl}^{-1/2}\mathbf{H}\mathbf{v}\neq 0$ with very high probability, because $\mathbf{H}$ is a realization of the random channel. If we choose $\mathbf{R}_{xl} = \alpha\mathbf{v}\mathbf{v}^H$ and $\alpha\to\infty$, the Lagrangian $\mathcal{L}(\{\mathbf{R}_{xl}\},0,\lambda_2)$ will be unbounded from below, which indicates that $\lambda_1 = 0$ is not dual feasible. This means that λ_1 is strictly larger than 0 if $\mathbf{G}_2^H\boldsymbol{\Delta}_l\mathbf{G}_2$ is singular for any l. Thus, the claim is proven.

Based on the above observations, we have the following lemma.

Lemma 7 ([122, 123])**.** *For given feasible dual variables $\lambda_1,\lambda_2\geq 0$, the optimal solution of* ($\mathbf{P}_1$-sub) *is given by*

$$\mathbf{R}_{xl}^*(\lambda_1,\lambda_2) = \boldsymbol{\Phi}_l^{-1/2}\mathbf{U}_l\boldsymbol{\Sigma}_l\mathbf{U}_l^H\boldsymbol{\Phi}_l^{-1/2}, \tag{6.11}$$

where $\boldsymbol{\Phi}_l \triangleq \mathbf{G}_2^H\boldsymbol{\Delta}_l\mathbf{G}_2+\lambda_1\mathbf{I}$; $\mathbf{U}_l$ is the right singular matrix of $\tilde{\mathbf{H}}_l \triangleq \mathbf{R}_{wl}^{-1/2}\mathbf{H}\boldsymbol{\Phi}_l^{-1/2}$; $\boldsymbol{\Sigma}_l = \mathrm{diag}(\beta_{l1},\ldots,\beta_{lr})$ with $\beta_{li} = (\lambda_2 - 1/\sigma_{li}^2)^+$, r and $\sigma_{li}, i=1,\ldots,r$, respectively being the rank and the positive singular vales of $\tilde{\mathbf{H}}_l$. It also holds that

$$\log_2\left|\mathbf{I}+\mathbf{R}_{wl}^{-1}\mathbf{H}\mathbf{R}_{xl}^*\mathbf{H}^H\right| = \sum\nolimits_{i=1}^{r}\left(\log(\lambda_2\sigma_{li}^2)\right)^+. \tag{6.12}$$

Based on Lemma 7, the solution of ($\mathbf{P}_1$) can be obtained by finding the optimal dual variables λ_1^*,λ_2^*. The cooperative spectrum sharing problem ($\mathbf{P}_1$) can be solved via the

procedure outlined in Algorithm 3. The convergence of Algorithm 3 is guaranteed by the convergence of the ellipsoid method [133].

Algorithm 3 Cooperative Spectrum Sharing ($\mathbf{P}_1$)

1: **Input:** $\mathbf{H}, \mathbf{G}_1, \mathbf{G}_2, \mathbf{\Omega}, P_t, C, \sigma_C^2$
2: **Initialization:** $\lambda_1 \geq 0, \lambda_2 \geq 0$
3: **repeat**
4: Calculate $\mathbf{R}_{xl}^*(\lambda_1, \lambda_2)$ according to (6.11) with the given λ_1 and λ_2;
5: Compute the subgradient of $g(\lambda_1, \lambda_2)$ as $\sum_{l=1}^{L} \mathrm{Tr}\left(\mathbf{R}_{xl}^*(\lambda_1, \lambda_2)\right) - P_t$ and $C - \mathrm{C}_{\mathrm{avg}}(\{\mathbf{R}_{xl}^*(\lambda_1, \lambda_2)\})$ respectively for λ_1 and λ_2;
6: Update λ_1 and λ_2 accordingly based on the ellipsoid method [133];
7: **until** λ_1 and λ_2 converge to a prescribed accuracy.
8: **Output:** $\mathbf{R}_{xl}^* = \mathbf{R}_{xl}^*(\lambda_1, \lambda_2)$

Based on Lemma 7, the coexistence model can be equivalently viewed as a fast fading MIMO channel $\tilde{\mathbf{H}}_l$. The covariance of the waveforms transmitted on $\tilde{\mathbf{H}}_l$ is $\tilde{\mathbf{R}}_{xl} \triangleq \mathbf{\Phi}_l^{1/2} \mathbf{R}_{xl} \mathbf{\Phi}_l^{1/2}$. It is well-known that the optimum $\tilde{\mathbf{R}}_{xl}$ equals $\mathbf{U}_l \mathbf{\Sigma}_l \mathbf{U}_l^H$ with power allocation obtained by the water-filling algorithm [108]. The achieved capacity is the average over all realization of the channel, *i.e.*, $\{\tilde{\mathbf{H}}_l\}_{l=1}^L$. This justifies the definition of average capacity in (6.8). Lemma 7 shows that the communication transmitter will allocate more power to directions determined by the left singular vectors of $\mathbf{H}$ corresponding to larger eigenvalues and by the eigenvectors of $\mathbf{\Phi}_l$ corresponding to smaller eigenvalues. In other words, the communication will transmit more power in directions that convey larger signal at the communication receivers and smaller interferences to the MIMO-MC radars.

Spectrum Sharing without knowledge of the radar's sampling scheme

If the MIMO-MC radar does not share $\mathbf{\Omega}$ with the communication system, the expression of EIP of (6.7) is also not available at the communication system. In this case, the communication system can design its covariance assuming that $\mathbf{\Omega}$ is full of 1's, *i.e.*, for the worst case of interference

$$\begin{aligned} (\mathbf{P}_0) \quad & \min_{\{\mathbf{R}_{xl}\} \succeq 0} \sum_{l=1}^{L} \mathrm{Tr}\left(\mathbf{G}_2 \mathbf{R}_{xl} \mathbf{G}_2^H\right) \\ & \text{s.t.} \quad \sum_{l=1}^{L} \mathrm{Tr}\left(\mathbf{R}_{xl}\right) \leq P_t, \mathrm{C}_{\mathrm{avg}}(\{\mathbf{R}_{xl}\}) \geq C. \end{aligned} \tag{6.13}$$

The same design would hold for the case in which a traditional MIMO radar is used instead of a MIMO-MC radar. Problem $(\mathbf{P}_0)$ is also convex and has exactly the same constraints as $(\mathbf{P}_1)$. The efficient algorithm based on the dual decomposition technique in Algorithm 3 could also be applied to solve $(\mathbf{P}_0)$.

The following theorem compares the minimum EIP achieved by the cooperative approaches of $(\mathbf{P}_0)$ and $(\mathbf{P}_1)$ under the same communication constraints.

Theorem 3. *For any P_t and C, the EIP achieved by the cooperative approaches of ($\mathbf{P}_1$) is less or equal than that achieved by the approach of ($\mathbf{P}_0$).*

Proof. Let $\{\mathbf{R}_{xl}^{*0}\}$ and $\{\mathbf{R}_{xl}^{*1}\}$ denote the solution of $(\mathbf{P}_0)$ and $(\mathbf{P}_1)$, respectively. We know that $\{\mathbf{R}_{xl}^{*0}\}$ satisfies the constraints in $(\mathbf{P}_1)$, which means that $\{\mathbf{R}_{xl}^{*0}\}$ is a feasible point of $(\mathbf{P}_1)$. The optimal $\{\mathbf{R}_{xl}^{*1}\}$ achieves an objective value no larger than any feasible point, including $\{\mathbf{R}_{xl}^{*0}\}$. It holds that $\text{EIP}(\{\mathbf{R}_{xl}^{*1}\}) \leq \text{EIP}(\{\mathbf{R}_{xl}^{*0}\})$, which proves the claim. □

There are certain scenarios in which $(\mathbf{P}_1)$ outperforms $(\mathbf{P}_0)$ significantly in terms of EIP. Let us denote by ϕ_1 the intersection of null space $\mathcal{N}(\mathbf{G}_{2l})$ and range space $\mathcal{R}(\mathbf{R}_{wl}^{1/2}\mathbf{H})$, and by ϕ_2 the intersection of null space $\mathcal{N}(\mathbf{G}_2)$ and range space $\mathcal{R}(\mathbf{R}_{wl}^{1/2}\mathbf{H})$. It holds that $\phi_2 \subseteq \phi_1$. Consider the case where ϕ_1 is nonempty while ϕ_2 is empty. This happens with high probability when $M_{r,R} \geq M_{t,C}$ but $pM_{r,R}$ is much smaller than $M_{t,C}$. Problem $(\mathbf{P}_1)$ will guide the communication system to focus its transmission power along the directions in ϕ_1 to satisfy both communication system constraints, while introducing zero EIP to the radar system. On the other hand, since ϕ_2 is empty, Problem $(\mathbf{P}_0)$ will guide the communication system transmit power along directions that introduce nonzero EIP. In other words, the subsampling procedure in the MIMO-MC radar essentially modulates the interference channel from the communication transmitter to the radar receiver by multiplying $\{\mathbf{\Delta}_l\}$. Compared to the original interference channel $\mathbf{G}_2$, the dimension of the row space of modulated channel $\mathbf{G}_{2l}$ may be greatly reduced. The cooperative approach allows the communication system to optimally design the communication precoding matrices w.r.t. the effective interference channel $\mathbf{G}_{2l}$. Therefore, it is expected that the cooperative approach based on the knowledge of $\mathbf{\Omega}$, *i.e.*, $(\mathbf{P}_1)$, introduces smaller EIP than its counterpart approach without knowledge of $\mathbf{\Omega}$, *i.e.*, $(\mathbf{P}_0)$, does under the same the communication constraints.

6.4.2 Joint Communication and Radar System Design for Spectrum Sharing

In the above described spectrum sharing strategies, the MIMO-MC radar operates with a predetermined pseudo random sampling scheme. In this section, we consider a joint design of the communication system transmit covariance matrices and the MIMO-MC radar random sampling scheme, *i.e.*, $\mathbf{\Omega}$. The candidate sampling scheme needs to ensure that the resulting data matrix can be completed. This means that $\mathbf{\Omega}$ is either a uniformly random sub-sampling matrix [36], or a matrix with a large spectral gap [124].

Recall that EIP $= \sum_{l=1}^{L} \mathrm{Tr}\left(\mathbf{\Delta}_l \mathbf{G}_2 \mathbf{R}_{xl} \mathbf{G}_2^H\right)$. The joint design scheme is formulated as

$$\begin{aligned}(\mathbf{P}_2) \quad \min_{\{\mathbf{R}_{xl}\}\succeq 0, \mathbf{\Omega}} \ & \sum\nolimits_{l=1}^{L} \mathrm{Tr}\left(\mathbf{\Delta}_l \mathbf{G}_2 \mathbf{R}_{xl} \mathbf{G}_2^H\right) \\ \text{s.t.} \ & \sum_{l=1}^{L} \mathrm{Tr}\left(\mathbf{R}_{xl}\right) \le P_t, \mathrm{C}_{\mathrm{avg}}(\{\mathbf{R}_{xl}\}) \ge C, \\ & \mathbf{\Delta}_l = \mathrm{diag}(\mathbf{\Omega}_{\cdot l}), \mathbf{\Omega} \text{ is proper.}\end{aligned}$$

The above problem is not convex. A solution can be obtained via alternating optimization. Let $(\{\mathbf{R}_{xl}^n\}, \mathbf{\Omega}^n)$ be the variables at the n-th iteration. We alternatively solve the following two problems:

$$\begin{aligned}\{\mathbf{R}_{xl}^n\} = & \arg\min_{\{\mathbf{R}_{xl}\}\succeq 0} \sum\nolimits_{l=1}^{L} \mathrm{Tr}\left(\mathbf{\Delta}_l^{n-1} \mathbf{G}_2 \mathbf{R}_{xl} \mathbf{G}_2^H\right), \qquad (6.14a) \\ & \text{s.t.} \ \sum_{l=1}^{L} \mathrm{Tr}\left(\mathbf{R}_{xl}\right) \le P_t, \mathrm{C}_{\mathrm{avg}}(\{\mathbf{R}_{xl}\}) \ge C, \\ \mathbf{\Omega}^n = & \arg\min_{\mathbf{\Omega}} \sum\nolimits_{l=1}^{L} \mathrm{Tr}\left(\mathbf{\Delta}_l \mathbf{G}_2 \mathbf{R}_{xl}^n \mathbf{G}_2^H\right), \qquad (6.14b) \\ & \text{s.t.} \ \mathbf{\Delta}_l = \mathrm{diag}(\mathbf{\Omega}_{\cdot l}), \mathbf{\Omega} \text{ is proper.}\end{aligned}$$

The problem of (6.14a) is convex and can be solved efficiently. By simple algebraic manipulation, the EIP can be reformulated as EIP $= \mathrm{Tr}(\mathbf{\Omega}^T \mathbf{Q})$, where the l-th column of $\mathbf{Q}$ contains the diagonal entries of $\mathbf{G}_2 \mathbf{R}_{xl} \mathbf{G}_2^H$. Based on the above reformulation of EIP, we can rewrite (6.14b) as

$$\mathbf{\Omega}^n = \arg\min_{\mathbf{\Omega}} \ \mathrm{Tr}(\mathbf{\Omega}^T \mathbf{Q}^n) \quad \text{s.t. } \mathbf{\Omega} \text{ is proper}, \qquad (6.15)$$

where the l-th column of $\mathbf{Q}^n$ contains the diagonal entries of $\mathbf{G}_2 \mathbf{R}_{xl}^n \mathbf{G}_2^H$. Therefore, the EIP can be reduced by carefully choosing $\mathbf{\Omega}$. Recall that the sampling matrix $\mathbf{\Omega}$ is proper

either if it is a uniformly random sampling matrix, or it has large spectral gap. However, it is difficult to incorporate such conditions in the above optimization problem.

Noticing that row and column permutation of the sampling matrix would not affect its singular values and thus the spectral gap, we propose to optimize the sampling scheme by permuting the rows and columns of an initial sampling matrix $\mathbf{\Omega}^0$, *i.e.*,

$$\mathbf{\Omega}^n = \arg\min_{\mathbf{\Omega}} \ \mathrm{Tr}(\mathbf{\Omega}^T \mathbf{Q}^n) \quad \text{s.t. } \mathbf{\Omega} \in \wp(\mathbf{\Omega}^0), \tag{6.16}$$

where $\wp(\mathbf{\Omega}^0)$ denotes the set of matrices obtained by arbitrary row and/or column permutations. The $\mathbf{\Omega}^0$ is generated with binary entries and $\lfloor pLM_{r,R} \rfloor$ ones. One good candidate for $\mathbf{\Omega}^0$ would be a uniformly random sampling matrix, as such matrix exhibit large spectral gap with high probability [124]. Brute-force search can be used to find the optimal $\mathbf{\Omega}$. However, the complexity is very high since $|\wp(\mathbf{\Omega}^0)| = \Theta(M_{r,R}!L!)$. By alternately optimizing w.r.t. row permutation and column permutation on $\mathbf{\Omega}^0$, we can solve (6.16) using a sequence of linear assignment problems [134].

To optimize w.r.t. column permutation, we need to find the best one-to-one match between the columns of $\mathbf{\Omega}^0$ and the columns of $\mathbf{Q}^n$. We construct a cost matrix $\mathbf{C}^c \in \mathbb{R}^{L \times L}$ with $[\mathbf{C}^c]_{ml} \triangleq (\mathbf{\Omega}^0_{\cdot m})^T \mathbf{Q}^n_{\cdot l}$. The problem turns out to be a linear assignment problem with cost matrix $\mathbf{C}^c$, which can be solved in polynomial time using the Hungarian algorithm [134]. Let $\mathbf{\Omega}^c$ denote the column-permutated sampling matrix after the above step. Then, we permute the rows of $\mathbf{\Omega}^c$ to optimally match the rows of $\mathbf{Q}^n$. Similarly, we construct a cost matrix $\mathbf{C}^r \in \mathbb{R}^{M_{r,R} \times M_{r,R}}$ with $[\mathbf{C}^r]_{ml} \triangleq \mathbf{\Omega}^c_{m\cdot}(\mathbf{Q}^n_{l\cdot})^T$. Again, the Hungarian algorithm can be used to solve the row assignment problem. The above column and row permutation steps are alternately repeated until $\mathrm{Tr}(\mathbf{\Omega}^T \mathbf{Q}^n)$ becomes smaller than a certain predefined threshold δ_1.

The complete joint-design spectrum sharing algorithm is summarized in Algorithm 4. The proposed algorithm stops when the value of EIP changes between two iterations drops below a certain threshold δ_2. It is easy to show that the objective function, *i.e.*, EIP, is nonincreasing during the alternating iterations between (6.14a) and (6.14b), and is lower bounded by zero. According to the monotone convergence theorem [135], the alternating optimization is guaranteed to converge. The proposed joint-design spectrum sharing strategy

is expected to further reduce the EIP at the MIMO-MC radar RX node compared to the cooperative methods in Section 6.4.1. However, ($\mathbf{P}_2$) has higher computational complexity than ($\mathbf{P}_1$) and ($\mathbf{P}_0$) (see detailed complexity analysis in Section 6.4.3). ($\mathbf{P}_1$) and ($\mathbf{P}_0$) could be preferable in cases of limited computing resources.

Algorithm 4 Joint design based spectrum sharing between MIMO-MC radar and a MIMO comm. system

Input: $\mathbf{H}, \mathbf{G}_1, \mathbf{G}_2, P_t, C, \sigma_C^2, \delta_1, \delta_2$
Initialization: $\mathbf{\Omega}^0$ is a uniformly random sampling matrix
repeat
  $\{\mathbf{R}_{xl}^n\} \leftarrow$ Solve problem (6.14a) using **Algorithm** 3 while fixing $\mathbf{\Omega}^{n-1}$
  $\mathbf{\Omega}^{prev} \leftarrow \mathbf{\Omega}^{n-1}$
  loop
    $\mathbf{\Omega}^c \leftarrow$ Find the best column permutation of $\mathbf{\Omega}^{prev}$ by solving the linear assignment problem with cost matrix $\mathbf{C}^c$
    $\mathbf{\Omega}^r \leftarrow$ Find the best row permutation of $\mathbf{\Omega}^c$ by solving the linear assignment problem with cost matrix $\mathbf{C}^r$
    if $|\mathrm{Tr}((\mathbf{\Omega}^r)^T\mathbf{Q}^n) - \mathrm{Tr}((\mathbf{\Omega}^{prev})^T\mathbf{Q}^n)| < \delta_1$ **then**
      Break
    end if
    $\mathbf{\Omega}^{prev} \leftarrow \mathbf{\Omega}^r$
  end loop
  $\mathbf{\Omega}^n \leftarrow \mathbf{\Omega}^r$; $n \leftarrow n+1$
until $|\mathrm{EIP}^n - \mathrm{EIP}^{n-1}| < \delta_2$
Output: $\{\mathbf{R}_{xl}\} = \{\mathbf{R}_{xl}^n\}, \mathbf{\Omega} = \mathbf{\Omega}^n$

6.4.3 Complexity

The adaptive communication transmission in the proposed spectrum sharing methods involves high complexity. A natural question would be how much would one lose by using a sub-optimal transmission approach of constant rate, *i.e.*, $\mathbf{R}_{xl} = \cdots = \mathbf{R}_{xL} \equiv \mathbf{R}_x$, which has lower implementation complexity. In such case, the spectrum sharing problem ($\mathbf{P}_1$) can be reformulated as

$$(\mathbf{P}_1') \min_{\mathbf{R}_x \succeq 0} \mathrm{EIP}(\mathbf{R}_x) \quad \text{s.t. } L\mathrm{Tr}(\mathbf{R}_x) \le P_t, \mathrm{C}_{\mathrm{avg}}(\mathbf{R}_x) \ge C, \tag{6.17}$$

where $\mathrm{EIP}(\mathbf{R}_x) \triangleq \mathrm{Tr}\left(\mathbf{\Delta}\mathbf{G}_2\mathbf{R}_x\mathbf{G}_2^H\right)$ and $\mathbf{\Delta}$ is diagonal and with each entry equal to the sum of the entries in the corresponding row of $\mathbf{\Omega}$. We can see that ($\mathbf{P}_1'$) is much easier to solve because there is only one matrix variable. However, as it will be seen in the simulations of

Section 6.6.2, the constant rate transmission based on solving (6.9) is inferior to the adaptive transmission based on solving (6.17).

It is clear that $(\mathbf{P}_0)$ and $(\mathbf{P}_1)$ have the same computational complexity, because the objectives and the constraints are similar. If an interior-point method [118] is used directly to the problems, the complexity is polynomial (cubic or slightly higher orders) in the number of real variables in each problem. For both $(\mathbf{P}_0)$ and $(\mathbf{P}_1)$, the semidefinite matrix variables $\{\mathbf{R}_{xl}\}$ have $LM_{t,C}^2$ real scalar variables. For the sub-optimal $(\mathbf{P}_1')$, there is only one semidefinite matrix variable $\mathbf{R}_x$, which results in $M_{t,C}^2$ real scalar variables. Therefore, the computational costs of $(\mathbf{P}_0)$ and $(\mathbf{P}_1)$ are at least L^3 times of that of $(\mathbf{P}_1')$, which are prohibitive if L is large. Fortunately, when $(\mathbf{P}_0)$ and $(\mathbf{P}_1)$ are solved using Algorithm 3 based on dual decomposition, the computation complexity is greatly reduced and scales linearly with L. Furthermore, the overall computation time of $(\mathbf{P}_0)$ and $(\mathbf{P}_1)$ using dual decomposition even becomes independent of L and thus equal to that of $(\mathbf{P}_1')$ if all L sub-problems ($\mathbf{P}_1$-sub) are solved simultaneously in parallel using the same computational routine [102].

To solve $(\mathbf{P}_2)$, several iterations of solving problems in (6.14a) and (6.14b) are required. The computational complexity of (6.14a) is identical to that of $(\mathbf{P}_1)$, which has been considered previously. Problem (6.14b) is in turn solved via several iterations of linear assignment problem, whose complexity cubically scales with L. Simulations show that the numbers of both inner and outer iterations in Algorithm 4 are relative small. In summary, the computational complexity of $(\mathbf{P}_2)$ is the sum of L times of a polynomial of $M_{t,C}^2$ and $\mathcal{O}(L^3)$.

6.5 Mismatched Systems

In Section 6.3, the waveform symbol duration of the radar system is assumed to match that of the communication system. In this section, we consider the mismatched case, and show that the proposed techniques presented in the previous sections can still be applied. Let $f_s^R = 1/T_R$ and f_s^C denote the radar waveform symbol rate and the communication symbol rate, respectively. Also, let the length of radar waveforms be denoted by L_R. The number of communication symbols transmitted in the duration of L_R/f_s^R is $L_C \triangleq \lceil L_R f_s^C f_s^R \rceil$. The communication average capacity and transmit power can be expressed in terms of $\{\mathbf{R}_{xl}\}_{l=1}^{L_C}$

as in Section 6.4. In the following, we will only focus on the effective interference to the MIMO-MC radar receiver.

If $f_s^R < f_s^C$, the interference arrived at the radar receiver will be down-sampled. Let $\mathcal{I}_1 \subset \mathbb{N}_{L_C}^+$ be the set of indices of communication symbols that are sampled by the radar in ascending order. It holds that $|\mathcal{I}_1| = L_R$. Following the derivation in previous sections, we have the following interference power expression:

$$\text{EIP} = \sum\nolimits_{l \in \mathcal{I}_1} \text{Tr}\left(\boldsymbol{\Delta}_{l'} \mathbf{G}_2 \mathbf{R}_{xl} \mathbf{G}_2^H\right),$$

where $l' \in \mathbb{N}_{L_R}^+$ is the index of l in ordered set $\mathcal{I}_1$. We observe that the communication symbols indexed by $\mathbb{N}_{L_C}^+ \setminus \mathcal{I}_1$, which are not sampled by the radar receiver, would introduce zero interference power to the radar system.

If $f_s^R > f_s^C$, the interference at the radar receiver will be over-sampled. One individual communication symbol will introduce interference to the radar system in $\lfloor f_s^R / f_s^C \rfloor$ consecutive symbol durations. Let $\tilde{\mathcal{I}}_l$ be the set of radar sampling time instances during the period of the l-th communication symbol. Note that $\tilde{\mathcal{I}}_l$ is with cardinality $\lfloor f_s^R / f_s^C \rfloor$, and the collection of sets $\tilde{\mathcal{I}}_1, \ldots, \tilde{\mathcal{I}}_{L_C}$ is a partition of $\mathbb{N}_{L_R}^+$. The effective interference power for both schemes of MIMO-MC radar is respectively

$$\text{EIP} = \sum\nolimits_{l=1}^{L_C} \text{Tr}\left(\tilde{\boldsymbol{\Delta}}_l \mathbf{G}_2 \mathbf{R}_{xl} \mathbf{G}_2^H\right),$$

where $\tilde{\boldsymbol{\Delta}}_l = \sum_{l' \in \tilde{\mathcal{I}}_l} \boldsymbol{\Delta}_{l'}$. We observe that each individual communication transmit covariance matrix will be weighted by the sum of interference channels for $\lfloor f_s^R / f_s^C \rfloor$ radar symbol durations instead of one single interference channel.

We conclude that in the above mismatched cases, the EIP expressions have the same form as those in the matched case except the diagonal matrix $\boldsymbol{\Delta}_l$. To calculate the corresponding diagonal matrices, the communication system only needs to know the sampling time of the radar system. Therefore, the spectrum sharing problems in such cases can still be solved using the proposed algorithms of Section 6.4.

6.6 Numerical Results

For the simulations, we set the number of symbols to $L = 32$ and the noise variance to $\sigma_C^2 = 0.01$. The MIMO radar system consists of colocated TX and RX antennas forming half-wavelength uniform linear arrays, and transmitting Gaussian orthogonal waveforms [32]. The channel $\mathbf{H}$ is taken to have independent entries, distributed as $\mathcal{CN}(0, 1)$. The interference channels $\mathbf{G}_1$ and $\mathbf{G}_2$ are generated with independent entries, distributed as $\mathcal{CN}(0, \sigma_1^2)$ and $\mathcal{CN}(0, \sigma_2^2)$, respectively. The channels are Rayleigh fading and are consistent with a flat fading model assumption [43–46, 51, 52, 66, 102, 122]. We fix $\sigma_1^2 = \sigma_2^2 = 0.01$ unless otherwise stated. The maximum communication transmit power is set to $P_t = L$ (the power is normalized w.r.t. the power of radar waveforms). The propagation path from the radar TX antennas to the radar RX antennas via the far-field target introduces a much more severe loss of power, γ^2, which is set to -30dB in the simulations. The transmit power of the radar antennas is fixed to $\rho^2 = \rho_0 \triangleq 1000L/M_{t,R}$ unless otherwise stated, and noise in the received signal is added at SNR= 25dB. The phase jitter variance is taken to be $\sigma_\alpha^2 = 10^{-3}$. The same uniformly random sampling scheme $\mathbf{\Omega}^0$ is adopted by the radar in both the cooperative spectrum sharing (SS) methods of $(\mathbf{P}_0)$ and $(\mathbf{P}_1)$. The joint-design spectrum sharing method uses the same sampling matrix as its initial sampling matrix. Recall that $(\mathbf{P}_0)$ is the cooperative spectrum sharing method when $\mathbf{\Omega}$ is not shared with the communication system. In $(\mathbf{P}_0)$, the communication system designs its waveforms by assuming $\mathbf{\Omega}$ as the all 1's matrix. Based on the obtained communication waveforms, an EIP value is calculated for $(\mathbf{P}_0)$ using the true $\mathbf{\Omega}$ for the ease of comparison. In the following figures, we denote the cooperative spectrum sharing method of $(\mathbf{P}_0)$ without knowledge of $\mathbf{\Omega}$ by "cooperative SS w/ $\mathbf{\Omega}$ unknown". We denote the cooperative spectrum sharing method of $(\mathbf{P}_1)$ by "cooperative SS"; and denote the joint-design spectrum sharing method of $(\mathbf{P}_2)$ by "joint-design SS". The TFOCUS package [136] is used for low-rank matrix completion at the radar fusion center. The communication covariance matrix is optimized according to the criteria of Section 6.4. The obtained $\mathbf{R}_{xl}$ is used to generate $\mathbf{x}(l) = \mathbf{R}_{xl}^{1/2}\text{randn}(M_{t,C}, 1)$. We use the EIP and MC relative recovery error as the performance metrics. The relative recovery error is defined as $\|\mathbf{DS} - \widehat{\mathbf{DS}}\|_F / \|\mathbf{DS}\|_F$, where $\widehat{\mathbf{DS}}$ is the completed result of

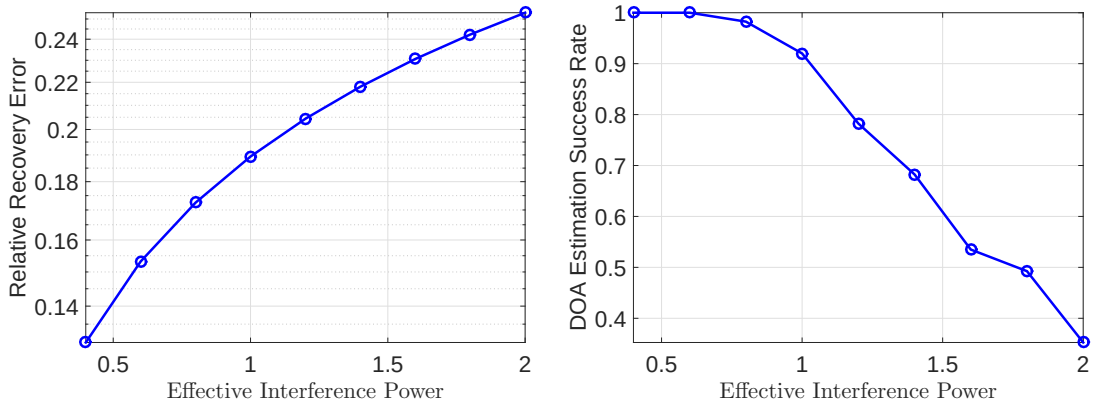

Figure 6.1: MC relative recovery errors and target angle estimation success rates under different levels of EIP for the MIMO-MC radar. $M_{t,R} = 16, M_{r,R} = 32, M_{t,C} = 4, M_{r,C} = 4$.

DS. For comparison, we also implement a "selfish communication" scenario, where the communication system minimizes the transmit power to achieve certain average capacity without any concern about the interferences it exerts to the radar system.

6.6.1 The Impact of EIP on Matrix Completion and Target Angle Estimation

In the following we provide simulation results in support of the use of EIP as a design objective. We take $M_{t,R} = 16, M_{r,R} = 32, M_{t,C} = 4, M_{r,C} = 4$. We consider two far-field targets at angle 30° and 32.5° w.r.t. the radar arrays, with target reflection coefficients equal to $0.2 + 0.1j$. The sub-sampling rate of MIMO-MC radar is fixed to 0.5. We simulate different levels of EIP by setting the communication TX covariance matrices equal to identity matrix and varying a scaling parameter. In Fig. 6.1, we show the MC relative recovery errors and target angle estimation success rates under different levels of EIP. The angle estimation is achieved by the MUSIC method based on 5 pulses [33]. A success occurs if the angle estimation error is smaller than 0.25°. The results are calculated based on 200 independent trials. One can see that the EIP indeed greatly affects the matrix completion accuracy and further the target angle estimation. In particular, a 0.5 unit increase of EIP causes a sharp 30% drop of the target angle estimation success rate. Therefore, in order to guarantee the function of the MIMO-MC radar, the EIP has to be maintained at a small level.

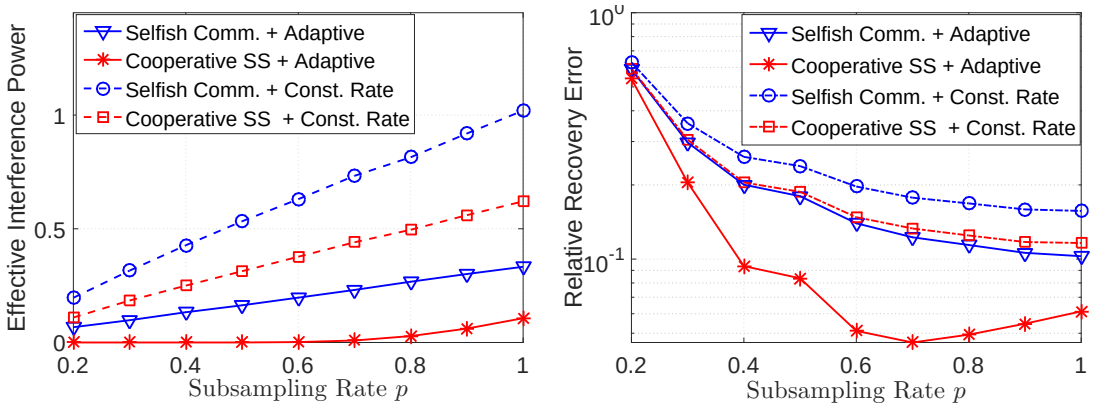

Figure 6.2: Spectrum sharing based on adaptive transmission and constant rate transmission for the MIMO-MC radar. $M_{t,R} = 4, M_{r,R} = M_{t,C} = 8, M_{r,C} = 4$.

6.6.2 Spectrum Sharing Based on Adaptive Transmission and Constant Rate Transmission

In this simulation, we compare the performance of the cooperative scheme of $(\mathbf{P}_1)$ based on adaptive transmission and the constant rate transmission scheme of $(\mathbf{P}_1')$. We also implement the selfish communication scenario using constant rate transmission. We take $M_{t,R} = 4, M_{r,R} = M_{t,C} = 8, M_{r,C} = 4$, and one far-field stationary target at angle 30° w.r.t. the radar arrays, with target reflection coefficient equal to $0.2+0.1j$. For the communication capacity constraint, we consider $C = 12$ bits/symbol. Fig. 6.2 shows the EIP and MC relative recovery error as functions of the sub-sampling rate at the MIMO-MC radar. We observe that the cooperative scheme of $(\mathbf{P}_1)$ (labeled as "Cooperative SS + Adaptive") achieves much smaller EIP and MC errors than the constant rate transmission scheme of $(\mathbf{P}_1')$ (labeled as "Cooperative SS + Const. Rate") does. It can also be seen that the constant rate transmission scheme is inferior even to the adaptive transmission based selfish communication scheme. This implies that the adaptive transmission technique plays an important role in reducing the EIP and MC errors. In the following, the performance of adaptive transmission based schemes is evaluated in more detail. As we already mentioned in Section 6.2, when the sub-sampling rate p equals 1, the MIMO-MC radar becomes the traditional MIMO radar. Therefore, the above comparison between the adaptive and the constant rate transmission scheme for MIMO-MC radars also holds for traditional MIMO radars.

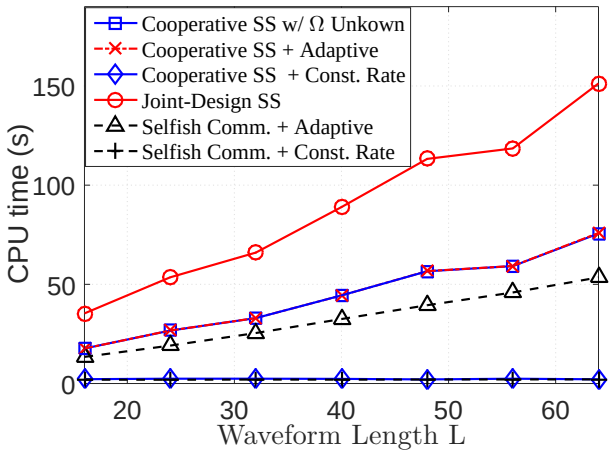

Figure 6.3: CPU time comparison for various spectrum sharing algorithms under different values of waveform length L.

To get an idea of the complexity involved in the aforementioned simulations, we recorded the CPU times for the various spectrum sharing algorithms executed on a laptop with Intel Core i7 CPU and 8GB memory. Fig. 6.3 shows the CPU times under different values of waveform length. One can observe that 1) the constant rate algorithms are the fastest and their running times are independent of L; 2) the running times of the adaptive rate algorithms, both selfish and cooperative ones, scale linearly with L; 3) the joint-design spectrum sharing method takes about 2-3 times of the cooperative spectrum sharing methods' running time. These observations match our complexity analysis in Section 6.4.3.

6.6.3 Spectrum Sharing between a MIMO-MC radar and a MIMO Communication System

Performance under different sub-sampling rates

There is a far-field stationary target at angle 30° w.r.t. the radar arrays, with target reflection coefficient equal to $0.2 + 0.1j$. For the communication capacity constraint, we consider $C = 12$ bits/symbol. The sub-sampling rate of MIMO-MC radar varies from 0.2 to 1. The following two scenarios are considered.

In the first scenario, we take $M_{t,R} = 4, M_{r,R} = M_{t,C} = 8, M_{r,C} = 4$. In Fig. 6.4(a) we plot the EIP results for 4 different realizations of $\mathbf{\Omega}^0$. For better visualization, Fig. 6.4(b) shows the relative recovery errors averaged over all 4 realizations of $\mathbf{\Omega}^0$. The cooperative scheme

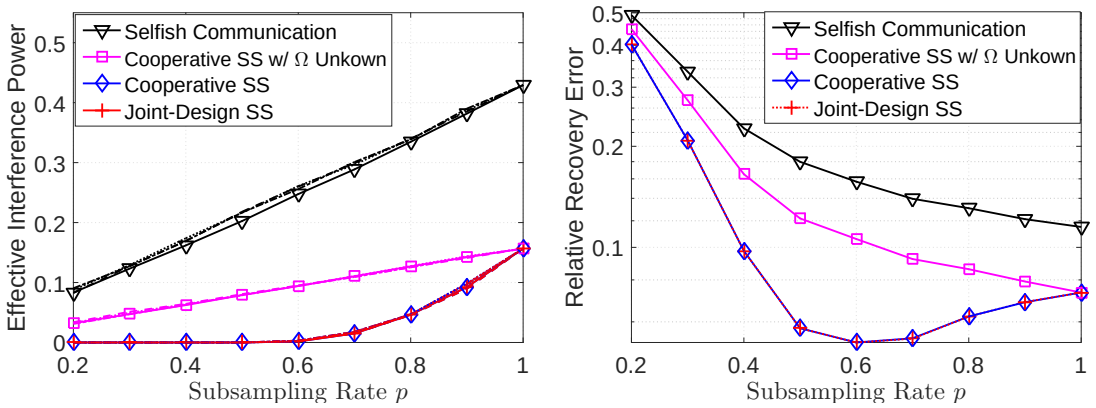

Figure 6.4: Spectrum sharing with the MIMO-MC radar under different sub-sampling rates. $M_{t,R} = 4, M_{r,R} = M_{t,C} = 8, M_{r,C} = 4$. Dashed curves correspond to EIP results using different realization of $\mathbf{\Omega}^0$.

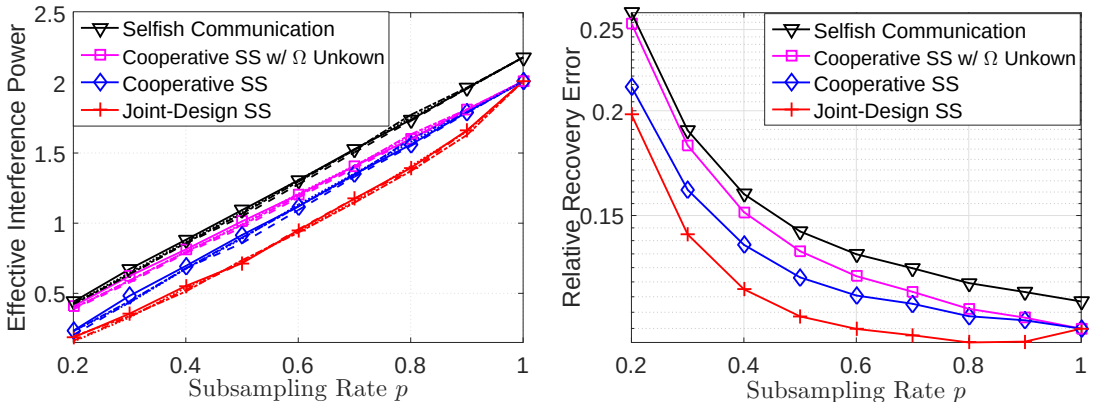

Figure 6.5: Spectrum sharing with the MIMO-MC radar under different sub-sampling rates. $M_{t,R} = 16, M_{r,R} = 32, M_{t,C} = M_{r,C} = 4$. Dashed curves correspond to EIP results using different realization of $\mathbf{\Omega}^0$.

(see $\mathbf{P}_1$) outperforms its counterpart without knowledge of $\mathbf{\Omega}$ (see $\mathbf{P}_0$) in terms of both the EIP and the MC relative recovery error. As discussed in Section 6.4, the EIP is significantly reduced by the cooperative method when $p < 0.6$, *i.e.*, when $pM_{r,R}$ is much smaller than $M_{t,C}$. The joint-design scheme in this scenario performs the same as the cooperative scheme, possibly because the row dimension of $\mathbf{\Omega}$ is too small to generate sufficient difference in EIP among the various permutations of $\mathbf{\Omega}$.

In the second scenario, we take $M_{t,R} = 16, M_{r,R} = 32, M_{t,C} = 4, M_{r,C} = 4$. In Fig. 6.5(a), we plot the EIP corresponding to 4 different realizations of $\mathbf{\Omega}^0$, taken as uniformly random sampling matrices. Again, Fig. 6.5(b) shows the relative recovery errors averaged over all 4 realizations of $\mathbf{\Omega}^0$. The cooperative scheme outperforms the cooperative scheme

without knowledge of $\mathbf{\Omega}$ only marginally. This is due to the fact that both $\mathbf{G}_2$ and $\mathbf{G}_{2l}$ are full rank. The joint-design scheme (see Section 6.4.2) optimizes $\mathbf{\Omega}$ starting from the same sampling matrix used by the other three methods. In this case, the joint-design scheme achieves smaller EIP and relative recovery errors than the other three methods.

In the above scenarios, we would like $p \geq 0.5$ for a small relative recovery error during matrix completion. However, values of $p > 0.7$ require more samples while achieving little or even no improvement on the recovery accuracy. Therefore, the optimal range of p is $[0.5, 0.7]$, where the proposed joint-design scheme significantly outperforms the "selfish communication method" and the "SS method w/o knowledge of $\mathbf{\Omega}$". We conclude that the proposed co-design based spectrum sharing methods utilize the sub-sampling procedure in the MIMO-MC radar to achieve small EIP and high matrix recovery accuracy.

Interestingly, for the joint-design based spectrum sharing method, the relative recovery error achieved by the sub-sampling rate $p \in [0.5, 0.9]$ is even smaller than that by full sampling $p = 1$. This indicates that due to the achieved small EIP, the full signal matrix is accurately completed. The completion process smoothes out the noise, and as result, the completed matrix enjoys higher SIR that the initial full signal matrix. Therefore, the sub-sampling procedure in MIMO-MC radar is beneficial for radar-communication spectrum sharing in terms of improving radar SINR as well as reducing the amount of data to be sent to the fusion center.

In addition, simulations indicate that the communication average capacity constraint holds with equality in both scenarios, confirming observation (1) of Section 6.4.1.

Performance under different capacity constraints

In this simulation, the constant C in the communication capacity constraint of (6.9b) varies from 6 to 14 bits/symbol, while the sub-sampling rate p is fixed to 0.5. Four different realizations of Ω^0 are considered. Fig. 6.6 shows the results for $M_{t,R} = 4, M_{r,R} = M_{t,C} = 8, M_{r,C} = 4$. For the "selfish communication" scheme and the cooperative scheme without knowledge of $\mathbf{\Omega}$, the EIP and relative recovery errors increase as the communication capacity increases. In contrast, the cooperative and joint-design schemes achieve significantly smaller EIP and relative recovery errors under all values of C. This indicates that the latter

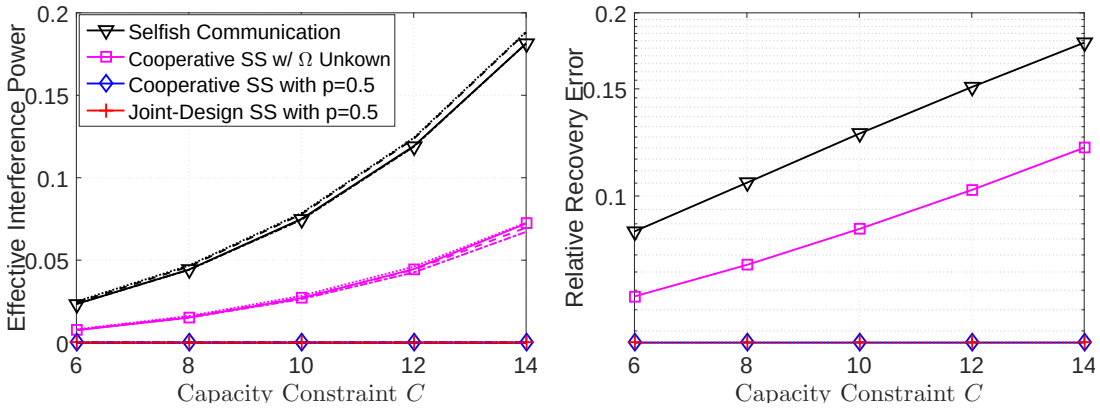

Figure 6.6: Spectrum sharing with the MIMO-MC radar under different capacity constraints C. $M_{t,R} = 4, M_{r,R} = M_{t,C} = 8, M_{r,C} = 4$. Dashed curves correspond to EIP results using different realization of $\mathbf{\Omega}^0$.

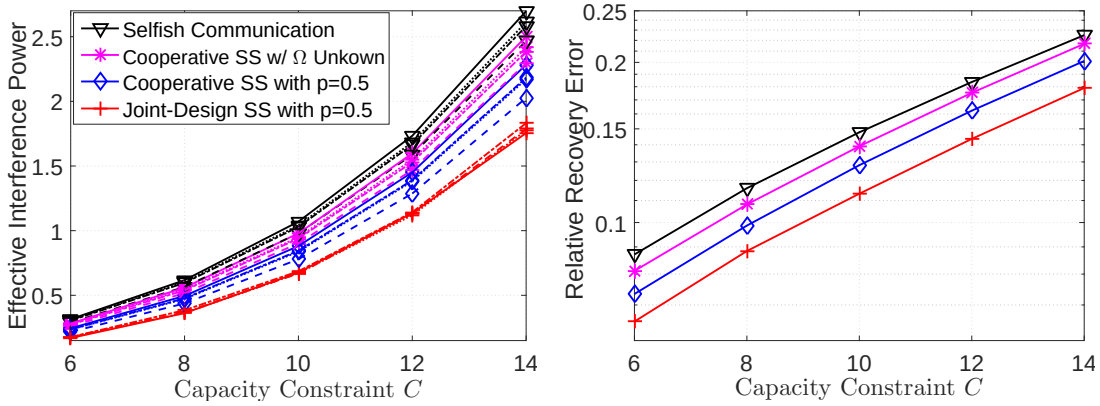

Figure 6.7: Spectrum sharing with the MIMO-MC radar under different capacity constraints C. $M_{t,R} = 16, M_{r,R} = 32, M_{t,C} = M_{r,C} = 4$. Dashed curves correspond to EIP results using different realization of $\mathbf{\Omega}^0$.

two spectrum sharing methods successfully allocate the communication transmit power in directions that result in high communication rate, but small EIP to the MIMO-MC radar.

The results for $M_{t,R} = 16, M_{r,R} = 32, M_{t,C} = M_{r,C} = 4$ are shown in Fig. 6.7. Since $M_{r,R}$ is much larger than $M_{t,C}$, the cooperative scheme with the knowledge of $\mathbf{\Omega}$ outperforms its counterpart without knowledge of $\mathbf{\Omega}$ only marginally. Meanwhile, the joint-design scheme can effectively further reduce the EIP and relative recovery errors.

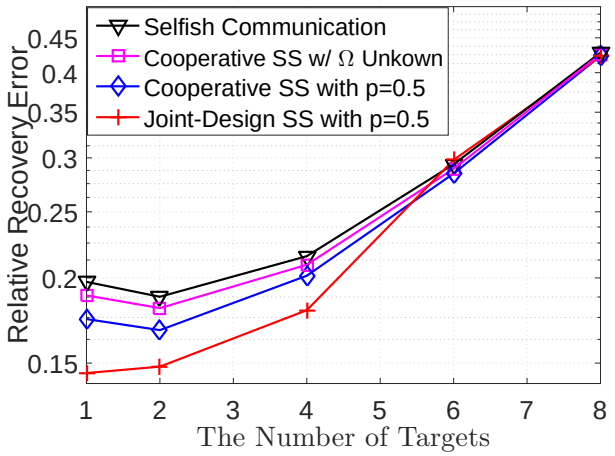

Figure 6.8: Spectrum sharing with the MIMO-MC radar when multiple targets present. $M_{t,R} = 16, M_{r,R} = 32, M_{t,C} = M_{r,C} = 4$, $p = 0.5$ and $C = 12$ bits/symbol.

Performance under different number of targets

In this simulation, we fix $p = 0.5$ and $C = 12$ and evaluate the performance when multiple targets are present. The target reflection coefficients are designed such that the target returns have fixed power, independent of the number of targets. We observe that the EIPs of different methods remain constant for different number of targets. This is because the design of the communication waveforms is not affected by the target number. Fig. 6.8 shows the results of the relative recovery error, which increases as the number of targets increases. All methods have large recovery error for large number of targets, because the retained samples are not sufficient for reliable matrix completion under any level of noise. The proposed joint-design scheme can work effectively for the MIMO-MC radar when a moderate number of targets are present.

Performance under different levels of radar TX power

In this simulation, we evaluate the effect of radar TX power ρ_2, while fixing $p = 0.5$, $C = 12$ and the target number to be 1. Fig. 6.9 shows the results of EIP and relative recovery errors for $M_{t,R} = 16, M_{r,R} = 32, M_{t,C} = M_{r,C} = 4$. Again, we see that the joint-design scheme performs the best, followed by the cooperative scheme with the knowledge of $\mathbf{\Omega}$ and then the cooperative scheme without knowledge of $\mathbf{\Omega}$. When the radar TX power increases, the EIP increases but with a much slower rate. Therefore, increasing the radar TX power

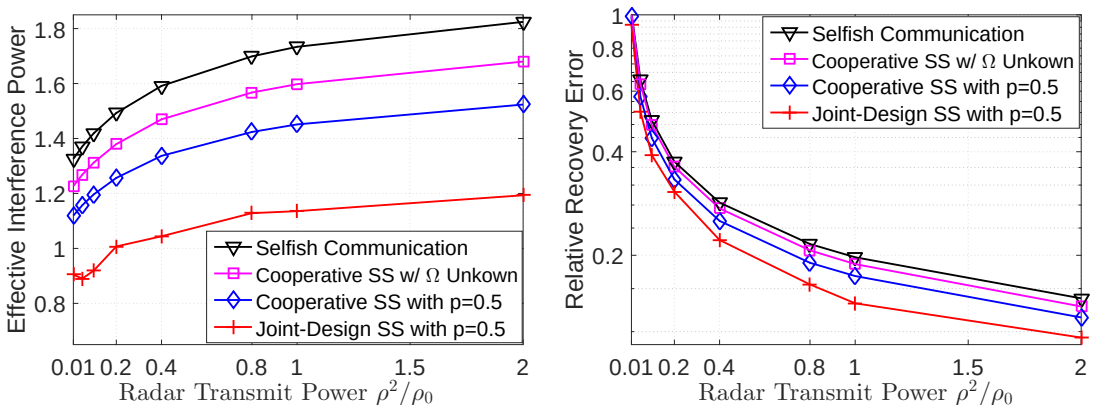

Figure 6.9: Spectrum sharing with the MIMO-MC radar under different levels of radar TX power. $M_{t,R} = 16, M_{r,R} = 32, M_{t,C} = M_{r,C} = 4$.

improves the relative recovery errors.

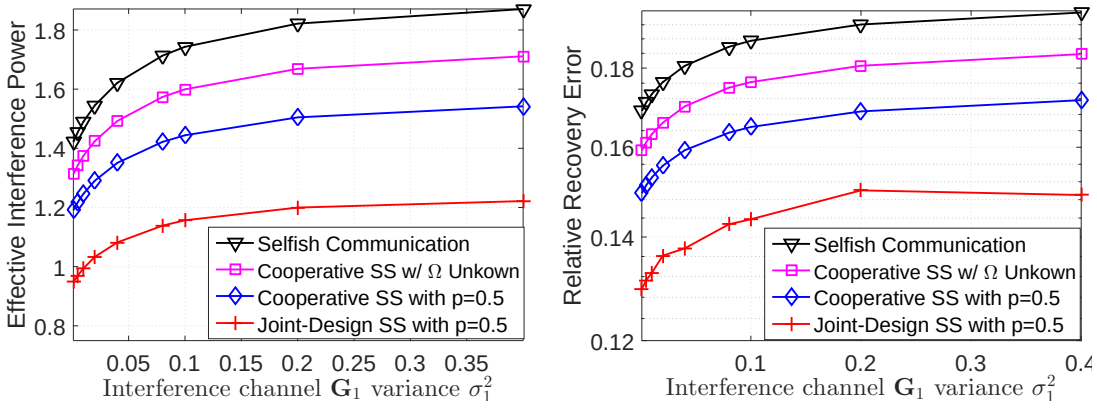

Figure 6.10: Spectrum sharing with the MIMO-MC radar under different channel variance σ_1^2 for the interference channel $\mathbf{G}_1$. $M_{t,R} = 16, M_{r,R} = 32, M_{t,C} = M_{r,C} = 4$.

Performance under different interference channel strength

In this simulation, we evaluate the effect the interference channel $\mathbf{G}_1$ with different σ_1^2, while fixing $p = 0.5$, $C = 12$ and the target number to be 1. As the communication RX gets closer to the radar TX antennas, σ_1^2 gets larger. Fig. 6.10 shows the results of EIP and relative recovery errors for $M_{t,R} = 16, M_{r,R} = 32, M_{t,C} = M_{r,C} = 4$. For all the spectrum sharing methods, when the interference channel $\mathbf{G}_1$ gets stronger, the communication TX increases its transmit power in order to satisfy the capacity constraint. Therefore, the EIP and the relative recovery errors increases with the variance σ_1^2. We also observe that the joint-design

scheme performs the best, followed by the cooperative scheme with the knowledge of $\mathbf{\Omega}$ and then the cooperative scheme without knowledge of $\mathbf{\Omega}$.

6.7 Conclusions

This chapter has considered spectrum sharing between a MIMO communication system and a MIMO-MC radar system. In order to reduce the effective interference power (EIP) at radar RX antennas, we have first considered the cooperative spectrum sharing method, which designs the communication transmit covariance matrix based on the knowledge of the radar sampling scheme. We have also formulated the spectrum sharing method for the case where the radar sampling scheme is not shared with the communication system. Our theoretical results guarantee that the cooperative approach can effectively reduce the EIP to a larger extent as compared to the spectrum sharing method without the knowledge of the radar sampling scheme. Second, we have proposed a joint design of the communication transmit covariance matrix and the radar sampling scheme to further reduce the EIP. The EIP reduction and the matrix completion recovery errors have been evaluated under various system parameters. We have shown that the MIMO-MC radars enjoy reduced interference by the communication system when the proposed spectrum sharing methods are considered. In particular, the sparse sampling at the radar RX antennas can reduce the rank of the interference channel. Our simulations have confirmed that significant EIP reduction is achieved by the cooperative approach; this is because in that approach, the communication power is allocated to directions in the null space of the effective interference channel. Our simulations have suggested that the joint-design scheme can achieve much smaller EIP and relative recovery errors than other methods when the number of radar TX and RX antennas is moderately large.

The adaptive communication transmission has been shown to be the optimal scheme for the considered spectrum sharing scenario. Compared to the constant rate transmission, the adaptive transmission requires higher computational and implementation complexity. To reduce the computation complexity, efficient algorithms have been provided based on the Lagrangian dual decomposition. As more and more powerful digital signal processors are used in modern communication terminals, advanced adaptive transmission approaches ought

to weigh heavily due to the increasing demand on high spectral efficiency. Nevertheless, the adaptive transmission approach considered in this chapter provides useful insights on the optimal design of the MIMO communication system coexisting with MIMO-MC radars, which deserves research attention despite the computational and implementation complexity.

Chapter 7

Joint Transmit Designs for Co-existence of MIMO Wireless Communications and Sparse Sensing Radars in Clutter

In this chapter, we design a scenario in which a MIMO radar system with matrix completion (MIMO-MC) optimally co-exists with a MIMO wireless communication system in the presence of clutter. By employing sparse sampling, MIMO-MC radars achieve the performance of MIMO radars but with significantly fewer data samples. To facilitate the co-existence, we employ transmit precoding at the radar and the communication system. First, we show that the error performance of matrix completion is theoretically guaranteed when precoding is employed. Second, the radar transmit precoder, the radar sub-sampling scheme, and the communication transmit covariance matrix are jointly designed to maximize the radar SINR while meeting certain rate and power constraints for the communication system. Efficient optimization algorithms are provided along with insight on the feasibility and properties of the proposed design. Simulation results show that the proposed scheme significantly improves the spectrum sharing performance in various scenarios.

7.1 Introduction

Spectrum congestion in commercial wireless communications is a growing problem as high-data-rate applications become prevalent. On the other hand, recent government studies have shown that huge chunks of spectrum held by federal agencies are underutilized in urban areas [39]. In an effort to relieve the problem, the Federal Communications Commission (FCC) and the National Telecommunications and Information Administration (NTIA) have proposed to make available 150 megahertz of spectrum in the 3.5 GHz band, which was primarily used by federal radar systems for surveillance and air defense, to be shared by both radar and communication applications [40, 41]. When communication and radar systems overlap in the

spectrum, they exert interference to each other. Spectrum sharing targets at enabling radar and communication systems to share the spectrum efficiently by minimizing interference effects.

The literature on spectrum sharing can be classified into three main classes. The first class comprises approaches which use large physical separation distances between radar and communication systems [42, 53, 54] to control interference. The second class includes approaches which optimally schedule dynamic access to spectrum [55–59], by using OFDM signals and optimally allocating subcarriers [62–64], or synthesize radar waveforms in frequency domain with controlled interference to the spectrally overlayed wireless communication systems [48, 49, 65]. The third class includes methods, which by using multiple antennas at both the radar and communication systems, allow radar and communication systems to co-exist on the same carrier frequency [43–47, 66, 67]. This greatly improves spectral efficiency as compared to the other two classes. Since our proposed method falls in this category, we will discuss this class in more detail.

Most of the existing multiple-input-multiple-output (MIMO) radar-communication spectrum sharing literature addresses interference mitigation either only for the communication system [43–46], or for the radar [47]. Spectrum sharing between traditional MIMO radars and communication systems was initially considered in [43–46, 66, 67], where the radar interference to the communication system was eliminated by projecting the radar waveforms onto the null space of the interference channel from radar to communication systems. However, projection-type techniques might miss targets lying in the row space of the interference channel. In addition, the interference from the communication system to the radar was not considered in [43–46, 66, 67]. Spatial filtering at the radar receiver was proposed in [47] to reduce interference from the communication systems. Since the output SINR of the optimal receive filter depends on the covariance matrix of the communication interference, the SINR performance could be further improved if the communication signaling was jointly designed with the radar waveforms. To the best of our knowledge, co-design of radar and communication systems for spectrum sharing was proposed in [99–101, 115] for the first time. Compared to radar design approaches of [43–47, 66, 67], the joint design has the potential to improve the spectrum utilization due to increased number of design degrees of freedom.

This chapter investigates spectrum sharing of a MIMO communication system and a matrix completion (MC) based, collocated MIMO radar (MIMO-MC) system [32–34]. MIMO radars transmit different waveforms from their transmit (TX) antennas, and their receive (RX) antennas forward their measurements to a fusion center for further processing. Based on the forwarded data, the fusion center populates a matrix, referred to as the "data matrix", which is then used by standard array processing schemes for target estimation. For a relatively small number of targets, the data matrix is low-rank [32], thus allowing one to fully reconstruct it (under certain conditions) based on a small, uniformly sampled set of its entries. This observation is the basis of MIMO-MC radars; the RX antennas forward to the fusion center a small number of pseudo-randomly sub-Nyquist sampled values of the target returns, along with their sampling scheme, each RX antenna partially filling a column of the data matrix. The full data matrix, corresponding to Nyquist sampling at the antennas, is provably recovered via MC techniques and can subsequently be used for target detection via standard array processing methods. The subsampling at the antennas avoids the need for high rate analog-to-digital converters, and the reduced amount of samples translates into power and bandwidth savings in the antenna-fusion center link. Further, the interference is confined only to the sampled entries of the data matrix, while after matrix completion the target echo power is preserved [32–34]. Compared to the compressive sensing (CS) based MIMO radars, MIMO-MC radars achieve data reduction while avoiding the basis mismatch issues inherent in CS-based approaches [24].

Spectrum sharing between a MIMO MC radar and a MIMO communication system was considered in [99] and [100], where the radar interference at the communication receiver was estimated and then subtracted from the received signal at the communication receiver. However, this approach might not work when the radar power is so high that saturates the communication receiver. Further, due to the random phase offset between the radar transmitter and the communication receiver, following the subtraction there will always be residual interference, which can degrade the communication system performance. The coexistence of traditional MIMO radars and a MIMO communication system was studied in [101, 115], where precoding was used both at the radar and the communication system, and the precoders were jointly designed to maximize the SINR at the radar receiver while

meeting certain communication system rate and power constraints. It was shown that radar TX precoding can effectively reduce the interference towards the communication receiver and maximize the radar SINR.

In this chapter, we propose a new spectrum sharing method for the MIMO-MC radars and MIMO communication systems by extending the work in [101, 137] with the following major contributions:

- We prove the feasibility of transmit precoding for MIMO-MC radars using random unitary waveforms. In particular, we show that the coherence of the data matrix of a transmit precoding based MIMO-MC radar is upper bounded by a small constant (see Theorem 6), a key condition for the applicability of matrix completion. Furthermore, the derived bound is independent of the transmit precoder as long as the resulted data matrix has rank equal to the number of targets. This means that we can design the precoder without affecting the incoherence property of the data matrix, for the purpose of transmit beamforming, interference suppression, *et al.*

- We propose a cooperative spectrum sharing algorithm for the coexistence of MIMO-MC radars and communication systems. The communication transmit covariance matrices, the radar precoding matrix, and the radar sub-sampling scheme are jointly designed in order to maximize the radar signal-to-interference-plus-noise ratio (SINR) subject to constraints on communication rate and power. The alternating optimization technique is leveraged to solve the joint design problem. We also provide insights on the problem feasibility and the rank of the solution of the radar precoding matrix. To the best of our knowledge, the joint design of transmit precoders and the radar clutter mitigation have not been considered in radar and communication coexistence literature.

Relation to literature: Our results on MIMO-MC radars using precoding extend the work in [33, 35], where transmit precoding was not considered, and the radar waveforms were required to be deterministically optimized. In contrast, in this chapter we derived a coherence bound for any radar waveform that is a random unitary matrix. This allows the radar waveform to be changed periodically, which would be good for security reasons,

without affecting the matrix completion performance.

This chapter is organized as follows. Section 7.2 starts with the background on MIMO-MC radars. We then provide the incoherence property for the MIMO-MC radars using random unitary waveforms and nontrivial precoders. Section 7.3 introduces the signal model when the MIMO-MC radar and communication systems are coexisted. The problem of MIMO communication sharing spectrum with MIMO-MC radar is studied in Sections 7.4. Numerical results and conclusions are provided in Sections 7.5-7.6.

7.2 MIMO-MC Radar Revisited

7.2.1 Background on MIMO-MC Radar

Consider a collocated MIMO radar system with $M_{t,R}$ TX antennas and $M_{r,R}$ RX antennas arranged as uniform linear arrays (ULA) with inter-element spacing d_t and d_r, respectively. The radar is pulse based with pulse repetition interval T_{PRI} and carrier wavelength λ_c. The K far-field targets are with distinct angles $\{\theta_k\}$, target reflection coefficients $\{\beta_k\}$ and Doppler shifts $\{\nu_k\}$ and are assumed to fall in the same range bin. Following the clutter-free model of [33–35], the data matrix at the fusion center can be formulated as

$$\mathbf{Y}_R = \mathbf{V}_r \mathbf{\Sigma} \mathbf{V}_t^T \mathbf{P} \mathbf{S} + \mathbf{W}_R, \tag{7.1}$$

where the m-th row of $\mathbf{Y}_R \in \mathbb{C}^{M_{r,R} \times L}$ contains the L samples forwarded by the m-th antenna; the waveforms are given in $\mathbf{S} = [\mathbf{s}(1), \cdots, \mathbf{s}(L)]$, with $\mathbf{s}(l) = [s_1(l), \cdots, s_{M_{t,R}}(l)]^T$ being the l-th snapshot across the transmit antennas; the transmit waveforms are assumed to be orthogonal, *i.e.*, it holds that $\mathbf{S}\mathbf{S}^H = \mathbf{I}_{M_{t,R}}$ [33]; $\mathbf{W}_R$ denotes additive noise; and $\mathbf{P} \in \mathbb{C}^{M_{t,R} \times M_{t,R}}$ denotes the transmit precoding matrix. $\mathbf{V}_t \triangleq [\mathbf{v}_t(\theta_1), \ldots, \mathbf{v}_t(\theta_K)]$ and $\mathbf{V}_r \triangleq [\mathbf{v}_r(\theta_1), \ldots, \mathbf{v}_r(\theta_K)]$ respectively denote the transmit and receive steering matrix and $\mathbf{v}_r(\theta) \in \mathbb{C}^{M_{r,R}}$ is the receive steering vector defined as

$$\mathbf{v}_r(\theta) \triangleq \left[e^{-j2\pi 0 \vartheta^r}, \ldots, e^{-j2\pi(M_{r,R}-1)\vartheta^r}\right]^T, \tag{7.2}$$

where $\vartheta^r = d_r \sin(\theta)/\lambda_c$ denotes the spatial frequency w.r.t. the receive array. $\mathbf{v}_t(\theta) \in \mathbb{C}^{M_{t,R}}$ is the transmit steering vector and is respectively defined. Matrix $\mathbf{\Sigma}$ is defined as $\mathbf{\Sigma} \triangleq \text{diag}([\beta_1 e^{j2\pi\nu_1}, \ldots, \beta_K e^{j2\pi\nu_K}])$. $\mathbf{D} \triangleq \mathbf{V}_r \mathbf{\Sigma} \mathbf{V}_t^T$ is also called the target response matrix.

After matched filtering at the fusion center, target estimation can be performed based on $\mathbf{Y}_R$ via standard array processing schemes [4].

When K is smaller than $M_{r,R}$ and L, the noise-free data matrix $\mathbf{M} \triangleq \mathbf{DPS}$ is low-rank and can be provably recovered based on a subset of its entries. This observation gave rise to MIMO-MC radars [33–35], where each RX antenna sub-samples the target returns and forwards the samples to the fusion center. The partially filled data matrix at the fusion center can be mathematically expressed as follows (see [33] Scheme I)

$$\mathbf{\Omega} \circ \mathbf{Y}_R = \mathbf{\Omega} \circ (\mathbf{M} + \mathbf{W}_R), \tag{7.3}$$

where $\circ$ denotes the Hadamard product; $\mathbf{\Omega}$ is the sub-sampling matrix containing 0's and 1's. The sub-sampling rate p equals $\|\mathbf{\Omega}\|_0/(LM_{r,R})$. When $p = 1$, the $\mathbf{\Omega}$ matrix is filled with 1's, and the MIMO-MC radar is identical to the traditional MIMO radar. At the fusion center, the completion of $\mathbf{M}$ can be achieved by the following nuclear norm minimization problem [36]

$$\min_{\mathbf{M}} \|\mathbf{M}\|_* \quad \text{s.t. } \|\mathbf{\Omega} \circ \mathbf{M} - \mathbf{\Omega} \circ \mathbf{Y}_R\|_F \leq \delta, \tag{7.4}$$

where $\delta > 0$ is a parameter determined by the sampled entries of the noise matrix, *i.e.*, $\mathbf{\Omega} \circ \mathbf{W}_R$. The recovery error of $\mathbf{M}$ is bounded with high probability, given that the following conditions hold [36]

- $\mathbf{M}$ is incoherennt with parameters (μ_0, μ_1),
- $\mathbf{\Omega}$ corresponds to uniformly at random sub-sampling operation with $m \triangleq M_{r,R}Lp \geq CKn \log n$, where $n \triangleq \max\{M_{r,R}, L\}$.

It is important to note that the data matrix $\mathbf{M}$ can be stably reconstructed with high accuracy and retaining all the received target echo power under the above conditions. The incoherence parameters (μ_0, μ_1) are given by $\mu_0 \geq \max(\mu(U), \mu(V))$, $\mu_1\sqrt{\frac{K}{M_{r,R}L}} \geq \|\sum_{k=1}^{K} \mathbf{U}_{\cdot k}\mathbf{V}_{\cdot k}^H\|_\infty$, where $\mathbf{U} \in \mathbb{C}^{M_{r,R} \times K}$ and $\mathbf{V} \in \mathbb{C}^{L \times K}$ contain the left and right singular vectors of $\mathbf{M}$; the coherence of subspace V spanned by basis matrix $\mathbf{V}$ is defined as

$$\mu(V) \triangleq \frac{L}{K} \max_{1 \leq l \leq L} \|\mathbf{V}_{l\cdot}\|^2 \in \left[1, \frac{L}{K}\right].$$

The upper bounds on the incoherence parameters of $\mathbf{M}$ are given in the following theorem [34, 35].

Theorem 4. *([35, Theorem 2] Coherence of* $\mathbf{M}$ *when* $\mathbf{P} = \mathbf{I}_{M_{t,R}}$ *) Let the minimum spatial frequency separation of the* K *targets be* ξ_t *and* ξ_r *w.r.t. the transmit and receive arrays. On denoting the Fejér kernel by* $F_n(x)$*, and for* $d_t = d_r = \lambda_c/2$ *and*

$$K \leq \min\left\{\sqrt{M_{r,R}/F_{M_{r,R}}(\xi_r)}, \sqrt{M_{t,R}/F_{M_{t,R}}(\xi_t)}\right\},$$

it holds that

$$\mu(U) \leq \frac{\sqrt{M_{r,R}}}{\sqrt{M_{r,R}} - (K-1)\sqrt{F_{M_{r,R}}(\xi_r)}} \triangleq \mu_0^r.$$

Further, if every snapshot of the waveforms satisfies that

$$|\mathbf{S}_{.l}^T \mathbf{v}_t(\theta)|^2 = \frac{M_{t,R}}{L},\ \forall l \in \mathbb{N}_L^+, \theta \in \left[-\frac{\pi}{2}, \frac{\pi}{2}\right], \tag{7.5}$$

then $\mu(\mathbf{V})$ *is upper bounded by*

$$\mu(V) \leq \frac{\sqrt{M_{t,R}}}{\sqrt{M_{t,R}} - (K-1)\sqrt{F_{M_{t,R}}(\xi_t)}} \triangleq \mu_0^t.$$

Consequently, the matrix $\mathbf{M}$ *is incoherent with parameters* $\mu_0 \triangleq \max\{\mu_0^r, \mu_0^t\}$ *and* $\mu_1 \triangleq \sqrt{K}\mu_0$.

In the following we discuss two points that motivate the contribution of this chapter.

1. In [35], the condition in (7.5) and the orthogonality property was used to design waveforms with good incoherence properties. However, radar waveforms need to be updates frequently as security against adversaries, which subsequently bring us the issue of computational complexity. The work of [35] involves numerical optimization on the complex Stiefel manifold [35], which has high computational complexity.

2. In radar system design, the adaptability of transmit waveforms and/or precoder is critical for the suppression of interference, including noise, clutter and jamming. In particular for MIMO-MC radars, the matrix completion performance will degrade severely when the SINR drops to as low as 10dB [33], which in turn emphasizes the importance of waveform and/or precoder design for MIMO-MC radar noise and interference mitigation. However, the results in Theorem 4 cannot be easily extended for a nontrivial transmit precoding.

To address the above two issues, we propose to use a random unitary matrix [138] as the waveform matrix $\mathbf{S}$. This choice is motivated by the simulations in [35] which show that the random unitary matrix performs almost the same as the optimally designed waveform.

7.2.2 MIMO-MC Radar Using Random Unitary Matrix

A random unitary matrix [138] can be obtained through performing the Gram-Schmidt orthogonalization on a random matrix with entries distributed as i.i.d Gaussian. This means that we can generate waveform candidates easily. The following theorem provides upper bounds on the incoherence parameter $\mu(U)$ and $\mu(V)$ of $\mathbf{M}$ when the random unitary waveform is used.

Theorem 5. *(Bounding $\mu(U)$ and $\mu(V)$) Consider the MIMO-MC radar presented in Section 7.2.1 with $\mathbf{S}$ being random unitary. For any transmit precoder $\mathbf{P}$ such that the rank of $\mathbf{M}$ is $K_0 \leq K$, and arbitrary transmit array geometry and target angles, the coherence of subspace V obeys the following:*

$$\mu(V) \leq \frac{K_0 + 2\sqrt{3K_0 \ln L} + 6 \ln L}{K_0} \triangleq \tilde{\mu}_0^t$$

with probability $1 - L^{-2}$, and the coherence of subspace U obeys $\mu(U) \leq \frac{K}{K_0}\mu_0^r$, where μ_0^r is defined in Theorems 4.

Proof. The proof can be found in Appendix 7.A. □

Based on Theorem 5, we have the following theorem for the incoherence parameters of $\mathbf{M}$.

Theorem 6. *(Coherence of $\mathbf{M}$ with random unitary waveform matrix) Consider the MIMO-MC radar presented in Section 7.2.1 with $\mathbf{S}$ being random unitary. For $d_r = \lambda_c/2$, arbitrary transmit array geometry, and*

$$K \leq \sqrt{M_{r,R}/F_{M_{r,R}}(\xi_r)},$$

the matrix $\mathbf{M}$ is incoherent with parameters $\mu_0 \triangleq \max\{\frac{K}{K_0}\mu_0^r, \tilde{\mu}_0^t\}$ and $\mu_1 \triangleq \sqrt{K}\mu_0$ with probability $1 - L^{-2}$, where μ_0^r and $\tilde{\mu}_0^t$ are defined in Theorems 4 and 5, respectively. The incoherence property of $\mathbf{M}$ holds for any precoding matrix $\mathbf{P}$ such that the rank of $\mathbf{M}$ is K_0.

Proof. The theorem can be proven by combining the bounds on $\mu(U)$ and $\mu(V)$ in Theorems 4 and 5, respectively. □

Remark 10. Some comments are in order. First, if K_0 is $\mathcal{O}(\ln L)$, the upper bound $\tilde{\mu}_0^t > 1$ is a small constant. Therefore, $\mathbf{M}$ has a good incoherent property. A similar bound was provided on the coherence of the subspaces spanned by random orthogonal basis in [139]. Second, unlike the results in Theorem 4, the probabilistic bound on $\mu(V)$ is independent of the target angles and array geometry. Third, the above results hold for any random unitary matrix $\mathbf{S}$. The radar waveform can be changed periodically, which would be good for security reason, without affecting the matrix completion performance. Finally, the probabilistic bound on $\mu(V)$ in Theorem 5 is independent of $\mathbf{P}$. This means that we can design $\mathbf{P}$, without affecting the incoherence property of $\mathbf{M}$, for the purpose of transmit beamforming and interference suppression. This key observation validates the feasibility of radar precoding based spectrum sharing approaches for MIMO-MC radar and communication systems in the sequel. □

7.3 System Model and Problem Formulation

We consider the coexistence scenario in [100], as shown in Fig. 4.1, where a MIMO-MC radar system and a MIMO communication system operate using the same carrier frequency. Note that the coexistence model is general, because when full sampling is adopted the MIMO-MC radar turns to be a traditional MIMO radar.

Suppose that the two systems use narrowband waveforms with the same symbol rate and are synchronized in sampling time (see [100] for the case of mismatched symbol rates). Consider the same target scene in a particular range bin as in Section 7.2.1 but with clutter. The signal received by the radar and communication RX antennas during L symbol durations

can be respectively expressed as

Radar fusion center:

$$\mathbf{\Omega} \circ \mathbf{Y}_R = \mathbf{\Omega} \circ \big(\underbrace{\mathbf{DPS}}_{\text{signal}} + \underbrace{\mathbf{CPS} + \mathbf{G}_2\mathbf{X}\mathbf{\Lambda}_2}_{\text{interference}} + \underbrace{\mathbf{W}_R}_{\text{noise}}\big), \tag{7.6a}$$

Communication receiver:

$$\mathbf{Y}_C = \underbrace{\mathbf{HX}}_{\text{signal}} + \underbrace{\mathbf{G}_1\mathbf{PS}\mathbf{\Lambda}_1}_{\text{interference}} + \underbrace{\mathbf{W}_C}_{\text{noise}}, \tag{7.6b}$$

where $\mathbf{Y}_R$, $\mathbf{D}$, $\mathbf{P}$, $\mathbf{S}$, $\mathbf{W}_R$, and $\mathbf{\Omega}$ are defined in Section 7.2.1. The waveform-dependent interference $\mathbf{CPS}$ contains interferences from point scatterers (clutter or interfering objects). Suppose that there are K_c point clutters with angles $\{\theta_k^c\}$, reflection coefficients $\{\beta_k^c\}$ in the same range bin as the targets. $\mathbf{C} \triangleq \sum_{k=1}^{K_c} \beta_k^c \mathbf{v}_r(\theta_k^c)\mathbf{v}_t^T(\theta_k^c)$ is the clutter response matrix. $\mathbf{Y}_C$ and $\mathbf{W}_C$ denote the received signal and additive noise at the communication RX antennas, respectively. The columns of $\mathbf{X} \triangleq [\mathbf{x}(1), \ldots, \mathbf{x}(L)]$ are codewords from the code-book of the communication system. We assume that $\mathbf{W}_{R/C}$ contains i.i.d random entries distributed as $\mathcal{CN}(0, \sigma_{R/C}^2)$. $\mathbf{H} \in \mathbb{C}^{M_{r,C} \times M_{t,C}}$ denotes the communication channel, where $M_{r,C}$ and $M_{t,C}$ denote respectively the number of RX and TX antennas of the communication system; $\mathbf{G}_1 \in \mathbb{C}^{M_{r,C} \times M_{t,R}}$ and $\mathbf{G}_2 \in \mathbb{C}^{M_{r,R} \times M_{t,C}}$ denote the interference channels between the communication and radar systems. All channels are assumed to be flat fading and remain the same over L symbol intervals [43, 44, 46, 102]. The flat fading assumption might be not valid for the communication and interference channels as the communication signal bandwidth increases. If the model needs to be treated as frequency selective, then one could consider OFDM type of radar transmissions and communication signals. In that scenario, the formulation discussed above, would apply on each carrier. Phase synchronization is assumed for the radar and communication systems separately. However, the random phase jitters of the oscillators at the transmitter and the receiver PLLs may result in time-varying phase offsets between the MIMO-MC radar and the communication system [100]. We model such phase offsets in the diagonal matrix $\mathbf{\Lambda}_i, i \in \{1, 2\}$, where its diagonal contains the random phase offset $e^{j\alpha_{il}}$ between the MIMO-MC radar and the communication system at the l-th symbol.

In the following we present a joint design of the communication TX signals and the

radar precoding matrix and sub-sampling scheme, so that we minimize the interference at the radar RX antennas for successful matrix completion, while satisfying certain communication system rate requirements.

Note that the application of traditional spatial filtering on $\mathbf{\Omega} \circ \mathbf{Y_R}$ for eliminating the interferences is not as straightforward as for the case where the entire $\mathbf{Y_R}$ matrix is available. Even if we somehow find the spatial filter $\mathbf{W}$ that maximizes the SINR, the filter output $\mathbf{W}(\mathbf{\Omega} \circ \mathbf{Y}_R)$ cannot be used by the matrix completion formulation in (7.4) because of the presentence of $\mathbf{W}$. The extension of the matrix completion working with the additional filtering matrix has not been considered in the MIMO-MC radar formulation [33–35] and general matrix completion literature [36], and is out the scope of this dissertation. Of course, one could apply filtering on the recovered data matrix $\mathbf{DS}$ as post processing. However, such post-filtering would first need the matrix completion to be successful.

7.4 The Proposed Spectrum Sharing Method

In this section, we first derive the communication rate and radar SINR in terms of communication and radar waveforms and formulate the MIMO-MC radar and MIMO communication spectrum sharing problem. In Section 7.4.1, an optimization algorithm is proposed using alternating optimization. Insight on the feasibility and properties of the proposed problem is provided in 7.4.2. We briefly discuss the spectrum sharing formulations for constant-rate communication transmission and traditional MIMO radars respectively in Section 7.4.3 and 7.4.4.

For the communication system, the covariance of interference plus noise is given by

$$\mathbf{R}_{\text{Cin}} = \mathbf{G}_1 \mathbf{\Phi} \mathbf{G}_1^H + \sigma_C^2 \mathbf{I} \tag{7.7}$$

where $\mathbf{\Phi} \triangleq \mathbf{P}\mathbf{P}^H/L$ is positive semidefinite. For $l \in \mathbb{N}_L^+$, the *instaneous* information rate is unknown because the interference plus noise is not necessarily Gaussian due to the random phase offset $\alpha_1(l)$. Instead, we are interested in a lower bound of the rate, which is given by [109]

$$\underline{C}(\mathbf{R}_{xl}, \mathbf{\Phi}) \triangleq \log_2 \left| \mathbf{I} + \mathbf{R}_{\text{Cin}}^{-1} \mathbf{H} \mathbf{R}_{xl} \mathbf{H}^H \right|,$$

which is achieved when the codeword $\mathbf{x}(l)$, $l \in \mathbb{N}_L^+$ is distributed as $\mathcal{CN}(0, \mathbf{R}_{xl})$. The average communication rate over L symbols is as follows

$$C_{\text{avg}}(\{\mathbf{R}_{xl}\}, \mathbf{\Phi}) \triangleq \frac{1}{L} \sum_{l=1}^{L} \underline{C}(\mathbf{R}_{xl}, \mathbf{\Phi}), \tag{7.8}$$

where $\{\mathbf{R}_{xl}\}$ denotes the set of all $\mathbf{R}_{xl}$'s.

The MIMO-MC radar only partially samples $\mathbf{Y}_R$. Therefore, only the sampled target signal and sampled interference determine the matrix completion performance. Based on this observation, we define the *effective signal power* (ESP) and *effective interference power* (EIP) at the radar RX node as follows

$$\begin{aligned} \text{ESP} &\triangleq \mathbb{E}\left\{\text{Tr}\left(\mathbf{\Omega} \circ (\mathbf{DPS})\left(\mathbf{\Omega} \circ (\mathbf{DPS})^H\right)\right)\right\} \\ &= pLM_{r,R}\text{Tr}\left(\mathbf{\Phi}\mathbf{D}_t\right), \end{aligned} \tag{7.9}$$

$$\begin{aligned} \text{EIP} &\triangleq \mathbb{E}\left\{\text{Tr}\left(\mathbf{\Omega} \circ (\mathbf{CPS})\left(\mathbf{\Omega} \circ (\mathbf{CPS})\right)^H\right)\right\} \\ &+ \mathbb{E}\left\{\text{Tr}\left(\mathbf{\Omega} \circ (\mathbf{G}_2\mathbf{X}\mathbf{\Lambda}_2)\left(\mathbf{\Omega} \circ (\mathbf{G}_2\mathbf{X}\mathbf{\Lambda}_2)\right)^H\right)\right\} \\ &= pLM_{r,R}\text{Tr}\left(\mathbf{\Phi}\mathbf{C}_t\right) + \sum\nolimits_{l=1}^{L} \text{Tr}\left(\mathbf{G}_{2l}\mathbf{R}_{xl}\mathbf{G}_{2l}^H\right), \end{aligned} \tag{7.10}$$

where $\mathbf{D}_t = \sum_{k=1}^{K} \sigma_{\beta_k}^2 \mathbf{v}_t^*(\theta_k)\mathbf{v}_t^T(\theta_k)$, $\mathbf{C}_t = \sum_{k=1}^{K_c} \sigma_{\beta_k^c}^2 \mathbf{v}_t^*(\theta_k^c)\mathbf{v}_t^T(\theta_k^c)$, σ_{β_k} and $\sigma_{\beta_k^c}$ denote the standard deviation of β_k and β_k^c, respectively; $\mathbf{G}_{2l} \triangleq \mathbf{\Delta}_l\mathbf{G}_2$ and $\mathbf{\Delta}_l = \text{diag}(\mathbf{\Omega}_{\cdot l})$. The derivation can be found in Appendix 7.B, which assumes that each of the target and clutter reflection coefficient is an independent complex Gaussian variable with zero mean, which is widely considered in the literature [113, 116, 117].

Remark 11. The sub-sampling at the radar receiver effectively modulates the interference channel $\mathbf{G}_2$ from the communication transmitter to the radar receiver. At sampling time l, only the interferences at radar RX antennas corresponding to 1's in $\mathbf{\Omega}_{\cdot l}$ are sampled. Equivalently, the effective interference channel during the l-th symbol duration is $\mathbf{G}_{2l}$. Therefore, adaptive communication transmission with symbol dependent covariance matrix $\mathbf{R}_{xl}$ is used in order to match the variation of the effective interference channel $\mathbf{G}_{2l}$ [100]. The disadvantage is high computational cost. A sub-optimal alternative is constant rate communication transmission, *i.e.*, $\mathbf{R}_{xl} \equiv \mathbf{R}_x, \forall l \in \mathbb{N}_L^+$, outlined in Section 7.4.3

Note that the effective target signal power and clutter interference power only depend on the scalar sub-sampling rate p instead of the complete sub-sampling matrix $\mathbf{\Omega}$. The effective

power of the sub-sampled target and clutter echoes is just the power of the full target and clutter echoes scaled by p. This simplification stems from the fact the covariance of the radar transmission $\mathbf{\Phi}$ is constant for any $l \in \mathbb{N}_L^+$. □

Incorporating the expressions for effective target signal, interference and additive noise, the *effective* radar SINR is given as

$$\text{ESINR} = \frac{\text{Tr}\left(\mathbf{\Phi}\mathbf{D}_t\right)}{\text{Tr}\left(\mathbf{\Phi}\mathbf{C}_t\right) + \sum_{l=1}^{L} \text{Tr}\left(\mathbf{G}_{2l}\mathbf{R}_{xl}\mathbf{G}_{2l}^H\right)/(pLM_{r,R}) + \sigma_R^2}.$$

In this chapter, we consider the scenario where the radar searches in particular directions of interest given by set $\{\theta_k\}$ for targets with unknown RCS variances [3, 113]. For the unknown $\{\sigma_{\beta_k}^2\}$, we instead use the worst possible target RCS variance $\{\sigma_0^2\}$, which is the smallest target RCS variance that could be detected by the radar. In practice, the prior on $\{\theta_k\}$ could be obtained in various ways. For example, in tracking applications, the target parameters obtained from previous tracking cycles are provided to focus the transmit power onto directions of interest. We assume that $\{\sigma_{\beta_k^c}^2\}$ and $\{\theta_k^c\}$ are known. In practice, these clutter parameters could be estimated when target is absent [116].

In a cooperative fashion, the radar and the communication system will jointly design the communication TX covariance matrices $\{\mathbf{R}_{xl}\}$, the radar precoder $\mathbf{P}$ (embedded in $\mathbf{\Phi}$), and the radar sub-sampling scheme $\mathbf{\Omega}$. Based on Theorem 6, the radar precoder $\mathbf{P}$ can be designed without affecting the incoherence property of $\mathbf{M}$. The sub-sampling scheme also needs to be designed to ensure that the data matrix can be completed from partial samples. In matrix completion literature, $\mathbf{\Omega}$ is either a uniformly random sub-sampling matrix [36], or a matrix with a large spectral gap[1] [124]. We will design $\mathbf{\Omega}$ with fixed sub-sampling rate p and a large spectral gap.

[1]The spectral gap of a matrix is defined as the difference between the largest singular value and the second largest singular value.

The above stated spectrum sharing problem can be formulated as follows

$$
\begin{aligned}
(\mathbf{P}_1) \quad & \max_{\{\mathbf{R}_{xl}\}\succeq 0, \mathbf{\Phi}\succeq 0, \mathbf{\Omega}} \mathrm{ESINR}\left(\{\mathbf{R}_x\}, \mathbf{\Omega}, \mathbf{\Phi}\right), \\
& \text{s.t.} \quad C_{\mathrm{avg}}(\{\mathbf{R}_{xl}\}, \mathbf{\Phi}) \geq C, && \text{(7.11a)} \\
& \quad \sum_{l=1}^{L} \mathrm{Tr}\left(\mathbf{R}_{xl}\right) \leq P_C, L\mathrm{Tr}\left(\mathbf{\Phi}\right) \leq P_R, && \text{(7.11b)} \\
& \quad \mathrm{Tr}\left(\mathbf{\Phi}\mathbf{V}_k\right) \geq \xi \mathrm{Tr}(\mathbf{\Phi}), \forall k \in \mathbb{N}_K^+, && \text{(7.11c)} \\
& \quad \mathbf{\Omega} \text{ is proper}, && \text{(7.11d)}
\end{aligned}
$$

where $\mathbf{V}_k \triangleq \mathbf{v}_t^*(\theta_k)\mathbf{v}_t^T(\theta_k)$. The constraint of (7.11a) restricts the communication rate to be at least C, in order to support reliable communication and avoid service outage. The constraints of (7.11b) restrict the total communication and radar transmit power to be no larger than P_C and P_R, respectively. The constraints of (7.11c) restrict that the power of the radar probing signal at interested directions must be not smaller than that achieved by the uniform precoding matrix $\frac{\mathrm{Tr}(\mathbf{\Phi})}{M_{t,R}}\mathbf{I}$, *i.e.*, $\mathbf{v}_t^T(\theta_k)\mathbf{\Phi}\mathbf{v}_t^*(\theta_k) \geq \xi \mathbf{v}_t^T(\theta_k)\frac{\mathrm{Tr}(\mathbf{\Phi})}{M_{t,R}}\mathbf{I}\mathbf{v}_t^*(\theta_k) = \xi\mathrm{Tr}(\mathbf{\Phi})$. $\xi \geq 1$ is a parameter used to control the beampattern at the interested target angles.

Problem $(\mathbf{P}_1)$ is non-convex w.r.t. optimization variable triple $(\{\mathbf{R}_x\}, \mathbf{\Omega}, \mathbf{\Phi})$. We propose an algorithm to find a local solution via alternating optimization in Subsection 7.4.1. In Subsection 7.4.2, we provide some insights on the feasibility and solution properties for $(\mathbf{P}_1)$.

7.4.1 Solution to $(\mathbf{P}_1)$ Using Alternating Optimization

The alternating iterations w.r.t. $\{\mathbf{R}_{xl}\}$, $\mathbf{\Omega}$, and $\mathbf{\Phi}$ are discussed in the following three subsections.

The Alternating Iteration w.r.t. $\{\mathbf{R}_{xl}\}$

We first solve $\{\mathbf{R}_{xl}\}$ while fixing $\mathbf{\Omega}$ and $\mathbf{\Phi}$ to be the solution from the previous iteration:

$$
\begin{aligned}
(\mathbf{P}_{\mathbf{R}}) \quad & \min_{\{\mathbf{R}_{xl}\}\succeq 0} \sum_{l=1}^{L} \mathrm{Tr}\left(\mathbf{G}_{2l}\mathbf{R}_{xl}\mathbf{G}_{2l}^H\right) \\
& \text{s.t.} \quad C_{\mathrm{avg}}(\{\mathbf{R}_{xl}\}, \mathbf{\Phi}) \geq C, \sum_{l=1}^{L} \mathrm{Tr}\left(\mathbf{R}_{xl}\right) \leq P_C.
\end{aligned} \tag{7.12}
$$

Problem ($\mathbf{P_R}$) is convex and involves multiple matrix variables, the joint optimization w.r.t. which requires high computational complexity. The semidefinite matrix variables $\{\mathbf{R}_{xl}\}$ have $LM_{t,C}^2$ real scalar variables, which will results in a complexity of $\mathcal{O}((LM_{t,C}^2)^{3.5})$ if an interior-point method [118] is used. An efficient algorithm for solving the above problem can be implemented based on the Lagrangian dual decomposition [118]. The Lagrangian of ($\mathbf{P_R}$) can be written as

$$\mathcal{L}(\{\mathbf{R}_{xl}\},\lambda_1,\lambda_2)=\sum_{l=1}^{L}\mathrm{Tr}\left(\mathbf{G}_{2l}\mathbf{R}_{xl}\mathbf{G}_{2l}^H\right)+\lambda_1\left(\sum_{l=1}^{L}\mathrm{Tr}\left(\mathbf{R}_{xl}\right)-P_C\right)+\lambda_2\left(C-\mathrm{C}_{\mathrm{avg}}(\{\mathbf{R}_{xl}\})\right),$$

where $\lambda_1\geq 0$ and $\lambda_2\geq 0$ are the dual variables associated with the transmit power and the communication rate constraints, respectively. The dual problem of ($\mathbf{P_R}$) is

$$(\mathbf{P_R}\text{-}D)\ \max_{\lambda_1,\lambda_2\geq 0} g(\lambda_1,\lambda_2),$$

where $g(\lambda_1,\lambda_2)$ is the dual function defined as

$$g(\lambda_1,\lambda_2)=\inf_{\{\mathbf{R}_{xl}\}\succeq 0}\mathcal{L}(\{\mathbf{R}_{xl}\},\lambda_1,\lambda_2).$$

The dual function $g(\lambda_1,\lambda_2)$ can be obtained by solving L independent subproblems, each of which can be written as follows

$$\begin{aligned}(\mathbf{P_R}\text{-sub})\ \min_{\mathbf{R}_{xl}\succeq 0}\ &\mathrm{Tr}\left(\left(\mathbf{G}_2^H\boldsymbol{\Delta}_l\mathbf{G}_2+\lambda_1\mathbf{I}\right)\mathbf{R}_{xl}\right)\\ &-\lambda_2\log_2\left|\mathbf{I}+\mathbf{R}_{wl}^{-1}\mathbf{H}\mathbf{R}_{xl}\mathbf{H}^H\right|.\end{aligned}\tag{7.13}$$

Given λ_1 and λ_2, ($\mathbf{P_R}$-sub) admits a closed-form solution, which can be used to solve the dual problem ($\mathbf{P_R}$-D) via the ellipsoid method [133], and thus solve ($\mathbf{P_R}$). Please refer to [100, Algorithm 1] for the detailed solution. The overall complexity of the dual decomposition based algorithm is only linearly dependent on L.

The Alternating Iteration w.r.t. $\boldsymbol{\Omega}$

By simple algebraic manipulation, the EIP from the communication transmission can be reformulated as

$$\sum_{l=1}^{L}\mathrm{Tr}\left(\mathbf{G}_{2l}\mathbf{R}_{xl}\mathbf{G}_{2l}^H\right)\equiv\mathrm{Tr}(\boldsymbol{\Omega}^T\mathbf{Q}),$$

where the l-th column of $\mathbf{Q}$ contains the diagonal entries of $\mathbf{G}_2\mathbf{R}_{xl}\mathbf{G}_2^H$. With fixed $\{\mathbf{R}_{xl}\}$ and $\mathbf{\Phi}$, we can solve $\mathbf{\Omega}$ via

$$\min_{\mathbf{\Omega}} \ \mathrm{Tr}(\mathbf{\Omega}^T\mathbf{Q}) \quad \text{s.t. } \mathbf{\Omega} \text{ is proper}, \tag{7.14}$$

Recall that the sampling matrix $\mathbf{\Omega}$ is required to have large spectral gap. However, it is difficult to incorporate such conditions in the above optimization problem. Based on the fact that row and column permutation of the sampling matrix would not affect its singular values and thus the spectral gap, our prior work [100] proposed a suboptimal approach to search the best sampling scheme by permuting rows and columns of an initial sampling matrix $\mathbf{\Omega}^0$, *i.e.*,

$$\min_{\mathbf{\Omega}} \ \mathrm{Tr}(\mathbf{\Omega}^T\mathbf{Q}) \quad \text{s.t. } \mathbf{\Omega} \in \wp(\mathbf{\Omega}^0), \tag{7.15}$$

where $\wp(\mathbf{\Omega}^0)$ denotes the set of matrices obtained by arbitrary row and/or column permutations. The $\mathbf{\Omega}^0$ is generated with binary entries and $\lfloor pLM_{r,R} \rfloor$ ones. One good candidate for $\mathbf{\Omega}^0$ would be a uniformly random sampling matrix, as such matrix exhibit large spectral gap with high probability [124]. Multiple trials with different $\mathbf{\Omega}^0$'s can be used to further improve the choice of $\mathbf{\Omega}$. However, the search space is very large since $|\wp(\mathbf{\Omega}^0)| = \Theta(M_{r,R}!L!)$. In [100], we iteratively solved (7.15) w.r.t. row and column permutation on $\mathbf{\Omega}^0$ by using two linear assignment problems [134]. The complexity of each iteration is $\mathcal{O}(M_{r,R}^3 + L^3)$. In this chapter, we propose to reduce the search space as follows

$$\min_{\mathbf{\Omega}} \ \mathrm{Tr}(\mathbf{\Omega}^T\mathbf{Q}) \quad \text{s.t. } \mathbf{\Omega} \in \wp_r(\mathbf{\Omega}^0), \tag{7.16}$$

where $\wp_r(\mathbf{\Omega}^0)$ denotes the set of matrices obtained by arbitrary row permutations. The search space in (7.16) $|\wp_r(\mathbf{\Omega}^0)| = \Theta(M_{r,R}!)$ is greatly reduced compared to that in (7.15). Furthermore, the following proposition shows that such reduction of search space comes without any performance loss.

Proposition 6. *For any $\mathbf{\Omega}^0$, searching for an $\mathbf{\Omega}$ in $\wp_r(\mathbf{\Omega}^0)$ can achieve the same EIP as searching in $\wp(\mathbf{\Omega}^0)$.*

Proof. We can prove the proposition by showing that the EIP achieved by any $\mathbf{\Omega}_1 \in \wp(\mathbf{\Omega}^0)$ can also be achieved by a certain $\mathbf{\Omega}_2 \in \wp_r(\mathbf{\Omega}^0)$. For the pair $(\mathbf{\Omega}_1, \{\mathbf{R}_{xl}\})$, the same EIP can be achieved by the pair $(\mathbf{\Omega}_2, \{\tilde{\mathbf{R}}_{xl}\})$, where

- $\mathbf{\Omega}_2$ is constructed by performing on $\mathbf{\Omega}^0$ the row permutations performed from $\mathbf{\Omega}^0$ to $\mathbf{\Omega}_1$, and
- $\{\tilde{\mathbf{R}}_{xl}\}$ is a permutation of $\{\mathbf{R}_{xl}\}$ according to the column permutations performed from $\mathbf{\Omega}^0$ to $\mathbf{\Omega}_1$.

In other words, the column permutations on $\mathbf{\Omega}$ is unnecessary because $\{\mathbf{R}_{xl}\}$ will be automatically optimized to match the column pattern of $\mathbf{\Omega}$. The claim is proven. □

To formulate (7.16) as a linear assignment problem, we construct a cost matrix $\mathbf{C}^r \in \mathbb{R}^{M_{r,R}\times M_{r,R}}$ with $[\mathbf{C}^r]_{ml} \triangleq \mathbf{\Omega}_{m\cdot}(\mathbf{Q}_{l\cdot})^T$. The optimal solution of (7.16) can obtained efficiently in polynomial time $\mathcal{O}(M_{r,R}^3)$ using the Hungarian algorithm [134].

The Alternating Iteration w.r.t. $\mathbf{\Phi}$

For the optimization of $\mathbf{\Phi}$ with fixed $\{\mathbf{R}_{xl}\}$ and $\mathbf{\Omega}$, the constraint in (7.11a) is nonconvex w.r.t. $\mathbf{\Phi}$. The first order Taylor expansion of $\underline{C}(\mathbf{R}_{xl}, \mathbf{\Phi})$ at $\bar{\mathbf{\Phi}}$ is given as

$$\underline{C}(\mathbf{R}_{xl}, \mathbf{\Phi}) \approx \underline{C}(\mathbf{R}_{xl}, \bar{\mathbf{\Phi}}) - \mathrm{Tr}\left[\mathbf{A}_l(\mathbf{\Phi} - \bar{\mathbf{\Phi}})\right],$$

where $\mathbf{A}_l$ is given by

$$\mathbf{A}_l \triangleq -\left(\frac{\partial \underline{C}(\mathbf{R}_{xl}, \mathbf{\Phi})}{\partial \Re(\mathbf{\Phi})}\right)^T_{\mathbf{\Phi}=\bar{\mathbf{\Phi}}} = \mathbf{G}_1^H[(\mathbf{G}_1\mathbf{\Phi}\mathbf{G}_1^H + \sigma_C^2\mathbf{I})^{-1} - (\mathbf{G}_1\mathbf{\Phi}\mathbf{G}_1^H + \sigma_C^2\mathbf{I} + \mathbf{H}\mathbf{R}_{xl}\mathbf{H}^H)^{-1}]\mathbf{G}_1\big|_{\mathbf{\Phi}=\bar{\mathbf{\Phi}}}. \tag{7.17}$$

The sequential convex programming technique is applied to solve $\mathbf{\Phi}$ by repeatedly solve the following approximate optimization problem

$$\begin{aligned} (\mathbf{P}_{\mathbf{\Phi}}) \ \max_{\mathbf{\Phi}\succeq 0} \ & \frac{\mathrm{Tr}(\mathbf{\Phi}\mathbf{D}_t)}{\mathrm{Tr}(\mathbf{\Phi}\mathbf{C}_t) + \rho}, \\ \text{s.t.} \ & \mathrm{Tr}\left(\mathbf{\Phi}\right) \le P_R/L, \mathrm{Tr}\left(\mathbf{\Phi}\mathbf{A}\right) \le \tilde{C}, \\ & \mathrm{Tr}\left(\mathbf{\Phi}\mathbf{V}_k\right) \ge \xi \mathrm{Tr}\left(\mathbf{\Phi}\right), \forall k \in \mathbb{N}_K^+, \end{aligned} \tag{7.18}$$

where $\tilde{C} = \sum_{l=1}^L(\underline{C}(\mathbf{R}_{xl}, \bar{\mathbf{\Phi}}) + \mathrm{Tr}(\bar{\mathbf{\Phi}}\mathbf{A}_l) - C)$, $\mathbf{A} = \sum_{l=1}^L \mathbf{A}_l$, $\rho = \sum_{l=1}^L \mathrm{Tr}\big(\mathbf{R}_{xl}\mathbf{G}_2^H\mathbf{\Delta}_l\mathbf{G}_2\big)$ $/(pLM_{r,R}) + \sigma_R^2$ are real positive constants w.r.t. $\mathbf{\Phi}$, and $\bar{\mathbf{\Phi}}$ is updated as the solution of the previous repeated problem. Problem (7.18) could be equivalently formulated as a

semidefinite programming problem (SDP) via Charnes-Cooper Transformation [116, 119].

$$\begin{aligned} \max_{\tilde{\mathbf{\Phi}}\succeq 0,\phi>0} \quad & \mathrm{Tr}(\tilde{\mathbf{\Phi}}\mathbf{D}_t), \\ \text{s.t.} \quad & \mathrm{Tr}(\tilde{\mathbf{\Phi}}\mathbf{C}_t) = 1-\phi\rho \\ & \mathrm{Tr}\left(\tilde{\mathbf{\Phi}}\right) \le \phi P_R/L, \mathrm{Tr}\left(\tilde{\mathbf{\Phi}}\mathbf{A}\right) \le \phi\tilde{C}, \\ & \mathrm{Tr}\left(\tilde{\mathbf{\Phi}}(\mathbf{V}_k-\xi\mathbf{I})\right) \ge 0, \forall k \in \mathbb{N}_K^+. \end{aligned} \tag{7.19}$$

The optimal solution of (7.19), denoted by $(\tilde{\mathbf{\Phi}}^*, \phi^*)$, can be obtained by using any standard interior-point method based SDP solver with a complexity of $\mathcal{O}((M_{t,R}^2)^{3.5})$. The solution of (7.18) is given by $\tilde{\mathbf{\Phi}}^*/\phi^*$. In each alternating iteration w.r.t. $\mathbf{\Phi}$, it is required to solve several iterations of SDP due to the sequential convex programming.

It is easy to show that the objective function, *i.e.*, ESINR, is nondecreasing during the alternating iterations of $\{\mathbf{R}_{xl}\}$, $\mathbf{\Omega}$ and $\mathbf{\Phi}$, and is upper bounded. According to the monotone convergence theorem [135], the alternating optimization is guaranteed to converge. The proposed efficient spectrum sharing algorithm in presence of clutter using a lower bound of the radar SINR is summarized in Algorithm 5.

Algorithm 5 Spectrum sharing algorithm for $(\mathbf{P}_1)$.

1: **Input:** $\mathbf{D}_t, \mathbf{C}_t, \mathbf{H}, \mathbf{G}_1, \mathbf{G}_2, P_{C/R}, C, \sigma_{C/R}^2, \delta_1$
2: **Initialization:** $\mathbf{\Phi} = \frac{P_R}{LM_{t,R}}\mathbf{I}$, $\mathbf{\Omega} = \mathbf{\Omega}^0$;
3: **repeat**
4: Update $\{\mathbf{R}_{xl}\}$ by solving $(\mathbf{P_R})$ with fixed $\mathbf{\Omega}$ and $\mathbf{\Phi}$;
5: Update $\mathbf{\Omega}$ by solving (7.16) with fixed $\{\mathbf{R}_{xl}\}$ and $\mathbf{\Phi}$;
6: Update $\mathbf{\Phi}$ by solving a sequence of approximated SDP problem (7.18) with fixed $\{\mathbf{R}_{xl}\}$ and $\mathbf{\Omega}$;
7: **until** ESINR increases by amount smaller than δ_1
8: **Output:** $\{\mathbf{R}_{xl}\}, \mathbf{\Omega}, \mathbf{P} = \sqrt{L}\mathbf{\Phi}^{1/2}$

7.4.2 Insights on the Feasibility and Solutions of $(\mathbf{P}_1)$

In this subsection, we provide some key insights on the feasibility of $(\mathbf{P}_1)$ and the rank of the solutions $\mathbf{\Phi}$ obtained by Algorithm 5.

Feasibility

A necessary condition on C for the feasibility of $(\mathbf{P}_1)$ w.r.t. $\{\mathbf{R}_{xl}\}$ is $C \leq C_{\max}(P_C)$ where

$$C_{\max}(P_C) \triangleq \max_{\{\mathbf{R}_{xl}\}\succeq 0} \frac{1}{L}\sum_{l=1}^{L} \log_2 \left|\mathbf{I} + \sigma_C^{-2}\mathbf{H}\mathbf{R}_{xl}\mathbf{H}^H\right|,$$
$$\text{s.t.} \sum_{l=1}^{L} \mathrm{Tr}\left(\mathbf{R}_{xl}\right) \leq P_C$$

The above optimization problem is convex and has a closed-form solution [52] based on water-filling. The optimal solution is given by $\mathbf{R}_{x1} = \cdots = \mathbf{R}_{xL} = \sum_{i=1}^{M_{\min}} P_i^* \mathbf{v}_{Hi}\mathbf{v}_{Hi}^H$, where $M_{\min} \triangleq \min(M_{t,C}, M_{r,C})$ and $\mathbf{v}_{Hi}$ is the right singular vector of the communication channel matrix $\mathbf{H}$, *i.e.*, $\mathbf{H} = \sum_{i=1}^{M_{\min}} \lambda_i \mathbf{u}_{Hi}\mathbf{v}_{Hi}^H$ and

$$P_i^* = \max\left(0, \mu - \frac{\sigma_C^2}{\lambda_i^2}\right),$$

with μ be chosen such that $\sum_{i=1}^{M_{\min}} P_i^* = P_C$. It can be shown that

$$C_{\max}(P_C) = \sum_{i=1}^{M_{\min}} \log_2\left(1 + \frac{P_i^*\lambda_i^2}{\sigma_C^2}\right) \text{bits/s/Hz},$$

which is a monotone increasing function of P_C. $C_{\max}(P_C)$ is essentially the largest achievable communication rate when there is no interference from radar transmitters to the communication receivers. Note that $C = C_{\max}(P_C)$ will generate a nonempty feasible set for $\{\mathbf{R}_{xl}\}$ only if $\mathbf{G}_1\mathbf{\Phi}\mathbf{G}_1^H = \mathbf{0}$, *i.e.*, the radar transmits in the null space of the interference channel $\mathbf{G}_1$ to the communication receivers[2].

A necessary condition on ξ for the feasibility of $(\mathbf{P}_1)$ w.r.t. $\mathbf{\Phi}$ is $\xi \leq \xi_{\max}$ where

$$\xi_{\max} \triangleq \max_{\mathbf{\Phi}\succeq 0, \xi \geq 0} \xi, \text{ s.t. } \mathrm{Tr}(\mathbf{\Phi}\mathbf{V}_k) \geq \xi \mathrm{Tr}(\mathbf{\Phi}), \forall k \in \mathbb{N}_K^+.$$

Note that the above optimization problem is independent of $\mathrm{Tr}(\mathbf{\Phi})$. Without loss of generality, we assume that $\mathrm{Tr}(\mathbf{\Phi}) = 1$, based on which we have the following equivalent SDP formulation

$$\xi_{\max} \triangleq \max_{\mathbf{\Phi}\succeq 0, \xi \geq 0} \xi, \text{ s.t. } \mathrm{Tr}(\mathbf{\Phi}) = 1,$$
$$\mathrm{Tr}(\mathbf{\Phi}\mathbf{V}_k) \geq \xi, \forall k \in \mathbb{N}_K^+.$$

It is easy to check that $\xi_{\max} \geq 1$, which can be achieved by set $(\mathbf{\Phi}, \xi)$ to be $(\mathbf{I}/M_{t,R}, 1)$.

The following proposition provides a sufficient condition for the feasibility of $(\mathbf{P}_1)$.

[2]We omit the trivial case $\mathbf{\Phi} = \mathbf{0}$.

Proposition 7. *If $C, \xi, P_C > 0, P_R > 0$ are chosen such that $C < C_{max}(P_C)$ and $\xi \leq \xi_{max}$, then $(\mathbf{P}_1)$ is feasible.*

Proof. If $C < C_{\max}(P_C)$, the feasible set for $\{\mathbf{R}_{xl}\}$ determined by constraints in (7.11a) and (7.11b) $\mathcal{F}_{\{\mathbf{R}_{xl}\}}$ is nonempty as long as $\mathrm{Tr}(\mathbf{\Phi})$ is sufficiently small. If $\xi \leq \xi_{\max}$, the feasible set for $\mathbf{\Phi}$ determined by constraints in (7.11c) $\mathcal{F}_{\mathbf{\Phi}1}$ is nonempty and has no restriction on $\mathrm{Tr}(\mathbf{\Phi})$. If $\mathbf{\Phi} \in \mathcal{F}_{\mathbf{\Phi}1}$, then $\alpha\mathbf{\Phi} \in \mathcal{F}_{\mathbf{\Phi}1}, \forall \alpha > 0$. The overall feasible set for $\mathbf{\Phi}$, $\mathcal{F}_{\mathbf{\Phi}}$, is the intersection of feasible sets determined by (7.11a), (7.11b) and (7.11c). $\mathcal{F}_{\mathbf{\Phi}}$ is nonempty as long as $\mathcal{F}_{\mathbf{\Phi}1}$ and $\mathcal{F}_{\{\mathbf{R}_{xl}\}}$ are nonempty because we can choose any $\mathbf{\Phi} \in \mathcal{F}_{\mathbf{\Phi}1}$ and scale it down to make $(\mathbf{P}_1)$ feasible. The claim is proven. □

The Rank of the Solutions $\mathbf{\Phi}$

We are also particularly interested in the rank of $\mathbf{\Phi}$ obtained using Algorithm 5. Since the sequential convex programming technique is used for solving $\mathbf{\Phi}$, it suffices to focus on the rank of the solution of $(\mathbf{P}_{\mathbf{\Phi}})$. To achieve this goal, we first introduce the following SDP problem

$$\begin{aligned} \min_{\mathbf{\Phi} \succeq 0} \mathrm{Tr}\left(\mathbf{\Phi}\right) \text{ s.t. } \mathrm{Tr}\left(\mathbf{\Phi}\mathbf{A}\right) \leq \tilde{C}, \frac{\mathrm{Tr}(\mathbf{\Phi}\mathbf{D}_t)}{\mathrm{Tr}(\mathbf{\Phi}\mathbf{C}_t) + \rho} \geq \gamma, \\ \mathrm{Tr}\left(\mathbf{\Phi}\mathbf{V}_k\right) \geq 0, \forall k \in \mathbb{N}_K^+. \end{aligned} \tag{7.20}$$

where γ is a real positive constant. The following proposition relates the optimal solutions of problems (7.18) and (7.20).

Proposition 8. *If γ in (7.20) is chosen to be the maximum achievable SINR of (7.18), denoted as $SINR_{max}$, the optimal $\mathbf{\Phi}$ of (7.20) is also optimal for (7.18).*

Proof. Denote $\mathbf{\Phi}_1^*$ and $\mathbf{\Phi}_2^*$ the optimal solutions of (7.18) and (7.20), respectively. It is clear that $\mathbf{\Phi}_1^*$ is feasible point of (7.20). This means that $\mathrm{Tr}(\mathbf{\Phi}_2^*) \leq \mathrm{Tr}(\mathbf{\Phi}_1^*) \leq P_R$. Therefore, $\mathbf{\Phi}_2^*$ is a feasible point of (7.18). It holds that

$$\mathrm{SINR}_{\max} \equiv \frac{\mathrm{Tr}(\mathbf{\Phi}_1^*\mathbf{D}_t)}{\mathrm{Tr}(\mathbf{\Phi}_1^*\mathbf{C}_t) + \rho} \geq \frac{\mathrm{Tr}(\mathbf{\Phi}_2^*\mathbf{D}_t)}{\mathrm{Tr}(\mathbf{\Phi}_2^*\mathbf{C}_t) + \rho} \geq \mathrm{SINR}_{\max}.$$

It is only possible when all the equalities hold. In other words, $\mathbf{\Phi}_2^*$ is optimal for (7.18). The claim is proved. □

In order to characterize the optimal solution of (7.20), we need the following key lemma:

Lemma 8. *Matrix* $\mathbf{A}_l$ *defined in (7.17) and thus* $\mathbf{A}$ *are positive semidefinite.*

Proof. Based on Lemma 6, we prove that $\mathbf{A}_l$ is semidefinite. Further, $\mathbf{A}$ is also semidefinte because it is the sum of L semidefinite matrices. □

Based on Lemma 8, we prove the following result by following the approach in [119]:

Proposition 9. *Suppose that (7.20) is feasible when* γ *is set to* $SINR_{max}$*. Then, any optimal solution of (7.20) has rank at most* K*. All rank-*K *solutions* $\mathbf{\Phi}_K^*$ *of (7.20) have the same range space. Any solution* $\mathbf{\Phi}_{K-}^*$ *with rank less than* K *has range space such that* $\mathcal{R}(\mathbf{\Phi}_{K-}^*) \subset \mathcal{R}(\mathbf{\Phi}_K^*)$*. Moreover, (7.18) and (7.19) always have solutions with rank at most* K *and with the same range space properties as that for (7.20).*

Proof. The proof can be found in Appendix 7.C. □

7.4.3 Constant-Rate Communication Transmission

The adaptive communication transmission in the proposed spectrum sharing methods involves high complexity. A sub-optimal transmission approach of constant rate, *i.e.*, $\mathbf{R}_{xl} \equiv \mathbf{R}_x, \forall l \in \mathbb{N}_L^+$, has a lower implementation complexity. In such case, the spectrum sharing problem can be reformulated as

$$\begin{aligned}(\mathbf{P}_1') \quad & \max_{\mathbf{R}_x \succeq 0, \mathbf{\Phi} \succeq 0} \text{ESINR}'(\mathbf{R}_x, \mathbf{\Omega}, \mathbf{\Phi}), \\ \text{s.t.} \quad & \underline{C}(\mathbf{R}_x, \mathbf{\Phi}) \geq C, \\ & L\text{Tr}\left(\mathbf{R}_x\right) \leq P_C, L\text{Tr}\left(\mathbf{\Phi}\right) \leq P_R, \\ & \text{Tr}\left(\mathbf{\Phi}\mathbf{V}_k\right) \geq 0, \forall k \in \mathbb{N}_K^+,\end{aligned}$$

where

$$\text{ESINR}' = \frac{\text{Tr}\left(\mathbf{\Phi}\mathbf{D}_t\right)}{\text{Tr}\left(\mathbf{\Phi}\mathbf{C}_t\right) + \text{Tr}\left(\mathbf{\Delta}\mathbf{G}_2\mathbf{R}_x\mathbf{G}_2^H\right)/(pLM_{r,R}) + \sigma_R^2}$$

and $\mathbf{\Delta} = \sum_{l=1}^{L} \mathbf{\Delta}_l$ is diagonal and with each entry equal to the number of 1's in the corresponding row of $\mathbf{\Omega}$. Similar techniques in Algorithm 5 can be used to solve $(\mathbf{P}_1')$.

We can see that $(\mathbf{P}_1')$ has much lower complexity because there is only one matrix variable for the communication transmission. However, the drawback of the constant-rate communication is that $\mathbf{R}_x$ cannot adapt to the variation of the effective interference channel $\mathbf{G}_{2l}$. On the other hand, the adaptive communication transmission considered in $(\mathbf{P}_1)$ can fully exploit the channel diversity introduced by the radar sub-sampling procedure. It will be seen in the simulations of Section 7.5.3, the constant-rate transmission from the solution of (7.21) is inferior to the adaptive transmission from the solution of (7.11).

Another consequence is that the ESINR$'$ depends on $\mathbf{\Omega}$ only through $\mathbf{\Delta}$. Since $\mathbf{\Omega}$ is searched among the row permutations of a uniformly random sampling matrix, the number of 1's in each row of $\mathbf{\Omega}$ is close to pL, or equivalently, $\mathbf{\Delta}$ will be very close to the scaled identity matrix $pL\mathbf{I}$. To further reduce the complexity, the optimization w.r.t. $\mathbf{\Omega}$ in $(\mathbf{P}_1')$ is omitted because all row permutations of $\mathbf{\Omega}$ will result in a very similar ESINR$'$. From a different perspective, if the radar sub-sampling matrix $\mathbf{\Omega}$ is not available for the radar and communication cooperation, we can safely replace $\mathbf{\Delta}$ with $pL\mathbf{I}$ in the ESINR$'$. The above discussion asserts that, for the case of constant-rate communication transmission almost no performance degradation occurs due to the absent of the knowledge of $\mathbf{\Omega}$.

7.4.4 Traditional MIMO Radars

The traditional MIMO radars without sub-sampling can be considered as special with $p = 1$, and thus there is no need for the matrix completion. In such case, the constant-rate communication transmission becomes optimal scheme because the interference channel $\mathbf{G}_2$ stays as a constant for the period of L symbol time due to the block fading assumption. The spectrum sharing problem has the same form as $(\mathbf{P}_1')$ with the objective function being

$$\text{SINR} = \frac{\text{Tr}\left(\mathbf{\Phi}\mathbf{D}_t\right)}{\text{Tr}\left(\mathbf{\Phi}\mathbf{C}_t\right) + \text{Tr}\left(\mathbf{G}_2\mathbf{R}_x\mathbf{G}_2^H\right)/M_{r,R} + \sigma_R^2}.$$

Note that SINR $\approx$ ESINR$'$ because $\mathbf{\Delta} \approx pL\mathbf{I}$. Therefore, traditional MIMO radars can achieve approximately the same spectrum sharing performance as MIMO-MC radars when the communication system transmits at a constant rate. However, for MIMO-MC radars, the adaptive communication transmission and the radar sub-sampling matrix can be designed

to achieve significant radar SINR reduction over the traditional MIMO radars. This advantageous flexibility is introduced by the sparse sensing (*i.e.* sub-sampling) in MIMO-MC radars.

7.5 Numerical Results

In this section, we provide simulation examples to quantify the performance of the proposed spectrum sharing method for the coexistence of the MIMO-MC radars and communication systems.

Unless otherwise stated, we use the following default values for the system parameters. The MIMO radar system consists of collocated $M_{t,R} = 16$ TX and $M_{r,R} = 16$ RX antennas, respectively forming transmit and receive half-wavelength uniform linear arrays. The radar waveforms are chosen from the rows of a random orthonormal matrix [99]. We set the length of the radar waveforms to $L = 16$. The wireless communication system consists of collocated $M_{t,C} = 4$ TX and $M_{r,C} = 4$ RX antennas, respectively forming transmit and receive half-wavelength uniform linear arrays. For the communication capacity and power constraints, we take $C = 16$ bits/symbol and $P_C = 64$ (the power is normalized by the power of the radar waveform). The radar transmit power budget $P_R = 1000 \times P_C$, which is typical in radar systems. The additive white Gaussian noise variances are $\sigma_C^2 = \sigma_R^2 = 0.01$. There are three stationary targets with RCS variance $\sigma_{\beta 0}^2 = 0.5$, located in the far-field with pathloss 10^{-3}, and clutter is generated by four point scatterers. All scatterers RCS variances are set to be identical and are denoted by σ_β^2, which is decided by the prescribed clutter to noise ratio (CNR) $10 \log \sigma_\beta^2 / \sigma_R^2$. The channel $\mathbf{H}$ is modeled as Rayleigh fading, *i.e.*, contains independent entries, distributed as $\mathcal{CN}(0, 1)$. The interference channels $\mathbf{G}_1$ and $\mathbf{G}_2$ are modeled as Rician fading. The power in the direct path is 0.1, and the variance of Gaussian components contributed by the scattered paths is 10^{-3}.

The performance metrics considered in this chapter include the following:

- The radar *effective* SINR, *i.e.*, the objective of the spectrum sharing problem;
- The matrix completion relative recovery error, defined as $\|\mathbf{M} - \hat{\mathbf{M}}\|_F / \|\mathbf{M}\|_F$, where $\hat{\mathbf{M}}$ is the completed data matrix at the radar fusion center;

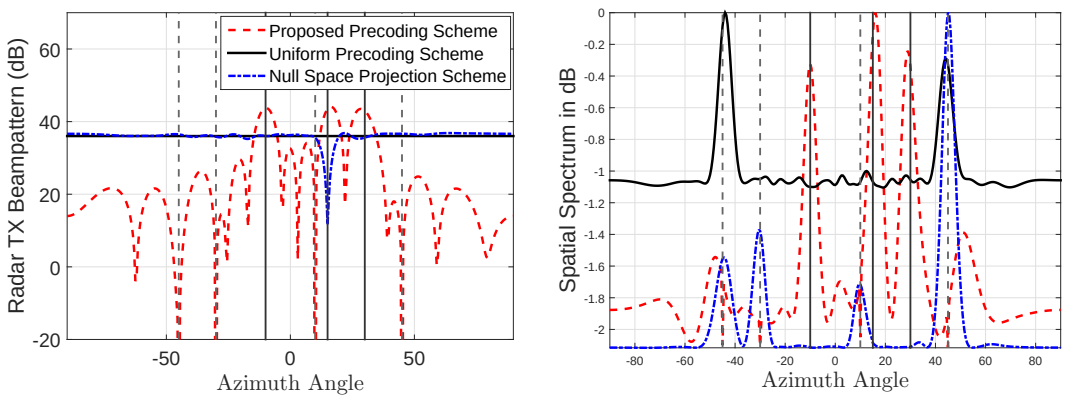

Figure 7.1: The radar transmit beampattern and the MUSIC spatial pseudo-spectrum for MIMO-MC radar and communication spectrum sharing. $M_{t,R} = M_{r,R} = 16, M_{t,C} = M_{r,C} = 4$. The true positions of the targets and clutters are labeled using solid and dashed vertical lines, respectively. CNR=30 dB.

- The radar transmit beampattern, *i.e.*, the transmit power for different azimuth angles $\mathbf{v}_t^T(\theta)\mathbf{P}\mathbf{v}_t^*(\theta)$;
- The MUSIC pseudo-spectrum and the relative target RCS estimation RMSE obtained using the least squares estimation on the completed data matrix $\hat{\mathbf{M}}$.

Monte Carlo simulations with 100 independent trials are carried out to get an average performance.

7.5.1 The Radar Transmit Beampattern and MUSIC Spectrum

In this subsection, we present an example to show the advantages of the proposed radar precoding scheme as compared to the trivial uniform precoding, *i.e.*, $\mathbf{P} = \sqrt{LP_R/M_{t,R}}\mathbf{I}$, and null space projection (NSP) precoding, *i.e.*, $\mathbf{P} = \sqrt{LP_R/M_{t,R}}\mathbf{V}\mathbf{V}^H$, where $\mathbf{V}$ contains the basis of the null space of $\mathbf{G}_1$ [46]. For the proposed joint-design based scheme in (7.11), we choose $\xi = \lfloor \xi_{\max} \rfloor$. The target angles w.r.t. the array are respectively $-10°$, $15°$, and $30°$; the four point scatterers are at angles $-45°$, $-30°$, $10°$, and $45°$. The CNR is 30 dB. In this simulation, the direct path in $\mathbf{G}_1$ is generated as $\sqrt{0.1}\mathbf{v}_t(\phi)\mathbf{v}_t^H(\phi)$, where $\phi = 15°$, with $\mathbf{v}_t(\phi)$ is defined in (7.2). In other words, the communication receiver is taken at the same azimuth angle as the second target.

The radar transmit beampattern and the spatial pseudo-spectrum obtained using the

Precoding schemes	ESINR	MC Relative Recovery Errors	Relative RCS Est. RMSE
Joint-design precoding	31.3dB	0.038	0.028
Uniform precoding	-44.3dB	1.00	1.000
NSP based precoding	-46.3dB	1.00	0.995

Table 7.1: The radar ESINR, MC relative recovery errors, and the relative target RCS estimation RMSE for MIMO-MC radar and communication spectrum sharing. The simulation setting is the same as that for Fig. 7.1.

MUSIC algorithm are shown in Fig. 7.1. The correspondingly achieved ESINR, MC relative recovery error, and relative target RCS estimation RMSE are listed in Table 7.1. From Fig. 7.1, we observe that the proposed joint-design based precoding scheme successfully focuses the transmit power towards the three targets and nullifies the power towards the point scatterers. The three targets can be accurately estimated from the pseudo-spectrum obtained by the proposed scheme. As expected, the uniform precoding scheme just spreads the transmit power uniformly in all directions. The NSP precoding scheme results in a similar beampattern as the uniform precoding scheme except the deep null at the direction of the communication receiver. This means that the transmit power towards the second target is severely attenuated by the NSP precoding scheme. It is highly possible that the second target will be missed. In addition, both the uniform and NSP precoding schemes have no capability of clutter mitigation. As shown in Fig. 7.1 and Table 7.1, the proposed joint-design based precoding scheme achieves significant improvement in ESINR, MC relative recovery error, and target RCS estimation accuracy.

7.5.2 Comparison of Different Levels of Cooperation

In this subsection, we compare several algorithms with different levels of radar and communication cooperation. The compared algorithms include

- Uniform radar precoding and selfish communication: the radar transmit antennas use the trivial precoding, *i.e.*, $\mathbf{P} = \sqrt{LP_R/M_{t,R}}\mathbf{I}$; and the communication system minimizes the transmit power to achieve certain average capacity without any concern about the interference it exerts to the radar system. This algorithm involves no radar and communication cooperation.

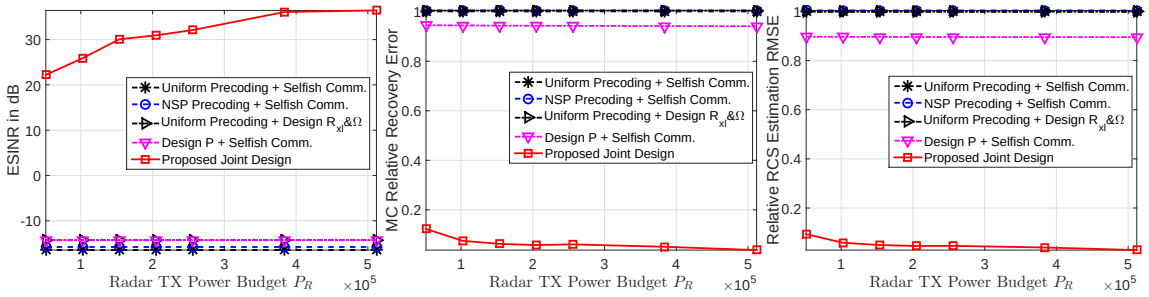

Figure 7.2: Comparison of spectrum sharing with different levels of cooperation between the MIMO-MC radar and the communication system under different P_R. $M_{t,R} = M_{r,R} = 16, M_{t,C} = M_{r,C} = 4$.

- NSP based radar precoding and selfish communication: the radar transmit antennas use the fixed precoding, *i.e.*, $\mathbf{P} = \sqrt{LP_R/M_{t,R}}\mathbf{V}\mathbf{V}^H$, while the selfish communication scheme is the same with the previous case.

- Uniform radar precoding and designing $\mathbf{R}_{xl}$ & $\mathbf{\Omega}$: only $\mathbf{R}_{xl}$ & $\mathbf{\Omega}$ are jointly designed to minimize the effective interference the radar receiver.

- Designing $\mathbf{P}$ and selfish communication: only the radar precoding matrix $\mathbf{P}$ is designed to maximize the radar ESINR.

- The proposed joint-design of $\mathbf{P}$, $\mathbf{R}_{xl}$, and $\mathbf{\Omega}$ in (7.11).

We use the same values for all parameters as in the previous simulation except that the radar transmit power budget P_R changes from $51,200$ to 2.56×10^6. Fig. 7.2 shows the achieved ESINR, the MC relative recovery error, and the relative target RCS estimation RMSE. The algorithms that use trivial uniform and NSP based radar precoding perform bad because the point scatterers are not properly mitigated. The scheme designing $\mathbf{P}$ only could mitigate the scatterers but the interference from the communication transmission is not controlled. The proposed joint design of $\mathbf{P}$, $\mathbf{R}_{xl}$, and $\mathbf{\Omega}$ simultaneously addresses the clutter and the mutual interference between the radar and the communication systems, and thus achieves the best performance amongst all the algorithms. The performance gains come from high level cooperation between the two systems.

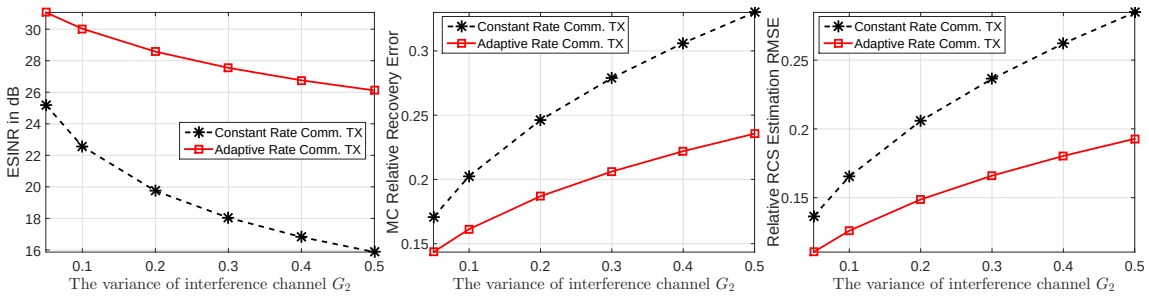

Figure 7.3: Comparison of spectrum sharing with adaptive and constant-rate communication transmissions under different levels of interference channel $\mathbf{G}_2$ from the communication transmitter to the radar receiver. $M_{t,R} = 16, M_{r,R} = M_{t,C} = 8, M_{r,C} = 2$.

7.5.3 Adaptive and Constant-rate Communication Transmissions

In this subsection, we evaluate the performance of two communication transmission schemes, namely, adaptive transmission with different $\mathbf{R}_{xl}$'s for all $l \in \mathbb{N}_L^+$, and constant-rate transmission with only one identical $\mathbf{R}_x$. We use the following parameter setting: $M_{t,R} = 16, M_{r,R} = M_{t,C} = 8, M_{r,C} = 2$, $C = 10$ bits/symbol, $P_C = 64$ and $P_R = 1000 \times P_C$. For the $\mathbf{G}_1$ and $\mathbf{G}_2$, Rayleigh fading is used with fixed $\sigma_{G_1}^2$ and varying $\sigma_{G_2}^2$. The results of ESINR, MC relative recovery error and the relative target RCS estimation RMSE for different values of $\sigma_{G_2}^2$ are shown in Fig. 7.3. The value of $\sigma_{G_2}^2$ varies from 0.05 to 0.5, which effectively simulates different distances between the communication transmitter and the radar receiver. It is clear that the adaptive communication transmission outperforms the constant-rate counterpart under various values of interference channel strength. As discussed in Section 7.4.3, the adaptive communication transmission can fully exploit the channel diversity of $\mathbf{G}_{2l}$ introduced by the radar sub-sampling procedure. The price for the performance advantages is high complexity. The average running times for the adaptive and constant-rate communication transmissions are respectively 15.6 and 4.8 seconds. The choice between these two transmission schemes can be made depending on the available computing resources.

7.5.4 MIMO-MC Radars and Traditional MIMO Radars

In this subsection, we present a simulation to show the advantages of MIMO-MC radars compared to the traditional full-sampled MIMO radars. The parameters are the same as those in the previous simulation but with fixed $\sigma_{G_1}^2 = 0.3$ and $\sigma_{G_2}^2 = 1$, which indicates

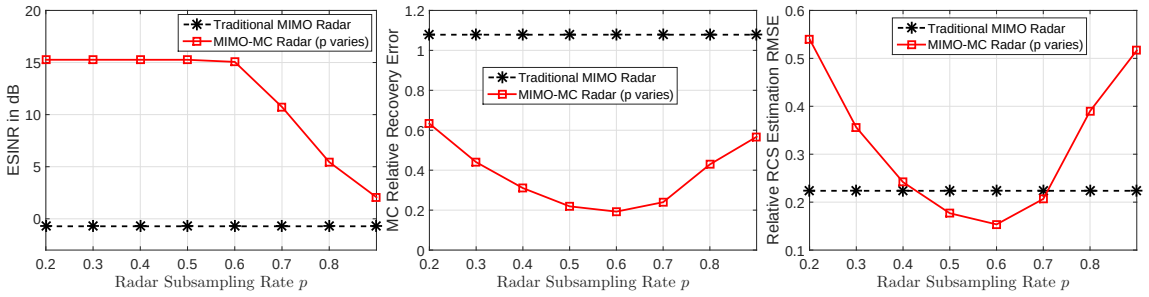

Figure 7.4: Comparison of spectrum sharing with traditional MIMO radars and the MIMO-MC radars with different subsampling rates p. $M_{t,R} = 16, M_{r,R} = M_{t,C} = 8, M_{r,C} = 2$.

strong mutual interference, especially the interference from the communication transmitter to the radar receiver. The radar transmit power budget P_R is taken to be equal to $10 \times P_C$. We consider two targets; one is randomly located and the other is taken to be 25° away. We also consider 4 randomly located point scatterers. Fig. 7.4 shows the results under different MIMO-MC sub-sampling rates p. Note that full sampling is used for the traditional MIMO radar. The MC relative recover error for the traditional radar is actually the output distortion to signal ratio. A smaller distortion to signal ratio corresponds to a larger output SNR. For ease of comparison, a black dashed line is used for the traditional MIMO radar. We observe that the MIMO-MC radar achieves better performance in ESINR than the traditional radar. This is due to the fact that the communication system can effectively prevent its transmission from interfering the radar system when the number of actively sampled radar RX antennas is small, *i.e.*, sub-sampling is small. In addition, the larger ESINR of the MIMO-MC radar results in a larger output SNR than that of the traditional radar. Furthermore, the MIMO-MC radar achieves better target RCS estimation accuracy than the traditional radar if its sub-sampling rate is between 0.4 and 0.7. For p larger than 0.7, the target RCS estimation accuracy achieved by the MIMO-MC radar is worse than that achieved by the traditional radar because small ESINRs for $p \geq 0.7$ introduce high distortion in the completed data matrix. The results in Fig. 7.4 could be used to help the selection of radar sub-sampling rate p. For the best target RCS estimation accuracy, $p = 0.6$ is the best choice, while for the biggest savings in terms of samples and similar performance as traditional radars, $p = 0.4$ is the best choice. We conclude that MIMO-MC radars can coexist with communication systems and achieve better target RCS estimation

than traditional radars while saving up to 60% data samples. Such significant advantage is introduced by the sparse sensing (*i.e.* sub-sampling) in MIMO-MC radars as discussed in Section 7.4.4.

7.6 Conclusions

In this chapter, we have considered the co-existence of a MIMO-MC radar and a wireless MIMO communication system by sharing a common carrier frequency. The radar transmit precoder, the radar sub-sampling scheme, and the communication transmit covariance matrix have been jointly designed to maximize the radar SINR while meeting certain rate and power constraints for the communication system. The proposed joint design based spectrum sharing algorithm has been evaluated via extensive simulations. Specifically, we have shown the superiority introduced by radar and communication cooperation in the proposed algorithm compared to noncooperative counterparts. The proposed joint-design based spectrum sharing scheme successfully focuses the transmit power towards the targets and nullifies the power towards the clutter. The proposed method achieves significant improvement in ESINR, MC relative recovery error, and target RCS estimation accuracy. We have also compared the performance and complexity of the adaptive and the constant-rate communication transmission schemes for radar-communication spectrum sharing. Finally, we have provided a simulation on the comparison of MIMO-MC radars and traditional MIMO radars co-existing with communication systems. We have observed that the MIMO-MC radar achieves better performance in ESINR and output SNR than the traditional radar. MIMO-MC radars can coexist with communication systems and achieve better target RCS estimation than traditional radars while saving up to 60% in data samples. The cost for these advantages is the additional computation for matrix completion.

7.A Proof of Theorem 5

Proof. The following proof extends the results in [34, 35] for the cases where the radar employs transmit precoder $\mathbf{P}$ and random unitary waveform matrix $\mathbf{S}$, *i.e.*, $\mathbf{M} = \mathbf{V}_r\mathbf{\Sigma}\mathbf{V}_t^T\mathbf{P}\mathbf{S}$. The following lemma is used.

Lemma 9 ([140]). *Let S_N be a χ^2 random variable with N degrees of freedom. Then for each $t > 0$*

$$Pr\left(S_N - N \geq t\sqrt{2N} + t^2\right) \leq e^{-t^2/2}.$$

Denoting the rank of $\mathbf{M}$ by K_0, it is clear that K_0 is not larger than K. Recall that $\mathbf{M}$ has a compact SVD given as

$$\mathbf{M} = \mathbf{U}\mathbf{\Gamma}\mathbf{V}^H$$

where $\mathbf{U} \in \mathbb{C}^{M_{r,R} \times K_0}$ and $\mathbf{V} \in \mathbb{C}^{L \times K_0}$ contain the left and right singular vectors of $\mathbf{M}$; $\mathbf{\Gamma} \in \mathbb{R}^{K_0 \times K_0}$ is diagonal containing the singular values. Consider the QR decomposition of $\mathbf{V}_r$ and $\mathbf{S}^T\mathbf{P}^T\mathbf{V}_t$:

$$\mathbf{V}_r = \mathbf{Q}_r\mathbf{R}_r,$$

$$\mathbf{S}^T\mathbf{P}^T\mathbf{V}_t = \mathbf{Q}_t\mathbf{R}_t,$$

where $\mathbf{Q}_r \in \mathbb{C}^{M_{r,R} \times K}$ and $\mathbf{Q}_t \in \mathbb{C}^{L \times K_0}$ are with orthonormal columns, $\mathbf{R}_r \in \mathbb{C}^{K \times K}$ is upper triangular, and $\mathbf{R}_t \in \mathbb{C}^{K_0 \times K}$ has an upper staircase form. The matrix $\mathbf{R}_r\mathbf{\Sigma}\mathbf{R}_t^T \in \mathbb{C}^{K \times K_0}$ is full column rank with a compact SVD given by $\mathbf{U}_1\mathbf{\Gamma}_1\mathbf{V}_1^H$, where $\mathbf{U}_1 \in \mathbb{C}^{K \times K_0}$, $\mathbf{V}_1 \in \mathbb{C}^{K_0 \times K_0}$, $\mathbf{U}_1^H\mathbf{U}_1 = \mathbf{V}_1^H\mathbf{V}_1 = \mathbf{I}_{K_0}$, and $\mathbf{\Gamma}_1$ is diagonal, containing the singular values of $\mathbf{R}_r\mathbf{\Sigma}\mathbf{R}_t^T$. Therefore, we have

$$\mathbf{M} = \mathbf{Q}_r\mathbf{U}_1\mathbf{\Gamma}_1\mathbf{V}_1^H\mathbf{Q}_t^T = \mathbf{Q}_r\mathbf{U}_1\mathbf{\Gamma}_1(\mathbf{Q}_t^*\mathbf{V}_1)^H,$$

which is a valid SVD of $\mathbf{M}$. The uniqueness of singular value of a matrix indicates that $\mathbf{\Gamma} \equiv \mathbf{\Gamma}_1$. Therefore, we can choose $\mathbf{U} = \mathbf{Q}_r\mathbf{U}_1$ and $\mathbf{V} = \mathbf{Q}_t^*\mathbf{V}_1$. We have

$$\begin{aligned} \mu(U) &= \frac{M_{r,R}}{K_0} \sup_{m \in \mathbb{N}^+_{M_{r,R}}} \|(\mathbf{Q}_r)_{m\cdot}\,\mathbf{U}_1\|_2^2 \\ &\leq \frac{M_{r,R}}{K_0} \sup_{m \in \mathbb{N}^+_{M_{r,R}}} \|(\mathbf{Q}_r)_{m\cdot}\|_2^2 = \frac{K}{K_0}\mu_0^r, \end{aligned} \tag{7.22}$$

where μ_0^r is defined in Theorem 4. We also have

$$\mu(V) = \frac{L}{K_0} \sup_{l \in \mathbb{N}^+_L} \|(\mathbf{Q}_t^*)_{l\cdot}\,\mathbf{V}_1\|_2^2 = \frac{L}{K_0} \sup_{l \in \mathbb{N}^+_L} \|(\mathbf{Q}_t)_{l\cdot}\|_2^2.$$

If K_0 is strictly smaller than K, we can not represent $\mathbf{Q}_t$ in terms of $\mathbf{S}^T\mathbf{P}^T\mathbf{V}_t$ and $\mathbf{R}_t$ because of the singularity of $\mathbf{R}_t$. To conquer this, we apply column permutations $\mathbf{F}$ on $\mathbf{R}_t$ to bring forward the first non-zero elements in each row $\mathbf{R}_t\mathbf{F} = \begin{pmatrix}\mathbf{R}_1 & \mathbf{R}_2\end{pmatrix}$ such that $\mathbf{R}_1 \in \mathbb{C}^{K_0 \times K_0}$ is

square, upper triangular and invertible. The QR decomposition $\mathbf{S}^T\mathbf{P}^T\mathbf{V}_t$ can be re-written as

$$\mathbf{S}^T\mathbf{P}^T\mathbf{V}_t\mathbf{F} = \mathbf{Q}_t\big(\mathbf{R}_1\ \mathbf{R}_2\big).$$

We can represent $\mathbf{Q}_t$ as

$$\mathbf{Q}_t = \mathbf{S}^T\mathbf{P}^T\mathbf{V}_t\mathbf{F}_{K_0}\mathbf{R}_1^{-1},$$

where $\mathbf{F}_{K_0}$ denotes the first K_0 columns of $\mathbf{F}$. Substituting $\mathbf{Q}_t$ into $\mu(V)$, we obtain

$$\begin{aligned}\mu(V) &= \frac{L}{K_0}\sup_{l\in\mathbb{N}_L^+}\|\big(\mathbf{S}^T\big)_{l\cdot}\mathbf{P}^T\mathbf{V}_t\mathbf{F}_{K_0}\mathbf{R}_1^{-1}\|_2^2 \\ &= \frac{L}{K_0}\sup_{l\in\mathbb{N}_L^+}\big(\mathbf{S}^T\big)_{l\cdot}\mathbf{P}^T\mathbf{V}_t\mathbf{F}_{K_0}\mathbf{R}_1^{-1}\left(\mathbf{R}_1^{-1}\right)^H\mathbf{F}_{K_0}^H\mathbf{V}_t^H\mathbf{P}^*\left(\mathbf{S}^*\right)_{\cdot l}\end{aligned} \tag{7.23}$$

We can show that

$$\begin{aligned}\mathbf{R}_1^{-1}\left(\mathbf{R}_1^{-1}\right)^H &= \left(\mathbf{R}_1^H\mathbf{R}_1\right)^{-1} = \left(\mathbf{R}_1^H\mathbf{Q}_t^H\mathbf{Q}_t\mathbf{R}_1\right)^{-1} \\ &= \left(\mathbf{F}_{K_0}^H\mathbf{V}_t^H\mathbf{P}^*\mathbf{S}^*\mathbf{S}^T\mathbf{P}^T\mathbf{V}_t\mathbf{F}_{K_0}\right)^{-1} \\ &= \left(\mathbf{F}_{K_0}^H\mathbf{V}_t^H\mathbf{P}^*\mathbf{P}^T\mathbf{V}_t\mathbf{F}_{K_0}\right)^{-1}\end{aligned} \tag{7.24}$$

where the last equality holds because $\mathbf{S}\mathbf{S}^H = \mathbf{I}_{M_{t,R}}$. Consider the QR decomposition of $\mathbf{P}^T\mathbf{V}_t\mathbf{F}_{K_0}$ given by

$$\mathbf{P}^T\mathbf{V}_t\mathbf{F}_{K_0} = \mathbf{Q}_a\mathbf{R}_a, \tag{7.25}$$

where $\mathbf{Q}_a \in \mathbb{C}^{M_{t,R}\times K_0}$ contains orthonormal columns, and $\mathbf{R}_a \in \mathbb{C}^{K_0\times K_0}$ is upper triangular and full rank. Substituting (7.24) and (7.25) into (7.23), we have

$$\begin{aligned}\mu(V) &= \frac{L}{K_0}\sup_{l\in\mathbb{N}_L^+}\mathbf{s}_l^T\mathbf{R}_a\left(\mathbf{R}_a^H\mathbf{R}_a\right)^{-1}\mathbf{R}_a^H\mathbf{s}_l^* \\ &= \frac{L}{K}\sup_{l\in\mathbb{N}_L^+}\mathbf{s}_l^T\mathbf{s}_l^* = \frac{L}{K}\sup_{l\in\mathbb{N}_L^+}\|\mathbf{s}_l\|_2^2\end{aligned} \tag{7.26}$$

where $\mathbf{s}_l \triangleq \mathbf{Q}_a^T\mathbf{S}_{\cdot l}$, and the second equality holds because $\mathbf{R}_a$ is invertible. Based on [107, Theorem 3], if $M_{t,R} = \mathcal{O}(L/\ln L)$, the entries of $\mathbf{S}$ can be approximated by i.i.d Gaussian random variables with distribution $\mathcal{CN}(0, 1/L)$. Since $\mathbf{Q}_a$ has orthonormal columns, $\mathbf{s}_l \in \mathbb{C}^{K_0}, \forall l \in \mathbb{N}_L^+$ also contains i.i.d Gaussian random variable with distribution $\mathcal{CN}(0, 1/L)$, and $L\|\mathbf{s}_l\|_2^2$ is distributed according to $\chi^2_{K_0}$. Based on Lemma 9 setting $t = \sqrt{6\ln L}$, it holds that

$$\Pr\left(L\|\mathbf{s}_l\|_2^2 \geq K_0 + 2\sqrt{3K_0\ln L} + 6\ln L\right) \leq L^{-3}. \tag{7.27}$$

Applying the union bound, we have

$$\Pr\left(\sup_{l\in\mathbb{N}_L^+}\|\mathbf{s}_l\|_2^2 \geq \frac{K_0+2\sqrt{3K_0\ln L}+6\ln L}{L}\right)\leq L^{-2}. \tag{7.28}$$

Combining (7.26) and (7.28) gives

$$\Pr\left(\mu(V)\geq \frac{K_0+2\sqrt{3K\ln L}+6\ln L}{K_0}\right)\leq L^{-2}. \tag{7.29}$$

From the derivation, the bound on $\mu(V)$ holds for any target angles, array geometry, and precoding matrix $\mathbf{P}$ as long as $\mathbf{P}^T\mathbf{V}_t\mathbf{F}_{K_0}$ is with full column rank K_0. Theorem 5 is proved.

□

7.B Derivation of ESP and EIP in (7.9) and (7.10)

The derivation of ESP is shown as bellow

$$\begin{aligned}
&\text{ESP} \triangleq \mathbb{E}\left\{\text{Tr}\left(\boldsymbol{\Omega}\circ(\mathbf{DPS})\left(\boldsymbol{\Omega}\circ(\mathbf{DPS})^H\right)\right)\right\}\\
&=\mathbb{E}\left\{\text{Tr}\left\{\left[\textstyle\sum_k \beta_k\boldsymbol{\Omega}\circ(\mathbf{D}_k\mathbf{PS})\right]\left[\sum_k \beta_k\boldsymbol{\Omega}\circ(\mathbf{D}_k\mathbf{PS})^H\right]\right\}\right\}\\
&=\mathbb{E}\left\{\text{Tr}\left\{\sum_k\sum_j \beta_k\beta_j\boldsymbol{\Omega}\circ(\mathbf{D}_k\mathbf{PS})\left[\boldsymbol{\Omega}\circ(\mathbf{D}_j\mathbf{PS})^H\right]\right\}\right\}\\
&=\text{Tr}\left\{\sum_k\sum_j \mathbb{E}\{\beta_k\beta_j\}\left[\sum_l \boldsymbol{\Delta}_l\mathbf{D}_k\mathbf{P}\mathbb{E}\{\mathbf{s}_l\mathbf{s}_l^H\}\mathbf{P}^H\mathbf{D}_j^H\boldsymbol{\Delta}_l\right]\right\}\\
&\overset{(a)}{=}\text{Tr}\left\{\sum_k \sigma_{\beta_k}^2\left[\sum_l \boldsymbol{\Delta}_l\mathbf{D}_k\boldsymbol{\Phi}\mathbf{D}_k^H\boldsymbol{\Delta}_l\right]\right\}\\
&\overset{(b)}{=}\text{Tr}\left(\sum_k \sigma_{\beta_k}^2\boldsymbol{\Delta}\mathbf{D}_k\boldsymbol{\Phi}\mathbf{D}_k^H\right)=\text{Tr}\left(\boldsymbol{\Phi}\sum_k \sigma_{\beta_k}^2\mathbf{D}_k^H\boldsymbol{\Delta}\mathbf{D}_k\right)\\
&=\text{Tr}\left(\boldsymbol{\Phi}\sum_k \sigma_{\beta_k}^2\mathbf{v}_t^*(\theta_k)\mathbf{v}_r^H(\theta_k)\boldsymbol{\Delta}\mathbf{v}_r(\theta_k)\mathbf{v}_t^T(\theta_k)\right)\\
&\overset{(c)}{=}pLM_{r,R}\text{Tr}\left(\boldsymbol{\Phi}\sum_k \sigma_{\beta_k}^2\mathbf{v}_t^*(\theta_k)\mathbf{v}_t^T(\theta_k)\right)\\
&=pLM_{r,R}\text{Tr}\left(\boldsymbol{\Phi}\mathbf{D}_t\right)
\end{aligned}$$

where $\mathbf{D}_k \triangleq \mathbf{v}_r(\theta_k)\mathbf{v}_t^T(\theta_k)$, $\mathbf{s}_l \triangleq \mathbf{s}(l)$. (a) follows from the fact that $\mathbb{E}\{\beta_k\beta_j\}=\delta_{jk}\sigma_{\beta_k}^2$; (b) follows from the fact that $\boldsymbol{\Delta}_l=\boldsymbol{\Delta}_l\boldsymbol{\Delta}_l$ and $\boldsymbol{\Delta}=\sum_{l=1}^L\boldsymbol{\Delta}_l$; (c) follows from the fact that $\mathbf{v}_r^H(\theta_k)\boldsymbol{\Delta}\mathbf{v}_r(\theta_k)=\|\boldsymbol{\Delta}\|_1=pLM_{r,R}$. The derivation for EIP is similar and is omitted for brevity.

7.C Proof of Proposition 9

Proof. Problem (7.20) is an SDP, whose Karush-Kuhn-Tucker (KKT) conditions are given as

$$\mathbf{\Psi} + \lambda_2 \mathbf{D}_t + \sum_{k=1}^{K} \nu_k \mathbf{V}_k = \mathbf{I} + \lambda_1 \mathbf{A} + \lambda_2 \gamma \mathbf{C}_t + \sum_{k=1}^{K} \nu_k \xi \mathbf{I} \tag{7.30a}$$

$$\mathbf{\Psi}\mathbf{\Phi} = \mathbf{0} \tag{7.30b}$$

$$\mathbf{\Psi} \succeq 0, \mathbf{\Phi} \succeq 0, \lambda_1 \geq 0, \lambda_2 \geq 0, \{\nu_k\} \geq 0 \tag{7.30c}$$

$$\mathrm{Tr}(\mathbf{\Phi}\mathbf{D}_t) \geq \gamma \mathrm{Tr}(\mathbf{\Phi}\mathbf{C}) + \gamma\rho \tag{7.30d}$$

$$\mathrm{Tr}(\mathbf{\Phi}\mathbf{V}_k) \geq 0, \forall k \in \mathbb{N}_K^+ \tag{7.30e}$$

where $\mathbf{\Psi} \succeq 0, \lambda_1 \geq 0, \lambda_2 \geq 0$, and $\{\nu_k\} \geq 0$ are dual variables. We can rewrite (7.30a) as follows

$$\begin{aligned} &\mathrm{rank}(\mathbf{\Psi}) + \mathrm{rank}\left(\lambda_2 \mathbf{D}_t + \sum_{k=1}^{K} \nu_k \mathbf{v}_t^*(\theta_k)\mathbf{v}_t^T(\theta_k)\right) \\ &\geq \mathrm{rank}\left(\mathbf{I} + \lambda_1 \mathbf{A} + \lambda_2 \gamma \mathbf{C}_t + \sum_{k=1}^{K} \nu_k \xi \mathbf{I}\right). \end{aligned} \tag{7.31}$$

Recall that $\mathbf{D}_t = \sum_k \sigma_{\beta_k}^2 \mathbf{v}_t^*(\theta_k)\mathbf{v}_t^T(\theta_k)$. It is clear to see that $\lambda_2 \mathbf{D}_t + \sum_{k=1}^{K} \nu_k \mathbf{v}_t^*(\theta_k)\mathbf{v}_t^T(\theta_k)$ has rank at most K. Since $\mathbf{A}$ and $\mathbf{C}$ are positive semidefinite, the matrix on right hand side of (7.31) has full rank. Therefore, $\mathrm{rank}(\mathbf{\Psi})$ is not smaller than $M_{t,R} - K$. From (7.30b) and (7.30d) we conclude that any optimal solution $\mathbf{\Phi}$ must have rank at most K.

The second claim asserts that if there are multiple solutions with rank K, they have the same range space. This can be proved using contradiction. Suppose that $\mathbf{\Phi}_1^*$ and $\mathbf{\Phi}_2^*$ are rank-K solutions of (7.20) and $\mathcal{R}(\mathbf{\Phi}_1^*) \neq \mathcal{R}(\mathbf{\Phi}_2^*)$. Based on convex theory, any convex combination of $\mathbf{\Phi}_1^*$ and $\mathbf{\Phi}_2^*$, saying $\mathbf{\Phi}_3^* \triangleq \alpha\mathbf{\Phi}_1^* + (1-\alpha)\mathbf{\Phi}_2^*, \forall \alpha \in (0,1)$, is also a solution of (7.20). However, $\mathbf{\Phi}_3^*$ is with rank at least $K+1$, which contradicts the fact that any solution must have rank at most K. The third claim could also be proved using contradiction. Suppose that $\mathbf{\Phi}_1^*$ and $\mathbf{\Phi}_2^*$ are respectively rank-K solution and solution with rank smaller than K, and $\mathcal{R}(\mathbf{\Phi}_2^*) \setminus \mathcal{R}(\mathbf{\Phi}_1^*)$ is nonempty. Then any convex combination of $\mathbf{\Phi}_1^*$ and $\mathbf{\Phi}_2^*$, saying $\mathbf{\Phi}_3^* \triangleq \alpha\mathbf{\Phi}_1^* + (1-\alpha)\mathbf{\Phi}_2^*, \forall \alpha \in (0,1)$, is also a solution of (7.20). However, $\mathbf{\Phi}_3^*$ is again with rank at least $K+1$, which contradicts the fact that any solution must have rank at most K.

The last claim on the solutions of (7.18) and (7.19) follows from Proposition 8. □

Chapter 8

Conclusions and Future Work

8.1 Conclusions

In Chapter 2 and 3, we have considered moving target estimation using sparsity based MIMO radars with collocated and widely distributed antennas, respectively. We have provided the uniform recovery guarantee by analyzing the RIP of the measurement matrices. For distributed MIMO radars using compressive sensing, two low-complexity approaches have been proposed to reduce the computation while maintaining the estimation performance. The first approach was an ADMM-based sparse signal recovery algorithm. Simulation results have indicated that this approach significantly lowers the computational complexity for target estimation with improved accuracy as compared to the approaches using proximal gradient algorithm and interior point method. The second approach decouples the location and speed estimation into two separate stages. The location estimation obtained in the first stage is used to prune the target location-speed space in the speed estimation stage. Simulations have indicated that the decoupled scheme can reduce both the computation and the required number of measurements, while maintaining high estimation accuracy.

In Chapter 4, we have considered a general spectrum sharing framework between a MIMO radar and a MIMO communication system. Depending on the availability of target range information, a knowledge-based and a robust spectrum sharing approach were proposed to maximize the radar SINR while satisfying the communication requirements. The resulting nonconvex problems were solved by using alternating optimization and sequential convex programming. Simulation results have validated the effectiveness of the proposed spectrum sharing methods. In Chapter 5, we have proposed the co-design based spectrum sharing of a MIMO radar and a communication system for a scenario in which the radar system operates in the presence of clutter.

In Chapter 6, we have considered spectrum sharing between a MIMO communication system and a MIMO-MC radar system. In order to reduce the effective interference power (EIP) at radar RX antennas, we have first considered the cooperative spectrum sharing method, which designs the communication transmit covariance matrix based on the knowledge of the radar sampling scheme. We have also formulated the spectrum sharing method for the case where the radar sampling scheme is not shared with the communication system. Our theoretical results guarantee that the cooperative approach can effectively reduce the EIP to a larger extent as compared to the spectrum sharing method without the knowledge of the radar sampling scheme. Second, we have proposed a joint design of the communication transmit covariance matrix and the radar sampling scheme to further reduce the EIP. The EIP reduction and the matrix completion recovery errors have been evaluated under various system parameters. Our simulations have suggested that the joint-design scheme can achieve much smaller EIP and relative recovery errors than other methods when the number of radar TX and RX antennas is moderately large.

In Chapter 7, we have extended spectrum sharing between a MIMO communication system and a MIMO-MC radar system by jointly designing the radar transmit precoder, the radar sub-sampling scheme, and the communication transmit covariance matrix to maximize the radar SINR while meeting certain rate and power constraints for the communication system. The proposed joint design based spectrum sharing algorithm has been evaluated via extensive simulations. Specifically, we have shown the superiority introduced by radar and communication cooperation in the proposed algorithm compared to noncooperative counterparts. The proposed joint-design based spectrum sharing scheme successfully focuses the transmit power towards the targets and nullifies the power towards the clutter. The proposed method achieves significant improvement in ESINR, MC relative recovery error, and target RCS estimation accuracy. We have also compared the performance and complexity of the adaptive and the constant-rate communication transmission schemes for radar-communication spectrum sharing. Finally, we have provided a simulation on the comparison of MIMO-MC radars and traditional MIMO radars co-existing with communication systems. We have observed that the MIMO-MC radar achieves better performance in ESINR and output SNR than the traditional radar. MIMO-MC radars can coexist with communication

systems and achieve better target RCS estimation than traditional radars while saving up to 60% in data samples. The cost for these advantages is the additional computation for matrix completion.

8.2 Future Work

MIMO radars and wireless MIMO communication coexistence is a new line of work with many interesting challenges. We highlight several potential directions for future work.

- Spectrum sharing between MIMO radars and multiple MIMO communication systems. The current work considered a MIMO radar system coexisting with a single MIMO communication system. It would be very interesting to extend current work to the scenario under which MIMO radars coexist with multiple pairs of MIMO transmitters and receivers. A centralized fusion center can be introduced to collect all the channel state information from all the co-existing systems and be responsible for the joint design based spectrum sharing algorithm. Distributed implementation for the centralized spectrum sharing algorithm in such case would be important for distributing the computation to local systems and thus reducing the need of a powerful fusion center.

- The flat fading assumption might fail for the communication and interference channels as the communication signal bandwidth increases. If the model needs to be treated as frequency selective, then one could consider OFDM type of radar transmissions and communication signals. OFDM has been used to turn the frequency selective fading into parallel flat fading channels. It is already the basis for many communication standards, such as LTE, WiFi and WiMax [52]. Motivated by results from wireless communications, OFDM-like signals have been increasingly used in radar system [81, 141, 142]. For the co-existence of OFDM radar and communication systems, the authors of [63] proposed a greedy based carrier allocation method. Based on a given carrier allocation, [64] proposed to jointly design the radar and communication waveforms' power spectrum. As future work, we will investigate the coexistence of MIMO-OFDM radars and MIMO-OFDM communication systems. It is possible to formulate an optimization problem which optimally allocates the radar and communication resources

to multiple antennas and multiple sub-carriers simultaneously. Compared to spectrum sharing in spatial and spectral domain separately, the increased degrees of freedom in the joint spatial-spectral domain are expected to greatly boost the spectral efficiency.

Bibliography

[1] M. I. Skolnik. *Introduction to Radar Systems, 2nd edition*. New York: McGraw-Hill, 1980.

[2] M. A. Richards. *Fundamentals of Radar Signal Processing*. New York: McGraw-Hill, 2005.

[3] P. Stoica, J. Li, and Y. Xie. "On probing signal design for MIMO radar". In: *IEEE Transactions on Signal Processing* 55.8 (2007), pp. 4151–4161.

[4] H. Krim and M. Viberg. "Two decades of array signal processing research: The parametric approach". In: *IEEE Signal Processing Magazine* 13.4 (1996), pp. 67–94.

[5] J. Li and P. Stoica. "MIMO radar with colocated antennas". In: *IEEE Signal Processing Magazine* 24.5 (2007), pp. 106–114.

[6] J. Li et al. "On parameter identifiability of MIMO radar". In: *IEEE Signal Processing Letters* 14.12 (2007), pp. 968–971.

[7] A. M. Haimovich, R. S. Blum, and L. J. Cimini. "MIMO radar with widely separated antennas". In: *IEEE Signal Processing Magazine* 25.1 (2008), pp. 116–129.

[8] H. Godrich, A. M. Haimovich, and R. S. Blum. "Target localization accuracy gain in MIMO radar-based systems". In: *IEEE Transactions on Information Theory* 56.6 (2010), pp. 2783–2803.

[9] E. Fishler et al. "MIMO radar: an idea whose time has come". In: *Proceedings of the IEEE Radar Conference*. 2004, pp. 71–78.

[10] J. Li and P. Stoica. "MIMO radar with colocated antennas". In: *IEEE Signal Processing Magazine* 24.5 (2007), pp. 106–114.

[11] J. Li et al. "On Parameter Identifiability of MIMO Radar". In: *IEEE Signal Processing Letters* 14.12 (2007), pp. 968–971.

[12] C. Y. Chen and P. P. Vaidyanathan. "MIMO Radar Space-Time Adaptive Processing Using Prolate Spheroidal Wave Functions". In: *IEEE Transactions on Signal Processing* 56.2 (2008), pp. 623–635.

[13] D. L. Donoho. "Compressed sensing". In: *IEEE Transactions on Information Theory* 52.4 (2006), pp. 1289–1306.

[14] E. J. Candes and M. B. Wakin. "An Introduction To Compressive Sampling". In: *IEEE Signal Processing Magazine* 25.2 (2008), pp. 21–30.

[15] R. Baraniuk et al. "A simple proof of the restricted isometry property for random matrices". In: *Constructive Approximation* 28.3 (2008), pp. 253–263.

[16] Y. C. Eldar and G. Kutyniok. *Compressed sensing: theory and applications*. Cambridge University Press, 2012.

[17] M. F. Duarte and Y. C. Eldar. "Structured compressed sensing: from theory to applications". In: *IEEE Transactions on Signal Processing* 59.9 (2011), pp. 4053–4085.

[18] Y. C. Eldar and M. Mishali. "Robust recovery of signals from a structured union of subspaces". In: *IEEE Transactions on Information Theory* 55.11 (2009), pp. 5302–5316.

[19] L. Meier, S. Geer, and P. Buhlmann. "The group lasso for logistic regression". In: *Journal of the Royal Statistical Society: Series B* 70.1 (2008), pp. 53–71.

[20] Y. C. Eldar, P. Kuppinger, and H. Bolcskei. "Block-sparse signals: uncertainty relations and efficient recovery". In: *IEEE Transactions on Signal Processing* 58.6 (2010), pp. 3042–3054.

[21] T. Blumensath and M. E. Davies. "Sampling theorems for signals from the union of finite-dimensional linear subspaces". In: *IEEE Transactions on Information Theory* 55.4 (2009), pp. 1872–1882.

[22] C. Chen and P. P. Vaidyanathan. "MIMO radar ambiguity properties and optimization using frequency-hopping waveforms". In: *IEEE Transactions on Signal Processing* 56.12 (2008), pp. 5926–5936.

[23] M. A. Herman and T. Strohmer. “High-Resolution Radar via Compressed Sensing”. In: *IEEE Transactions on Signal Processing* 57.6 (2009), pp. 2275–2284.

[24] Y. Yu, A. P. Petropulu, and H. V. Poor. “MIMO Radar Using Compressive Sampling”. In: *IEEE Journal of Selected Topics in Signal Processing* 4.1 (2010), pp. 146–163.

[25] Y. Yu, A. P. Petropulu, and H. V. Poor. “CSSF MIMO RADAR: Compressive-Sensing and Step-Frequency Based MIMO Radar”. In: *IEEE Transactions on Aerospace and Electronic Systems* 48.2 (2012), pp. 1490–1504.

[26] T. Strohmer and B. Friedlander. “Analysis of Sparse MIMO Radar”. In: *Applied and Computational Harmonic Analysis* 37.3 (2014), pp. 361–388.

[27] M. Hugel, H. Rauhut, and T. Strohmer. “Remote sensing via ℓ_1 minimization”. In: *Foundations of Computational Mathematics* 14.1 (2013), pp. 115–150.

[28] M. Rossi, A. M. Haimovich, and Y. C. Eldar. “Spatial Compressive Sensing for MIMO Radar”. In: *IEEE Transactions on Signal Processing* 62.2 (2014), pp. 419–430.

[29] B. Li and A. P. Petropulu. “RIP analysis of the measurement matrix for compressive sensing-based MIMO radars”. In: *Proceedings of the IEEE Sensor Array and Multichannel Signal Processing Workshop*. A Coruna, Spain, 2014, pp. 497–500.

[30] S. Gogineni and A. Nehorai. “Target estimation using sparse modeling for distributed MIMO radar”. In: *IEEE Transactions on Signal Processing* 59.11 (2011), pp. 5315–5325.

[31] A. P. Petropulu, Y. Yu, and J. Huang. “On exploring sparsity in widely separated MIMO radar”. In: *Proceedings of the 45th Asilomar Conference on Signals, Systems, and Computers*. 2011, pp. 1496–1500.

[32] S. Sun, A. P. Petropulu, and W. U. Bajwa. “Target estimation in colocated MIMO radar via matrix completion”. In: *IEEE International Conference on Acoustics, Speech and Signal Processing*. 2013, pp. 4144–4148.

[33] S. Sun, W. Bajwa, and A. P. Petropulu. “MIMO-MC Radar: A MIMO Radar Approach Based on Matrix Completion”. In: *IEEE Transactions on Aerospace and Electronic Systems* 51.3 (2015), pp. 1839–1852.

[34] D. S. Kalogerias and A. P. Petropulu. “Matrix Completion in Colocated MIMO Radar: Recoverability, Bounds and Theoretical Guarantees”. In: *IEEE Transactions on Signal Processing* 62.2 (2014), pp. 309–321.

[35] S. Sun and A. P. Petropulu. “Waveform Design for MIMO Radars with Matrix Completion”. In: *IEEE Journal of Selected Topics in Signal Processing* 9.8 (2015), pp. 1400–1414.

[36] E. J. Candès and Y. Plan. “Matrix Completion With Noise”. In: *Proceedings of the IEEE* 98.6 (2010), pp. 925–936.

[37] Y. Chi et al. “Sensitivity to Basis Mismatch in Compressed Sensing”. In: *IEEE Transactions on Signal Processing,* 59.5 (2011), pp. 2182–2195.

[38] B. Li and A. P. Petropulu. “Performance guarantees for distributed MIMO radar based on sparse modeling”. In: *Proceedings of the IEEE Radar Conference*. 2014, pp. 1369–1372.

[39] The Presidents Council of Advisors on Science and Technology (PCAST). *Realizing the full potential of government-held spectrum to spur economic growth*. 2012. URL: `https://www.whitehouse.gov/sites/default/files/microsites/ostp/pcast_spectrum_report_final_july_20_2012.pdf`.

[40] Federal Communications Commission (FCC). *FCC proposes innovative small cell use in 3.5 GHz band*. 2012. URL: `https://apps.fcc.gov/edocs_public/attachmatch/DOC-317911A1.pdf`.

[41] Gary Locke and Lawrence E. Strickling. *An Assessment of the Near-Term Viability of Accommodating Wireless Broadband Systems in the 1675-1710 MHz, 1755-1780 MHz, 3500-3650 MHz, and 4200-4220 MHz, 4380-4400 MHz Bands*. Technical Report TR-13-490. US Dept. of Commerce, the National Telecommunications and Information Administration, 2012.

[42] A. Lackpour, M. Luddy, and J. Winters. “Overview of interference mitigation techniques between WiMAX networks and ground based radar”. In: *20th Annual Wireless and Optical Communications Conference*. 2011, pp. 1–5.

[43] S. Sodagari et al. “A projection based approach for radar and telecommunication systems coexistence”. In: *IEEE Global Telecommunication Conference*. 2012, pp. 5010–5014. DOI: 10.1109/GLOCOM.2012.6503914.

[44] A. Babaei, W. H. Tranter, and T. Bose. “A practical precoding approach for radar communications spectrum sharing”. In: *8th International Conference on Cognitive Radio Oriented Wireless Networks*. 2013, pp. 13–18.

[45] S. Amuru et al. “MIMO Radar Waveform Design to Support Spectrum Sharing”. In: *IEEE Military Communication Conference*. 2013, pp. 1535–1540.

[46] A. Khawar, A. Abdel-Hadi, and T. C. Clancy. “Spectrum sharing between S-band radar and LTE cellular system: A spatial approach”. In: *IEEE International Symposium on Dynamic Spectrum Access Networks,* 2014, pp. 7–14.

[47] H. Deng and B. Himed. “Interference Mitigation Processing for Spectrum-Sharing Between Radar and Wireless Communications Systems”. In: *IEEE Transactions on Aerospace and Electronic Systems* 49.3 (2013), pp. 1911–1919.

[48] A. Aubry et al. “Radar waveform design in a spectrally crowded environment via non-convex quadratic optimization”. In: *IEEE Transactions on Aerospace and Electronic Systems* 50.2 (2014), pp. 1138–1152.

[49] A. Aubry et al. “A new radar waveform design algorithm with improved feasibility for spectral coexistence”. In: *IEEE Transactions on Aerospace and Electronic Systems* 51.2 (2015), pp. 1029–1038.

[50] Simon Haykin. “Cognitive radio: brain-empowered wireless communications”. In: *Selected Areas in Communications, IEEE Journal on* 23.2 (2005), pp. 201–220.

[51] T. Rappaport. *Wireless Communications Principles And Practice Edition*. Prentice Hall, 2001.

[52] D. Tse and P. Viswanath. *Fundamentals of wireless communication*. Cambridge university press, 2005.

[53] F. H. Sanders et al. *Analysis and resolution of RF interference to radars operating in the band 2700–2900 MHz from broadband communication transmitters*. Technical Report TR-13-490. US Dept. of Commerce, NTIA, 2012.

[54] M. R. Bell et al. "Results on spectrum sharing between a radar and a communications system". In: 2014 International Conference on Electromagnetics in Advanced Applications (ICEAA). 2014, pp. 826–829.

[55] Q. Zhao and B. M. Sadler. "A Survey of Dynamic Spectrum Access". In: *IEEE Signal Processing Magazine* 24.3 (2007), pp. 79–89.

[56] E. Hossain, D. Niyato, and Z. Han. *Dynamic spectrum access and management in cognitive radio networks*. Cambridge university press, 2009.

[57] Y. Wang et al. "A new alternating minimization algorithm for total variation image reconstruction". In: *SIAM Journal on Imaging Sciences* 1.3 (2008), pp. 248–272.

[58] S. S. Bhat, R. M. Narayanan, and M. Rangaswamy. "Bandwidth sharing and scheduling for multimodal radar with communications and tracking". In: *IEEE Sensor Array and Multichannel Signal Processing Workshop*. 2012, pp. 233–236.

[59] R. Saruthirathanaworakun, J. M. Peha, and L. M. Correia. "Opportunistic sharing between rotating radar and cellular". In: *IEEE Journal on Selected Areas in Communications* 30.10 (2012), pp. 1900–1910.

[60] B. D. Cordill, S. A. Seguin, and L. Cohen. "Electromagnetic interference to radar receivers due to in-band OFDM communications systems". In: *Electromagnetic Compatibility (EMC), 2013 IEEE International Symposium on*. 2013, pp. 72–75. DOI: 10.1109/ISEMC.2013.6670384.

[61] B. D. Cordill, S. A. Seguin, and L. Cohen. "Radar performance degradation with in-band OFDM communications system interference". In: *Radio Science Meeting (USNC-URSI NRSM), 2013 US National Committee of URSI National*. 2013, pp. 1–1. DOI: 10.1109/USNC-URSI-NRSM.2013.6525039.

[62] S. C. Surender, R. M. Narayanan, and C. R. Das. "Performance analysis of communications & radar coexistence in a covert UWB OSA system". In: *IEEE Global Telecommunications Conference*. 2010, pp. 1–5.

[63] S. Gogineni, M. Rangaswamy, and A. Nehorai. "Multi-modal OFDM waveform design". In: *IEEE Radar Conference*. 2013, pp. 1–5.

[64] A. Turlapaty and Y. Jin. "A joint design of transmit waveforms for radar and communications systems in coexistence". In: *IEEE Radar Conference*. 2014, pp. 0315–0319.

[65] Kuan-Wen Huang et al. "Radar waveform design in spectrum sharing environment: Coexistence and cognition". In: *Radar Conference (RadarCon), 2015 IEEE*. IEEE. 2015, pp. 1698–1703.

[66] C. Shahriar, A. Abdelhadi, and T. C. Clancy. "Overlapped-MIMO radar waveform design for coexistence with communication systems". In: *IEEE Wireless Communications and Networking Conference*. 2015, pp. 223–228.

[67] Awais Khawar, Ahmed Abdelhadi, and T Charles Clancy. *MIMO Radar Waveform Design for Spectrum Sharing with Cellular Systems: A MATLAB Based Approach*. Springer, 2016.

[68] Haya Shajaiah, Ahmed Abdelhadi, and Charles Clancy. "Impact of Radar and Communication Coexistence on Radar's Detectable Target Parameters". In: *arXiv preprint arXiv:1408.6736* (2014).

[69] A. Khawar, A. Abdelhadi, and C. Clancy. "Target Detection Performance of Spectrum Sharing MIMO Radars". In: *IEEE Sensors Journal* 15.9 (2015), pp. 4928–4940. ISSN: 1530-437X. DOI: 10.1109/JSEN.2015.2424393.

[70] Carl W Rossler, Emre Ertin, and Randolph L Moses. "A software defined radar system for joint communication and sensing". In: *Radar Conference (RADAR), 2011 IEEE*. IEEE. 2011, pp. 1050–1055.

[71] Christian Sturm and Werner Wiesbeck. "Waveform design and signal processing aspects for fusion of wireless communications and radar sensing". In: *Proceedings of the IEEE* 99.7 (2011), pp. 1236–1259.

[72] M. Fitz, T. Halford, and I. H. S. Enserink. "Towards simultaneous radar and spectral sensing," in: *IEEE International Symposium on Dynamic Spectrum Access Networks (DYSPAN)*. IEEE, 2014, pp. 15–19.

[73] Shannon D Blunt, Padmaja Yatham, and James Stiles. "Intrapulse radar-embedded communications". In: *Aerospace and Electronic Systems, IEEE Transactions on* 46.3 (2010), pp. 1185–1200.

[74] Jerome Euziere et al. "Dual function radar communication time-modulated array". In: *Radar Conference (Radar), 2014 International*. IEEE. 2014, pp. 1–4.

[75] Aboulnasr Hassanien et al. "A dual function radar-communications system using sidelobe control and waveform diversity". In: *2015 IEEE Radar Conference (RadarCon)*. IEEE. 2015, pp. 1260–1263.

[76] Aboulnasr Hassanien et al. "Dual-function radar-communications using phase-rotational invariance". In: *Signal Processing Conference (EUSIPCO), 2015 23rd European*. IEEE. 2015, pp. 1346–1350.

[77] JR Guerci et al. "Joint design and operation of shared spectrum access for radar and communications". In: *Radar Conference (RadarCon), 2015 IEEE*. IEEE. 2015, pp. 0761–0766.

[78] Aboulnasr Hassanien et al. "Signaling strategies for dual-function radar-communications: An overview". In: *IEEE Aerospace and Electronic Systems Magazine* (2016).

[79] Daniel W Bliss. "Cooperative radar and communications signaling: The estimation and information theory odd couple". In: *Radar Conference, 2014 IEEE*. IEEE. 2014, pp. 0050–0055.

[80] Alex R Chiriyath et al. "Inner Bounds on Performance of Radar and Communications Co-Existence". In: *IEEE Transactions on Signal Processing* 64.2 (2016), pp. 464–474.

[81] BJ Donnet and ID Longstaff. "Combining MIMO radar with OFDM communications". In: *Radar Conference, 2006. EuRAD 2006. 3rd European*. IEEE. 2006, pp. 37–40.

[82] Christian Sturm, Thomas Zwick, and Werner Wiesbeck. "An OFDM System Concept for Joint Radar and Communications Operations." In: *VTC Spring*. 2009.

[83] Dmitriy Garmatyuk et al. "Wideband OFDM system for radar and communications". In: *Radar Conference, 2009 IEEE*. IEEE. 2009, pp. 1–6.

[84] Steve C Thompson and John P Stralka. "Constant envelope OFDM for power-efficient radar and data communications". In: *2009 International Waveform Diversity and Design Conference*. 2009.

[85] Yoke Leen Sit et al. "The OFDM joint radar-communication system: An overview". In: *Proc. Third Int. Conf. Advances in Satellite and Space Communications, Budapest, Hungary*. 2011, pp. 69–74.

[86] J. R. Krier et al. "Performance bounds for an OFDM-based joint radar and communications system". In: *IEEE Military Communications Conference*. 2015, pp. 511–516.

[87] M. Rossi, A. M. Haimovich, and Y. C. Eldar. "Conditions for target recovery in spatial compressive sensing for MIMO radar". In: *Proceedings of the IEEE International Conference on Acoustic, Speech, and Signal Processing*. 2013, pp. 4115–4119.

[88] J. Haupt et al. "Toeplitz compressed sensing matrices with applications to sparse channel estimation". In: *IEEE Transactions on Information Theory* 56.11 (2010), pp. 5862–5875.

[89] Y. Yu, S. Sun, and A. P. Petropulu. "A capon beamforming method for clutter suppression in colocated compressive sensing based MIMO radars". In: *Proceedings of SPIE 8717, Compressive Sensing II*. 87170J, 2013.

[90] A. R. Hunt. "Use of a frequency-hopping radar for imaging and motion detection through walls". In: *IEEE Transactions on Geoscience and Remote Sensing* 47.5 (2009), pp. 1402–1408.

[91] F. Ahmad and M. G. Amin. "Through-the-wall human motion indication using sparsity-driven change detection". In: *IEEE Transactions on Geoscience and Remote Sensing* 51.2 (2013), pp. 881–890.

[92] B. Li and A. P. Petropulu. "Structured sampling of structured signals". In: *Proceedings of the IEEE Global Conference on Signal and Information Processing*. 2013, pp. 1009–1012.

[93] H. Rauhut. "Compressive sensing and structured random matrices". In: *Theoretical foundations and numerical methods for sparse recovery* Chapter 9 (2010), pp. 1–92.

[94] B. Li and A. P. Petropulu. "Efficient target estimation in distributed MIMO radar via the ADMM". In: *Proceedings of the 48th Conference on Information Sciences and Systems*. 2014, pp. 1–5.

[95] S. Boyd et al. "Distributed optimization and statistical learning via the alternating direction method of multipliers". In: *Foundations and Trends in Machine Learning* 3.1 (2011), pp. 1–122.

[96] D. P. Bertsekas, A. Nedic, and A. E. Ozdaglar. *Convex Optimization Theory*. Belmont: Athena Scientific, 2009.

[97] D. Malioutov, M. Cetin, and A. S. Willsky. "A sparse signal reconstruction perspective for source localization with sensor arrays". In: *IEEE Transactions on Signal Processing* 53.8 (2005), pp. 3010–3022.

[98] "Radar Spectrum Regulatory Overview". In: *[online] 2013* (`http://www.darpa.mil/WorkArea/DownloadAsset.aspx?id=2147486331`, (Accessed: July 2014)).

[99] B. Li and A. P. Petropulu. "Spectrum sharing between matrix completion based MIMO radars and a MIMO communication system". In: *IEEE International Conference on Acoustics, Speech and Signal Processing*. 2015, pp. 2444–2448.

[100] B. Li, A. P. Petropulu, and W. Trappe. "Optimum Co-Design for Spectrum Sharing between Matrix Completion Based MIMO Radars and a MIMO Communication System". In: *IEEE Transactions on Signal Processing* 64.17 (2016), pp. 4562–4575.

[101] B. Li and A. P. Petropulu. "Radar precoding for spectrum sharing between matrix completion based MIMO radars and a MIMO communication system". In: *IEEE Global Conference on Signal and Information Processing*. 2015, pp. 737–741. DOI: 10.1109/GlobalSIP.2015.7418294.

[102] R. Zhang and Y. Liang. "Exploiting Multi-Antennas for Opportunistic Spectrum Sharing in Cognitive Radio Networks". In: *IEEE Journal of Selected Topics in Signal Processing* 2.1 (2008), pp. 88–102.

[103] M. Filo et al. "Cognitive pilot channel: Enabler for radio systems coexistence". In: *2nd International Workshop on Cognitive Radio and Advanced Spectrum Management*. 2009, pp. 17–23.

[104] F. M. Gardner. *Phaselock techniques*. John Wiley & Sons, 2005.

[105] R. Poore. "Phase noise and jitter". In: *Agilent EEs of EDA* (2001).

[106] R. Mudumbai, G. Barriac, and U. Madhow. "On the feasibility of distributed beamforming in wireless networks". In: *IEEE Transactions on Wireless Communications* 6.5 (2007), pp. 1754–1763.

[107] T. Jiang. "How Many Entries of a Typical Orthogonal Matrix Can Be Approximated by Independent Normals?" In: *The Annals of Probability* 34.4 (2006), pp. 1497–1529. ISSN: 00911798.

[108] A. Goldsmith et al. "Capacity limits of MIMO channels". In: *IEEE Journal on Selected Areas in Communications* 21.5 (2003), pp. 684–702.

[109] S. N. Diggavi and T. M. Cover. "The worst additive noise under a covariance constraint". In: *IEEE Transactions on Information Theory* 47.7 (2001), pp. 3072–3081.

[110] B. Friedlander. "Waveform design for MIMO radars". In: *IEEE Transactions on Aerospace and Electronic Systems* 43.3 (2007), pp. 1227–1238.

[111] C. Chen and P. P. Vaidyanathan. "MIMO radar waveform optimization with prior information of the extended target and clutter". In: *IEEE Transactions on Signal Processing* 57.9 (2009), pp. 3533–3544.

[112] E. Grossi, M. Lops, and L. Venturino. "Robust waveform design for MIMO radars". In: *IEEE Transactions on Signal Processing* 59.7 (2011), pp. 3262–3271.

[113] G. Cui, H. Li, and M. Rangaswamy. "MIMO radar waveform design with constant modulus and similarity constraints". In: *IEEE Transactions on Signal Processing* 62.2 (2014), pp. 343–353.

[114] A. Leshem, O. Naparstek, and Arye Nehorai. "Information Theoretic Adaptive Radar Waveform Design for Multiple Extended Targets". In: *IEEE Journal of Selected Topics in Signal Processing* 1.1 (2007), pp. 42–55.

[115] B. Li, H. Kumar, and A. P. Petropulu. "A Joint Design Approach for Spectrum Sharing between Radar and Communication Systems". In: *IEEE International Conference on Acoustics, Speech and Signal Processing*. 2016, pp. 3306–3310.

[116] Z. Chen et al. "Adaptive Transmit and Receive Beamforming for Interference Mitigation". In: *IEEE Signal Processing Letters* 21.2 (2014), pp. 235–239.

[117] C. Y. Chen and P. P. Vaidyanathan. "MIMO Radar Spacetime Adaptive Processing and Signal Design". In: *MIMO Radar Signal Processing*. John Wiley & Sons, Inc., 2008, pp. 235–281. ISBN: 9780470391488. DOI: 10.1002/9780470391488.ch6. URL: http://dx.doi.org/10.1002/9780470391488.ch6.

[118] S. Boyd and L. Vandenberghe. *Convex optimization*. Cambridge university press, 2004.

[119] Qiang Li and Wing-Kin Ma. "Optimal and robust transmit designs for MISO channel secrecy by semidefinite programming". In: *IEEE Transactions on Signal Processing* 59.8 (2011), pp. 3799–3812.

[120] K. Letaief and W. Zhang. "Cooperative Communications for Cognitive Radio Networks". In: *Proceedings of the IEEE* 97.5 (2009), pp. 878–893.

[121] S. Haykin. "Cognitive radar: A way of the future". In: *IEEE Signal Processing Magazine* 23.1 (2006), pp. 30–40.

[122] R. Zhang, Y. Liang, and S. Cui. "Dynamic Resource Allocation in Cognitive Radio Networks". In: *IEEE Signal Processing Magazine* 27.3 (2010), pp. 102–114.

[123] S. J. Kim and G. B. Giannakis. "Optimal Resource Allocation for MIMO Ad Hoc Cognitive Radio Networks". In: *IEEE Transactions on Information Theory* 57.5 (2011), pp. 3117–3131.

[124] S. Bhojanapalli and P. Jain. "Universal Matrix Completion". In: *Proceedings of The 31st International Conference on Machine Learning*. 2014, pp. 1881–1889.

[125] B. Razavi. "A study of phase noise in CMOS oscillators". In: *IEEE Journal of Solid-State Circuits* 31.3 (1996), pp. 331–343.

[126] C. Kopp. "Search and acquisition radars (S-band, X-band)". In: *Technical Report APA-TR-2009-0101, [online] 2009* (`http://www.ausairpower.net/APA-Acquisition-GCI.html`, (Accessed: July 2015)).

[127] "Radar performance". In: *Radtec Engineering Inc., [online]* (`http://www.radar-sales.com/PDFs/Performance\_RDR\%26TDR.pdf`, (Accessed: July 2015)).

[128] Telesystem Innovations. "LTE in a nutshell: The physical layer". In: *White paper* (2010).

[129] A. Goldsmith. *Wireless communications*. Cambridge university press, 2005.

[130] R. P. Jover. "LTE PHY fundamentals". In: *[online] 2015* (`http://www.ee.columbia.edu/~roger/LTE\_PHY\_fundamentals.pdf`, (Accessed: July 2015)).

[131] L. Lu et al. "Ten years of research in spectrum sensing and sharing in cognitive radio." In: *EURASIP J. Wireless Comm. and Networking* 2012 (2012), p. 28.

[132] G. Taubock. "Complex-valued random vectors and channels: Entropy, divergence, and capacity". In: *IEEE Transactions on Information Theory* 58.5 (2012), pp. 2729–2744.

[133] R. G. Bland, D. Goldfarb, and M. J. Todd. "The ellipsoid method: A survey". In: *Operations research* 29.6 (1981), pp. 1039–1091.

[134] H. W. Kuhn. "The Hungarian method for the assignment problem". In: *Naval research logistics quarterly* 2.1-2 (1955), pp. 83–97.

[135] J. Yeh. "Real analysis". In: *Theory of measure and integration*. Theory of measure and integration. Singapore: World Scientific, 2006.

[136] S. R. Becker, E. J. Candès, and M. C. Grant. "Templates for convex cone problems with applications to sparse signal recovery". In: *Mathematical Programming Computation* 3.3 (2011), pp. 165–218.

[137] B. Li and A. P. Petropulu. "MIMO Radar and Communication Spectrum Sharing with Clutter Mitigation". In: *IEEE Radar Conference*. 2016, pp. 1–6.

[138] Karol Zyczkowski and Marek Kus. "Random unitary matrices". In: *Journal of Physics A: Mathematical and General* 27.12 (1994), p. 4235.

[139] E. J. Candès and B. Recht. "Exact matrix completion via convex optimization". In: *Foundations of Computational mathematics* 9.6 (2009), pp. 717–772.

[140] B. Laurent and P. Massart. "Adaptive estimation of a quadratic functional by model selection". In: *Annals of Statistics* (2000), pp. 1302–1338.

[141] GEA Franken, H Nikookar, and Piet van Genderen. "Doppler tolerance of OFDM-coded radar signals". In: *2006 European Radar Conference*. 2006.

[142] Satyabrata Sen and Arye Nehorai. "Adaptive OFDM radar for target detection in multipath scenarios". In: *Signal Processing, IEEE Transactions on* 59.1 (2011), pp. 78–90.